Hydrogen Production from Liquefied Petroleum Gas (LPG) by Oxidative Steam Reforming Over Bimetallic Catalysts

by

Zuhair Malaibari

A thesis
presented to the University of Waterloo
in fulfillment of the
thesis requirement for the degree of

Doctor of Philosophy

in
Chemical Engineering

Waterloo, Ontario, Canada, 2011

Author's Declaration

I hereby declare that I am the sole author of this thesis. This is a true copy of the thesis, including any required final revisions, as accepted by my examiners.

I understand that my thesis may be made electronically available to the public.

Abstract

Hydrogen is a promising renewable fuel for producing energy in transportation and domestic applications. This study investigates the production of H_2 from reforming of liquefied petroleum gas (LPG). LPG is a mixture of gases, mainly propane and butane, produced from petroleum or natural gas. It is a liquid under moderate pressure and therefore a favourable feedstock for distributed hydrogen production since it is easy to store and transport with a distribution network already in place. With its wide range of propane and butane compositions world wide, in this study LPG was considered as a mixture of propane and butane. H_2 production from LPG was investigated through oxidative steam reforming of propane and butane.

Oxidative steam reforming (OSR) can be viewed as a combination of two reactions: partial oxidation (PO) and steam reforming (SR). By carefully controlling the steam to carbon (S/C) and oxygen to carbon (O_2/C) ratios in the feed, OSR can produce higher H_2 yields than PO at operational temperatures lower than SR.

In the first part of this study, based on the literature and preliminarily experiments, two Ni based bimetallic catalysts, Pt-Ni/Al_2O_3 and Mo-Ni/Al_2O_3, were selected to be compared to a monometallic 15 wt% Ni/Al_2O_3 catalyst for OSR of a 1:1 propane to butane LPG mixture under different operational conditions. This catalysts screening study evaluated the performance of the catalysts on the basis of a statistical factorial experimental design. The factorial design was efficient in optimizing experimental runs, while testing the activity and product distribution of the catalysts at different operational limits. The importance of the factorial design was clearer when analyzing results for the Pt-Ni catalysts, as the catalyst showed different product compositions at the two selected loadings (0.2 and 1 wt%) under different conditions compared to the unpromoted catalyst. However, at both loadings, the Pt-Ni catalyst did not have a significant effect on fuel conversion or catalyst selectivity to different products. On the other had, under all stable conditions in the factorial design experiments, the Ni-Mo catalyst had higher H_2

and CO yields and lower CH_4 yields compared to the unpromoted catalyst. To our knowledge these product composition variations were not reported before in the literature for hydrocarbon reforming reactions over Mo promoted catalysts.

The catalyst screening study also included time on stream catalysts stability tests. These experiments illustrated the high potential for solving the Ni stability problem associated with LPG reforming as the unpromoted 15Ni catalyst suffered from deactivation by coking and could not sustain its high conversion. On the other hand, promoting the Ni catalysts with 1 wt% Pt or 0.1 wt% Mo improved the catalyst resistance to coking and sustained its activity and product composition throughout the 18 hours of the stability tests. However, an increase in the Mo loading to 0.3 wt% in the Mo-Ni bimetallic catalyst, led to lower fuel conversions and loss of stability with time.

Because of the interesting performance of the Mo-Ni /Al_2O_3 catalyst observed in the catalyst screening tests, and the lack of explanations of different aspects of this performance in the literature, especially in the presence of O_2, the second part of the study was concerned with the investigation of the effect of small amounts of Mo addition on the activity, selectivity and stability of Ni catalysts when used for H_2 production from LPG OSR. Individual fuels and reactions experiments showed that butane OSR gave the highest fuel conversions and H_2 production rates. These experiments also revealed the importance of O_2 for the catalyst activity and stability as for both hydrocarbons the catalyst suffered deactivation by coking under SR conditions. However, O_2 compositions in the feed should be carefully optimized as characterization of fresh and aged catalysts showed that the loss of stability observed earlier in the catalyst screening tests for higher Mo catalysts loading, was caused by the oxidation of active Ni species to inactive Ni and Ni-Mo phases which resulted from the oxidative environment of the reaction during aging.

In the last part of this study, surface and bulk properties of the monometallic Ni catalyst was compared to the Mo-Ni bimetallic catalyst using different catalyst characterization techniques (TPR, TPO, TGA, XRD, H_2 and O_2 chemisorption and

DRIFTS) in order to understand the structural effect of Mo addition on the catalytic properties. It was found that the improvements in the catalytic properties of the catalyst and the change in its selectivity to different products were caused by an electronic effect of Mo and its different oxide phases on Ni species. These electronic effects enhanced the O_2 mobility over the catalysts surface leading to higher gasification rates of CHx species and hence, preventing coking of the catalyst. They also affected the stability of adsorbed reaction intermediates over the catalysts surface which affected the selectivity of the catalyst to different reaction products.

Acknowledgments

My profound gratitude is to Allah (God Almighty) who guided me in his infinite wisdom and blessings through every facet of this work.

To start, I would like to thank King Fahd University of Petroleum and Minerals (KFUPM) in Dhahran, Saudi Arabia, for offering me the scholarship to achieve my PhD degree and for their generous financial support for me and my family throughout my years of study here in Canada.

I am sincerely grateful to my supervisors, Dr. Eric Croiset and Dr. William Epling, who showed great confidence in me, provided me with a tremendous deal of support and shared their knowledge and expertise with me. I also would like to thank the members of my final PhD defense committee for their time, efforts and valuable comments that improved the quality of this thesis. They were:

Dr. Chuck Mims (University of Toronto)
Dr. Xianguo Li, represented by Prof. Zhongchao Tan (Department of Mechanical Engineering)
Dr. Bob Hudgins (Department of Chemical Engineering)
Dr. Joao Soares (Department of Chemical Engineering)

I would like to acknowledge the Chemical Engineering Department at the University of Waterloo for their invaluable contributions and assistance throughout the course of my PhD graduate program.

It would have been very difficult for me when I first came to the city of Waterloo, having left my family back home, if it had not been for a few friends who helped me to stand on my own two feet. Thank you Dr. Mohammed Ba-shammak, Dr. Ibrahem Maffa and Dr. Mamdoh Al-Harthi for all that you did.

Two very good friends and lab mates, Dr. Ashraf Amin and Dr. Moshari Al-Harbi, were essential to the successful completion of this thesis. Ashraf, thank you for all your technical and moral support. We spent long nights in the lab which included running experiments and discussing results, as well as eating, chatting and laughing a lot. I can't imagine better times. Moshari, I will never forget your smile; it always boosted my self esteem. After talking to you, I always felt encouraged to continue my work and finish it. Thank you my friends, and I assure you, this will not be the end of our personal and professional relationship.

I would like also to thank other members of the Reaction Engineering group in our lab that helped me at the beginning of my research to construct my experimental set-up: Dr. Luke Columen, Dr. Monrudee Phongaksorn and Dr. Tuan Amran,

Throughout my PhD studies, I made many good friends at the University of Waterloo. We had good times together and I am sure they will continue in the future. Also, I would like to thank the Saudi community in the city of Waterloo for their social and moral support for me and my family.

To my lovely wife Noha, you sacrificed a lot, you made the perfect study environment for me, you took care of the kids, the house, my health, etc. – you took care of every thing. I was the only PhD student that was married and had children who didn't have any responsibilities interfering with my studies. I couldn't imagine having done it without you, my love. May Allah (God Almighty) reward you for I don't think I can repay all that you have done for me.

Finally, my prayers go to my parents: my father, Mr.Omar Malaibari and my mother, Mrs. Khayriyh Al-Safar. May Allah (God Almighty) bless them with mercy and rewards now and always. If it weren't for them, I wouldn't be who I am today. Mom and Dad, all your sacrifices and tears paid off; be proud of yourselves – this is your achievement, too.

Dedication

To My Loving Parents, My Wife and All My Big Family in Saudi Arabia

Table of Contents

List of Figures

List of Tables

Chapter 1

Introduction and Motivation

Recent environmental concerns of using fossil fuels and improving energy efficiency for producing electricity and for propulsion of vehicles, led to remarkable progress in fuel cell research and development. Fuel cell systems operating on pure hydrogen produce only water, thus eliminating all emissions locally. Hydrogen as a fuel powers a wide range of fuel cells. It is a promising future fuel for fuel cell applications. It has the highest energy content by weight of any fuel, and has almost no emissions when burned and when used in a fuel cell, the only by-product is water. Hydrogen is very abundant and is found readily in many compounds on earth.

The fuel cell most often targeted for vehicle applications uses hydrogen and oxygen to produce an electric current. It is similar to a battery in terms of use only it creates the electricity as it is needed instead of storing the energy for later use. Fuel cells work by utilizing hydrogen gas (H_2), which must be supplied, and oxygen gas (O_2) from the air. The hydrogen gas goes through the anode (-) side and the oxygen through the cathode (+) side. The anode side contains a platinum catalyst that breaks the hydrogen atoms into H^+ ions and electrons. In between the cathode and anode is a PEM or proton exchange membrane. This membrane allows only the H^+ ions to travel though from the anode to the cathode. The electrons must travel through an external wire. This creates the electric current that can be utilized to drive accessories and the propulsion motor. At the cathode the hydrogen and oxygen combine to form water, which is the only by-product of the fuel cell process. Individual fuel cells generally do not produce large amounts of power. In order to create an amount of current that is useful, they must be combined into stacks, similar to batteries being grouped to provide a greater power source.

The projected commercialization of fuel cells requires a readily available hydrogen source. Hydrogen can be supplied from a number of storage methods, such as liquid hydrogen storage, compressed hydrogen storage, and metal hydride. The most efficient

way for storage is liquid hydrogen, which offers high storage density and allows fast refuelling times, but this method suffers significant evaporative loss, also high energy is required to liquefy hydrogen. Metal hydride overcomes the problem of losing hydrogen by evaporation but has low hydrogen storage density.

These storage difficulties in addition to the lack of an infrastructure for producing and distributing hydrogen led to a research effort to develop fuel processing technologies for reforming hydrocarbon fuels to generate hydrogen. In addition, for a hydrogen fuel cell-based system to be practical and reliable it must ensure the following features: rapid start-up, good dynamic response, high-fuel conversion, small size and weight, simple construction and operation, and of course low cost (Appleby, 1995). Therefore the choice of a correct fuel and fuel processor is one of the main key features for the commercialization of the electric vehicle fuel cell with an on-board hydrogen generator.

One of the promising hydrocarbon fuels recently investigated for hydrogen production in fuel cell applications is liquefied petroleum gas (LPG). LPG is a mixture of gases, mainly propane and butane, produced from petroleum or natural gas. It is a liquid under moderate pressure and therefore a favourable feed stock for distributed hydrogen production since it is easy to store and transport with a distribution network already developed. Hydrogen can be produced from LPG through partial oxidation, steam reforming or dry reforming. Oxidative steam reforming is a combination of partial oxidation and steam reforming, where the exothermic oxidation reactions provide heat for the endothermic reforming reactions. Provided that the heat from oxidation can be readily transferred to the steam reforming zone of the catalytic system, OSR is more energy conservative by overcoming high operational temperatures of steam reforming while having higher hydrogen yields than partial oxidation reactions

Ni-based catalysts are by far the preferred systems for steam reforming, due to their activity as well as cost considerations. They are thus probably the preferred catalysts for oxidative steam reforming. However, the ability of Ni catalysts to sustain their activity had always been a concern. With high hydrocarbon feeds such as butane enriched LPG,

Ni catalysts are always under the risk of deactivating by carbon formation because of cracking of hydrocarbons especially at high temperatures. In addition, Ni is not the best oxidation catalyst, since it can be oxidized to non-active phases in high oxidation environments. Moreover, when running steam reforming reactions at high temperatures, as in the case of methane steam reforming, and/or at high steam pressures for gasoline or diesel reforming, Ni catalysts will be at a high risk of sintering; the growth of metal crystallites and the collapse of catalyst support. Sintering of Ni catalysts will lead to losses in Ni surface area and hence, the activity of the catalyst with time. Although, optimizing operational parameters can lower the risk of Ni catalysts deactivation, it is usually accompanied with a loss of activity and/or selectivity of the catalysts to desired products. Therefore, more attention has been given to understanding the effect of different Ni deactivation modes on the catalyst structure, and how it can be modified or improved to enhance catalyst stability. As a well developed industrial process, deactivation of Ni catalysts in CH_4 steam reforming was studied extensively in the literature. On the other hand, less attention was given to deactivation of LPG reforming catalysts, as the feed was considered for H_2 production only in the last decade.

Among the ways to improve Ni catalysts stability, is to combine the Ni catalyst with small amounts of another metal, in which the interaction of the two metals will lead to structural changes in the catalyst. The resulting catalyst is known as a bimetallic catalyst capable of resisting Ni deactivation while sustaining the catalyst activity and selectivity. Noble metals such as Pt and Rh have been known to be highly resistant to carbon formation and to have high sulfur tolerance, in addition to their highly oxidation properties. Therefore, they were added to Ni catalyst in oxidative steam reforming of high hydrocarbons such as gasoline and diesel. However, because of the high cost of these metals, more attention was drawn to cheaper transition metals that can improve Ni stability. Metals like Co, Ce and Mo showed promising results when added to Ni to sustain its activity. However, the structural role of these metals in Ni reforming catalysts are still not as clearly understood as for bimetallic noble metals which have been investigated more extensively for their role as hydrocarbon oxidation and steam reforming catalysts in automotive emission control applications. Moreover, the effect of

adding O_2 to the reaction in oxidative steam reforming over these bimetallic catalysts is undefined since most of the catalysts are applied to hydrocarbons steam reforming at high temperatures and in the absence of O_2.

Research Objectives

The overall objective of this study was to develop an active and stable Ni based bimetallic catalyst, suitable for reforming a wide range of LPG compositions through oxidative steam reforming, with the goal of achieving high hydrogen yields. This general objective was achieved through the following key objectives:

- To carry out a thermodynamic equilibrium study, to provide insights on the expected product distribution for a wide range of operating conditions. The thermodynamic analysis also help to limit examined parameter ranges and concentrate experiments on optimum operational conditions, under which maximum hydrogen yields are achieved.

- To run a variety of preliminarily experiments that set foundations for evaluating the performance of bimetallic catalysts that were selected to compare their catalytic properties under different operational conditions.

- To screen the performance of two selected catalysts (chosen to be Pt-Ni/Al_2O_3 and Mo-Ni/Al_2O_3 based on the literature and preliminarily experiments) under different operating conditions and compare their performance under the selected conditions to the monometallic Ni/Al_2O_3 catalyst based on a statistical factorial experimental design.

- To analyze the effect of the Mo-Ni/Al_2O_3 catalyst (as the selected catalyst from the screening tests) on the activity and selectivity of individual reactions taking place during oxidative steam reforming for propane and butane separately.

- To investigate the role of Mo in preventing catalyst deactivation by coking through analyzing carbon deposition relations that resulted in the deactivation of the monometallic Ni catalyst.

- To investigate the nature of structural interactions between Mo and Ni in the bimetallic catalyst, and how these interactions affect the activity, selectivity and stability of the catalyst. This investigation was carried out by characterizing both the bimetallic and monometallic catalysts to compare the effect of small amounts of Mo on the surface and bulk properties of the catalyst.

- To predict the effect of Mo on different pathways in the general oxidative steam reforming scheme.

CHAPTER 2

Background Material and Literature Review

Hydrogen can be extracted by reforming various readily available hydrocarbons, such as methanol, ethanol, natural gas, gasoline, diesel and jet fuel. Reforming has been intensively developed for both on-board (vehicle), and off board (stationary, residential) applications. The conversion of hydrocarbon fuels to hydrogen can be carried out by several reaction processes, including steam reforming (SR), partial oxidation (PO), dry reforming (DR) and oxidative steam reforming (OSR). The choice of the reaction process to be used for reforming in small fuel cell systems depends on many factors, including the operating characteristics of the application (e.g, varying power demand, rapid start-up, frequent shutdowns) and the type of fuel cell stack (e.g, PEMFC or SOFC).

Steam Reforming (SR) involves the reaction of steam with the fuel in the presence of a catalyst to produce hydrogen and CO. Steam methane reforming (SMR) is the most common method of producing commercial bulk hydrogen. At high temperatures (700 – 1100°C) and in the presence of a metal-based catalyst, steam reacts with methane to yield carbon monoxide and hydrogen.

$$CH_4 + H_2O = CO + 3\ H_2 \qquad (2.1)$$

$$\Delta H^{\circ}_{298} = +206.2\ \text{kJ mol}^{-1}$$

The residence time is generally on the order of several seconds, for a gas-hourly space velocity (GHSV) of 2000–4000 h^{-1}.

Steam reforming can also be used to produce hydrogen from propane and butane (the two main components of LPG):

$$C_3H_8 + 3H_2O = 3CO + 7H_2 \qquad (2.2)$$

$$\Delta H°(298\text{K}) = +497\ \text{kJ/mol}$$

n-$C_4H_{10} + 4H_2O = 4CO + 9H_2$ (2.3)

$\Delta H°$ (298K) =+649.9 kJ/mol

The high hydrogen yield from the endothermic reaction (up to 70%) makes steam reforming a potential way to provide fuel for fuel cells. The basic idea is that a light hydrocarbon fuel tank and a steam reforming unit would replace the bulky pressurized hydrogen tanks that would otherwise be necessary. This might mitigate the distribution problems associated with hydrogen vehicles. However, the reforming reactions take place at high temperatures, making the process slow to start up and requiring costly high temperature materials. Another problem associated with steam reforming catalysts is deactivation by coking. Coking produced by thermal cracking of hydrocarbons (Eq. (2.4) & (2.5)) or by CO disproportionation (Boudouard reaction) (Eq. (2.6)) leads to catalyst deactivation. These processes are problematic when the steam-to-carbon ratios are low.

$CH_4 = C + 2H_2$ (2.4)

$C_3H_8 = CH_4 + 2C(s) + 2H_2$ (2.5)

$2CO = C + CO_2$ (2.6)

To minimize coke formation, excess steam is used to ensure that any carbon formed is gasified (Eq. (2.7)).

$C + H_2O = CO + H_2$ (2.7)

For methane and propane, a steam-to-carbon ratio of approximately 2.5 is sufficient to avoid coking. For higher hydrocarbons, a steam-to-carbon ratio of 6–10 is not uncommon (Pesce, et al., 1992). Nonetheless the biggest problem for steam reforming based systems remains the fuel cell itself, in terms of both cost and durability. The catalyst used in the common polymer-electrolyte-membrane fuel cell, the device most likely to be used in transportation roles, is very sensitive to any leftover carbon monoxide

in the fuel, which some reformers do not completely remove. The membrane is poisoned by carbon monoxide even at levels as low as 10 ppm and its performance degrades, making it necessary to include complex CO-removal systems.

A reaction taking place with steam reforming which helps to remove some of the CO by converting it to H_2 and CO_2 is the heterogeneous catalyzed water-gas-shift reaction:

$$CO + H_2O = CO_2 + H_2 \qquad (2.8)$$

$$\Delta H°(298K) = -41 \text{ kJ/mol}$$

The water-gas shift reaction is limited by its thermodynamic equilibrium, which may be calculated using the equilibrium constant expression (Eq. 2.9) (Moe, 1962):

$$K=\exp((4577.8/T)-4.33) \qquad (2.9)$$

From an industrial design prospective, in order to decrease the size of the reactor, water-gas-shift reactions are usually performed in two stages with intermediate cooling preferably by water injection (Twigg, 1989). In the first stage, the so-called high-temperature water-gas shift (HTS), most of the carbon monoxide is converted, which is performed industrially at temperatures between 350 and 450°C. Fe_2O_3/Cr_2O_3 catalysts are applied industrially for HTS which are robust but suffer from low activity. This is less crucial for the industrial process rather than for a compact fuel processor application (Ghenciu, 2002). The second stage (low-temperature water-gas shift, LTS) is performed between 200 and 300°C depending on the application and the CO concentration required for the product. The reaction is performed industrially over CuO/ZnO catalysts with an alumina carrier (Twigg and Spencer, 2001). These two stages are necessary since the HTS stage is fast because of high temperatures but it is thermodynamically limited. Therefore, lowering the temperatures in the LTS stage shifts the equilibrium to the right producing more products. However, the challenges for an automotive application are fundamentally different from those of industrial use. As mentioned before the high sensitivity of the fuel cell to any CO content has driven researchers to come up with

catalysts systems that can reduce the CO content to very low concentrations, shifting the reaction toward the production of H_2 and CO_2 as much as possible.

Partial oxidation (PO) involves the reaction of oxygen with fuel to produce H_2 and CO when the oxygen-to-fuel ratio is less than that required for total combustion, i.e. complete conversion to CO_2 and H_2O. The following equations represent partial and total oxidation reactions for both propane ((2.10) and (2.11), respectively) and butane ((2.12) and (2.13), respectively):

$$C_3H_8 + 1.5\ O_2 = 3CO + 4H_2 \qquad (2.10)$$
$$\Delta H°(298K) = -229\ kJ/mol$$

$$C_3H_8 + 5O_2 = 3CO_2 + 4H_2O \qquad (2.11)$$
$$\Delta H°(298K) = -2046\ kJ/mol$$

$$C_4H_{10} + 2O_2 = 4CO + 5H_2 \qquad (2.12)$$
$$\Delta H°(298K) = -568\ kJ/mol$$

$$C_4H_{10} + 6.5O_2 = 4CO_2 + 5H_2O \qquad (2.13)$$
$$\Delta H°(298K) = -2658.5\ kJ/mol$$

The use of PO to generate H_2 (in particular synthesis gas [H_2 + CO]) for large-scale commercial applications has received some attention recently; however, such processes have not been extensively commercialized (Bharadwaj et al., 1995). Although PO reactions have higher rates than SR, the hydrogen yield is much lower. Furthermore, in order to achieve optimal rates in PO, some of the fuel must be combusted to preheat the feed. (Pesce, et al., 1992) .The reaction can be conducted with a catalyst (catalytic PO) or without a catalyst (non-catalytic PO). Recently, there has been an interest in catalytic PO, because it operates at lower temperatures than the non-catalytic route, thus providing better control over the reaction, minimizing coke formation, and allowing for a wider choice of materials of construction for the reactor. Catalysts are typically group VIII

metals, such as rhodium, platinum, palladium, ruthenium, cobalt, nickel, and iridium, which are supported on oxide substrates (Hofstad et al., 1998).

Oxidative Steam Reforming (OSR) involves the reaction of oxygen, steam, and fuel to produce H_2 and CO_2. Equation 2.14 defines the idealized reaction stoichiometry for the production of H_2 from a carbonaceous fuel during OSR, where x is the oxygen-to-fuel molar ratio.

$$C_nH_mO_p + x(O_2 + 3.7N_2) + (2n - 2x - p)H_2O \rightarrow nCO_2 + (2n - 2x - p + (0.5m))H_2 + 3.7xN_2 \quad (2.14)$$

In essence, this process can be viewed as a combination of PO and SR. The oxidative steam reformer is composed of a thermal zone and a catalytic zone. The feed enters a burner and mixes with specific amounts of steam and oxygen or air. In the thermal zone partial and total oxidation reactions take place. By adjusting the oxygen-to-carbon and the steam-to-carbon ratios, the oxidation reactions provide the required heat for the subsequent endothermic steam reforming and water-gas shift reactions taking place in the catalytic zone. Thus, gas compositions of the product stream are fixed thermodynamically through pressure, temperature, steam to carbon ratio and oxygen to carbon ratio. In principle, the oxygen-to-carbon (O_2/C) and the steam-to-carbon (S/C) ratios can be chosen independently, as long as there is a supply of O_2 in the system sufficient to convert the entire C to CO_2. However, as mentioned earlier, these ratios determine the energy released or adsorbed by the reaction, which defines the adiabatic reaction temperature and consequently, the concentration of H_2 in the product.

When no external heating source is required in OSR, such that the exothermic oxidation reaction provides the heat necessary for the endothermic SR reaction the adiabatic process ($\Delta H = 0$) is referred to as autothermal reforming (ATR). Although expressed by autothermal reforming, most definitions in the literature consider the process as composed of partial oxidation and steam reforming with $\Delta H < 0$ (which is

really OSR not ATR). This choice depends on some considerations about the integration of the fuel processor system (faster start-up, good transient response, closer heat balance of the total fuel processor).

As discussed by Ahmed and Krumpelt (2001), the lower operating temperature of catalytic OSR has several advantages over the higher operating temperature of endothermic SR. Three advantages are particularly important:

1) Less complicated reactor design and lower reactor weights, because less thermal integration is required
2) A wider choice of materials of construction
3) Lower fuel consumption during startup because, for a given reactor mass, the energy required to heat a reformer to its operating temperature is proportional to its operating temperature.

However, since more than 70% of the hydrogen on a dry basis is produced during the steam reforming stage and it is a slow reaction (Ahmed and Krumpelt, 2001), it is necessary to study the kinetics of steam reforming as a step towards understanding OSR in which, partial oxidation occurs first, followed by steam reforming.

Various transition metals (Ni, Co, Fe) or noble metals (Pt, Rh, Pd) supported on oxide supports are the standard catalyst formulations for OSR of hydrocarbons. Recently, efforts have focus on formulating new catalysts that prevent carbon deposition and/or sulphur deactivation while keeping high thermal and mechanical stability. In this respect, new catalysts including substrates like ceria and zirconia have been developed.

In the absence of a clear, well-defined base line and as a result of significant differences in fuel properties for different hydrocarbons, there is only little research work done to compare different types of hydrocarbons used in hydrogen production reforming processes. Two studies that compared propane and methane reforming using computer simulation were presented by Avcı et al. in 2001 and by Minutillo in 2005.

Avcı et al. (2001) compared catalytic PO and OSR of methane, propane, octane and methanol under conditions similar to those used for hydrogen production for fuel cell applications. Both reactions for each fuel have been simulated, based on conversion data and kinetic equations reported in the literature for various catalyst configurations and hydrocarbons using computer codes. Table 2.1 shows some of their interesting simulation results.

Table 2.1: Weight-based hydrogen yields obtained from the simulations of PO and OSR of different fuels (Avcı et. al., 2001)

Oxidative Steam Reforming

Fuel	T (K)	[a]H_2 at 353K (ml/g) x 100	[b]Water:fuel
Methane	1100	500	3.45
Methanol	600	440	3.26
Propane	1100	850	5.98
Octane	1100	1050	11.41

Direct Partial Oxidation

Fuel	T (K)	H_2 at 353K (ml/g) x 100	Water:fuel
Methane	1490	1060	1.4
Methanol	1370	318	0.2
Propane	1770	850	5.5
Octane	1840	770	14.4

[a]Weight-based hydrogen yield = volumetric flow rate of hydrogen at 353K (operating temperature of the fuel cell) (ml)/(weight of the fuel + water injected into Reactor 1 (g)).
[b]Water:fuel = moles of water injected/moles of fuel injected.

The results showed that in terms of hydrogen produced per weight of fuel, partial oxidation of propane and oxidative steam reforming of octane were the best alternatives, while methanol was much less efficient.

In 2005 Minutillo developed a numerical model of a simple reforming system, based on a partial oxidation process. He investigated the conversion of methane, propane, heptane, toluene and gasoline to hydrogen by a thermodynamic analysis of the reforming system using AspenPlus software. The reformer efficiency was calculated by considering both hydrogen and carbon monoxide in the synthesis gas.

Although the main objective of his work was to validate the proposed model compared to experimental results, based on his simulation results Minutillo also showed that the reforming efficiency of propane was higher than that of methane for on-board fuel processors (as shown in Table 2.2).

Table 2.2: Methane vs. propane reforming efficiencies (Minutillo, 2005)

	Operating conditions			Experimental results			
	Fuel flow rate	Air flow rate (Nm^3/h)	O/C	H_2+CO (vol%)	CO_2 (vol%)	CH_4 (vol%)	Efficiency (%
Propane	0.39 kg/h	1.9	0.36	43.0	3.0	2.0	72.0
Propane	0.35 kg/h	1.9	0.40	40.0	3.1	0.5	73.0
Methane	0.70 Nm^3/h	3.2	0.45	34.0	4.5	0.5	63.0
Methane	0.56 Nm^3/h	2.6	0.46	33.0	4.5	0.4	65.0

2.1 Propane Reforming

Because of its easy storage and existing infrastructure, propane is a fuel that has a high potential as a hydrogen carrier for future applications. Investigations on propane reforming began in the early 1980's. At those times partial and total oxidation of propane were studied not for the purpose of hydrogen production in fuel cell applications, but to investigate hydrocarbon oxidation into carbon dioxide and water over three way catalysts. Three way catalysts were used in catalytic converters for controlling the pollutants emitted by exhaust gases from automobile engines. By the 90's researchers began to look at propane reforming (mainly steam reforming) as a process to supply hydrogen for fuel cell applications. Consequently, studies on OSR of propane did not take place until the beginning of the new millennium, where researchers began to think of combining endothermic high hydrogen yield steam reforming with exothermic oxidation reactions in order to get a more efficient process.

2.1.1 Propane Steam Reforming

On an industrial scale, steam reforming of light alkanes is one of the most economical routes for the manufacturing of synthesis gas (H_2/CO mixture). Therefore, even modest improvements in the steam reforming operation translate to substantial gains in plant economics. As illustrated before, propane reforming produces hydrogen and carbon monoxide from the reaction of propane with steam as illustrated by equation 2.2:

$C_3H_8 + 3H_2O = 3CO + 7H_2$ (2.2)

$\Delta H°(298K) = +497$ kJ/mol

Subsequently carbon monoxide is converted to carbon dioxide by the thermodynamic equilibrium limited water gas shift reaction (2.8):

$CO + H_2O = CO_2 + H_2$ (2.8)

$\Delta H°(298) = -41$ kJ/mol

A significant amount of work on propane steam reforming for both industrial and fuel cell applications has been published in the literature. Different aspects of both the reaction and the process have been investigated including: kinetics of the reactions, activity and stability of the catalyst and optimum process conditions. Table 2.3 gives an overview of the current state of propane steam reforming studies in the open literature.

Table 2.3: An overview of the current state of the propane steam reforming filed.

Author	Year	Fuels	Catalyst	Temp. °C (S/C)	Fuel Con%	Objectives
Hardiman et al.	2004	propane	5%Co-15%Ni/80%γ-Al_2O_3	500-600 (0.8& 1.6)	95	study effect of S/C ratio & T on deactivation of catalyst
Kolb et al.	2004	propane	Rh/γ-Al_2O_3, Pt/γ-Al_2O_3, Pd/γ-Al_2O_3, Rh/CeO_2/γ-Al_2O_3, Pt/CeO_2/γ-Al_2O_3, Rh/Pt/CeO_2/γ-Al_2O_3	450-750 (0.5-3)	70-100	Study of propane steam reforming on different noble catalyst combinations in micro-channel reactors.
Hardiman et al.	2005	propane	Co-Ni/γ-Al_2O_3 with pH of the impregnating solution varying from 2-8	NR (1)	NR	Study the influence of impregnating pH on steam reforming characteristics.
Natesakhawat et al.	2005	propane	20% Ni–2% Ce/Al_2O_3 20% Ni–2% La/Al_2O_3 20% Ni–2% Yb/Al_2O_3	400-550 (1.3)	66-80	Study effect of lanthanide promotion on catalytic performance of sol–gel Ni/Al_2O_3 catalysts in steam reforming of propane
Resini et al.	2005 2006	Propane, propene, Isopropanol and acetone	Pd-Cu/ γ-Al_2O_3 Ni/$NiAl_2O_4$	427-827 (6)	70-90	Study of SR of C3 organics over two catalysts that can be used as anodes in directly fueled fuel cells.
Laosiripojana et al.	2006	Mix. of 65% ethane and 35% propane	14%CeO_2-doped Ni/Al_2O_3	600-900	95	Study reactivity toward steam reforming of ethane and propane, as well as the resistance toward carbon formation of CeO_2-doped Ni/Al_2O_3 and comparing to conventional Ni/Al_2O_3.
Hardiman et al.	2006	propane	5%Co-15%Ni/80%γ-Al_2O_3	500-600 (0.8& 1.6)	NR	Using microscopic, spectroscopic and thermal analysis techniques to study the chemical nature of carbon deposited during propane reforming over a Co–Ni catalyst and relate the qualitative features to the mechanistic and kinetic details of the coke removal process under oxidizing and reducing environments.
Schadel et al.	2009	CH_4, C_2H_6, propane, butane	Honeycomb monoliths Rh based	300-900 (2.5 & 4)	10-100	Developing a detailed mechanism for natural gas SR including higher alkanes components
Zhang et al.	2009	propane	Sol-gel 20 % Ni/Al_2O_3	500 (1.3)	60	compared the activity and stability of a conventionally impregnation prepared Ni/Al_2O_3 catalyst with a one step sol-gel prepared one for propane steam reforming
Fauteux-Lefebvre et al.	2010	Propane, hexadecane and tetralin	$NiAl_2O_4$/Al_2O_3–YSZ	700-750 (3)	NR	Test the suggested catalyst for diesel steam reforming
Rakib et al.	2010	propane	Naphtha SR catalyst provided by Haldor Topsoe	475-550 (5)	60-75	Improving H_2 purity from propane SR by using a fluidized bed membrane reactor.

Catalysts for Propane Steam Reforming

For many years, nickel has been the most suitable metal for steam reforming of hydrocarbons as far as cost effectiveness is concerned. Usually nickel is supported on alumina, magnesia, zirconia and recently ceria. These supports provide high crush strength and stability. However, coke formation is still a major problem associated with nickel catalysts. The formation of coke during the steam reforming of hydrocarbons results mainly from catalytic reactions. Filamentous carbon is formed at the surface of the metal particle by a consecutive process of formation, diffusion and dissolution (Race, 2000). As the coke is gradually produced, the degradation of the catalyst is accelerated until the catalyst is deactivated by coking and continuation of catalyzed reforming becomes impossible.

Nickel Metal Based Catalysts

In an effort to improve Ni catalysts stability and coking resistance, Hardiman et al. (2004-2006) investigated propane steam reforming in a fluidized bed reactor on Co-Ni/Al_2O_3 bimetallic catalysts. Beginning in 2004 the group examined the effects of temperature and steam-to-carbon ratio on carbon formation and deactivation of the catalysts. As their total organic carbon analysis showed in Table 2.4, carbon content decreased with increasing both temperature and S:C ratio.

Table. 2.4: Total organic carbon analysis at different S/C ratios and temperatures (Hardiman et al., 2004)

S:C ratio	Temperature (K)		
	773	823	873
0.8	60.83%	56.34%	55.15%
1.2	24.67%	9.17%	7.49%
1.6	15.09%	1.27%	0%

In 2005 Hardiman's group studied the influence of pH during the impregnation step during catalyst preparation on the steam reforming characteristics of a Co-Ni/Al_2O_3

catalyst. Different catalysts were prepared by impregnation under low (2) and high (8) pH values. They found that support dissolution due to acid attack appeared to be responsible for the low BET surface area for catalysts obtained at pH 2. However, this low-pH catalyst possesses higher dispersion. They continued their work in 2006 by investigating the physicochemical properties of used catalysts obtained from propane steam reforming under steam-to-carbon (S:C) of 0.8 and 1.6 at operating temperatures of 773–873°K using BET, H_2 chemisorption, total organic carbon (TOC) content analysis, XRD, TEM, as well as carbon reactivity analysis via gravimetric temperature-programmed (TPO–TPR and TPR–TPO–TPR) runs. Interpretation of the results from these techniques provided good agreement with their previous results in 2004 especially those regarding the types of atomic carbon phases (C_α and C_β).

Another interesting study to improve the resistance of Ni/Al_2O_3 catalysts toward carbon formation was done by Laosiripojana et al. (2006) where they investigated the steam reforming of a mixture of 65% ethane and 35% propane on Ni/Al_2O_3 and the effect of doping with 0 to 20% CeO_2. Compared to conventional Ni/Al_2O_3, 14% CeO_2-doped Ni/Al_2O_3 provided significantly higher reforming reactivity and resistance toward carbon deposition. These enhancements were mainly due to the influence of the redox properties of doped ceria. Although by increasing the ceria content the amount of carbon formation decreased, Ni was easily oxidized when more than 16% of ceria was doped as presented in Table 2.5. Another effect of increasing the ceria content was the increase in the redox properties and the oxygen storage capacity (OSC) as shown by their temperature programmed reduction experiments.

Table 2.5: Change in hydrogen production % and carbon formation with the increase in CeO_2 content (Laosiripojana et al., 2006)

Catalyst	Yield of H_2 production (%) at steady state	C formation[b] (monolayers)
Ni/Al_2O_3	15.2	4.85
2%Ce-Ni/Al_2O_3	25.1	4.28
4%Ce-Ni/Al_2O_3	36.9	4.04
6%Ce-Ni/Al_2O_3	46.2	3.21
8%Ce-Ni/Al_2O_3	60.8	3.09
10%Ce-Ni/Al_2O_3	66.6	2.76
12%Ce-Ni/Al_2O_3	71.8	1.98
14%Ce-Ni/Al_2O_3	74.5	1.07
16%Ce-Ni/Al_2O_3	72.1	1.06
18%Ce-Ni/Al_2O_3	64.3	1.02
20%Ce-Ni/Al_2O_3	49.4	1.11

Early studies done on methane reforming showed that the addition of lanthanide elements can improve the activity of Ni-based catalysts. In 1991 Zhuang et al. found that carbon deposition rate can be decreased in methane steam reforming by promoting the nickel catalysts with cerium oxide. They suggested that the reaction of steam with adsorbed species on the nickel surface, thus decreasing the carbon deposition as well as increasing or maintaining the catalytic activity, was increased by the promoter. Su and Guo (1999) also found that Ni sintering of Ni/Al_2O_3 catalysts can be reduced by doping the catalyst with rare earth oxides in methane steam reforming. The role of these promoters was to suppress the growth of Ni particles and the formation of inactive NiO and $NiAl_2O_4$ phases. Moreover, the oxides of heavy rare earth elements (Gd, Er, Dy) exhibited more effect than those of the light ones (La, Pr, Nd). Cheng et al. (1996) studied the effect of impregnation order of nickel and lanthanides during the preparation of the promoted catalyst. Although impregnating lanthanides prior to nickel did not affect the reforming activity to a large extent, an enhanced reducibility of nickel and a decrease in nickel particle size were observed. These and other promising results drove Natesakhawat et al. in 2005 to study the effect of lanthanide elements (La, Ce, and Yb)

on the catalytic behaviour of sol–gel Ni/Al_2O_3 catalysts in propane steam reforming. Comparing the three promoters, they found that 20% Ni–2% Ce/Al_2O_3 had the best effect in terms of enhancing the catalyst reducibility as their characterization results suggested that positive effects of the lanthanide promoters were due to easier reduction of nickel species to a metallic state and larger nickel surface area.

Although a number of researchers suggested doping Ni catalysts with other metals to improve their performance, until recently, studies were still conducted to improve the stability of Ni catalyst without the addition of any promoters. In 2009 Zhang et al. compared the activity and stability of a conventionally impregnation prepared Ni/Al_2O_3 catalyst with a one step sol-gel prepared one for propane steam reforming. They found that preparing the catalyst with the sol-gel method increased H_2 yields and suppressed carbon diffusion in Ni particles.

Precious Metals Based Catalysts

Precious metals based catalysts have been reported to be more effective catalysts for hydrocarbon reforming by preventing carbon deposition and having a high sulphur tolerance; so they are proposed to replace conventional based metal catalysts in fuel cell applications. As mentioned earlier in the chapter, due to the presence of steam, hydrocarbons and carbon monoxide in the automotive combustion off-gas, valuable information about noble metal catalyst performance was gained from the extensive work performed on automotive three-way catalysts (TWC). In 1977 Gandhi et al. tested steam reforming activity of various noble metals for a mixture of propene and propane. At that time their work was for TWC and therefore, the concentration of propane and propene were around 1500 ppm. At a temperature of 450°C they ranked the noble metals:

Rh, Ir> Pt> Co> Ru> Ni,Re

Another work on industrial hydrogen production by Rostrup-Nielsen in 1973 showed the following ranking for alumina and magnesia based catalysts:

Rh; Ru> Ni; Pd; Pt> Re> Co

Much later (1999), authors from the same group stated that Group VIII metals (rhodium, ruthenium) are one order of magnitude more active in steam reforming than platinum and nickel. A rationalization of the higher activity of rhodium in steam reforming compared to platinum catalysts was given by Schmidt and Huff in 1994. They expected this higher activity because of the reformation of adsorbed hydroxyl groups from adsorbed hydrogen and oxygen, the latter supplied by the support to the noble metal has a slower rate on rhodium.

An important oxide used in steam reforming as a promoter or as a support with noble metals is ceria. It is known to stabilize both the alumina support and the noble metal dispersion. Additionally, ceria reduces coke formation by increased carbon gasification. Barbier et al. in 1993 tested different alumina based noble catalysts promoted with 12% CeO_2 at a temperature of 450°C for propane steam reforming. They came up with the following rank:

$Rh/Pt/CeO_2 > Rh/Pt > Rh/CeO_2 > Rh >> Pt/CeO_2 = Pt$

However, when the propane feed concentration was increased under almost the same conditions (T= 400°C), Engler et al. (1991) found that for both supports, alumina and ceria, platinum activity was higher than rhodium:

$Pt/CeO_2 > Pt/Al_2O_3 > Rh/CeO_2 > Rh/Al_2O_3$

As a noble metal from the same group (VIII B), palladium was also used as a steam reforming catalyst. In 2005 Resini et al. compared steam reforming of propane and propene on Pd-Cu/Al_2O_3 and $Ni/NiAl_2O_4$. They found that steam reforming of propane over the Pd catalyst was inhibited by site poisoning; therefore propene steam reforming was faster and more selective. Compared to the Ni catalysts, propane steam reforming over the Pd catalyst was worse than over the Ni catalyst.

An extensive study that investigated propane steam reforming with different noble metals (Rh, Pt and Pd), different loadings, different combinations of bimetallic noble metals and on two different supports (ceria and alumina) was accomplished by Kolb et al. in 2004. The group ran a couple of experiments in microchannel reactors. As their results show in Table 2.6, rhodium was the best candidate when considering selectivity and activity. The introduction of platinum as a second metal and CeO_2 as a support further improved the performance of the rhodium catalyst. Figure 2.1 illustrates their six hours stability test on the $Rh/Pt/CeO_2$ catalysts. At a steam-to-carbon ratio of 2.3 and a reaction temperature of 750°C, the catalyst showed full conversion at a turnover frequency of 63 (g H_2/g catalyst).

Table 2.6: Selectivity and selectivity ratio of the rhodium, platinum, palladium and Rh/Pt catalyst samples at 550°C reaction temperature. (Kolb et al., 2004).

component	$Rh/\gamma\text{-}Al_2O_3$	$Pt/\gamma\text{-}Al_2O_3$	$Pd/\gamma\text{-}Al_2O_3$	$Rh/Pt/\gamma\text{-}Al_2O_3$
CO	30	5	80	62
CO_2	70	20	12	33
C_3H_6	0	70	5	3
CH_4	0	6	1	0
CO/CO_2	0.4	0.2	6.7	1.9

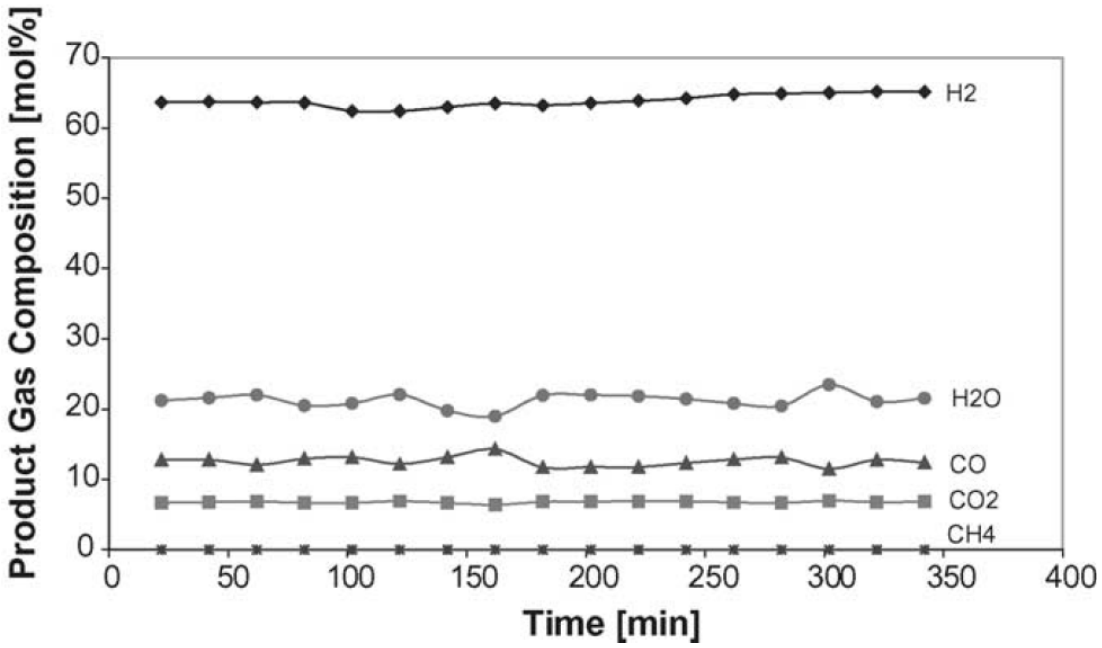

Figure 2.1: A six hour stability test on the Rh/Pt/CeO_2 catalysts at a steam-to-carbon ratio of 2.3 and a reaction temperature of 750°C (Kolb et al. in 2004).

2.1.2 Propane Oxidation

As a fuel used for heating in many applications for many years, propane oxidation has been extensively studied in the literature. However, in recent years partial oxidation of propane has been considered for the generation of H_2 from fossil fuels. In the presence of oxygen (air) propane can react to form a wide range of products and intermediates, depending on the propane/oxygen ratio in the feed. These reactions are:

Partial oxidation

$$C_3H_8 + 1.5\ O_2 \longrightarrow 3CO + 4H_2 \qquad (2.15)$$

Total oxidation

$$C_3H_8 + 5O_2 \longrightarrow 3CO_2 + 4H_2O \qquad (2.16)$$

Oxidative dehydrogenation

$$C_3H_8 + 0.5\ O_2 \longrightarrow C_3H_6 + H_2O \qquad (2.17)$$

Thermal dehydrogenation

$$C_3H_8 \longrightarrow C_3H_6 + H_2 \quad (2.18)$$

Cracking to ethylene and methane

$$C_3H_8 \longrightarrow C_2H_4 + CH_4 \quad (2.19)$$

In 1994 Huff et al. studied the production of synthesis gas from partial oxidation of propane. The study considered not only the partial oxidation reaction but also the other reactions taking place (those shown above). They used a catalytic monolith configuration with α/Al_2O_3 foam monolith disks and Pt, Rh and Pd. For a 4.3% Pt catalyst they found that below 4% propane in air the products were primarily CO_2 and H_2O as described by equation 2.16. As this percentage increases to 12 % the partial oxidation reaction (2.17) also takes place forming H_2 and CO, above that percentage ethylene begins to form by the cracking reaction (2.19). For the Rh catalyst under the same experimental conditions the only product was syngas meanwhile for Pd carbon deposition was a problem. The same results when comparing Rh/Al_2O_3 and Pt/Al_2O_3 catalysts in annular reactors were achieved by Beretta and Forzatti in 2004. They found that the partial oxidation of ethane and propane led to large amounts of gas-phase olefinic products over Pt, whereas high selectivities to synthesis gas were found over Rh. Their mechanistic results suggest that these different behaviours could be due to the varying capability of Pt and Rh surface reactions in competition with homogeneous reactions.

In an attempt to improve the activity of Pd in propane oxidation reactions Zhou et al. (2002) used perovskite oxides as supports instead of the traditional alumina. They found that $Pd/LaFe_{0.8}Co_{0.2}O_3$ was more active than the Pd/Al_2O_3 catalyst in propane oxidation with higher conversions at lower temperatures.

Corbo and Migliardini (2007) compared the activity and stability of three catalysts for partial oxidation of methane and propane at 700°C for different space velocities. They found that the commercial 12 % $NiO\text{-}CaO/Al_2O_3$ catalyst had the highest H_2 production

compared to a Ni based catalyst modified with K_2O and a Pt-CeO_2 catalyst. However, the K_2O catalyst offered the best resistance to carbon deposition, while the Pt catalyst had the lowest light off temperature. Partial oxidation of propane over Pt /CeO_2 was also studied recently by Dadyburjor et al. (2011). Based on their experimental runs at different flow rates and catalyst lodgings they proposed the following independent set of reactions taking place over high surface area ceria at a loading of 0.02 g of the catalyst: partial oxidation, total oxidation, WGS reaction and dehydrogenation. At lower catalyst loading the WGS reaction is replaced by water formation.

2.1.3 Propane Oxidative Steam Reforming (OSR)

Propane OSR has gained a lot of attention in the last few years especially for hydrogen production in fuel cell applications. The relatively low temperature of the process leads to more energy conservation and expands the material selection range, lowering the design cost and complexity. Since the process is a combination of steam reforming and oxidation, all reactions associated with both process can take place depending on different reaction parameters including temperature, pressure, steam-to-carbon ratio and oxygen-to-carbon ratio. Upon screening the literature for work done on propane OSR, it was not surprising to find that although steam reforming and partial oxidation of propane have been extensively investigated, their distinguishable combined effect in the OSR process had not been investigated well and needs further research for efficient hydrogen production in especially small scale applications. Table 2.7 gives a summary of the work done on OSR of propane in the literature so far (note that the researches that considered propane to be a model for LPG reforming is going to be discussed in the LPG section).

Ramp et al. (2000) studied autothermal reforming of propane on a catalyst system which was a metal honeycomb structure coated with platinum. 30 to 40% of the fuel was oxidized by injecting air, releasing heat. This heat was required to convert the remaining fuel with steam to hydrogen, carbon monoxide and carbon dioxide by the endothermic steam reforming reaction. Their optimum reforming conditions were: 700°C, S/C= 1.0 and mol air $_{reaction}$/ mol air $_{stoichometric}$ (λ)=0.4. They also investigated the influence of air preheating, in which the air flow was mixed with water and this stream flowed together

over the vaporizer to the reformer; in the other case, the air was directly injected into the reformer. The preheated operation mode was favoured because the H_2 and CO mole content in the reformer product gas was higher. They concluded that higher inlet air temperature led to a higher temperature level in the reaction zone, which improved the kinetics of the reforming reaction.

In 2003 Ayabe et al. used a 10 % Ni/Al_2O_3 catalyst for autothermal reforming of propane to investigate carbon deposition of hydrocarbons higher than methane during OSR. Autothermal reforming was carried out at 800°C in a fixed bed reactor at an O_2/C ratio of 2 and S/C ratios ranging from 0 (dry conditions) to 1.5 (wet conditions). The conversion was kept at 100% but hydrogen concentrations were around 53%. After running the experiment without the catalyst and analyzing the results, they found that the conversion of propane was initiated by the decomposition into lower hydrocarbons at the inlet zone of the catalyst bed, and then the steam reforming of lower hydrocarbons proceeded in the rear zone of the catalyst bed. This explanation agreed well with results previously discussed by Ramp et al. (2000) in their metal honeycomb catalyst structure. Ayabe et al. (2003) also concluded that although methane autothermal reforming did not suffer from carbon deposition, use of propane always gave rise to carbon deposition even in regions expected to be deposition free from equilibrium calculations.

Table 2.7: work done on propane oxidative steam reforming

Author	Year	Fuel	Catalyst	Temp. °C	Reaction Ratios	Fuel Conv.%	Objectives
Rampe	2000	propane	A metal honeycomb coated with Pt	700	S/C=1 λ=0.4	NR	Investigate the efficiency of the propane autothermal reforming process and the hydrogen production rate.
Ayabe et al.	2003	propane Methane	10%Ni/Al_2O_3	800	S/C=0 -1.5 O_2/C = 2	100	To determine the general behavior of the autothermal reforming using supported metal catalysts with methane and propane fuel.
Aartun et al.	2004	propane	Rh/Al_3O_2 /Fecralloy microchannel reactor	500-1000	C/O_2 (including O_2 & H_2O oxygen)= 0.5 S/O_2= 2	100 at 1000oC	Study small-scale hydrogen production by partial oxidation and oxidative steam reforming of propane in microstructured reactors.
Silberova et al.	2005	propane	0.01% Rh/Al_2O_3 foam	700	C/O_2 (including O_2 & H_2O oxygen)= 0.5 S/O_2= 2	100	Study Rh-impregnated alumina foams for PO and OSR of propane as potential high-throughput, structured catalysts for hydrogen or synthesis gas production.
Lee et al.	2006	propane	Ni/δ-Al_2O_3 promoted with: Co, CeO_2, MgO and La_2O_3	400-700	S/C = 3 O_2/C =0.4	100	H_2 production by OSR of propane over a water-alcohol Ni catalyst promoted with different metals
Lim et al.	2007	propane	Ni/MgAl promoted with Pt, Pd, Ce, Sr, Ba and Ca	300-700	S/C =3 O_2/C = 0.37	100	H_2 production by OSR of propane over a hydrotalcite-like Ni/MgAl catalyst promoted with different metals
Pino et al.	2008	propane	$Ce_{0.95}Ni_{0.05}O_2$ & $Ce_{0.90}Ni_{0.10}O_2$	650	S/C = 1.2 O_2/C = 1.3	100	Evaluation of the performance of a CeNiO2 catalyst prepared with a combustion synthesis method for propane OSR
Faria et al.	2008 2009	propane	Pd/Al_2O_3 and Pd/$CeO_2Al_2O_3$	500-800	S/C = 6 O_2/C = 0.83	100	Investigate the effect of O2/C ratio on the activity and product distribution of the catalyst and in-situ characterization of the catalyst
Lee et al.	2009	propane	Ni/MgAl promoted with Pt, Pd and Ru	300-700	S/C=3 O_2/C= 0.37	100	H_2 production by OSR of propane over a hydrotalcite-like Ni/MgAl catalyst promoted with three noble metals
Li et al.	2009	propane	Ru –doped Ni/Mg(Al)O	700-600	S/C=2 O_2/C= 0.5	95-100	Testing the catalyst stability under daily start-up and shut-down conditions
Park et al.	2010	propane	Ni/MgAl promoted with Fe, Pd and Ru	300-700	S/C =3 O_2/C = 0.37	100	Comparing hydrotalcite-like Ni/MgAl based catalysts prepared with different solvents for propane OSR
Faro et al.	2010	propane	A composite Ni-La-$Ce_{0.8}Gd_{0.2}O_2$	600-800	S/C = 2.5 O_2/C = 0.5	100	Develop a low cost catalyst for direct utilization in SOFC of propane with high stability and activity at intermediate temperatures
Álvarez-Galván et al.	2011	propane	$LaCoO_3$ and Ru/$LaCoO_3$	750	S/C = 3 O_2/C = 0.5	NR	Compare the differences in surface reactivity of $LaCoO_3$ and Ru/$LaCoO_3$ solids after pre-treatment in a hydrogen or oxygen gas atmosphere towards oxidative steam reforming (OSR) of propane

Holman et al. (2004 and 2005) investigated hydrogen production from propane by partial oxidation (PO) and oxidative steam reforming (OSR) in short contact time reactors. In 2004 the group investigated propane PO and OSR in a microstructure reactor. The reactor was a Fecralloy metal alloy made of 72.6% Fe, 22% Cr and 4.8% Al. In order to achieve a porous layer of α-Al_2O_3 on the surface, the reactor was first oxidized at high temperature and subsequently impregnated with Rh. Their results showed that the OSR of propane in the Rh/Al_2O_3/Fecralloy reactor give the highest hydrogen yields compared to the Ni/Al_2O_3/Fecralloy and Rh reactors. Methane and ethane by-products were only detected at high temperatures. The catalyst was characterized using different techniques including XRD, SEM/EDX and XPS. Catalyst characterizations confirmed the presence of Rh in a metallic phase, while Ni was present in both metallic and oxide phases. Deactivation including coke formation was not observed for the Rh/Al_2O_3/Fecralloy system under the conditions applied. Results from Ni/Al_2O_3/Fecralloy are more ambiguous, and it appears that sintering, oxidation of Ni or possibly loss of material have occurred in this system.

Holmen et al. (2005) then studied the same two reactions (PO & OSR) but this time over 0.01 % Rh-impregnated alumina foams in a short contact time regime. After determining the optimum operational temperature of 700°C, they investigated the effect of residence time on the product distribution during both PO and OSR. The production of hydrogen was hardly affected by the residence time, but an influence on the selectivity to all other products was observed. Hydrocarbon by-products were increasingly formed at shorter residence times while formation of partial and complete oxidation products increased with longer residence times. An interesting study that they also made was on the variation in the pressure difference usually applied for sampling from the product stream. As they show in Figure 2.2 this pressure difference had small effects on product distribution with a minor increase in propane conversion.

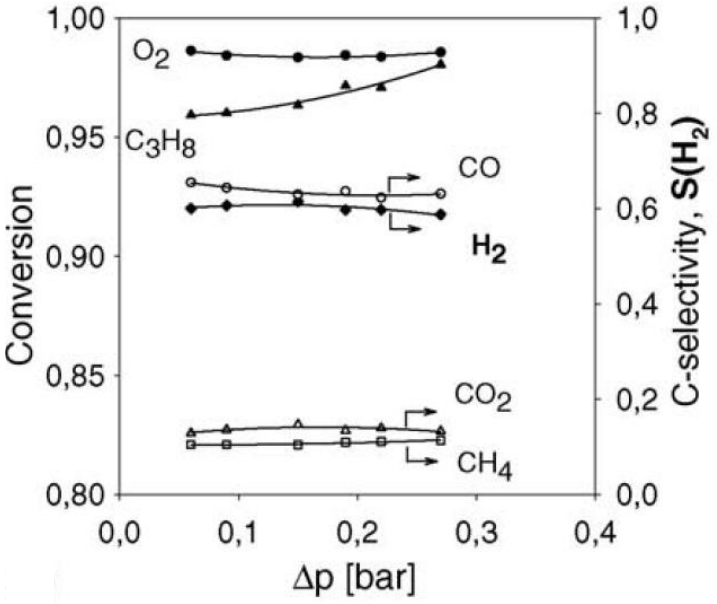

Figure 2.2: Sampling pressure difference effect during OSR of propane over 0.01% Rh/Al_2O_3 foam. (Holmen et al., 2005)

Later in 2005 the same group (Holmen et al., 2005) published an article comparing two types of short contact time reactors (alumina foams and metallic microchannel reactors) impregnated with Rh for PO and OSR of propane. Temperature profiles obtained along the catalyst/reactor axis under comparable conditions showed that the gradients are smaller in the Rh/Al_2O_3/Fecralloy microchannel reactors than in the Rh/Al_2O_3 foams. The Rh/Al_2O_3 foams showed higher initial activity and syngas selectivity than the Rh/Al_2O_3/Fecralloy microchannel monolith, resulting in a product composition closer to equilibrium. The group also investigated formation of byproducts, especially methane and ethane as cracking products. These homogenous gas phase reactions took place within the region near the entrance of the Rh/Al_2O_3 foams, while in the microchannel monolith system, gas phase reactions appear to be suppressed and by-product formation was very low.

Another group that studied propane OSR extensively was by Park et al. from 2006 to 2010. This group examined different combinations of Ni based catalysts. In 2006 they

prepared a Ni/δ-Al_2O_3 catalyst by a water-alcohol method and found that it was more active and had higher H_2 yields than the regular impregnated one. Then they promoted the water-alcohol catalyst with different metals and oxides, including Co, Ce, Mg and La. The highest H_2 production was achieved on a Ni-Co-CeO_2/Al_2O_3 catalyst. Later in 2007 they began using Ni/ Mg-Al hydrotalcite-like catalyst. They used co-precipitation to add different metals to the catalyst including, Ce, Sr, Ba and Ca. They found that except for Ca the addition of the three metals enhanced the H_2 yield at temperatures below 450°C. However, at temperatures higher than 600°C the Ni/Mg-Al catalyst had higher H_2 yields. In 2009 they used three noble metals (Pt, Pd and Ru) to promote the same Ni/Mg-Al catalyst; all three noble metals decreased the catalyst light off temperature with Pt having the highest H_2 yield. They continued their work in 2010 by comparing the activity and carbon resistance of the Ru and Pd catalysts prepared with different solvents. In agreement with their previous study in 2006 they found that catalysts prepared with alcohol and water as solvents had higher H_2 yields than those prepared with water only.

2.2 Butane Reforming

Cost considerations make butane an attractive hydrocarbon fuel for different applications. It is easily stored and can be found in remote sites where battery power is expensive. However, because of its relatively high content of carbon compared to lower hydrocarbons, a major concern when discussing any butane reforming reaction is carbon deposition or coking. Considering this issue, compared to propane reforming, work done on butane reforming is covered to a lesser extent in the literature and reported data are scarce.

2.2.1 Butane Steam Reforming

Hydrogen can be produced from butane by the well-known steam reforming reaction according to equation 2.3:

$$n\text{-}C_4H_{10} + 4H_2O = 4CO + 9H_2 \qquad (2.3)$$

$$\Delta H°(298K) = +649.9 \text{ kJ/mol}$$

As stated before, carbon deposition on the catalyst (especially Ni-based catalysts) is a common problem associated with butane steam reforming. Therefore, approximately half of the work presented in the literature on butane steam reforming is directed at overcoming this restriction. For this purpose different approaches were investigated, mainly introducing different promoters to existing catalysts or using noble metal based catalysts. Table 2.8 gives an overview of the current state of the butane reforming in the open literature.

Borowiecki et al. (2000-2004) worked for several years on improving Ni- based catalysts activity and coking resistance in butane steam reforming by the addition of different promoters. In 2000 they studied the effect of adding small amounts of Mo to Ni/Al_2O_3 catalyst on butane steam reforming. As shown in Figure 2.3, the addition of Mo improved the catalyst resistance to coking by decreasing the rate of coking. Although the morphology of both catalysts were the same, on the $Ni–Mo/Al_2O_3$ catalyst much lower numbers of Ni particles were observed that were active toward carbon filament growth.

In 2004 the Borowiecki et al. group investigated the influence of adding different amounts of potassium to a Ni/Al_2O_3 catalyst. The method of its addition on physico-chemical and kinetic properties as well as on resistance to coking was also determined. Although the addition of potassium increased the resistance of the catalysts to coking it decreased its activity. However, addition of potassium in amounts not greater than 1 wt.% K_2O caused a decrease in activity not higher than 20 %.

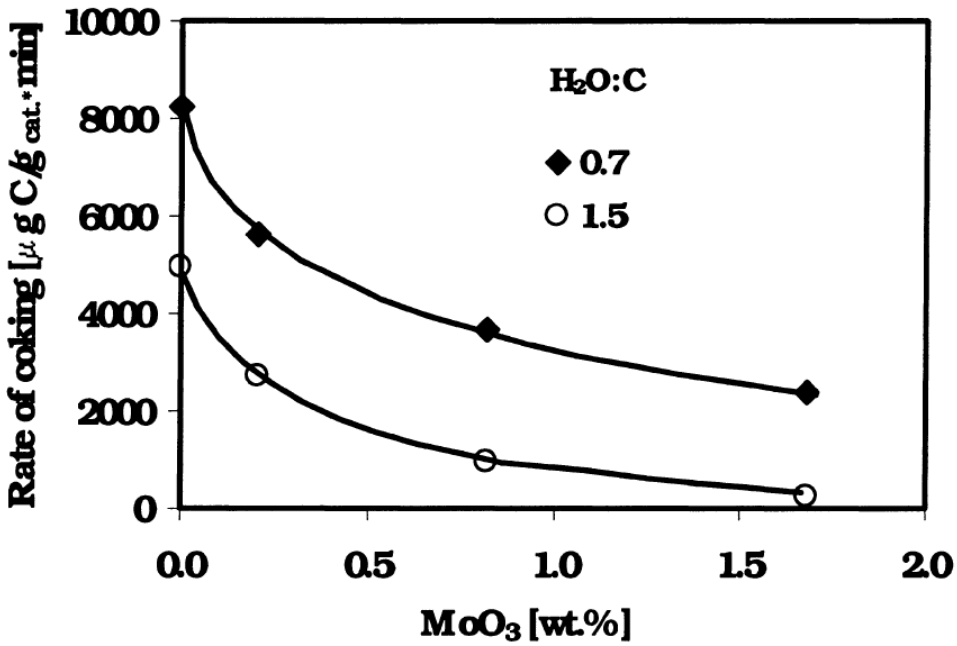

Figure 2.3: Effect of the promoter amount on the coking rate of the catalyst in the steam reforming of *n*-butane. Borowiecki et al. (2000).

In general, precious metals are more resistant to coking than Ni, and therefore they are expected to be able to function under more severe conditions. As a result some works have been done in butane steam reforming over precious metal catalysts, essentially Pd and Pt based catalysts. In 2001, Wang and Gorte examined butane steam reforming on ceria, 1 wt% Pd/ceria, 1 wt% Pd/alumina, and 15 wt% Ni/silica. No rates could be obtained for Ni/silica because of rapid coking. Under the same conditions, the three other catalysts were much more stable, with 1 wt% Pd/ceria having the best activity. They later (in 2002) compared butane steam reforming on three different catalysts, Pd/ceria, Pd/alumina and Pt/ceria with the aim to study the effect of different supports. The two ceria supported catalysts had similar activities but had better activities than the Pd/alumina catalyst.

Table 2.8 An overview on the work done on butane reforming in the literature

Author	Year	Fuel	Catalyst	Temp. °C	Reaction Ratios	Fuel Conv.%	Objectives
Kendall & Williams	1998	n-butane	Ceria, Ni, Pt, Ru	600-850	[a]PO C:air= 1:10 And 1:5	40-100	Find a catalyst capable of favoring the production of syngas from butane in zirconia fuel cells .
Finnerty et al.	2000	n-butane & methane	5% Ru-doped	600-900	PO O:C=4.5	[e]NR	Define catalyst compositions, which would allow integration of the pre-reforming, fuel cell operation and total oxidation at the exhaust, while generating power from the SOFCs.
Kepinski et al.	2000	n-butane	Ni/Al_2O_3 & $Ni-Mo/Al_2O_3$	500	[b]SR S/C=0.7 & 1.5	NR	Use of the HRTEM method to determine the effect of small amounts of molybdenum promoter on the morphology of deposits formed on Ni and Ni–Mo catalysts used in SR of n-butane
Wang and Gorte	2001	n-butane	Pd/ceria, Ni/silica Pd/alumina	300-600	SR (1) and (2)	10 Diff. condi.	Study steam reforming of *n*-butane on Pd/ceria
Borowiecki et al.	2002	n-butane	Ni/Al_2O_3 & $Ni-Mo/Al_2O_3$	640	SR (0.4-2.0)	NR	Determine quantitatively the effect of temperature and reagent ratio on the initiation of the coking process.
Wang and Gorte	2002	ethane,*n*-butane, *n*-hexane, *n*-octane, 2,4-dimethylhexane, cyclohexane, benzene, and toluene	1 wt.% Pd/ceria 1 wt.%Pd/alumina 1 wt.% Pt/ceria.	347-497	SR (1:1)-(3:1)	NR	Investigate the effect of hydrocarbon size and structure on steam reforming reactions by examining rates, selectivities, and reaction stabilities for linear alkanes from methane to *n*-octane and for aromatics and a branched alkane and to examine the effect of replacing Pd with Pt catalysts.
Costa-Nunes et al.	2003	n-butane	Pd/ceria Pt/ceria	700	PO and [c]TO	70	Study direct-conversion SOFC with *n*-Butane at higher fuel utilization
Borowiecki et al.	2004	n-butane & methane	$Ni-K/Al_2O_3$ Ni/Al_2O_3-K	600-800	SR S/C = 0.33-3.0	NR	To study the influence of potassium amount in a commercial nickel catalyst and the way of its addition affects physico-chemical and kinetic properties as well as on resistance to coking.
Avci et al.	2004	Butane	15% Ni/Al_2O_3 0.2%Pt-15%Ni/Al_2O_3	305-405	SR S/C=3	100	Study hydrogen production by steam reforming of *n*-butane over supported Ni and Pt-Ni catalysts
Nagaoka et al	2007	Butane	Ni over:SiO_2, TiO_2, Al_2O_3, ZrO_2 and MgO	450	[d]OSR, S/C = 1 O_2/C = 0.5	60-100	Compare the activity and stability of Ni over different supports before and after oxidation treatment to simulate startup and shutdown conditions in fuel cell applications
Sago et al.	2009	Butane	$Ni/Zr_{0.5}Ti_{0.5}O_2$-SiO_2	450	[d]OSR, S/C = 1 O_2/C = 0.5	50-90	Study the effect of a composite oxide support $Zr_{0.5}Ti_{0.5}O_2$, in which they impregnated Ni, and compare its activity and stability to Ni/TiO_2 and Ni/ZrO_2 catalysts
Seyed-Reihani and Jackson	2010	Butane	Rh/γ-Al_2O_3 coated foam monolith	300-450	PO O_2/C = 1	50-85	Study the effect of reactor length on operating conditions and heat loss in butane PO
Jeong and Kang	2010	Butane	Ni(9)/Ag(1)/$MgAl_2O_4$	700	SR S/C = 1	100	Study the effect of adding Ag to Ni-$MgAl_2O_4$ to resist sintering between Ni and Al during butane SR.
Sato et al.	2010	Butane	Ni/MgO	450	[d]OSR, S/C = 1 O_2/C = 0.5	30-100	Study the effect of pH preparation solution on the activity of the catalyst
Ferrandon et al.	2010	Butane	Ni and Rh monometallic and bimetallic over La-Al_2O_3, $CeZrO_2$ and $CeMgO_x$	700	SR S/C = 3 OSR S/C = 2 O_2/C = 0.5	NR	Investigate synergistic effects that occur between nickel and rhodium in butane SR and OSR. To compare the ability of reducible supports to resist coking to that of refractory supports such as La-Al_2O_3.

[a] PO: partial oxidation, [b] SR: steam reforming, [c] TO: total oxidation, [d] OSR: oxidative steam reforming, [e] NR: not reported

In a step aimed at combining the high production yields of Ni catalysts with high coking resistance of noble metal catalysts, Avci et al. (2004) compared steam reforming of butane on Ni/Al_2O_3 and a $Pt\text{-}Ni/Al_2O_3$ bimetallic catalyst. The bimetallic catalyst showed better performance in terms of selective hydrogen production which resulted in lower carbon dioxide and methane formation (see Table 2.9). The activity of both catalysts increased with temperature, however, at 405°C, complete *n*-butane conversion was achieved over the bimetallic catalyst while only 67% conversion was obtained over the Ni catalyst.

Table 2.9: Rate of production of species formed at different temperatures during steam reforming of *n*-butane over $15\%Ni/Al_2O_3$ and $0.2\%Pt\text{-}15\%Ni/Al_2O_3$ catalysts. (Avci et al., 2004)

T (K)	Production rate $\times 10^3$ (mol/(kg cat·s)							
	$15\%Ni/\delta\text{-}Al_2O_3$				$0.2\%Pt\text{-}15\%Ni/\delta\text{-}Al_2O_3$			
	CO	CO_2	CH_4	H_2	CO	CO_2	CH_4	H_2
578	0	0.8	0.6	2.7	0	1.1	0.5	4.0
598	0	2.0	0.9	7.7	0	1.4	0.7	6.2
648	0	3.0	1.4	11.0	0	2.4	0.8	10.3
678	1.1	9.9	16.6	23.0	1.1	9.9	24.8	24.3

Studies on OSR of butane for H_2 production are very rare in the literature. A group that covered this aspect began their work in 2007 by investigating butane OSR at 450°C, S/C = 1 and O_2/C = 0.5 over five different Ni supported catalysts. Nagaoka et al. compared the activity and stability of Ni over SiO_2, TiO_2, Al_2O_3, ZrO_2 and MgO, before and after oxidation treatment to simulate start-up and shutdown conditions in fuel cell applications. They found that before oxidation the Al_2O_3 and MgO catalysts had the best activity and stability with high resistance to coking compared to the other supports. However, after the oxidation treatment the Ni/Al_2O_3 catalyst was non active, while the

Ni/MgO catalyst sustained a 60% conversion for the whole 15 hr run. In 2009 (sago et al.) they developed a composite oxide support $Zr_{0.5}Ti_{0.5}O_2$, on which they impregnated Ni and compared its activity and stability to those of Ni/TiO_2 and Ni/ZrO_2 catalysts. The composite catalyst was indeed more active than the other two other catalysts, however, it suffered from high carbon depositions. In order to reduce carbon depositions they added SiO_2 to the support. High SiO_2 loadings had negative effects on the fuel conversion; however, lower amounts of SiO_2 did sustain the activity of the catalyst while preventing carbon deposition. In the following year (2010) they (Sato et al.) went back to study butane OSR over the Ni/MgO catalyst prepared at two pH levels; 7 and 3.5. Under the same operational conditions specified in their first study in 2007 they found that H_2 production from the Ni/MgO catalyst prepared at pH 7 was 2.3 times higher than that of the one prepared at the lower pH.

2.2.2 Butane Oxidation

Hydrogen can also be produced from butane by partial oxidation. However, the reaction of butane with oxygen can give different products depending on the reaction conditions; primarily the fuel-to-oxygen ratio. The following reactions can take place during butane oxidation:

Partial oxidation

$$C_4H_{10} + 2O_2 \longrightarrow 4CO + 5H_2 \qquad (2.12)$$

Total oxidation

$$C_4H_{10} + 6.5O_2 \longrightarrow 4CO_2 + 5H_2O \qquad (2.13)$$

Oxidative dehydrogenation

$$C_4H_{10} + 0.5\ O_2 \longrightarrow C_4H_8 + H_2O \qquad (2.20)$$

Thermal dehydrogenation

$$C_4H_{10} \longrightarrow C_4H_8 + H_2 \qquad (2.21)$$

Oxidative cracking

$$C_4H_{10} + 0.5\ O_2 \longrightarrow 2C_2H_4 + H_2O \quad (2.22)$$

Thermal cracking to ethylene and ethane

$$C_4H_{10} \longrightarrow C_2H_4 + C_2H_6 \quad (2.23)$$

Thermal cracking to propylene and methane

$$C_4H_{10} \longrightarrow C_3H_6 + CH_4 \quad (2.24)$$

Early investigations on butane oxidation were related to studying hydrocarbon autoignition in relation to combustion engine knocking. Different mechanisms were developed to study the modeling of the oxidation reactions. Another wide range of applications for butane oxidation is the production of maleic anhydride. Maleic anhydride was traditionally manufactured by the oxidation of benzene or other aromatic compounds (Eq. 2.25). Due to rising benzene prices, most maleic anhydride plants now use n-butane as a feedstock:

$$CH_3CH_2CH_2CH_3 + 3.5\ O_2 \rightarrow C_2H_2(CO)_2O + 4\ H_2O \quad (2.25)$$

Therefore, a lot of work in the literature has been done on this topic.

Some of the literature work that dealt with butane PO as an individual process to some extent is presented in Table 2.8 (together with the work done on butane steam reforming).

2.3 Reforming of Liquefied Petroleum Gas (LPG)

Liquefied Petroleum Gas (LPG) is often incorrectly identified as propane. In fact, LPG is a mixture of petroleum gases that exist in a liquid state at ambient temperatures under moderate pressures (less than 1.5 MPa or 200 psi). The common interchanging of the two terms is explained by the fact that in the U.S. and Canada LPG consists primarily of propane. In many countries around the world, however, the propane content in LPG can

be as low as 10%. LPG is composed primarily of propane and butane along with other hydrocarbons (such as pentane, propylene, iso-butane, butylenes and ethylene).

As early as 1860, LPG was used as a portable fuel source for heating, cooking and some times for lighting in rural areas. However, the extensive use of LPG did not develop until the 1940's through the 1960's. Transport LPG is delivered to the consumer as a liquid in cylinders of various sizes, weighing from 1 pound to 1,000 pounds and maintained under relatively low pressures of about 100 psi. (HEARTH Gas Appliance Training Manual, 1997).

A recent application of LPG is in powering automotive vehicles. Over 4 million LPG vehicles are in operation in about 30 countries, such as Japan, the Netherlands, Australia, Austria, and Italy, and with proven safety records (Demirbas, 2002). LPG is an attractive fuel for internal-combustion engines for many reasons. It burns with little air pollution and little solid residue. In fact, switching to LPG fuel in combustion engines can reduce CO emissions in half and decrease NOx emissions by 25 % (Demirbas, 2002). Table 2.10 shows typical emissions from an LPG engine.

Table 2.10: Emissions from the LPG Engine (Net Technologies Inc., 2005)

CO volume %	HC ppm	NOx vppm
0.2-2	50-750	250-2000

Since LPG burns cleaner than gasoline with less carbon build-up and oil contamination, engine wear is reduced and the life of some components such as rings and bearings is much longer than with gasoline engines. Compared to gasoline which has an octane number ranging between 84 and 97, LPG has an average octane number of 104 (Demirbas, 2002). This higher octane number minimizes wear caused by engine knock. Although LPG has a lower energy density than gasoline that results in fewer miles per gallon, its higher octane number allows higher compression ratios and therefore, higher power and fuel efficiency.

2.3.1 LPG Properties and Compositions

As a vapor, LPG is colorless, odorless and heavier than air, it does not disperse easily without wind or ventilation. Although sometimes an odorant is added to aid detection of LPG presence, shops servicing LPG vehicles must be ventilated to minimize the risk of asphyxiation and explosions and underground parking garages should not permit parking of LPG fuelled vehicles in their premises. Depending on its composition LPG has a boiling point ranging from -44 to 0°C. Compared to gasoline and diesel having ignition temperatures of 260 and 316°C respectively, LPG has a higher ignition temperature of 482°C. In air, LPG is flammable in concentrations between 2 and 10 %.

The major sources of commercial LPG are natural gas processing and petroleum refining. Raw natural gas often contains excess propane and butane, which must be removed to prevent their condensation in high-pressure pipelines. In petroleum refining, LPG is collected during distillation, from lighter compounds dissolved in the crude oil, as well as generated in the cracking of heavy hydrocarbons. Therefore, LPG can be considered a by-product and its exact composition and properties will vary greatly with the source. The variations in LPG composition can be seen when looking at the composition of the two major components (propane and butane) of LPG worldwide (see Table 2.11).

Table 2.11: compositions of the two major components (propane and butane) of LPG worldwide.

Country (organization)	Propane %	Butane %
Austria	50	50
Belgium	50	50
Denmark	50	50
France	35	65
Greece	20	80
Ireland	100	-
Italy	25	75
Netherlands	50	50
Spain	30	70
Sweden	95	5
United Kingdom	100	-
Germany	90	10
U.S. (HD-5 standard)	85	2.5
Malaysia (GAS Malaysia)	40	60
Thailand (PTT Co.)	60	40
North China (Platts, refinery grade)	30	70
South China (Platts, import grade)	10	90
Australia (Australian LPG Asso.)	40	60
New Zealand (Taranaki Basin gas fields)	60	40

2.3.2 Hydrogen Production from LPG Reforming

In light of the above considerations, LPG is found to be a cleaner and more efficient fuel to be used directly in internal combustion engines. This will definitely require a slight change in the design and operational conditions of the engine. However, attention is focused more and more on developing hydrogen fuel cells as alternative energy conversion devices. And in the absence of a hydrogen refuelling structure and problems related to hydrogen storage, LPG is considered as a promising fuel for on board fuel processors to produce hydrogen rich reformate gases. With its well established

distribution network and safe storage methods, this gas is also proposed to be an attractive fuel for systems in remote areas where natural gas pipeline is not available. LPG can also be used for auxiliary power units (APU). The last two examples would be particularly suitable for solid oxide fuel cells (SOFCs).

As a mixture composed mainly of propane and butane, understanding and investigating the different reforming processes of these two gases individually are basic steps in developing LPG reforming processes. Therefore, all possible reactions considered for propane and butane; steam reforming, partial oxidation and oxidative steam reforming in previous chapters are thought to be involved in LPG reforming. However, looking at the mixture in an integrated reforming process might be a different story. In addition, as discussed in the previous section, the wide range of LPG propane and butane mixtures increases the challenge of coming up with a reforming process that accommodates this wide range of compositions. In fact, each part or factor in the reforming process (feed, catalyst, operation conditions, reactor design, etc.) should be investigated individually.

Although the reforming of propane and butane has been investigated to some extent in the literature as seen in previous sections, not enough attention has been given to LPG reforming. In addition, among these scattered works on LPG reforming in the literature, some of these studies considered pure propane to be a model for LPG which really does not represent the actual LPG compositions worldwide as stated before.

Recupero et al. (2005) studied the autothermal reforming of propane on 1% Pt/CeO_2. Their study was the first step of a project oriented for the development of a compact and reliable fuel processor, fed by LPG, to be used in a PEFC vehicle. This group studied the effects of O_2/C and S/C ratios on both the conversion of propane and the product distribution as shown in Figures 2.4 and 2.5. They also found that their catalyst was stable under the specified conditions for 100 h, sustaining an experimental hydrogen yield of 74 %.

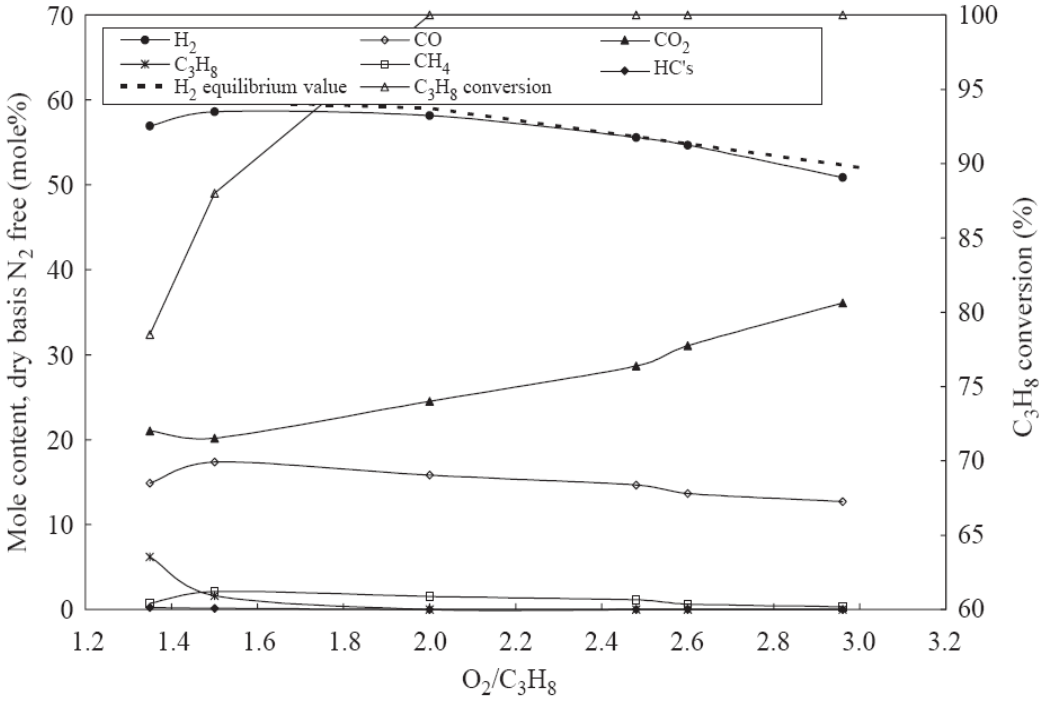

Figure 2.4: Product gas compositions (dry basis, N_2 free) and conversion from the autothermal reforming of propane as a function of the O_2/C_3H_8 molar ratio at 600°C, GHSV = 10 000 h^{-1} with H_2O/C_3H_8 = 3.6; (Dashed line = thermodynamic H_2 value). Recupero et al. (2005).

Another study on propane reforming as a pre-step for LPG reforming was the research of Caglayan et al. in 2005. This group investigated the production of hydrogen over bimetallic 0.2%Pt–15%Ni/δ-Al_2O_3 catalyst by OSR of propane. Their main objective was to show the advantages of using a bimetallic catalyst over monometallic in OSR of propane. Their results showed that the Pt–Ni bimetallic system has superior performance characteristics compared to the monometallic catalysts reported in literature. As they explained via Figure 2.6, this higher performance obtained over Pt–Ni at lower temperatures compared to those obtained from monometallic Ni catalysts are thought to result from the enhanced heat transfer occurring in the bimetallic catalyst, from Pt sites catalyzing the exothermic oxidation reactions to Ni sites catalyzing the endothermic SR reaction. During this process, the catalyst acts as a micro heat exchanger.

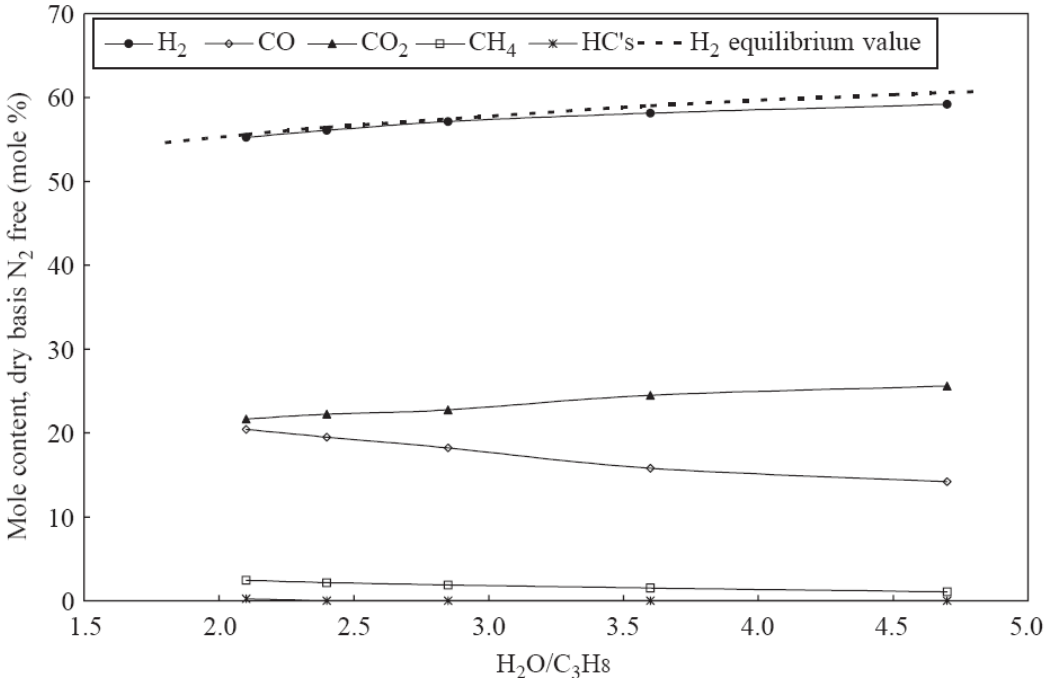

Figure 2.5: Product gas compositions (dry basis, N_2 free) from the autothermal reforming of propane as a function of the H_2O/C_3H_8 ratio, carried out at T = 600°C, GHSV = 10 000 h^{-1} and O_2/C_3H_8 = 2; (Dashed line = thermodynamic H_2 value). Recupero et al. (2005).

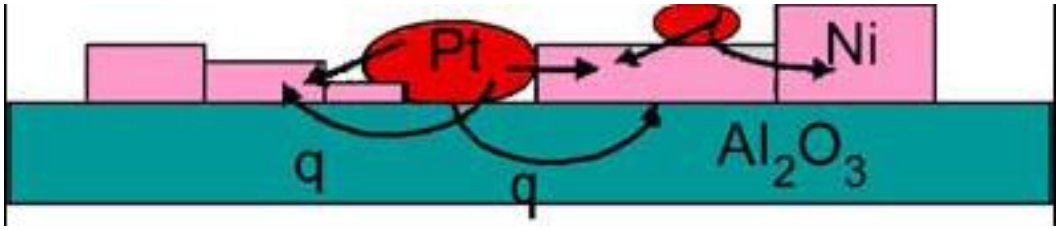

Figure 2.6: Catalyst surface acting as a micro heat exchanger transferring heat from the oxidation reactions favorable on Pt to the steam reforming reactions favorable on Ni. (Caglayan et al., 2005)

This group also studied different reaction conditions including temperature, S/C and C/O_2 ratios and resident time. The optimal conditions were found as S/C = 3, C/O_2 = 2.70 and resident time = 0.51 g_{cat} h/mol HC for OSR of propane on the basis of high hydrogen productivity and selectivity between 350 and 470°C for the experimental conditions tested. The catalyst stability was also tested and the catalyst was found to be very stable under the 12-h testing period. The same year (2005) the group (Caglayan et al., 2005) studied the OSR over the same catalyst for a 75:25 propane : butane mixture used as a model for LPG. They ran the same set of experiments under the same conditions, with only the S/C ratio increased to 5. When comparing the results of the mixture to pure propane LPG, they found that the presence of butane increased the amount of heat produced on Pt sites and hence, more heat was transferred to Ni for SR. This resulted in higher activity and H_2 yields for the butane propane LPG mixture. In 2008 (Gokaliler et al.) they repeated the same set of experiments for a 1:1 propane: butane mixture at three S/C ratios: 5, 6 and 7. They found that although, the presence of butane improved activity and selectivity, the catalysts was more exposed to deactivation by coking at the moderate S/C ratios, and sustained its stability only at the highest S/C ratio. They concluded their study by recommending further work to improve the stability of the Pt-Ni catalysts especially for butane-enriched LPG feeds.

Laosiripojana and Assabumrungrat (2006) also studied OSR of a 60:40 propane : butane LPG mixture over high surface area CeO_2, synthesized by a surfactant-assisted approach under solid oxide fuel cell (SOFC) operating conditions. In their study they covered a temperature range from 700 to 900°C, and studied the effect of different S/C and O_2/C ratios at 900°C on different reaction products. They found that at 900°C their suggested catalyst had excellent resistance toward carbon deposition compared to the conventional Ni/Al_2O_3 catalyst. They attributed this high resistance, to redox properties of CeO_2. They also suggested optimizing the O_2/C ratio, as they found that O_2/C ratios higher than 0.6 had a negative effect on H_2 selectivity.

In 2010, Laosiripojana et al. considered the same LPG mixture in their previous study for partial oxidation over a Ce-ZrO_2 catalyst doped with La, Sm, Gd and Nb at 850°C.

They found that doping the catalyst with La, Sm and Gd considerably improved catalytic reactivity, whereas Nb-doping reduced its reactivity. The high reactivity of the three elements was related to their oxygen storage capacity (OSC) with the La doped catalyst having the highest OSC and hence the best performance among the three.

Recently, they (Laosiripojana et al.) continued their work on the 60:40 propane: butane LPG mixture by comparing LPG steam reforming over Ni and Rh based catalysts over two supports; Gd-CeO_2 (CGO) and Al_2O_3 in a 750 to 900°C temperature range. The order of activity was found to be Rh/CGO> Ni/CGO = Rh/Al_2O_3 > Ni/Al_2O_3. They attributed the comparable activity of Ni/CGO to the precious metal Rh/Al_2O_3 catalyst to the occurring of gas–solid reactions between hydrocarbons and lattice oxygen on the CGO surface, along with the reactions taking place on the active site of Ni, which helps to prevent carbon depositions. In the same study the addition different amounts of O_2 and H_2 to the reaction feed was also investigated over the Ni/CGO catalyst at 900°C. For O_2 addition, the results were the same as their study in 2006; however, the addition of H_2 had a negative effect on the catalyst activity due to catalyst active site competition and the inhibition of gas–solid reactions between the gaseous hydrocarbon compounds and lattice oxygen on the surface of the CGO support.

2.4 Mechanistic Studies on LPG Reforming

With this very small amount of work done on LPG reforming, obviously there are no mechanistic studies on LPG (as a mixture) reforming reported in the literature. However, since propane and butane are the two main components in LPG, evaluating their reforming mechanisms should be an essential step in developing any model for LPG reforming. As a well-known reaction, mechanistic studies on propane oxidation reactions have been developed before propane steam reforming reactions. Based on their product selectivity results from propane oxidation reactions, Huff et al. (1994) found that over the Pt catalyst they used, ethylene was the dominating product. With a 2:1 ethylene to methane ratio, they suggested that the oxidation reaction proceeds through a cracking mechanism:

C_3H_8 reacts with O_s (oxygen atom on the surface) to form propyl groups on the surface:

$$C_3H_8 + O_s \longrightarrow C_3H_{7,s} + OH_s \quad (2.26)$$

The propyl group may be adsorbed at either a primary carbon to form:

$$CH_3\,CH_2\,CH_{2,\,s} \longrightarrow CH_{3,\,s} + C_2H_4 \quad (2.27)$$

Or on a secondary carbon to form:

$$CH_3\,CHCH_{3,\,s} \longrightarrow H_s + C_3H_6 \quad (2.28)$$

By differential measurements at a conversion of less than 10%, Ma et al. (1996) estimated kinetic parameters for the total oxidation of propane over $Pt/\delta\text{-}A1_2O_3$ based on the power rate expression:

$$\frac{-d(propane)}{dt} = k\,(propane)^{\alpha}\,(O_2)^{\beta} \quad (2.29)$$

Where the kinetic parameters were:

k (mol/m^2 h $kPa^{(\alpha+\beta)}$) = $1.87*10^9$

Ea (kJ/mol) = 104.7

$\alpha = 1.1$ $\beta = -0.6$

When comparing predicted data from this power rate expression with experimental observations, the correlation coefficients were better than 0.99.

For catalytic partial oxidation, two different mechanisms have been proposed in the literature. The first mechanism suggests that CO and H_2 form as direct products from catalytic partial oxidation. This has been confirmed experimentally in the case of very short contact times (Bharadwaj and Schmidt, 1994). The yield of synthesis gas through

this direct route is, however, limited because these products are more readily reactive for combustion than the reactant. The other mechanism involves first total oxygen consumption by total combustion of the fuel. This is followed by endothermic dry and steam reforming as well as the water-gas shift reaction (Dissanayake, et al., 1991). Since water–gas shift and reforming are relatively slow reactions compared to oxidation reactions, these reactions may not strongly affect the product distribution at very short contact times.

The results of Rostrup-Nielsen and Alstrup (1999) showed that the reaction rate was not affected by carbon monoxide or carbon dioxide during propane steam reforming. Therefore the dissociative adsorption of propane is most likely an irreversible step and they suggested the following mechanism for propane steam reforming:

$$C_3H_8 + (y+1)\,[site] \longrightarrow C_3H_{x,\,ads} + yH_{ads} + 0.5(8- x -y)H_2 \qquad (2.30)$$

$$2H_{ads} = H_2 + [site] \qquad (2.31)$$

$$C_3H_{x,\,ads} + H_2 + [site] = 3CH_{z,\,ads} + (0.5+1-3z)H_2 \qquad (2.32)$$

$$H_2O + \{support\ site\} \longrightarrow \{support\ site\}\text{-}H_2O \qquad (2.33)$$

$$\{support\ site\}\text{-}H_2O + [site] \longrightarrow O_{ads} + H_2 + \{support\text{-}[site]\} \qquad (2.34)$$

$$CH_{z,\,ads} + O_{ads} \longrightarrow CO + (0.5z)H_2 + [site] \qquad (2.35)$$

Possible side reactions are the formation of propene due to the desorption of the dehydrogenated C_3 carbon species formed during steam reforming as shown in the reaction scheme above in equation 2.17. Methane might also be formed by either the hydrogenation of a C_1 carbon species formed by equation 2.4 or the subsequent hydrogenation of carbon monoxide (methanation reaction):

$$CO + 3H_2 \longrightarrow CH_4 + H_2O \quad (2.36)$$

Based on the observed surface species transformations from their in situ DRIFTS studies, Natesakhawat et al. (2005) suggested the following major reaction pathways for adsorbed propane in the presence of steam over reduced sol–gel Ni–Ce/Al_2O_3 catalysts:

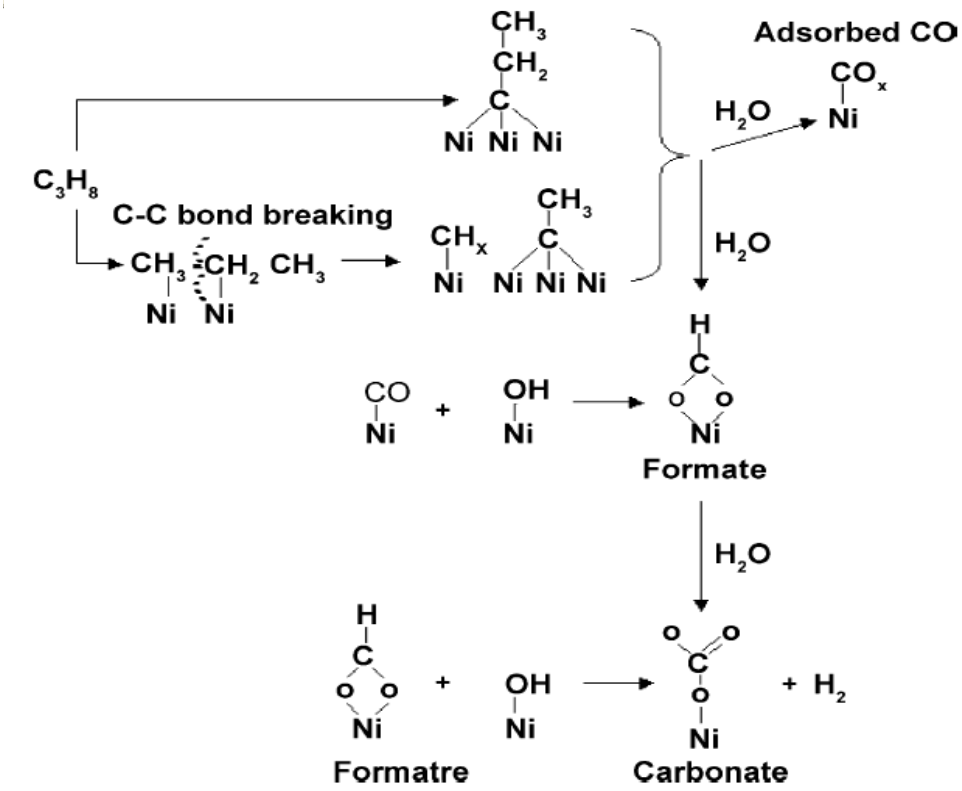

Laosiripojana et al., (2006) also investigated the mechanism of the resistance to carbon formation in propane steam refroming for a CeO_2-doped Ni/Al_2O_3 catalyst. They found that carbon deposition due to decomposition of hydrocarbons (ethane, propane, ethylene and methane) could be inhibited by gas-solid reactions between these hydrocarbons and the lattice oxygen (O_x) at the CeO_2 surface forming hydrogen and carbon dioxide according to the following suggested mechanism:

$$C_3H_8 + 3S = 2(CH_3\text{-}S) + CH_2\text{-}S \quad (2.37)$$

$C_2H_6 + 2S = 2(CH_3\text{-}S)$ (2.38)

$CH_4 + 2S = CH_3\text{-}S + H\text{-}S$ (2.39)

$C_2H_4 + 2S = 2(CH_2\text{-}S)$ (2.40)

$CH_3\text{-}S + S = CH_2\text{-}S + H\text{-}S$ (2.41)

$CH_2\text{-}S + S = CH\text{-}S + H\text{-}S$ (2.42)

$CH\text{-}S + S = C\text{-}S + H\text{-}S$ (2.43)

$C\text{-}S + O_x = CO + O_{x-1} + S$ (2.44)

$2H\text{-}S = H_2 + 2S$ (2.45)

Where S is the catalyst surface site which can be a unique site, or the same site as the lattice oxygen (O_x).

Although the few previous studies showed some suggested mechanisms for propane steam reforming and propane oxidation, developing a mechanism for the combination of the two reactions in OSR is expected to be more complicated.

Chapter 3
Experimental

This chapter addresses experimental techniques used to prepare and evaluate the performance of the different examined catalysts. It describes a detailed catalyst synthesis procedure. Different pre-treatment procedures for the catalysts (calcination-reduction) before each experimental run(s) are addressed when discussing each set of runs in subsequent chapters. The chapter also describes the primary experimental setup used to evaluate packed bed runs for different catalysts. Different catalyst characterization techniques are briefly mentioned at the end of the chapter, more details on each technique will be given when discussing their results, in Chapter 7.

3.1 Catalyst Preparation

All catalysts in this study were prepared by applying the wet impregnation method, described in detail in Bartholomew and Farrauto (2006). Impregnation is the simplest and most common procedure for dispersing active catalytic particles on different supports, especially for high metal loadings.

Commercial γ-Al_2O_3, in the form of a 3 micron powder with a surface area of 80-120 m^2/g and 99.97% metal basis, was purchased from Alfa Aesar, Ward Hill, MA, USA. To determine the maximum amount of Ni to cover a monolayer on this support surface, the following simple calculation was performed based on the lower limit of the support specified surface area:

For a nickel atomic radius (r_{Ni}) of 125 pm

The projected area (A_p) of a nickel atom is:

$$A_p = \pi r_{Ni}^2 = 4.91 \times 10^{-20}\ m^2 \qquad (3.1)$$

Therefore, for 1 mole of nickel (or 58.6 g_{Ni}), the area (A_m) is:

$$A_m = N \cdot A_p = 6.02 \times 10^{23}.A_p = 29{,}559\ m^2 \qquad (3.2)$$

and, the specific coverage area of Ni (A_s) is:

$$A_s = A_m / 58.6 = 504\ m^2 / g_{Ni} \qquad (3.3)$$

Assuming an 80 m^2/g support surface area, the maximum amount of Ni (monolayer) that can be deposited on 1 g of support is:

80/504 = $\boxed{0.159\ g_{Ni}/g_{sup}}$ = $\boxed{15.9\ wt\%}$

Based on the previous calculation, 15% wt Ni was used as the Ni loading for both the monometallic and bimetallic catalysts in this study.

Prior to using the amount required for each preparation, a batch of γ- Al_2O_3 was heated in the furnace at 110°C overnight to evaporate any moisture that may affect the calculations. $Ni(NO_3)_2.6\ H_2O$ (also obtained from Alfa Aesar) was used as Ni precursor. After calculating the amounts of the support and the precursor to obtain the specified 15% wt Ni loading, the precursor was dissolved in distilled water and the support powder was added to it. The solution was magnetically stirred while being heated at 70°C to evaporate the water until a paste-like mixture is obtained. The paste was then dried over night at 110°C. After drying, the catalyst was crushed and sieved to obtain 35-45 mesh particles.

When preparing bimetallic catalysts, the second metal could be co-impregnated with Ni by adding the right amount of both metal precursors with support powder, or by sequentially impregnating the metal over the already dried 15%Ni/Al_2O_3 catalyst. These bimetallic catalyst preparation methods will be investigated in Chapter 4.

3.2 Packed Bed Experimental Setup

The experimental setup is designed to perform a variety of reactions without modification of the setup. These reactions include catalytic and non-catalytic steam reforming and partial oxidation and oxidative steam reforming. The reactions can be run in both

differential and integral modes. A schematic diagram of the fixed bed setup is illustrated in Figure 3.1.

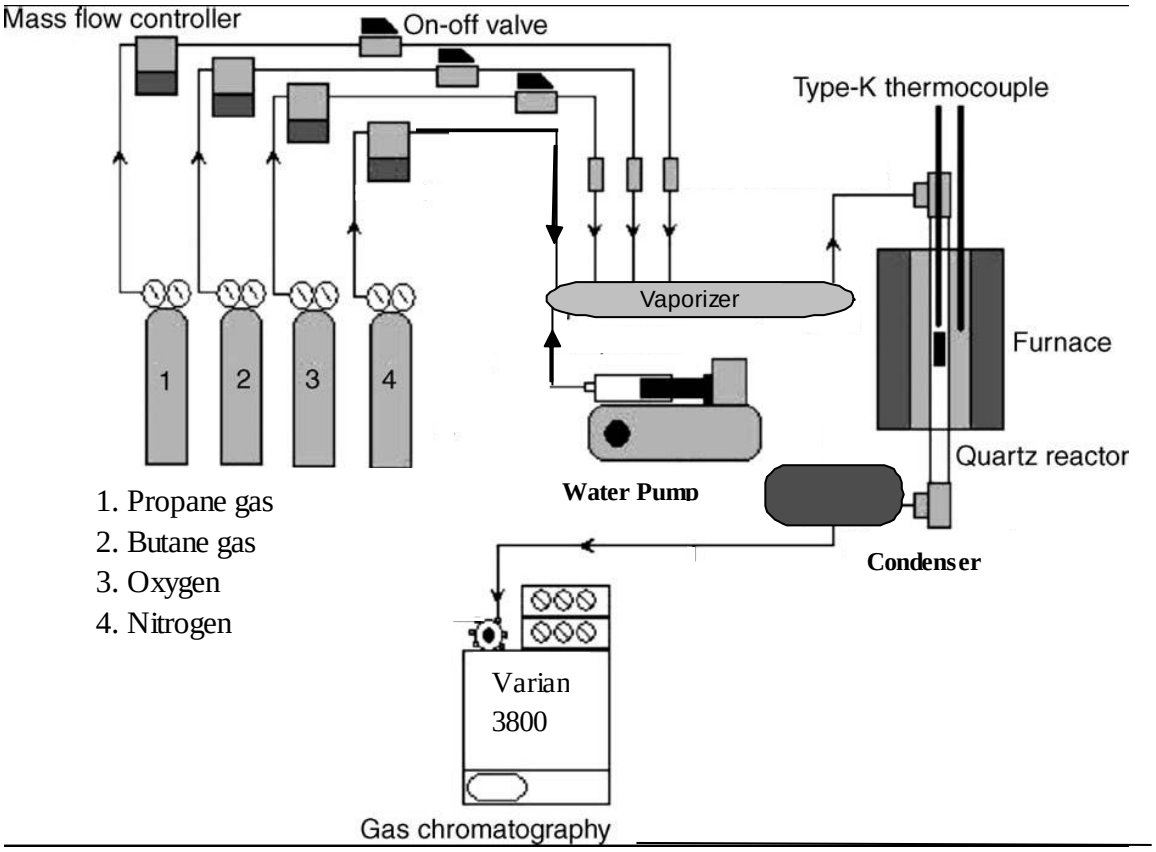

Figure 3.1. A Schematic diagram of the fixed bed experimental setup.

Gases are supplied from different gas cylinders at regulated pressures. The flow rates of the different gases are controlled by mass flow controllers. The gases join at a point and then travel to the vaporizer. A T-connection allows the feed to by-pass the vaporizer and directly enters the gas chromatograph (GC) for calibration or occasional feed analysis. Liquid water is pumped to the vaporizer. Gases mix with steam in the vaporizer before entering the reactor from the top. The reactor is installed inside a vertical tube furnace and consists of a quartz tube, where the catalyst bed sits on a quartz frit located in the middle of the isothermal zone of the reactor. After the reaction takes place, the hot product steam enters a condenser, where the water is removed. The non-condensable gas products exit the condenser and travel to the GC for compositional analysis.

Different parts of the experimental setup will be discussed in more details in the following sections.

3.2.1 Reactants Delivery System and Vaporizer

Gas Supply

All gases were supplied from gas cylinders by Praxair. Propane and butane were supplied in small cylinders and had a quality grade of 99.5%, with sulphur contents less than 1 ppmw, while O_2, H_2 and N_2 were supplied in large cylinders with quality grades of 99.99%. All gas cylinders were equipped with dual-stage regulators, also supplied by Praxair. Outlet gas pressures from all cylinders were kept below 50 psig to ensure consistent flow from the mass flow controllers.

Mass Flow Controllers

Propane and butane flow rates were controlled with two Brooks 5850E mass controllers, while Unit UFC 1000 mass controllers were used to control O_2, H_2 and N_2 flow rates. Each mass controller was calibrated with its respective gas using a bubble flow meter. Calibration curves relating the gas volumetric flow rate to the signal percent were generated and found to be linearly related with a coefficient of determination (r^2) higher than 0.99 for all gases.

Water Pump

The specified amount of steam was generated by delivering distilled water to the vaporizer through a KDS model 200 syringe pump supplied by KD Scientific, MA, USA. The pump covered a wide rang of flow rates with different syringe sizes. For short period activity tests 20 ml syringes were used, while in long time on stream tests 60 ml syringes were used. The required water volumetric flow rate was calculated and was given to the pump through a microcontroller that controlled the delivered volume based on the syringe diameter and the liner motion of the pusher block. Water was deliverer from the pump to the vaporizer through a 1/16” OD micro pipe.

Vaporizer

The heater, or vaporizer, was constructed from an 18" long, 1/8" OD stainless steel tube, wrapped in an STH 101 heating tape obtained from Omega Inc. The temperature of the vaporizer was set and controlled by a controlling system connected to a computer with WinGen^{TM} software. The vaporizer temperature was maintained at 230°C to ensure complete vaporization of the water. At this temperature, the feed components do not thermally decompose. At the end of the vaporizer, just before the reactor, a K-type thermocouple (obtained from Omega Inc.) was installed inside the vaporizer to measure the actual temperature of the feed entering the reactor. To reduce heat losses to the surroundings, thick insulation tape was wrapped around the vaporizer.

3.2.2 The Reactor

The reactor was a quartz tube 555 mm long with an ID of 9.9 mm and wall thickness of 2 mm. Quartz was selected as the reactor construction material, because of its inert chemical structure and inactivity towards reforming reactions. On the other hand, construction materials such as stainless steel, Hastalloy and Inconel, contain metals like nickel, cobalt and iron, well-known to have catalytic activity for OSR reactions under the specified operational conditions. When loading the reactor, the catalyst was kept in place by a quartz frit located 220 mm from the top of the reactor, as shown in Figure 3.2. The location of the frit was found to be in the middle of the isothermal zone of the reactor, as will be illustrated in Chapter 4.

The temperature of the catalyst bed inside the reactor was measured via a quartz sheathed micro K-type thermocouple obtained from Omega Engineering Inc. The thermocouple was inserted from the top of the reactor by a bored-through style 0.5" NPT x 0.5" Swagelok Ultra-Torr vacuum fitting. The thermocouple is connected for the same controlling system as the vaporizer. The bed's temperature is monitored and recorded over time using WinGen^{TM} software.

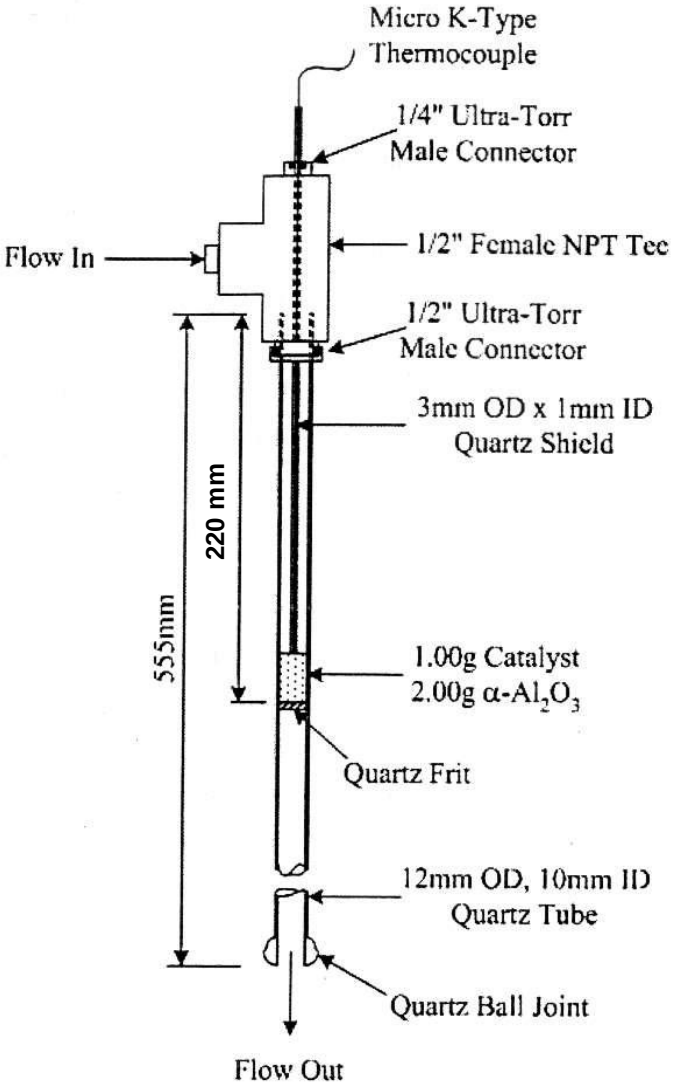

Figure 3.2: The fixed bed quartz reactor (Adapted from Coleman, 2008)

A bored-through style 0.5" NPT x 0.5" Swagelok Ultra-Torr vacuum fitting was used to attach the top end of the reactor to the vaporizer. The fitting is composed of a finger-tightened knurled nut and a metal ferrule to compress a Viton O-ring. The fitting was an effective choice to prevent any feed leakage and to provide more flexibility when installing, or removing, the reactor after each run. As illustrated in Figure 3.2, the reactor

ends with a ball joint to connect it to the condenser through a ball-socket joint fitting. A compression clamp was applied on the joint fitting to ensure a tight fit.

3.2.3 The Analytical System

Developing an analytical system to qualitatively and quantitatively analyze the reformate was a challenging task, because of the wide range of gases required to be detected and quantified. These gases include: light gases (H_2, O_2, N_2, CO, CH_4 and CO_2) and light hydrocarbons (ethylene, ethane, propylene, propane and n-butane). The analytical apparatus used was a Varian CP3800 GC. To cover the entire gas range and, at the same time, increase the number of injections for each run, the GC was fitted with two parallel analyzing configurations. The first configuration consisted of a 10 port valve (Valco Inc.), a 15' x 1/8" stainless steel 60/80 mesh Carboxen 1000 column (spherical carbon molecular sieve partials, Supelco Inc.) and a thermal conductivity detector (TCD). This configuration was used to analyze the light gases: H_2, O_2, N_2, CO, CH_4 and CO_2. Light hydrocarbons from C1 to C4 were analyzed by another configuration through a 6 port valve (Valco Inc.), a 50m x 0.53mm Al_2O_3/KCl fused silica PCOT column (Varian Inc.) and a flame ionization detector (FID). The two configurations with their different components are presented in Figure 3.3.

When the GC is in the fill mode, the product stream enters the 10 port valve and then the 6 port valve, by-passing the columns to be ventilated. When the GC is in the injection mode, two parallel injections take place at the same time through the two valves. In the first injection, the 10 port valve delivers a 50 microliter sample of the product through a sample loop. Before reaching the Carboxen column, the sample passes through a 2' porapak N pre-column. In this column, light hydrocarbons larger than CH_4 are back-flushed. In other words, the porapak N precolumn will hold the hydrocarbons allowing only gases (H_2, O_2, N_2, CO, CH_4 and CO_2) to proceed to the downstream Carboxen 1000 column. The gases are separated in the Carboxen 1000 column and their concentrations are quantified by the TCD.

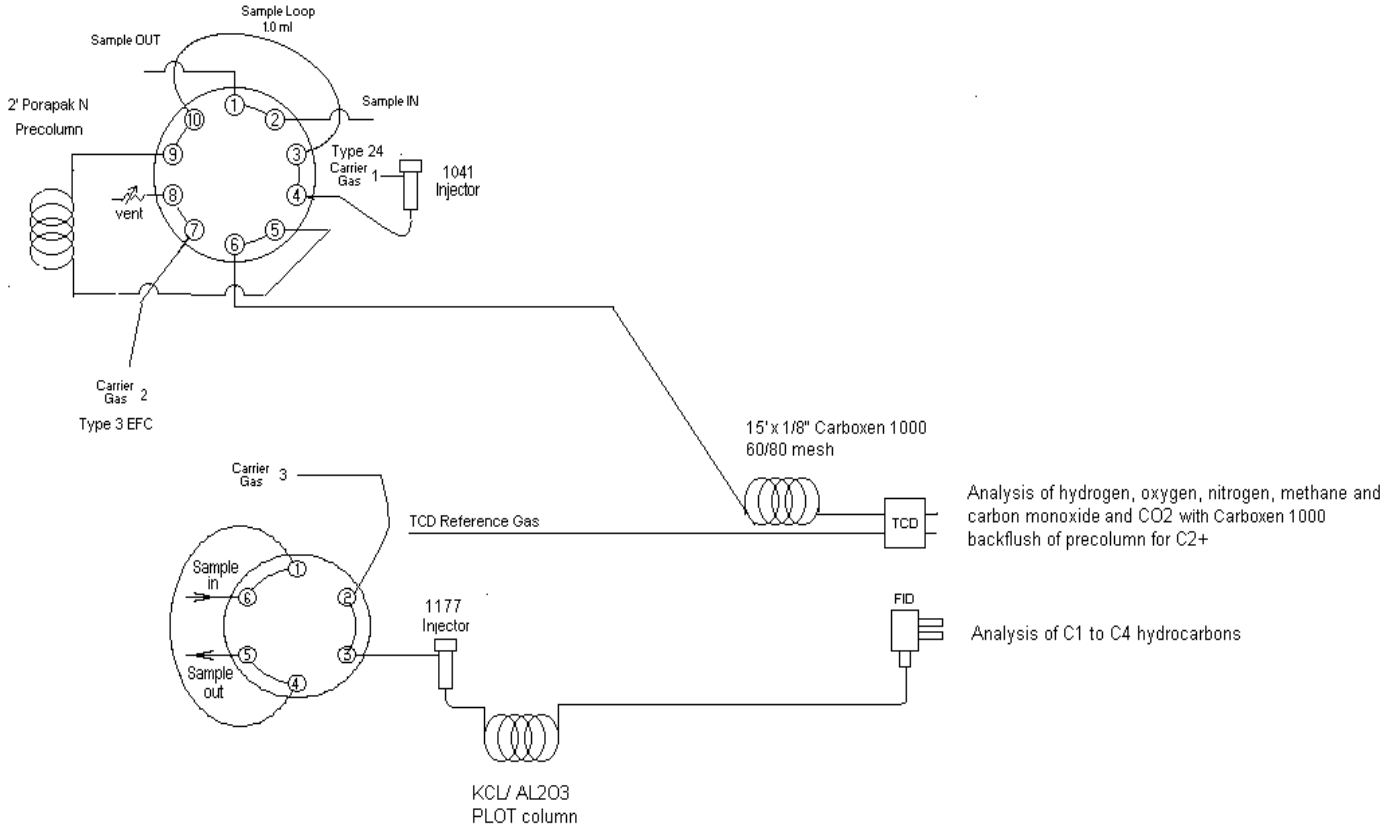

Figure 3.3: GC configurations; a Carboxen 1000 column with the TCD and a KCL/Al_2O_3 Plot column with the FID.

At the same time of the first injection, the 6 port valve delivers a 50 microliter sample of the product through a sample loop to the Al_2O_3/KCl fused silica column for gas separation. The alumina column is deactivated using very small salt crystals, providing a reproducible and stable deactivation up to 200°C. Depending on the type of deactivation salt, the column will present a different selectivity. KCl salt deactivation results in a relatively non-polar Al_2O_3 surface, while Na_2SO_4 deactivation results in a polar surface, where unsaturated compounds like ethylene, acetylene and methylacetylene (propyne) are retained longer.

After separation, the concentrations of different hydrocarbons were determined by the FID. Helium (supplied from Praxair) was used as a carrier gas in both configurations with a flow rate of 55 ml/min. To elude the different gases in a discernable and timely manner, a simple temperature program was employed for the GC oven that contains both columns. A Varian Star control software system was used to control and monitor different GC parts.

Two custom Praxair certified standard gases were used to calibrate TCD and FID peak areas. The compositions of the two standard gases are shown in Tables 3.1 and 3.2.

Table 3.1 Compositions of Standard Calibration Gas #1

Species	Concentration (volume %)
H_2	30.03
O_2	3.0
Ar	9.0
CO	30.0
CH_4	7.97
CO_2	20.0

Table 3.2 Compositions of Standard Calibration Gas #2

Species	Concentration (volume %)
C_2H_2	0.499
C_2H_4	3.09
C_2H_6	3.00
N_2	93.013
Traces of unsaturated hydrocarbons	0.398

A calibration procedure was developed to establish a relationship between peak areas and concentrations of different gases for the two standard mixtures. First, each gas mixture was run through the GC and different peaks were obtained for each gas in the two mixtures. Pure nitrogen (from Praxair) was used to dilute the two mixtures to obtain different concentrations of each gas in each mixture. After determining the concentration of each gas in its mixture and calculating the corresponding peak area for that concentration, calibration curves were generated for each gas relating the gas concentration to the peak area.

For all calibrated gases (H_2, O_2, N_2, CO, CH_4, CO_2, C_2H_4 and C_2H_6), a linear relationship was found between the gas concentration and peak area. The coefficient of determination (r^2) for all calibrated gases was higher than 0.99. Propane and butane

calibration curves were generated following the same procedure with different concentrations obtained by direct dilution of the pure gas with N_2. During the study period, when the GC parts, or settings, were subjected to any change, the calibration procedure for all gases was repeated to ensure calibration curves certainty.

3.3 Evaluation of Catalytic Performances

Catalytic performance was evaluated based on the total conversion of propane and butane in the LPG mixture and on the product distribution of the four main products resulting from LPG oxidative steam reforming: H_2, CO, CO_2 and CH_4. The total conversion was calculated as:

$$X_{total} = \frac{n_{prop}^{in} + n_{but}^{in} - n_{prop}^{out} - n_{but}^{out}}{n_{prop}^{in} + n_{but}^{out}} \times 100$$

Where:

n_{prop}^{in} : molar flow rate of propane in the feed

n_{but}^{in} : molar flow rate of butane in the feed

n_{prop}^{out} : molar flow rate of propane in the product

n_{but}^{out} : molar flow rate of butane in the product

Products are usually compared in their direct molar flow rate in mol/min × 10^5 or in their mol% in the dry product stream. However, in some comparisons, product yield was used, defined as:

$$Y_i = \frac{n_i^{out}}{n_{fuel}^{in} \times X_{fuel}}$$

Where:

n_i^{out} : molar flow rate of product i

n_{fuel}^{in} : molar flow rate of the fuel(s) in the feed

X_{fuel} : Conversion of the fuel(s)

A detailed calculation in an Excel spread-sheet was prepared to calculate different product molar flow rates from each GC injection. A sample calculation from the sheet is provided in Appendix A.

3.4 Catalyst Characterization Techniques

Surface and bulk properties of fresh and spent catalysts were characterized for both monometallic and bimetallic catalysts. A brief description of different characterization techniques applied in this study and the catalysts properties they investigated are given in Table 3.3. More details on each technique will be given in chapter 7 when discussing the results of the characterizations.

Table 3.3: Different characterization techniques applied in this study and the catalysts properties they investigated

Property Investigated	Characterization Technique	Apparatus
Calcination temperature	Temperature programmed oxidation (TPO)	Cahn TG 151 thermal gravimetric analyzer (TGA)
Reduction temperature	Temperature programmed reduction (TPR)	Cahn TG 151 thermal gravimetric analyzer (TGA)
Effect of metal-support interaction on the reducibility of the catalyst	Temperature programmed reduction (TPR)	The main experimental setup connected to a an Agilent 3000 micro GC to measure H_2 consumption
Amount of carbon deposits on spent catalysts	Temperature programmed oxidation (TPO)	Cahn TG 151 thermal gravimetric analyzer (TGA)
Carbon morphology on spent catalysts	Temperature programmed oxidation (TPO)	The main experimental setup connected to an Agilent 3000 micro GC to measure O_2 consumption or CO_2, CO
Catalyst coking rate	Measuring % increase of catalyst weight with time	Cahn TG 151 thermal gravimetric analyzer (TGA)
Different chemical phases and their crystallization degree of fresh and aged catalysts	X-ray diffraction measurements (XRD)	Bruker AXS D8 Advance difractometer using a Bragg-Brentano geometry with Ni-filtered Cu Kα radiation
Dispersion and average crystallite size of fresh and aged catalysts	H_2 chemisorption	a Hiden CatLab reactor connected to a Hiden QIC mass spectrometer to measure H_2 up take
Oxygen storage capacity (OSC)	O_2 chemisorption	a Hiden CatLab reactor connected to a Hiden QIC mass spectrometer to measure O_2 up take
Identify and quantify different adsorbed species on catalysts during reactions	*in-situ* Diffusion Reflectance Infrared Fourier Transform Spectroscopy (DRIFTS)	Nicolet Nexus spectrometer, equipped with a MCT detector and a KBr beam splitter

Chapter 4
Thermodynamics and Preliminary Experimental Studies

The experimental design for measuring catalyst activity and stability was preceded by a series of screening experiments to provide a solid starting base. Although some of the catalysts and reactions used in this study were reported in previous studies, the interpretation and comparison of results from these studies could be misleading in some cases. This can be attributed to different reasons: (1) non-systematic experimental design and using non-standard experimental methods, (2) underestimation of reaction limitations and catalysts' surface or bulk properties, (3) unspecified properties of the catalyst (purity, surface area, loading or support materials), and (4) unspecified critical operational conditions or analysis parameters. Because of such limitations, a variety of preliminary experiments were run to determine experimental design parameters and operational limitations, as well as to ensure measurement accuracy.

Before any experiments were run, a thermodynamic equilibrium study was performed. This study is useful in providing insight on different expected product patterns under a wide range of operational conditions. The thermodynamic analysis will also help to limit examined parameter ranges and concentrate experiments on optimum operating conditions, under which maximum hydrogen yields are achieved.

4.1 Thermodynamic Study of Oxidative Steam Reforming of Propane, Butane and their mixtures

The objective of this study was to predict the effect of different operating parameters on total conversion and product distribution during LPG oxidative steam reforming (OSR). These predictions, together with the few data available in the literature, were to serve as guidelines for choosing the starting values of several operating parameters for the screening tests. The investigated parameters were:

Temperature (°C)
Steam to carbon ratio (S/C)
Oxygen to carbon ratio (O_2/C)
LPG composition (mixtures of propane and butane in the feed)

4.1.1 Methodology

Two general methods can be used to investigate the effect of operating parameters on thermodynamic equilibrium of chemical reactions: stoichiometric and non-stoichiometric approaches. In the stoichiometric approach, equilibrium constants of independent reactions are required for calculating equilibrium compositions. In the non-stoichiometric approach, the minimization of the Gibbs free energy is used to determine the compositions at equilibrium without specification of the reactions taking place in the system. Inputs include temperature, pressure, reactants and expected products. The non-stoichiometric equilibrium model is widely used in thermodynamic analysis of hydrocarbon steam reforming and partial oxidation reactions [Chan and Wang, 2000; Faria et al., 2008; Zeng et al., 2010] and was used here.

The total Gibbs free energy G of a system, composed of n_i moles of each of the N gaseous elements, is expressed as (Zeng et al., 2010):

$$G = \sum_{i=1}^{N} n_i \left[\Delta G_{fi}^{0} + RT \ln\left(\frac{f_i}{f_i^{0}}\right) \right] \qquad (4.1)$$

where:

ΔG_{fi}^{0} : the standard Gibbs function of the formation of species i

f_i : fugacity of the i[th] species at operating conditions

$f_i^{\,0}$: fugacity of the i[th] species at standard conditions

For reaction equilibrium in the gaseous phase:

$$(\frac{f_i}{f_i^{\,0}}) = y_i \gamma_i \; P = (\frac{n_i}{n}) \; \gamma_i \; P$$

where:

y_i : the mole fraction of species i

n : the total number of molecules in the gaseous phase

γ_i : the fugacity coefficient of the i[th] species

P : the pressure of the system

Substituting for $(\frac{f_i}{f_i^{\,0}})$ in Equation (4.1) and rearranging:

$$G = \sum_{i=1}^{N} n_i \left[\Delta G_{fi}^{0} + RT \ln P + RT \ln y_i + RT \ln \gamma_i \right] \qquad (4.2)$$

Assuming ideal gas behaviour for all reaction components under the examined conditions, then:

$\gamma_i = 1$ for all components

Consequently, Equation (4.2) becomes:

$$G = \sum_{i=1}^{N} n_i \left[\Delta G_{fi}^{0} + RT \ln P + RT \ln y_i \right] \qquad (4.3)$$

Since, under some examined conditions, carbon formation is expected, a term was added to Equation (4.3) to account for solid carbon:

$$G = \sum_{i=1}^{N} n_i \left[\Delta G_{fi}^{0} + RT \ln P + RT \ln y_i \right] + n_c G_{fc}^{0} \qquad (4.4)$$

where:

n_c : moles of solid carbon

G_{fc}^{0} : the standard Gibbs function of the formation of solid carbon

All thermodynamic calculations were performed using AspenPlus™, a commercially available simulation software that has a built-in Gibbs reactor module to perform thermodynamic equilibrium reaction calculations. The Gibbs reactor setup is simple and composed of an inlet stream, the Gibbs reactor and an outlet stream. The parameters required for the inlet stream and the reactor will be illustrated.

After screening the literature and conducting some preliminary simulation runs, we chose a base case as a starting point for the simulation. The base case operating parameters were chosen such that they were between the maximum and minimum of each parameter. The base case feed composition and operating conditions are illustrated in Tables 4.1 and 4.2, respectively.

Table 4.1 Base case molar composition

Component	Composition mol %
Propane	2.049
n-butane	2.049
O_2	9.02
N_2	33.60
Steam	53.27
Total	100

These feed compositions were chosen to provide a steam to carbon (S/C) ratio of 3.7 and an O_2 to carbon ratio (O_2/C) of 0.61. The two ratios were defined as:

$$S/C = \frac{\text{moles of steam fed into the reactor}}{3\times(\text{moles of propane fed}) + 4\times(\text{moles of butane fed})}$$

$$O_2/C = \frac{\text{moles of oxygen fed into the reactor}}{3\times(\text{moles of propane fed}) + 4\times(\text{moles of butane fed})}$$

Table 4.2 Base case feed stream and reactor operational conditions

Parameter	Specification
Feed temperature	Inlet T (stream 1) = 200°C
Feed pressure	Inlet P (stream 1) = 1 atm
Reactor temperature	500°C
Reactor pressure	1 atm

In addition to specifying feed and operating conditions for the Gibbs reactor simulation, all possible expected products, including undesired products, should be included in both inlet and outlet streams. The specified gaseous components were propane, butane, oxygen, nitrogen, steam, hydrogen, carbon monoxide, carbon dioxide, methane, ethane, ethylene, propylene and iso-butane. These products were selected based on the reaction products mentioned in the literature. In addition to these products, solid carbon was also defined as a possible product to check the possibility of carbon formation under the specified conditions in each run.

4.1.2 Results and Discussion

After running the simulation in different ranges of the four parameters (temperature, S/C, O_2/C and LPG composition), a couple of observations were found to be common for all simulations:

- Under all conditions, the conversion of fuels, propane and butane, was greater than 99%.

- Under all conditions, the percentages of ethane and ethylene in the product stream were less than 1×10^{-5} mol %, which was considered negligible. Also, no propylene or iso-butane was predicted.

- According to the thermodynamic calculations, no solid carbon was formed in any of the simulation runs.

Based on the above general points, only the four major products were considered in the subsequent discussion: hydrogen, carbon monoxide, carbon dioxide and methane. For each parameter, the mole percentage of each product in the product stream was plotted versus different operating parameters.

Temperature Effect

As a combination of endothermic and exothermic reactions, temperature is expected to have a critical effect on oxidative steam reforming reactions. In this part of the study, the temperature of the reactor varied from 200 to 900°C, calculating the major product distribution every 50°C. In each run, the feed and operating conditions were kept at the base case conditions stated previously. The significant effect of temperature on product distribution is clearly illustrated in Figure 4.1. Hydrogen composition sharply increases as the temperature increases from 200 to 550°C, reaching a maximum between 550 and 600°C. As the temperature increases above 650°C, hydrogen composition in the product stream decreases. At temperatures above 550°C, CO_2 % decreases while at temperatures above about 400°C, more CO is produced as temperature is increased.

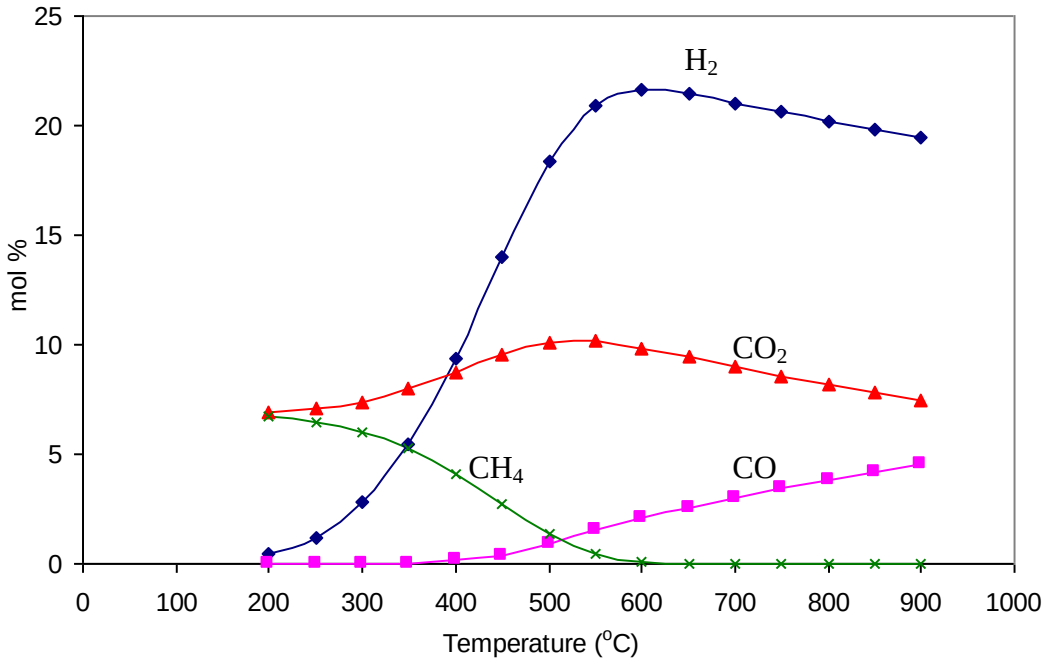

Figure 4.1: mol % of products at different temperatures at S/C = 3.71, O_2/C = 0.61 and 1:1 propane butane LPG mixture

Steam to Carbon Ratio (S/C)

The S/C ratio is an important parameter affecting hydrocarbon steam reforming (SR) and oxidative steam reforming (OSR). Relatively high S/C ratios are not only required to achieve high hydrogen yields, but they also are essential to prevent the formation of solid carbon, especially with feeds containing large-chain (higher) hydrocarbons. As stated previously, the S/C ratio used in the base case was 3.7. The change in product distribution was calculated by varying the S/C ratio from 0, where only oxidation reactions are taking place, to 6.

The S/C ratio was changed by manipulating the steam flow rate and balancing that with the nitrogen flow rate to keep a constant total flow rate to the reactor. All other conditions were kept at the base case conditions. The results are shown in Figure 4.2. Increasing the S/C ratio up to 0.5 caused an increase in all four products. However, above 0.5, a larger increase was observed for H_2 with increasing S/C. H_2 and CO_2 continued

increasing with increasing S/C ratio, while CO and CH_4 decreased above a S/C ratio of 0.5.

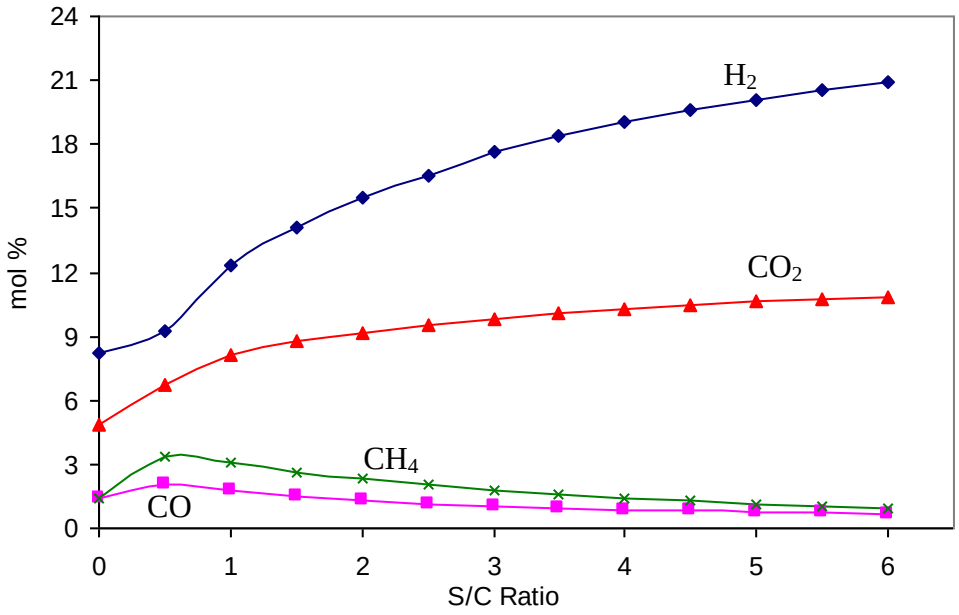

Figure 4.2: Effect S/C ratio at base case conditions, T = 500°C, O_2/C = 0.61 and 1:1 propane butane LPG mixture

It is clear that the S/C ratio has a positive effect on H_2 production. However, from Figure 4.1, the results show that temperature had a significant effect, where H_2 produced peaked between 550 and 600°C, after which, H_2 mol % started decreasing. Figure 4.3 shows the combined effect of temperature and the S/C ratio at four temperatures (400, 500, 600 and 700°C) and S/C ratios ranging from 2 to 5. A positive effect occurs on the H_2 % when increasing S/C ratios at almost all temperatures, although this positive effect is more significant at lower temperatures. The only situation where H_2% decreased when increasing the S/C ratio was found at the highest temperature (700°C) and for the highest S/C ratios (above 4.5).

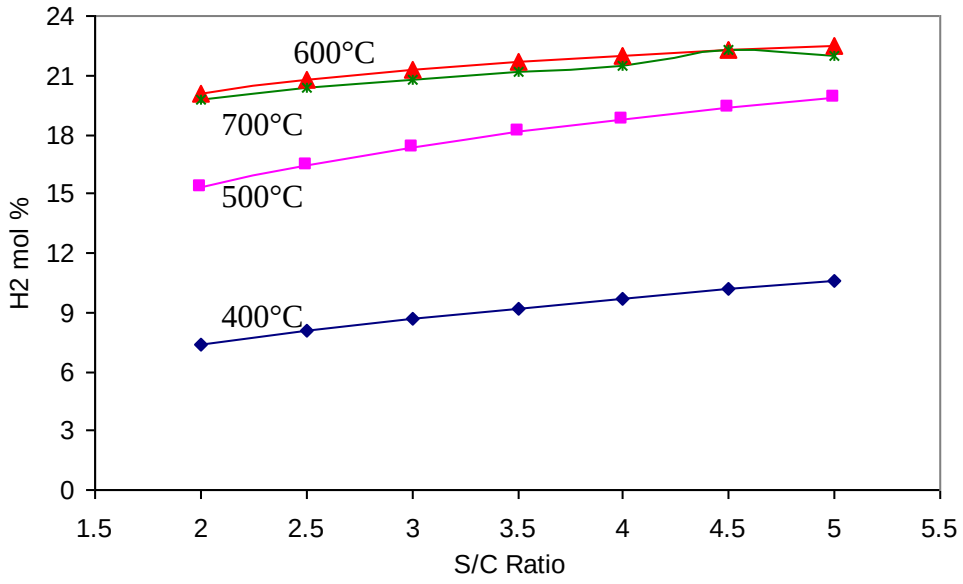

Figure 4.3: Combined temperature and S/C effects on H_2 mol% at O_2/C = 0.61 and 1:1 propane butane LPG mixture

Oxygen to Carbon Ratio

The O_2/C ratio used in the base case was 0.61. To study the effect of the O_2/C ratio, the change in product distribution was calculated by varying the O_2/C ratio from 0, where only the steam reforming reaction takes place, to 1. The O_2/C ratio was changed by changing the oxygen flow rate and balancing that with nitrogen to keep constant mole fractions for H_2O, propane and butane in the feed. All other parameters were kept at the base case conditions. The results are illustrated in Figure 4.4.

The increase in the O_2/C ratio led to a decrease in hydrogen production. This is the result of the increasing contribution of the complete combustion reactions of the fuel and CH_4 produced, yielding more CO_2 and H_2O and less CO and H_2 as more oxygen is supplied to the system.

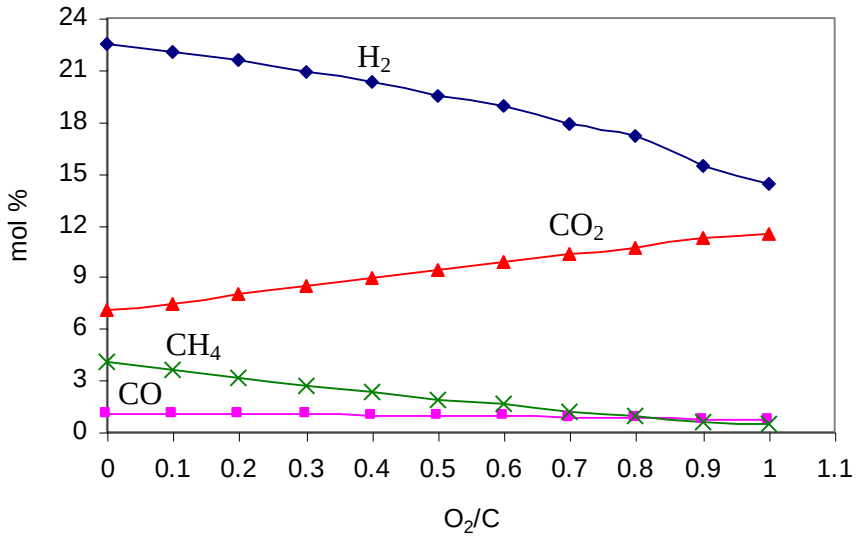

Figure 4.4: Effect of varying the O_2/C ratio of different products at base case conditions, T = 500°C, S/C = 3.71 and 1:1 propane butane LPG mixture

A review of the experimental data reported in the literature showed that there is no clear relationship between the O_2/C ratio and hydrogen production in OSR reactions. While hydrogen production was reported to decrease with the O_2/n-octane ratio when n-octane was used as a hydrocarbon feed in the OSR of gasoline (Whittington et al., 1995), H_2% was found to increase by increasing the O_2/CH_4 ratio in CH_4 OSR (Ma et al., 1996). However, when studying propane OSR over 1% Pt/CeO_2, Recupero et al. (2005), found a similar trend for the effect of increasing the O_2/C ratio on hydrogen production as the one in this thermodynamic study.

Although higher O_2/C ratios led to lower equilibrium H_2 production, experimentally (Laosiripojana and Assabumrungrat, 2006), the addition of O_2 in OSR was found to reduce the amount of carbon deposition and improve product selectivity by eliminating the formation of C_2H_6 and C_2H_4. O_2 prevents any by-product hydrocarbons formed from having an impact via carbon deposition resulting from hydrocracking reactions, by oxidizing these by-products (Laosiripojana and Assabumrungrat, 2006). Therefore,

although higher O_2/C ratios led to lower hydrogen production at equilibrium, there may be an optimum value of the O_2/C ratio for the OSR of LPG that minimizes the formation of undesired hydrocarbons and improve catalyst resistance to carbon build-up, while maintaining reasonable H_2 production.

The O_2/C and temperature combined effects on H_2 mol% was calculated at four temperatures (400, 500, 600 and 700°C) for O_2/C ratios ranging from 0.2 to 0.6 (Figure 4.5). The decrease in H_2 production with increasing O_2/C was more pronounced at higher temperatures.

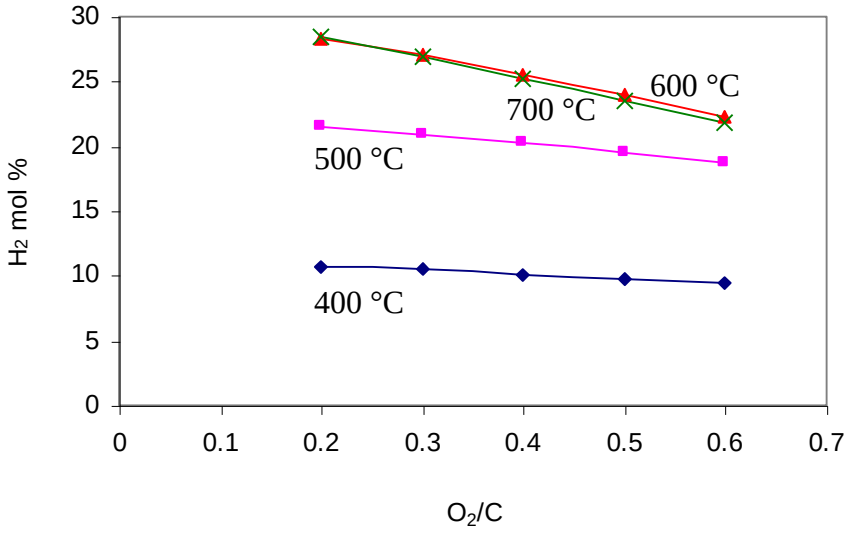

Figure 4.5: Combined temperature and O_2/C effects on H_2 mol% at S/C = 3.71 and 1:1 propane butane LPG mixture

The O_2/C and S/C ratios had opposite effects on H_2 mol%, therefore, their combined effect was investigated. The O_2/C and S/C combined effect on H_2 mol% was calculated at five O_2/C ratios, from 0 to 0.8, when varying the S/C ratio from 0 to 5. The results of these calculations are shown in Figure 4.6. When no steam is introduced and only oxidation reactions are taking place at 500°C, a small amount of H_2 can be produced from partial oxidation. This amount increases as the amount of O_2 is increased from 0.2 to 0.8. As steam is introduced at S/C ratios lower than 1, H_2 production increases, especially for

lower O_2/C ratios. However, at a S/C ratio of 1, the increase in H_2 with S/C ratio becomes independent of the O_2/C ratio, as at this S/C ratio, all O_2/C ratios produced the same amount of H_2. As the S/C ratio is increased above 2, increasing the O_2/C ratio will have a negative effect on equilibrium H_2 production. Under operating S/C ratios ranging from 3 to 6, the highest H_2 production is achieved when no O_2 is introduced and only SR is running (Figure 4.4), because when any amount of O_2 is introduced, a portion of the fuel is oxidized to provide heat for the endothermic SR reaction, causing a decrease in the fuel supply for SR.

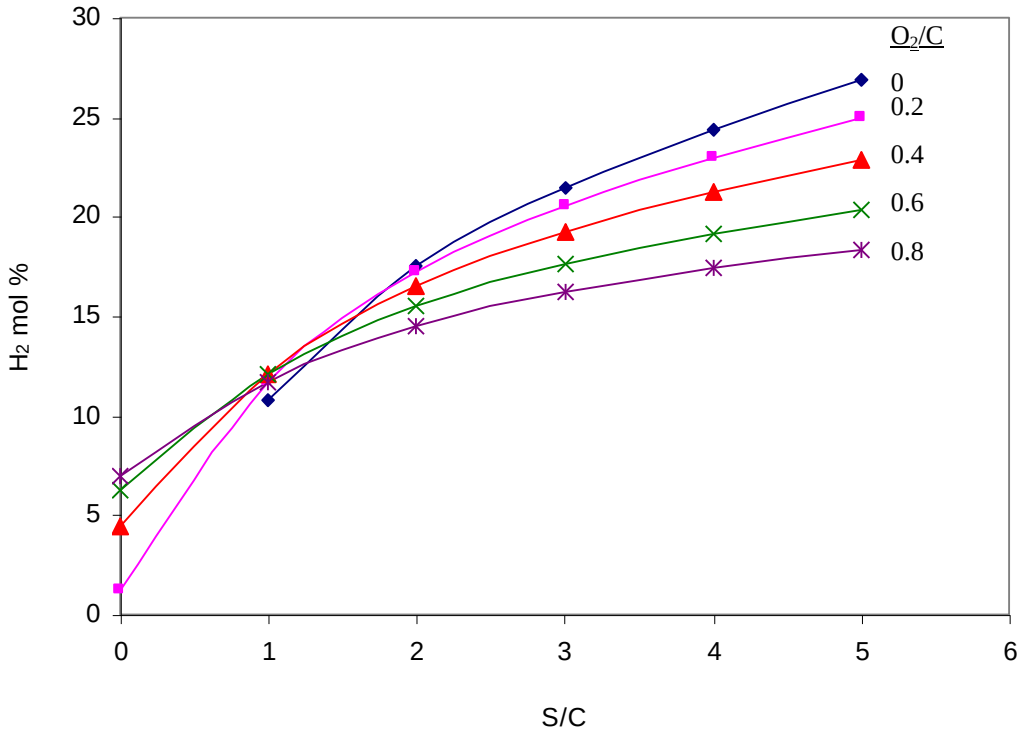

Figure 4.6: Combined S/C and O_2/C effect on H_2 mol% at 500°C and 1:1 propane butane LPG mixture

Effect of LPG Composition

As illustrated in the background chapter, LPG is actually a mixture of hydrocarbons with propane and/or butane having the highest concentrations. LPG mixtures of propane and butane have wide compositions worldwide, ranging from highly enriched propane LPG to

highly enriched butane. Therefore, it is interesting to look into equilibrium predictions investigating the effect of different propane/butane LPG compositions on the product distribution under the base case specified conditions.

To investigate different LPG mixtures, the 1:1 ratio of propane to butane was varied from pure propane to pure butane, maintaining the base case total fuel percent of 4.1%. However, from the definitions of the S/C and O_2/C ratios, given previously, it is clear that changing the compositions of propane and butane in the feed will change both ratios if we want to keep the total composition of both hydrocarbons constant at 4.1% in the feed. This change is a result of the different carbon content in butane and propane. Since, at the base case value of 3.7, the S/C ratio is higher than the stoichometric value (S/C=2) for both fuels, it will be more affected by changing the propane:butane ratio than the relatively lower O_2/C ratio. When keeping the steam and oxygen flow rate at their base case value, because butane has a higher carbon content, an LPG mixture enriched in butane will lead to lower S/C and O_2/C ratios than in the base case. Consequently, a propane enriched mixture will lead to higher ratios. Therefore, two cases were considered to study the effect of varying LPG compositions on OSR product distribution.

Case I:

In this case, the composition of LPG was varied from 0% propane, where the feed was pure butane, to 100% propane, maintaining a constant fuel percent of 4.1 mol% in the feed. The S/C and O_2/C ratios were kept constant at each run at the base case ratios. This was achieved by changing the steam, oxygen and nitrogen compositions in the feed each run and maintaining a constant total flow rate to the reactor.

Case II:

In this case, compositions of LPG were varied in the same way as in Case I. The flow rates of steam and oxygen were kept constant at their base case value. Although the LPG composition was changed, the total fuel molar flow rate was constant. Therefore, in all of these experiments the total mole fraction of fuel in the feed remained constant at 4.1 mol%. Consequently, S/C and O_2/C ratios changed for each run in the manner described

previously. Mol% of different products resulting from the simulation of both cases are presented together in Figure 4.7, where the solid lines represent the simulation from Case I, while the dashed lines are those of Case II for the same product.

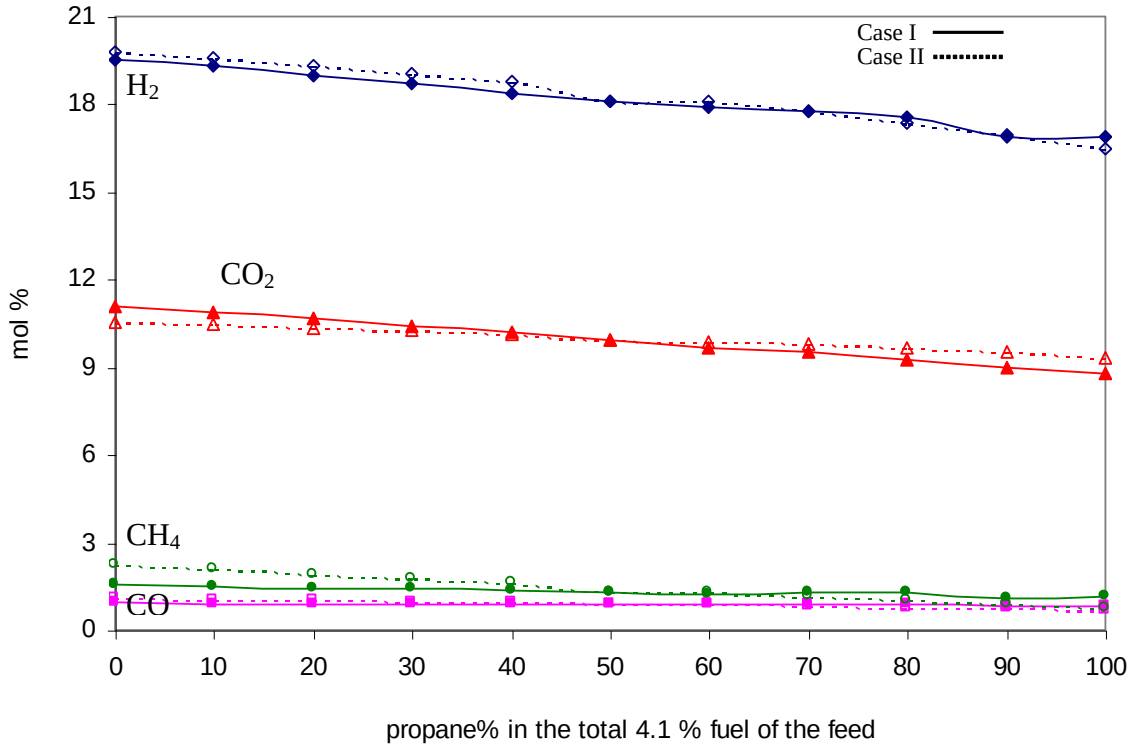

Figure 4.7: Effect of changing LPG propane/butane ratio on the product distribution at 500°C when S/C and O_2/C ratios are constant (Case I) and when the ratios vary (Case II)

In general, no significant differences were observed between the product trends for both cases. However, the change in the S/C and O_2/C ratios in Case II did have some effect on the CH_4 mol%, as pure butane LPG resulted in lower S/C ratios, which led to higher CH_4 production. On the other hand, a pure propane feed resulted in higher S/C ratios in Case II and a lower CH_4 production than in the base case. As a result of higher H_2 and carbon contents, LPG mixtures enriched in butane produced more H_2 and CO_2, while the concentrations of the two gases decreased by enriching the feed with more propane to reach the minimum value at pure propane. Although thermodynamically

butane-enriched LPG mixtures produced more H_2, their higher C/H_2 ratio, compared to propane, is a primary concern when considering the greater possibility of catalyst deactivation by carbon deposition resulting from hydrocarbon cracking under higher temperature conditions.

4.2 Blank Reactor Preliminary Experiments

Before any catalysts in the reactor described in Chapter 3 were used, a series of experiments were run with an empty reactor. The first group of experiments was used to determine the isothermal zone along the reactor tube, which is where the quartz frit supporting catalyst material would be placed. The other group was to investigate the possibility of thermal (non-catalytic) cracking of the fuels, or any homogenous reactions that might occur at different parameter limits.

4.2.1 Temperature Profile of the Reactor

To position the quartz frit that supports the catalyst bed in the isothermal zone of the reactor, preliminary tests were performed to study the effect of furnace temperature on the axial temperature profile of the reactor. Experiment runs were performed using the experimental setup described in Chapter 3. The reactor was the same as that described in Figure 3.2 except that it was only a quartz tube without a quartz frit. Beginning from the top of the reactor, defined to be 4 cm from the top of the quartz tube where the reactor enters the furnace, the temperature was measured every 2 cm. A quartz sheathed micro K-type thermocouple obtained from Omega Engineering Inc. was used to measure the temperature at the specified position. A ¼" ultra–torr male connector was used to adjust and seal the thermocouple at the required position.

The feed to the reactor for each run consisted of nitrogen flowing at 90 ml/min and steam flowing at 100 ml/min. These feed compositions were assumed to represent the reaction flow conditions. The vaporizer temperature was kept at 200°C for all runs. The thermocouple was left for 15 minutes to stabilize at each axial position before recording the temperature. The temperature reading of the thermocouple vs. time was displayed on a WinGen™ computer software. The WinGen™ screen also displayed the temperature of

the feed entering the reactor, measured by a thermocouple located at the end of the vaporizer.

In these tests, three furnace temperatures were chosen: 400, 500 and 600°C. For each temperature, the furnace set point was programmed to the required temperature. Temperature profiles of the three chosen set points are presented in Figure 4.8. From the top of the reactor, the temperature begins to increase as we move down the reactor. The increase continues until the set point is reached. Towards the end of the reactor, a slight decrease in temperature was observed as a result of heat losses from the bottom opening of the reactor. For all three set points, the isothermal zone was determined to be between axial positions 18 and 24 cm from the top end of the quartz tube. Therefore, the quartz frit, which supports the catalyst bed, was positioned in the center of the isothermal zone, 22 cm from the top of the quartz tube (Figure 4.8).

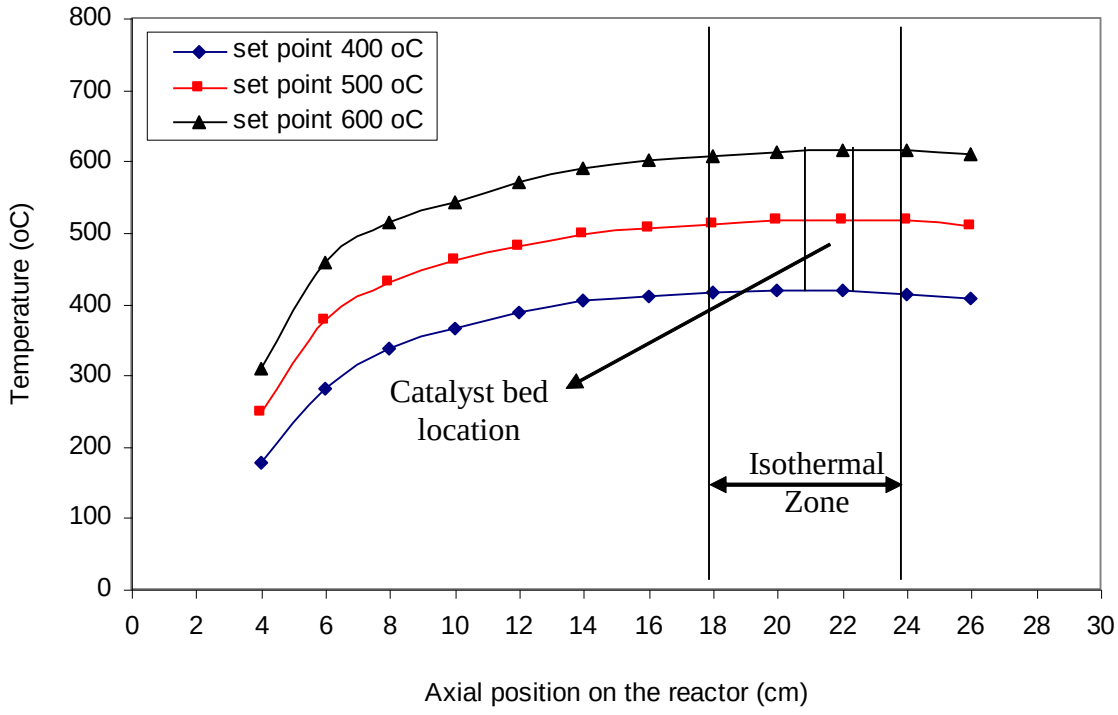

Figure 4.8: Temperature profiles in an empty quartz reactor at three different furnace set points: 400, 500 and 600°C.

4.2.2 Investigating the Occurrence of Non-Catalytic Homogenous Reactions

When evaluating the performance of a catalyst for a certain reaction, it is important to ensure that only heterogeneous catalytically driven reactions are taking place, as the occurrence of non-catalytic reactions will mislead the understanding of the exact role of the catalyst in activating the reaction. Moreover, in most reactions involving higher hydrocarbons, there is always a possibility of thermal (non-catalytic) cracking, especially at high operating temperatures. Such thermal cracking reactions will not only affect the reaction scheme of the catalytic process, but also are known to produce carbon deposition precursors which will often cause catalyst deactivation by coking. Therefore, when evaluating catalyst performance for OSR reactions, operating parameters should be selected such that no homogenous reactions will occur.

With butane having a longer carbon backbone than propane, the thermal decomposition of butane is more likely to occur at lower temperatures. Therefore, homogenous reactions experiments were first run for pure butane to determine the higher temperature limit, which is expected to be higher for propane.

Homogenous reaction experiments were run in the same experimental setup described in Chapter 3, using an empty reactor having the quartz frit. Feed compositions and operating conditions were selected from the literature and the thermodynamic equilibrium study to cover parameter ranges in which catalyst performance is expected to be evaluated. In the first set of experiments, 3 mol% butane (considerably high for butane reforming experiments) was fed to the reactor, while the S/C = 3 and the O_2/C = 0.6. The furnace temperature was set at 400°C and the product was analyzed 1 hour after introducing the feed to the reactor. For all three GC injections, no reaction took place and gas compositions were the same as that in the feed.

Two set of experiments, at 450 and 500°C, were run under the same feed conditions, also with no reaction. However, when the temperature was raised to 525°C, traces of different hydrocarbons were detected, most were identified, and included methane, ethane, ethylene, propylene, butylenes and propane. Possible reactions to produce these

hydrocarbons from butane were illustrated earlier in the butane background section of Chapter 2. Although the hydrocarbons couldn't be quantified, it was clear that there were only traces, as the total butane conversion was less than 3.4%. When the reactor temperature increased to 550°C, larger FID peaks were detected for the previously identified hydrocarbons, in addition to new, but unidentified peaks. At this temperature, the occurrence of homogenous reactions was clear, and the butane conversion increased to 26%. It is worth mentioning that after cooling down and taking the reactor out of the furnace, no soot or any carbon deposition was observed on the quartz frit or the reactor walls.

To further investigate the possibility and significance of butane homogenous reactions at different S/C and O_2/C limits, and since 525°C was proven to be a critical temperature for these reactions to occur, different ratios were chosen at this temperature. High and low limits were selected for the two ratios, and butane conversion resulting from running homogenous experiments at the combination of these limits are illustrated in Table 4.3.

Table 4.3: Homogenous reactions from the butane conversion for the variety of S/C and O_2/C combinations at 525°C

O_2/C \ S/C	1.5	**3**	4.5
0.35	3.2%		4%
0.6		**3.4%**	
0.9	4.9%		9.6%

As expected, increasing both ratios caused more homogenous reactions to occur; the lowest butane conversion was at the lowest ratio limits, while the highest conversion was at the highest limits. However, it is clear that under the selected limits, the O_2/C ratio had a stronger effect than the S/C ratio. This is clear when comparing the butane conversion at the lower S/C ratio for the two O_2/C limits and the lower O_2/C ratio for the two S/C

limits. When S/C = 1.5, increasing the O_2/C ratio from 0.35 to 0.9 causes a 1.7% increase in conversion, while at 0.35 O_2/C, increasing S/C from 1.5 to 4.5 increased the conversion by only 0.8%. This effect at the higher O_2/C ratio is expected as higher amounts of O_2 will shift equilibrium toward butane homogenous oxidation reactions/products. However, a 0.9 O_2/C ratio is not a practical ratio for OSR reactions and will not be reached when running catalytic reactions. A more practical O_2/C ratio is expected to be in the range of 0.3 to 0.6.

Since at 525°C butane homogenous reactions began to occur, propane homogenous experiments were also tested at this temperature. Two experiments were run for a 3% mol propane feed at the conditions leading to the two highest conversions in Table 4.4; the first was at S/C = 1.5 and O_2/C = 0.9, while the second was at S/C = 4.5 and O_2/C = 0.9. No reaction was detected under both sets of conditions.

Based on these experiments, it is clear that under practical OSR conditions, homogenous reactions for an LPG mixture, composed mainly of butane and propane, are likely to occur at temperatures higher than 500°C. To avoid these reactions, all catalyst evaluation experiments were run below this temperature, even for pure propane.

4.3 Catalysts Evaluation - Preliminary Experiments

In this section, a variety of experiments were run to establish operating boundaries and begin establishing performance baselines for evaluating and screening bimetallic catalysts that will be selected, discussed in Chapter 5. The first set of experiments was only run for the monometallic 15% wt Ni/Al_2O_3 (15Ni) catalyst to characterize the pre-treatment procedures necessary to achieve the best catalyst performance. Monometallic catalyst experiments were also run to determine the amount of catalyst used in the reactor for each run. The second sets of experiments were run for both the 15Ni catalyst and the selected bimetallic catalysts. These experiments were run to select catalysts for further comparison in the screening chapter and to optimize ranges of operating parameters for each catalyst.

4.3.1 Ni/Al_2O_3 Calcination – Reduction Experiments Using TGA

Most heterogeneous catalysts should be pre-treated, or activated, prior to using them for the required reaction. The first pre-treatment, usually performed directly after drying the catalyst, is calcination. The purpose of the calcination step is to decompose and volatilize the undesired compounds that formed, for example from the precursor materials, during the catalyst preparation process. The process is carried out in air at different temperatures and for different times. For reforming catalysts, a second pre-treatment is performed directly before using the catalyst and is referred to as reduction.

From the literature, Ni/Al_2O_3 calcination temperatures cover a wide range, from 400 to 900°C, with no rationalization for using any of these temperatures. However, selecting the calcination temperature has a direct effect on the textural properties of the catalysts which may, in turn, affect the activity of the catalyst. For example, at high calcination temperatures, exothermic reactions due to the decomposition of salts can cause localized high temperatures within the catalyst and, hence, accelerate catalyst aging. Moreover, the calcination process affects catalyst metal-support interactions, which play an important role in determining the activity and stability of Ni-based catalysts.

In the reduction step, the calcinated Ni catalyst is treated with a stream of H_2 to reduce different Ni oxide phases to metallic Ni, which is the active phase for catalyzing SR reactions. The reduction temperature needs to be carefully optimized, as each metal-support system has a temperature at which the maximum number of Ni active sites could be achieved. Like calcination temperatures, a wide range of reduction temperatures has been reported in the literature, ranging from 600 to 900°C (Coleman, 2008).

With these scattered calcination and reduction temperatures in the literature, experiments had to be run to characterize the 15Ni catalyst calcination and reduction temperatures. Both treatments are accompanied with a minor loss in weight, due to losing material (e.g. volatilizing the precurors, reducing the oxides to metal); the loss is more in

the case of calcination. Therefore, a thermo-gravimetric analysis (TGA) was used to relate the catalyst weight loss to temperature for each process.

Calcination experiments were run by measuring the fresh catalyst weight loss under a stream of air while ramping the temperature. Reduction experiments were run following the same procedure but for an already calcined catalyst and with a high purity H_2 stream. All experiments were run in a Cahn TG 151 thermal gravimetric analyzer, manufactured by Thermo Cahn, which measures the weight changes of a sample over a given temperature and pressure range under specified reaction conditions. A schematic diagram of the apparatus with its different parts is illustrated in Figure 4.9. The apparatus is composed of three main parts:

- The main frame: supported by a stand and containing a microbalance, a quartz chamber located in a furnace and an elevator used to close the furnace/chamber. Samples are placed in a sample holder suspended from the balance, located in the isothermal zone of the chamber when running experiments.

- The console: the TGA controlling unit is used to control temperature and pressure inside the furnace. It is connected to a computer in which all results are monitored and analyzed by WinTGA software.

- The gas delivery system: gas cylinders and mass control flow meters are used to deliver the required gases at the specified flow rates to the furnace.

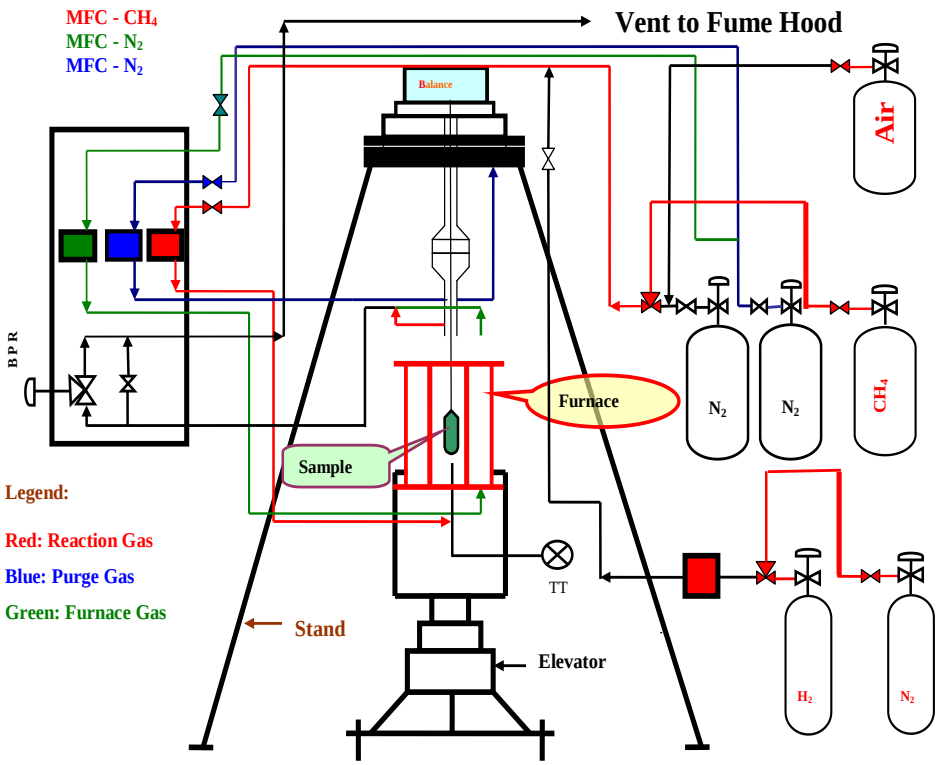

Figure 4.9: A schematic diagram of different parts of the TGA apparatus and different gas paths (adapted from Amin, 2011)

Calcination Temperature by Temperature Program Oxidation (TPO)

For each run, 50 mg of the freshly prepared 15Ni catalyst was pre-weighed and placed in a sample container. The sample was attached carefully to the balance and the elevator was lifted to close the furnace. N_2 gas was introduced to the sample, in addition to other gases; purge gas and furnace gas, which were also N_2. Before starting the temperature ramp, the sample was left to stabilize at room temperature for 10 min. After that, air was introduced and the temperature was ramped at 5°C/min to 800°C. The change in the sample weight according to temperature was recorded by the WinTGA software every 5 sec and is shown in Figure 4.10.

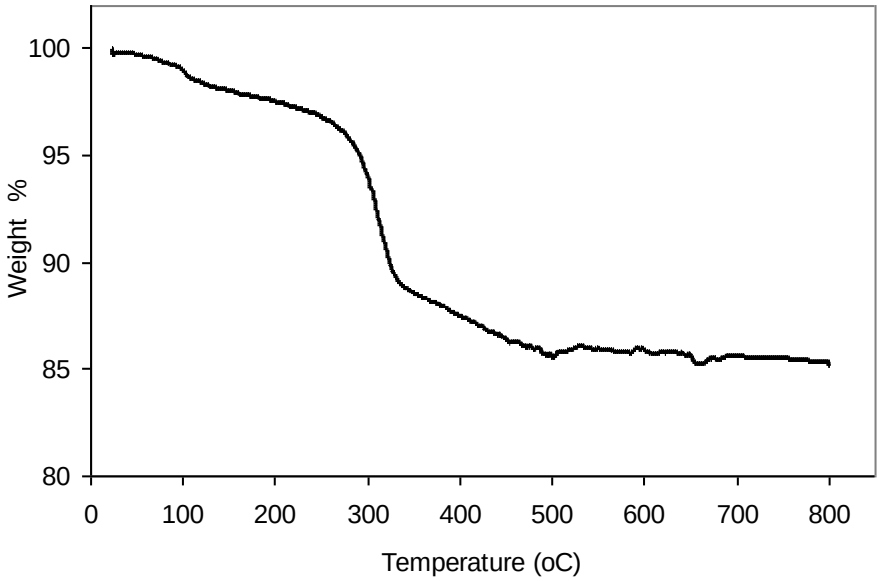

Figure 4.10: Normalized change in a 50 mg 15Ni sample versus temperature during calcination with air in the TGA.

The slight decrease in weight above 100°C is related to H_2O evaporating from the catalyst pores. The sharp decrease at 260°C and decrease at 335°C are due to the decomposition of precursor species or their by-products. It is clear from Figure 4.10 that above 500°C the weight is stable and all undesired precursor compounds were removed. These results are in agreement with TGA TPO experiments run in air for a freshly synthesized 7.6% wt Ni/Al_2O_3 catalyst, reported by Kim et al. (2004).

Temperature-programmed Reduction (TPR)

Since 500°C was determined to be the temperature necessary to remove all precursor residues, the 15Ni catalyst was calcined in an external furnace at 550°C for 1 hour before running TPR experiments. TPR experiments were run in the TGA following the same TPO procedure; however, air was replaced with a 10% mol H_2/N_2 stream. The change in the sample weight with temperature was recorded by the WinTGA software every 5 sec and the results are shown in Figure 4.11.

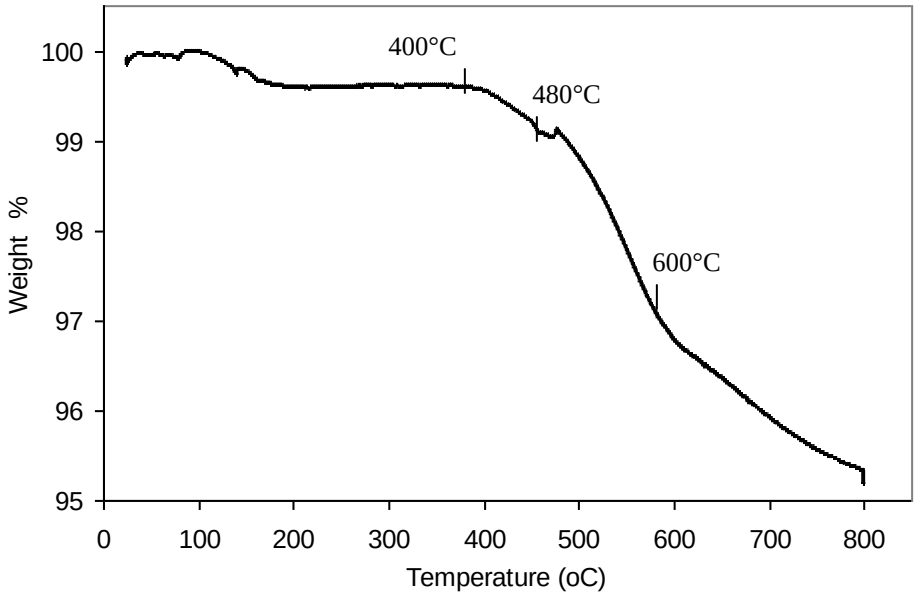

Figure 4.11: TPR run in TGA of a 15Ni catalyst calcined at 550°C for an hour

A slight decrease in weight above 120°C is the result of water evaporation. The weight was then stable, until a slow loss began at about 400°C, which is attributed to the reduction of bulk NiO interacting weakly with the alumina support. As the temperature increased to 480°C, another change in weight loss was detected. This change could be related to the reduction of strong NiO-Al_2O_3 interacting phases. A further change in the graph slope was observed at 600°C and continued to the end of the run at 800°C. This catalyst weight loss was likely attributed to the reduction of the hard to reduce $NiAl_2O_4$ spinel structures, which was observed in XRD pattern, as discussed later in Chapter 7. These structures start to form during Ni catalyst calcination, even at temperatures as low as 450°C (Bartholomew and Farrauto, 2006). These TGA results illustrated that to fully reduce the Ni catalyst, it should be treated with H_2 at temperatures over 800°C. However, heating the catalyst above 700°C will cause a loss in the Ni metal surface area, leading to a lower number of active sites, and hence, lower overall activities (Natesakhawat et al, 2005). Since all of our experiments were run at temperatures below 500°C, the reduction temperature was selected to be 600-650°C. On the other hand, to reduce the probability of the formation of hard to reduce Ni phases, the calcination temperature was kept below 450°C. A detailed investigation on TPR of the selected bimetallic catalysts and the effect

of their metal-support interactions on catalyst activity and stability is discussed in Chapter 7 of the thesis.

4.3.2 Optimizing the Amount of Catalyst in the Reactor and Operating Parameters

In the first couple of experiments with the 15Ni catalyst, 50 mg of the pre-calcined catalyst was used in the reactor, which gave a bed thickness of 1-2 mm. The feed introduced to the reactor was 2 mol% propane + 2 mol% butane with a S/C = 3 and O_2/C = 0.3. The reaction was run at 400°C at atmospheric pressure for two hours. A GC injection from the product stream was taken every 25 min and the results (conversion, H_2, CO, CO_2, CH_4 mol flow rates and carbon balance) were calculated from GC peak areas. Sample calculations of those parameters are given in Appendix A.

Once steady state was reached, the results from this run after 1 hour time-on-stream gave a total conversion higher than 95% with relatively high H_2 product rates. However, due to exothermic oxidation reactions, the temperature measured inside the reactor was always 70°C above the set point for the whole two hour run. This means that the reaction was not running at the set temperature, and also high temperatures could cause hot spots in the reactor and perhaps, a temperature gradient for thicker beds. In addition, at high conversions and product rates it will be hard to distinguish between the activities of different catalysts. In order to reduce the temperature increase in the reactor, silicon carbide (SiC) particles were used as a diluent for the catalyst bed. SiC served as a heat sink, thereby decreasing temperature gradients inside the reactor. SiC was tested in the reactor at the previous conditions and was found to be inert.

In order to determine operating conditions (catalyst:diluent ratio, temperature, S/C, O_2/C) that limit the temperature rise in the bed, while still showing some activity, a set of experiments were run with different parameter combinations. Values for the different parameters tested are shown in Table 4.4.

Table 4.4: Parameter ranges tested to optimise feed compositions and operating conditions for a 2 mol% propane + 2 mol% butane feed

Parameter	Tested values
Amount of catalyst (mg)	100, 50, 30 and 20
Amount of silicon carbide (mg)	500, 1000 and 2000
Temperatures (°C)	360, 380, 400 and 450
S/C	2 and 3
O_2/C	0.15, 0.2 and 0.3

To investigate the effect of different amounts of SiC on catalyst performance, the first set of experiments was run at the previously specified conditions using 50 mg of the 15Ni catalyst at 400°C, S/C = 3 and O_2/C = 0.3, where the temperature rise of the bed was ~55°C. Three experiments were run for three amounts of SiC; 500, 1000 and 2000 mg. The 50 mg in 2000 mg SiC combination was chosen since it had the lowest bed temperature rise (~20°C). At the same conditions two other combinations were tested; 100 mg of catalysts in 2000 mg of SiC and 20 mg of catalyst in 2000 mg of SiC. The first combination gave a high conversion (98%) and a high bed temperature rise, while the 20 mg catalyst combination showed no conversion. However, when using 30 mg of the catalyst in 2000 mg of SiC, a stable run was obtained with a lower conversion (81%) and a lower temperature rise (14°C) than the 50/2000 mg combination. Therefore, the 30/2000 mg combination was used in further preliminarily experiments.

Using 30 mg of catalyst in 2000 mg of SiC, at temperatures lower than 380°C there was no conversion, even at S/C =3 and O_2/C = 0.3. Running experiments at lower S/C and O_2/C ratios (2 and 0.15, respectively) at 400°C did not yield any conversion either. However, increasing the temperature to 450°C and the O_2/C ratio to 0.2 at S/C = 2 gave 89% conversion. It was concluded that 400°C was the lower temperature limit while 2 and 0.2 were the lower limits for S/C and O_2/C ratios, respectively.

4.3.3 Preliminarily Activity Experiments on Selected Bimetallic Catalysts from the Literature

Literature shows a couple of Ni-based catalysts were used for H_2 production from both propane and butane fuels. However, in most of these studies the reaction temperatures were higher than 450°C with a wide range of operating conditions. Also, in most of these studies the catalyst preparation method was either different or not addressed in detail, which makes it difficult to reproduce similar catalyst morphology even for the same loadings. Therefore, it is difficult to select a bimetallic catalyst from the literature without performing some preliminarily experiments to verify the activity and product selectivity results reported in the literature and compare it to our reference 15Ni monometallic catalyst.

Three Ni-based bimetallic catalysts were selected for activity experiments, Co-Ni/Al_2O_3, Mo-Ni/Al_2O_3 and Pt-Ni/Al_2O_3. The Co-Ni catalyst was reported to be active and stable in propane steam reforming (Hardiman et al, 2004), while the Mo-Ni was reported to resist coking during butane steam reforming, but had less activity than the corresponding Ni catalyst (Borowiecki et al, 2002). However, to the best of our knowledge neither of the two catalysts were tested in the presence of O_2, i.e. for oxidative steam reforming, and hence, in both studies the reaction temperature was higher than 500°C to supply enough heat for the endothermic reaction. Pt-based catalysts on different supports were investigated for both fuels. Furthermore, a study by Caglayan et al. (2005) showed that doping a Ni/Al_2O_3 catalyst with 0.2 % wt Pt improved the activity and H_2 production of propane OSR under different operating conditions.

All three bimetallic catalysts were prepared by co-impregnating the two precursor salts at the same time on alumina in distilled water. Precursor salts for different metals were supplied by Alfa Aesar and they were: $Ni(NO_3)_2.6H_2O$, $Co(NO_3)_2{\cdot}6H_2O$, $(NH_4)_6Mo_7O_{24}.4H_2O$ and $(NH_3)_4Pt(NO_3)_2$. When sequential impregnation was used to prepare bimetallic catalysts, a monometallic Ni catalyst was first prepared and calcined (as described in detail in Chapter 3, Section 3.1). Then, the second metal was impregnated on

it by dissolving the metal salt in distilled water with the Ni catalyst. From there, the same steps were followed to obtain the final catalysts.

Activity experiments were run in the experimental setup described in detail in Chapter 3. The reactor was loaded with 30 mg of each catalyst diluted in 2000 mg of silicon carbide. Prior to each run the tested catalyst was reduced in a 30 mol% H_2/N_2 stream at 650°C. The fuel composition was 2 mol% propane + 2 mol% butane. All reactions were run at 450°C, S/C = 2 and O_2/C = 0.2 at atmospheric pressure. These conditions were selected to ensure a stable run, reduce the temperature gradient resulting from oxidation reactions and obtain an activity spectrum to compare the catalysts. A GC injection from the product stream was taken every 25 min and the catalyst evaluation parameters (conversion, H_2, CO, CO_2, CH_4 mol flow rates in mol/min × 10^{-5}) were calculated from GC peak areas at the fourth injection, i.e. after 75 min from introducing the feed. The fourth injection was selected as all experiments reached steady-state by then. Conversions and products flow rates for the catalysts at different loadings are presented in Table 4.5; all bimetallic catalysts were prepared by the co-impregnation procedure.

Table 4.5: Activity obtained during preliminarily runs for selected bimetallic catalysts at different loadings, products flow rates are in mol/min × 10^5

Catalyst loading wt %	Conversion %	H_2	CO	CO_2	CH_4
15Ni	89.9 ±0.7	93.2 ±1.3	4.36 ±0.1	49.8 ±1.3	49.9 ±2.5
5Co-10Ni	73.4 ±1.1	87.1 ±1.5	4.11 ±0.2	45.2 ±1.7	30.2 ±2.4
2Co-13Ni	91.5 ±1.1	96.2 ±1.5	4.68 ±0.2	51.6 ±1.7	47.5 ±2.4
0.5Co-15Ni	87 ±1.1	88.6 ±1.5	4.28 ±0.2	48.6 ±1.7	47.2 ±2.4
2Mo-13Ni	0	0	0	0	0
0.5Mo-15Ni	77.1 ±1.2	122 ±2.3	15.2 ±0.9	47.1 ±1.2	27.2 ±1
3Pt-14Ni	23.5 ±1.7	32.6 ±2.8	0.6 ±0.3	22.9 ±2.1	3.11 ±2.7
1Pt-15Ni	90 ±1.7	96.1 ±2.8	4.0 ±0.3	52.1 ±2.1	49.4 ±2.7
0.5Pt-15Ni	87.1 ±1.7	104 ±2.8	3.9 ±0.3	51.6 ±2.1	48.3 ±2.7

Lowering the O_2/C ratio to 0.2 did decrease the temperature inside the reactor to only 8°C above the set point. In general, Ni-Co catalysts did not show a significant effect on the conversion or product flow rates compared to the un-promoted 15Ni catalyst. In fact, higher Co loadings caused a decrease in the fuel conversion. The higher Mo loading (2% Mo) resulted in no reaction. However, when Mo loadings were decreased to 0.5 wt%, high hydrogen production was observed even at lower conversions. In addition, the CO production was notably higher than any other catalysts listed in Table 4.6. The higher 3 wt% Pt loading led to lower conversion and products flow rates, while 1 wt% Pt gave almost the same results as 15Ni. Decreasing the Pt loading to 0.5 did not have a significant effect on conversion, however, H_2 production increased from 93×10^{-5} mol/min for the 15Ni catalyst to 104×10^{-5} mol/min for the Pt-promoted catalyst. Since the 0.5Mo-15Ni and the 0.5Pt-15Ni catalysts produced higher H_2, they were selected for further investigation.

The effect of the metal impregnation method on the activity of the two selected bimetallic catalysts was investigated. A batch from each catalyst was prepared by sequentially impregnating the precursor salt of the metal over the 15Ni calcined catalyst. Experiments were run for these two catalysts under exactly the same operating conditions as specified earlier for runs in Table 4.5. Conversions and product flow rates from the two impregnation methods for the two bimetallic catalysts are compared in Table 4.6. The sequentially impregnated 15Ni-0.5Mo catalyst showed higher activity than the co-impregnated one. It had a slight increase in conversion and in both H_2 and CO production. The 15Ni-0.5Pt catalysts also led to higher conversion, but the H_2 production was reduced. However, for both bimetallic catalysts, the resulting pellets after drying, pressing and sieving, were fragile and easy to break when mixed with SiC. This led to a non-uniform particle size distribution in the catalyst bed. On the other hand both bimetallic catalysts produced from co-impregnation had a solid consistent structure after drying, and were meshed without pressing. The two catalysts retained their particle size even after running the experiments. Therefore, in order to keep a consistent reproducible

bed for each run, all bimetallic catalysts in the study were prepared by the co-impregnation method described earlier.

Table 4.6: Activity preliminarily runs for selected bimetallic catalysts prepared with different impregnation methods, product flow rates are in mol/min × 10^{-5}

Catalyst loading wt %	Impregnation method	Conversion %	H_2	CO	CO_2	CH_4
15Ni	---	89.9 ±0.7	93.2 ±1.3	4.36 ±0.1	49.8 ±1.3	49.9 ±2.5
0.5Mo-15Ni	co-impregnation	77.1 ±1.2	122 ±2.3	15.2 ±0.9	47.1 ±1.2	27.2 ±1
15Ni-0.5Mo	sequential-impregnation	81	130 ±2.3	19 ± 0.9	48.7 ±1.2	38.4 ±1
0.5Pt-15Ni	co-impregnation	87.1 ±1.7	104 ±2.8	3.9 ±0.3	51.6 ±2.1	48.3 ±2.7
15Ni-0.5Pt	sequential-impregnation	89.4	94 ±2.8	4.03 ±0.3	49.2 ±2.1	50.6 ±2.7

In order to ensure the reproducibility of the co-impregnation preparation method, two batches of a bimetallic catalyst were prepared and were tested at experimental conditions. The results for these batches reproducibility tests are given in Appendix B.

Chapter 5
Catalyst Screening for LPG Oxidative Steam Reforming

The aim of the screening study is to identify a promising catalyst system(s) for the oxidative steam reforming (OSR) of LPG mixtures consisting mainly of propane and butane gases. When selecting a catalyst, five important criteria are usually considered: activity, selectivity, stability, mechanical strength and cost. In this screening study the first three criteria were considered to compare between different chosen catalysts. The importance of these three criteria rises from their direct effect on capital and operating costs. The activity of the catalyst affects the size of the reactor, while the selectivity will determine the separation, recycling and by-product management units of the process. However stability of the catalyst is also at the top of the list, as in many catalytic processes activity and selectivity will be sacrificed to keep the catalyst active, to avoid high costs associated with shutdown and start up phases of the process.

Based on the literature review presented in previous chapters, and based on the preliminary tests described in Chapter 4, Pt-Ni was chosen to be further investigated during the catalyst screening test. Considering cost issues associated with noble metals, a relatively cheap metal that showed promising results when added in small amounts during the preliminary tests, and was reported in the literature to be effective in coke resistance during butane steam reforming, was Mo. Therefore Mo-Ni bimetallic catalysts were also considered in the screening tests. These two bimetallic catalysts were compared to a monometallic 15% wt Ni catalyst. To keep an equivalent comparison basis at this stage of the study, Al_2O_3 was used as the support for all catalysts.

5.1 Methodology & Experimental Parameters

It is important when comparing catalysts to maintain equivalent conditions, while at the same time different parameters need to be considered. Therefore, when designing experiments for catalyst comparison they should cover representative ranges of important experimental variables. Another important principle in experimental design is to consider statistical evaluation of the experimentally collected data. This statistical analysis is important to determine the accuracy, precision and reproducibility of the data. Bearing these two important principles in mind, and in order to reduce the number of experimental runs, the screening study was conducted on the basis of a statistical factorial experimental design with two levels. Although this design could not fully explore a wide range in each factor space, it indicates major trends, and so determines promising directions for further experimentation.

In the experimental design four factors were considered: temperature, steam to carbon ratio (S/C), oxygen to carbon ratio (O_2/C) and loading of the metals in the catalysts. The first three factors are the most frequent parameters considered in the literature when investigating OSR reactions and found to have significant effects on conversion of the fuel and product distributions (Wang et. al, 2007). Based the results of Chapter 2, two levels of each factor were identified, a high level and a low level. A center point between the two levels was also identified for each factor. Center point experiments were repeated three times to account for variances between different runs. Different factors with their levels, center points and notations used in the factorial experimental design for the metal catalysts are presented in Table 5.1.

Table 5.1 High and Low levels for different factors considered in the factorial experimental design

Factor	Notation	High level (+)	Low level (-)	Center point (0)
Temperature (°C)	T	450	400	425
Steam: Carbon ratio (S/C)	S	3.5	2	2.5
Oxygen: Carbon ratio (O/C)	O	0.6	0.2	0.3
Loadings of the metal (wt %)	L	0.8Mo-15Ni 1Pt-15Ni	0.3Mo-15Ni 0.2Pt-15Ni	0.3Mo-15Ni 0.5Pt-15Ni

The high temperature level was limited to 450°C to avoid homogenous thermal cracking of butane in the LPG mixture. Also rapid start-up and shutdown is a critical property considered for fuel cell application reformers and thus it is desirable to operate at a reforming temperature as low as possible. Preliminarily experiments showed that at high Mo loadings, the LPG mixture could not light off at 380°C. Therefore, the low temperature level was kept at 400°C. When reviewing the literature, the common S/C ratio used for propane OSR or SR was 3, while for butane SR it was around 5. Therefore, the high S/C ratio level was chosen to be 3.5 while the low was 2 to be higher than the stoichiometric S/C ratio for SR of both fuels. To avoid high temperature gradients in the reactor, the high O_2/C ratio was chosen to be 0.6 which is slightly higher than the stoichiometric value for both fuels (0.5). The low O_2/C level was 0.2, which is necessary for light off at lower temperatures levels.

The fourth factor in Table 5.1 is metal loadings for the Pt-Ni and Mo-Ni bimetallic catalysts. These loadings were chosen based on preliminarily tests for both catalysts, as presented in Chapter 4. All catalysts were prepared following the method described in detail in Chapter 3 (section 3.1). The bimetallic catalysts were prepared by co-impregnating the metal salt and the Ni salt for the specified loading. Experiments were run in the setup described in detail in Chapter 3. For each run 30 mg of the required catalyst was mixed with 2000 mg of silicon carbide to reduce temperature gradients and hot spots at high O_2/C ratio levels. The catalyst mixture was then loaded in the 9 mm ID quartz reactor and prior to the actual run it was reduced at 650°C for 30 min with a 30% vol. H_2/N_2 stream. The reactor was then cooled down to the reaction temperature in a N_2 stream. After flushing the GC with N_2, the specified feed was introduced and the first GC injection was taken after 10 min from feed introduction. After reaching steady state, the results of the 4^{th} GC injection, i.e. after 85 min from introducing the feed, were collected and analyzed for each run. The feed to all runs consisted of 2 % vol propane + 2% vol butane, and when varying the S/C and O_2/C factors. A 361,300 ml/hr.g_{cat} GHSV was kept constant in all runs by adjusting the N_2 flow rate.

5.2 Factorial Design Analysis of the 15% Ni/Al_2O_3 Catalyst

The 2^3 two level factorial experiment results for the 15Ni catalyst are shown in Table 5.2. The total conversion of propane and butane, and gas product compositions were calculated as illustrated in the sample calculation sheet in Appendix A. Compositions of all gases are given in mol% of dry gas in the product and compared to the equilibrium values for each condition. Equilibrium values for conversions and product gases were calculated based on minimizing the Gibbs free energy using AspenPlus^{TM} software package (following the same procedure described in the thermodynamic study in Chapter 4). Under the specified conditions for the factorial design, the main gas products were H_2, CO, CO_2 and CH_4. Traces of other hydrocarbons were negligible as the carbon atomic balance was 98% ± 3, in addition O_2 was totally consumed in all runs.

In the 2^3 factorial analyses, the three factors considered were T, S and O for the five responses (conversion, H_2 %, CO%, CO_2% and CH_4%). For each of the 5 responses, the main factor effect (T, S, O), two factor interactions (TS TO, SO), and three factor interactions (TSO) were calculated. These calculations were done by constructing a contrast coefficient table for each response (Box, 2005). Different factor effects on an individual response were analyzed first then an integral analysis of the effect of the factors on the reaction products distribution was discussed.

Table 5.2: Experimental and equilibrium results for different factorial design experiments of the 15Ni catalyst

Data	T	S	O	Conv.	H_2	CO	CO_2	CH_4
Equil. Mol%				100	9.8	0.22	6.7	9.0
Exp. Mol%	400	2	0.2	55.0	7.5	0.13	5.3	3.7
Equil. Mol%				100	14.4	0.66	7.3	7.1
Exp. Mol%	450	2	0.2	89.9	12.9	0.61	6.9	6.9
Equil. Mol%				100	16.3	0.21	9.5	10.4
Exp. Mol%	400	3.5	0.2	70.9	14.1	0.16	8.4	7.4
Equil. Mol%				100	23.1	0.62	10.5	7.4
Exp. Mol%	450	3.5	0.2	90.6	21.6	0.55	10.0	7.9
Equil. Mol%				100	9.8	0.25	10.5	6.4
Exp. Mol%	400	2	0.6	89.7	12.9	0.51	10.7	4.6
Equil. Mol%				100	14.5	0.69	10.9	4.7
Exp. Mol%	450	2	0.6	96.1	15.9	1.05	10.9	3.2
Equil. Mol%				100	16.1	0.25	14.5	7.6
Exp. Mol%	400	3.5	0.6	91.7	20.3	0.54	14.6	4.3
Equil. Mol%				100	22.7	0.67	15.0	4.9
Exp. Mol%	450	3.5	0.6	96.2	25.7	0.96	15.2	3.2
Error				± 0.6	± 0.2	± 0.01	± 0.2	± 0.4

The conversion contrast coefficient table is shown in Table 5.3. The first row is a column number to keep track of it in the explanation. Column (1) in the table represents the run number, followed by three columns labeled as T, S and O that define the design matrix of the 2^3 factorial design. The four columns after that, which are labeled as TS, TO, SO and TSO, represent the two and three factor interactions. The signs for these interactions are simply obtained by multiplying the signs of there individual factors. The 9^{th} column shows the results for the response that is being discussed, in this case total conversion. To calculate the average effect of each factor (whether is it a main, two interaction or three interaction), first the conversion of each run is multiplied by the sign of the factor. Then for each factor (columns 10 to 16), the conversions are summed and the average effect is obtained by dividing the summation by 4 since each effect is a difference between two averages, one from 4 high level observations and the other from 4 low level observations. The effect of each factor is shown in the last row of Table 5.3.

Table 5.3: A 2^3 factorial analysis contrast coefficient table to calculate main factors and their interaction effects on the conversion of 15Ni

1	2	3	4	5	6	7	8	9	10	11	12	13	14	15	16
Run	T	S	O	TS	TO	SO	TSO	Total conv.	T	S	O	TS	TO	SO	TSO
1	-1	-1	-1	1	1	1	-1	55.05	-55.1	-55.1	-55.1	55.1	55.1	55.1	-55.1
2	1	-1	-1	-1	-1	1	1	89.92	89.9	-89.9	-89.9	-89.9	-89.9	89.9	89.9
3	-1	1	-1	-1	1	-1	1	70.87	-70.9	70.9	-70.9	-70.9	70.9	-70.9	70.9
4	1	1	-1	1	-1	-1	-1	90.58	90.6	90.6	-90.6	90.6	-90.6	-90.6	-90.6
5	-1	-1	1	1	-1	-1	1	89.69	-89.7	-89.7	89.7	89.7	-89.7	-89.7	89.7
6	1	-1	1	-1	1	-1	-1	96.08	96.1	-96.1	96.1	-96.1	96.1	-96.1	-96.1
7	-1	1	1	-1	-1	1	-1	91.67	-91.7	91.7	91.7	-91.7	-91.7	91.7	-91.7
8	1	1	1	1	1	1	1	96.16	96.2	96.2	96.2	96.2	96.2	96.2	96.2
								Sum	65.6	18.5	67.2	-17.1	-43.7	-14.4	13.3
								Effect	16.36	4.632	16.79	-4.26	-10.9	-3.6	3.318

A method was developed to evaluate the effect of each factor, in order to determine whether the effect is real or a result of noise and uncertainty in the experiments. The method is based on measuring the deviation of the effect within the 95% confidence interval and the standard error (Box, 2005). Center points were chosen for each factor (Table 5.1) and runs were repeated three times at these center points as shown in Table 5.4. Error variance and standard error in conversion were calculated for the center point runs. The standard error for each response was assumed to be that calculated at the center points.

Table 5.4: Replicates of center point runs and the standard error for each response of the 15Ni catalysts, at 425°C. S/C = 2.5 and O_2/C = 0.3

	Conversion	H_2	CO	CO_2	CH_4
Equilibrium Mol%	100	14.40	0.39	8.87	7.67
Run # 1	89.87	14.63	0.45	8.96	6.95
Run # 2	89.33	14.56	0.45	8.88	6.37
Run # 3	90.50	14.97	0.44	9.19	7.09
Standard Error (SD)	0.58	0.22	0.01	0.16	0.39

Assuming a normally identical and independent distribution (NIID), the ratio of the effect over the SD will have a t distribution with 3 degrees of freedom, in this case, since the SD was calculated from the repetition of three runs. Referring to the statistical table for a t distribution (Box, 2005), a significant value of t at the 5% level with 3 degrees of freedom is 3.18. Therefore, the 95% confidence interval for an effect is given by:

$SD \times 3.18$

This will be for the conversion effect:

$0.58 \times 3.18 = 1.84$

Table 5.5 shows each factor and its effect deviation calculated for the total conversion of each run: although the effects of all factors were higher than the effect deviation, it was clear that the effect of T, O and their combination, TO, on conversion was higher than the effect of S. However, the S and the TS effects are significantly higher than the deviation and should also be considered.

Table 5.5: The effect of each factor on conversion over 15Ni and its 95% confidence interval

Factor	Effect and deviation
Main Effects	
Temperature, T	16.4 ± 1.8
Steam to carbon ratio, S	4.6 ± 1.8
Oxygen to carbon ratio, O	16.8 ± 1.8
Two factor interaction:	
TS	-4.3 ± 1.8
TO	-10.9± 1.8
SO	-3.6 ± 1.8
Three factor interaction:	
TSO	3.3 ± 1.8

The effects of T and O cannot be individually interpreted since their interaction TO have a significant effect on conversion. A better understanding of the TO interaction effect can be represented by a simple contrast diagram, as shown in Figure 5.1. The diagram is obtained by averaging conversion values for the same T and O levels at different S levels.

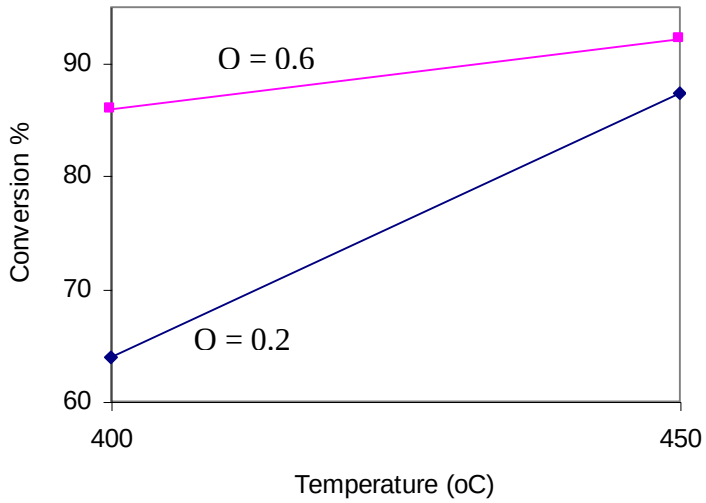

Figure 5.1: A contrast diagram of the TO interaction effect on the total conversion of the 15Ni catalyst

It is clear from Figure 5.1 that the conversion increases significantly when both factors are at low levels and one of them is increased to a higher level. While increasing a factor from a low level to a high level when operating at a high level of either factor will result in a slight increase in conversion. i.e. if the experiment is operated at O = 0.6, which is a high O level, then increasing the T form 400 to 450 will slightly increase the conversion, while increasing T from 400 to 450 at an operating condition of O= 0.2 will increase the conversion dramatically. Looking at the factorial design for different reaction products will help to explain the TO effect on conversion in terms of the role of different reactions taking place.

Similarly, the contrast diagram in Figure 5.2 was constructed to represent the TS interaction effect on conversion. In this interaction effect, the conversion increases significantly when both factors are at low levels and one of them is increased to a higher level. When operating at a high S level, increasing T will have a lower effect as the conversion increased only by 10% compared to 20% when operating at 400°C. On the other hand the diagram showed that when operating at high T the conversion is independent of the S/C ratio.

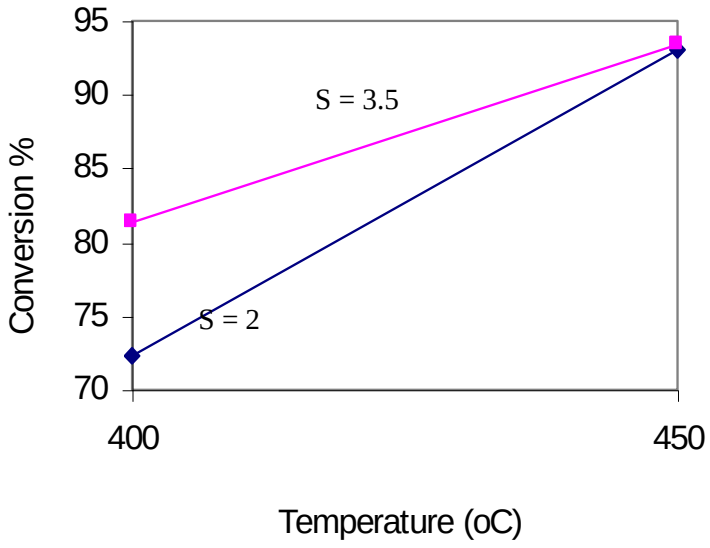

Figure 5.2: A contrast diagram of the TS interaction effect on the total conversion of the 15Ni catalyst

The factorial design contrast coefficient tables for mol% of the four reaction products were constructed and analyzed in the same way done for the total conversion, and hence, only effects deviation tables will be given for each product. All results for different gas products are given in mol% of dry product stream. Table 5.6 shows all five responses; the total conversion and the four reaction products, with their effect deviation calculated for each factor in the factorial design for the 15Ni catalyst.

Table 5.6: The effect of each factor on different products over the 15Ni catalyst and their 95% confidence interval (bold being significant)

	Effect and deviation				
Factor	Conv. %	H_2 mol%	CO mol %	CO_2 mol%	CH_4 mol%
Main Effects :					
Temperature, T	**16.4 ± 1.8**	**5.34 ± 0.69**	**0.46 ± 0.02**	1.0 ± 0.51	0.28 ± 1.23
Steam to carbon ratio, S	**4.6 ± 1.8**	**8.14 ± 0.69**	-0.02 ± 0.02	**3.6 ± 0.51**	1.08 ± 1.23
Oxygen to carbon ratio, O	**16.8 ± 1.8**	**4.63 ± 0.69**	**0.40 ± 0.02**	**5.2 ± 0.51**	**-2.7 ± 1.23**
Two factor interaction:					
TS	**-4.3 ± 1.8**	1.1 ± 0.69	**-0.05 ± 0.02**	0.14 ± 0.51	-0.61± 1.23
TO	**-10.9± 1.8**	-1.11± 0.69	0.02 ± 0.02	-0.6 ± 0.51	-1.6 ± 1.23
SO	-3.6 ± 1.8	0.46± 0.69	-0.01 ± 0.02	0.52 ± 0.51	-1.3 ± 1.23
Three factor interaction:					
TSO	3.3 ± 1.8	0.07± 0.69	-0.01 ± 0.02	0.12 ± 0.51	0.81 ± 1.23

Looking at the H_2 effect deviation column in Table 5.6, it is clear that H_2 production is affected by the three main effects individually and not by their interactions. All three factors had a positive effect, which indicates a direct proportional relationship to the H_2 mol% produced. However, the S factor had the highest effect among all three, supporting the suggestion that most of the H_2 in OSR reactions is produced by steam reforming reactions for both butane and propane. That being said, increasing T for the endothermic steam reforming reaction will result in an increase in both steam reforming products: H_2 and CO. This observation is also clear from the CO effect column in Table 5.6 as the T factor has a main effect. However, the effect of T on CO can not be discussed individually since, the TS interaction is higher than the deviation and hence, a two factor interaction should be considered. The contrast diagram of the TS interaction effect on CO is shown in Figure 5.3. The diagram shows a major effect of T on CO % when increased to higher level regardless of S. In fact, at the high T level increasing S had a negative effect on CO %. This probably occurs because of higher water gas shift reaction rates at

higher steam concentrations in the feed. Higher water gas shift reaction rates at high S resulted in a major positive effect of S on CO_2 production as indicated in Table 5.6

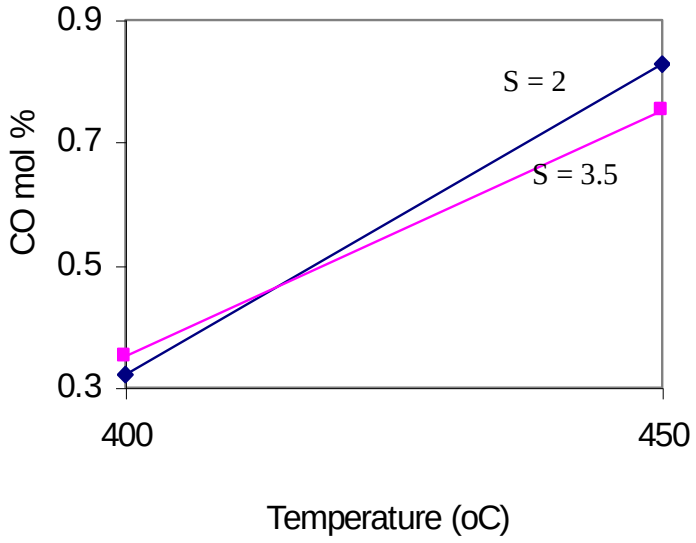

Figure 5.3: A contrast diagram of the TS interaction effect on CO mol % of the 15Ni catalyst

All products were positively affected by the O factor as all product effects were significantly higher than their deviations. This could be a result of the large difference between the two chosen levels for the O_2/C ratios. As the lower level was 0.2, which was below the stoichiometric value of the partial oxidation reaction (0.5) for both fuels, while the higher level (0.6) was above that value. The higher production rate of CO and CO_2 is from the addition of more O_2. Also, increasing the rate of the highly exothermic oxidation reaction will supply more heat for the endothermic steam reforming reaction and therefore increases the H_2 production rate. Indeed, for all high level O_2 runs (the last four runs in Table 5.2) the temperature measured inside the reactor bed was around 30°C above the set point for both temperature levels, 400 and 450°C, even with using silicon carbide particles as a heat sink.

A general suggested scheme of reactions taking place during OSR reforming for saturated hydrocarbons given in the literature is:

$$C_aH_b + a\ H_2O = a\ CO + (\frac{b}{2} + a)\ H_2 \quad (5.1)$$

$$C_aH_b + \frac{a}{2}\ O_2 = a\ CO + \frac{b}{2}\ H_2 \quad (5.2)$$

$$CO + H_2O = CO_2 + H_2 \quad (5.3)$$

$$CO + 3\ H_2 = CH_4 + H_2O \quad (5.4)$$

The above reaction scheme was used as a model by Recupero et al. (2005) to calculate thermodynamic values of H_2 at different conditions for propane OSR over a Pt/CeO_2 catalyst. It was also suggested by Dinka and Mukasyan (2007) to express OSR of jet fuel on complex $LaFeO_3$ based catalysts with a variety of noble and non-noble metal additives including, Co, Mo and Pt. Nagaoka et al. (2007) added the dry reforming reaction to the scheme and used it for screening different supported nickel catalysts in butane OSR.

According to the reaction scheme, in addition to the steam reforming reaction (5.1) and the partial oxidation reaction (5.2), H_2 is also produced from the water gas shift reaction (5.3) which is thermodynamically controlled. The fourth reaction (5.4) in the scheme is the methanation reaction which consumes H_2. The methanation reaction has long been known as a clean up reaction in ammonia synthesis; recently it has also been used to clean hydrogen streams in PEM fuel cells. It is the reversed methane steam reforming reaction and hence it is an exothermic reaction with $-\Delta H^{\circ}_{298} = 206$ kJ/mol.

If the scheme above is assumed to take place, the H_2 is assumed to form through these reactions. Therefore, theoretically, the H_2 content in the product can be calculated from the measured amounts of CO, CO_2 and CH_4 in the product and O_2 fed in the feed. If this

H_2 calculated amount was to agree with the measured H_2 downstream, then indeed the given scheme is followed (Dink and Mukasyan, 2007).

H_2 can be calculated in the product, applying the concept of extent of reaction to the following multiple reaction scheme:

$$\xi_1 C_aH_b + a\xi_1 H_2O = a\xi_1 CO + \xi_1 (\frac{b}{2} + a) H_2 \quad (5.5)$$

$$\xi_2 C_aH_b + \frac{a}{2}\xi_2 O_2 = a\,\xi_2 CO + \xi_2 \frac{b}{2} H_2 \quad (5.6)$$

$$x\,CO + x\,H_2O = x\,CO_2 + x\,H_2 \quad (5.7)$$

$$z\,CO + 3z\,H_2 = z\,CH_4 + z\,H_2O \quad (5.8)$$

Where ξ_1 is the extent of reaction (5.5) and ξ_2 is the extent of reaction (5.6)

Directly from equation (5.7), since it is the only equation that contains CO_2:

CO_2 out = CO_2 in + x

But CO_2 in= 0 → $\boxed{CO_2 \text{ out} = x}$

Similarly from equation (5.8):

$\boxed{CH_4 \text{ out} = z}$

For CO:

CO out = CO in + $a\xi_1$ + a ξ_2 - x – z

But CO in = 0

CO out = $a\xi_1$ + a ξ_2 - x – z (5.9)

For O_2:

O_2 out = O_2 in - $\frac{a}{2}\xi_2$

If all O_2 is totally consumed then O_2 out = 0

O_2 in = $\frac{a}{2}\xi_2$ (5.10)

For H_2:

H_2 out = H_2 in + ξ_1 ($\frac{b}{2}$ + a) + ξ_2 $\frac{b}{2}$ + x – 3z also H_2 in = 0

H_2 out = ξ_1 ($\frac{b}{2}$ + a) + ξ_2 $\frac{b}{2}$ + x – 3z (5.11)

Now : x and z values are already known and rearranging Eq. (5.10):

$$\xi_2 = \frac{2}{a}\ O_2 \text{ in}$$

Substituting for ξ_2 in Eq. (5.9) and solving for ξ_1 :

$$\xi_1 = \frac{CO_{out} + x + z - 2O_2}{a}$$

Substituting for ξ_1, ξ_2, x and z in Eq. (5.11) and rearranging:

$$H_2 = CO \text{ out } (\frac{b}{2a} + 1) + CO_2 \text{ out } (\frac{b}{2a} + 2) + CH_4 \text{ out } (\frac{b}{2a} - 2) - 2\ O_2 \text{ in} \quad (5.12)$$

Applying the suggested scheme and equation (5.12) to both propane and butane OSR:

$C_3H_8 + 3H_2O = 3CO + 7H_2$ (5.13)

$$C_3H_8 + 1.5\ O_2 = 3CO + 4H_2 \quad (5.14)$$

$$C_4H_{10} + 4H_2O = 4CO + 9H_2 \quad (5.15)$$

$$C_4H_{10} + 2O_2 = 4CO + 5H_2 \quad (5.16)$$

$$CO + H_2O = CO_2 + H_2 \quad (5.17)$$

$$CO + 3\ H_2 = CH_4 + H_2O \quad (5.18)$$

Equation (5.12) for propane with a = 3 and b = 8 is:

$$H_2 = 2.33\ CO + 3.33\ CO_2 - 0.67\ CH_4 - 2\ O_2 \quad (5.20)$$

Equation (5.12) for butane with a = 4 and b = 10 is:

$$H_2 = 2.25\ CO + 3.25\ CO_2 - 0.75\ CH_4 - 2\ O_2 \quad (5.21)$$

Although in all screening tests the ratio of propane to butane was 1:1, looking at the scheme of the two fuels, the ratios of CO and H_2 produced and O_2 consumed are slightly different. Moreover if O_2 was not totally consumed, then the term O_2 out should be included in both equations (5.20 and 5.21). Accounting for the ratios of each gas and assuming a 1:1 ratio for CO_2 and CH_4 Equations (5.20) and (5.21) will be:

$$H_2\ prop = 0.93\ CO + 1.67\ CO_2 - 0.33\ CH_4 - 0.86\ (O_2\ in - O_2\ out) \quad (5.22)$$

$$H_2\ but = 1.35\ CO + 1.62\ CO_2 - 0.38\ CH_4 - 1.14\ (O_2\ in - O_2\ out) \quad (5.23)$$

And hence if the suggested reaction scheme is followed then:

H_2 exp = H_2 propane from Eq. (5.22) + H_2 butane from Eq. (5.23) (5.24)

Calculating H_2 from equations (5.22) and (5.23) and then adding them, H_2 calculated and H_2 experemental for each run in the factorial design is added to Table 5.2. The H_2 calculated and H_2 experemental columns together with their error are shown in Table 5.7. Excluding the first run, it is clear that there is a good agreement between H_2 exp. and H_2 calc. which indicates that indeed the suggested scheme is followed at the given conditions for the 15Ni catalyst. What characterizes the first run is the lower conversion obtained (55%) because of the combined operating conditions of low temperature, low S/C and low O_2/C. Conversions far from equilibrium conversion indicate that other reactions, not taken into account in the suggested reaction mechanism, play an important role, thus the larger error in predicting H_2 production.

Table 5.7: Comparing H_2 production rates in mol/min for different runs of the factorial design for the 15Ni catalyst

Data	Conv.	H_2	CO	CO_2	CH_4	T	S	O	H_2 exp. mol/min	H_2calc mol/min	Error H_2 %
Equl. Mol%	100	9.8	0.22	6.73	9.01						
Exp. Mol%	55.1	7.5	0.13	5.3	3.7	400	2	0.2	49.1	54.0	9
Equl. Mol%	100	14.4	0.66	7.3	7.14						
Exp. Mol%	89.9	12.9	0.61	6.9	6.9	450	2	0.2	93.2	92.9	-0.3
Equl. Mol%	100	16.3	0.21	9.5	10.4						
Exp. Mol%	70.9	14.2	0.17	8.4	7.4	400	3.5	0.2	73.7	74.4	0.9
Equl. Mol%	100	23.1	0.62	10.5	7.42						
Exp. Mol%	90.6	21.7	0.55	10	7.9	450	3.5	0.2	127.6	122.7	-3.8
Equl. Mol%	100	9.77	0.25	10.5	6.44						
Exp. Mol%	89.7	12.9	0.51	10.7	4.6	400	2	0.6	86.0	85.6	-0.5
Equl. Mol%	100	14.5	0.69	10.9	4.69						
Exp. Mol%	96.1	15.9	1.05	10.9	3.2	450	2	0.6	109.1	110.0	0.8
Equl. Mol%	100	16.1	0.25	14.5	7.56						
Exp. Mol%	91.7	20.3	0.54	14.6	4.3	400	3.5	0.6	106.1	106.4	0.2
Equl. Mol%	100	22.8	0.68	15	4.87						
Exp. Mol%	96.2	25.7	0.96	15.3	3.2	450	3.5	0.6	145.4	147.1	1.2

5.3 Factorial Design Analysis of the Mo-15% Ni/Al_2O_3 Catalyst

For this catalyst the same two level factorial design as for the 15Ni catalyst was used. In our preliminarily experiments a 0.5% Mo-15Ni catalyst was used, therefore two loadings of Mo were prepared and tested, 0.3Mo and 0.8Mo wt%. As shown in Table 5.8 by performing a couple of runs at different conditions the high level Mo loading catalyst lost activity after a specific period of time, preventing us from constructing a complete factorial design table that accounts for two levels of Mo loadings. Therefore, at this stage of the study the factorial design analysis was done only for the 0.3 Mo loading. Center point runs for the 0.3Mo catalyst are shown in Table 5.9.

Table 5.8: Experimental and equilibrium results for different factorial design experiments of the 0.3Mo and 0.8Mo catalysts

	0.3Mo								0.8Mo				
	Conv.	H_2	CO	CO_2	CH_4	T	S	O	Conv.	H_2	CO	CO_2	CH_4
Equl. Mol%	100	9.79	0.22	6.73	9.01								
Exp. Mol%	61.8	12.1	1.7	5.5	3.6	400	2	0.2		lost	activity	30	min
Equl. Mol%	100	14.4	0.66	7.33	7.14				100	14.4	0.66	7.33	7.14
Exp. Mol%	86.0	16.9	1.9	6.8	4.5	450	2	0.2	66.4	16.6	3.2	5.3	2.0
Equl. Mol%	100	16.3	0.21	9.52	10.4								
Exp. Mol%	65.7	20.2	1.8	8.3	3.8	400	3.5	0.2					
Equl. Mol%	100	23.1	0.62	10.5	7.41				100	23.1	0.62	10.5	7.41
Exp. Mol%	85.3	27.7	1.9	10	3.4	450	3.5	0.2	42.7	20.6	4.3	6.1	0.75
Equl. Mol%	100	9.77	0.25	10.5	6.44								
Exp. Mol%	70	14.7	2.4	9.6	1.1	400	2	0.6					
Equl. Mol%	100	14.5	0.69	10.9	4.69								
Exp. Mol%	88.0	19.7	2.7	10.4	1.1	450	2	0.6					
Equl. Mol%	100	16.1	0.25	14.5	7.56								
Exp. Mol%	64.3	17.9	2.7	11.9	0.44	400	3.5	0.6		lost	activity	10	min
Equl. Mol%	100	22.8	0.67	15	4.86								
Exp. Mol%	82.3	24.6	2.7	13.2	0.43	450	3.5	0.6		lost	activity	10	min

Table 5.9: Replicates of center point runs and the standard error for each respond of the 0.3Mo catalyst, at 425°C. S/C = 2.5 and O_2/C = 0.3

	Conv.	H_2	CO	CO_2	CH_4
Equilibrium	100	14.4	0.39	8.87	7.67
Run # 1	80.6	19.0	1.98	8.26	3.12
Run # 2	82.4	18.76	1.85	8.30	3.24
Run # 3	81.8	18.39	1.80	8.15	3.01
Standard Error (SD)	0.90	0.30	0.10	0.10	0.11

Similar to the 15Ni catalyst, a 2^3 factorial design was applied to study the effect of temperature (T), steam to carbon ratio (S) and oxygen to carbon ratio (O) on five responses: conversion and the four main product mol compositions (H_2, CO, CO_2 and CH_4). The same statistical analysis and calculations were followed to construct the effect and deviation table (Table 5.10) for the 0.3Mo catalyst factorial design. It is clear from Table 5.10 that conversion in the case of the Mo catalyst is a strong function of T as the deviation in the T factor is significantly higher than other factors. Also from Table 5.8 for similar conditions of S and O the conversion at 450°C is about 20% higher than that at 400°C. On the other hand, regardless of the S or O values, the variation in conversion for the same T is less than 5%.

To better interpret these effect results, Table 5.11 was used to compare the factorial design runs for the 0.3Mo catalyst and the 15Ni catalyst. Excluding the first run in Table 5.11, where all factors were at low levels, the Mo catalyst always had a lower conversion than 15Ni and these differences were higher at low T.

Table 5.10: The effect of each factor on conversion and mol % of different products over the 0.3Mo catalyst and their 95% confidence interval

	Effect and deviation				
Factor	Conv. %	H_2 mol%	CO mol %	CO_2 mol%	CH_4 mol%
Main Effects :					
Temperature, T	**20.2 ± 2.8**	**6 ± 0.97**	0.19 ± 0.3	**1.27 ± 0.26**	0.11 ± 0.35
Steam to carbon ratio, S	-1.8 ± 2.8	**6.78 ± 0.97**	0.08 ± 0.3	**2.76 ± 0.26**	-0.54 ± 0.35
Oxygen to carbon ration, O	1.2 ± 2.8	-0.02 ± 0.97	**0.81 ± 0.3**	**3.61 ± 0.26**	**-3.07 ± 0.35**
Two factor interaction:					
TS	-1.4 ± 2.8	1.08 ± 0.97	-0.1± 0.3	0.23 ± 0.26	-0.31 ± 0.35
TO	-1.7 ± 2.8	-0.2 ± 0.97	-0.03 ± 0.3	-0.2 ± 0.26	-0.11 ± 0.35
SO	-3.4 ± 2.8	**-2.71 ± 0.97**	0.05 ± 0.3	-0.3 ± 0.26	-0.09 ± 0.35
Three factor interaction:					
TSO	0.89 ± 2.8	-0.26 ± 0.97	-0.04± 0.3	0 ± 0.26	0.3 ± 0.35

Table 5.11: Comparing the results of factorial experiments of the 0.3Mo catalyst to 15Ni

	15%Ni								0.3% Mo				
Data	Conv.	H_2	CO	CO_2	CH_4	T	S	O	Conv.	H_2	CO	CO_2	CH_4
Equl.	100	9.8	0.22	6.73	9.01				100	9.79	0.22	6.73	9.01
Exp.	55.1	7.5	0.13	5.3	3.7	400	2	0.2	61.8	12.1	1.7	5.5	3.6
Equl.	100	14.4	0.66	7.3	7.14				100	14.4	0.66	7.33	7.14
Exp.	89.9	12.9	0.61	6.9	6.9	450	2	0.2	86.0	16.9	1.9	6.8	4.5
Equl.	100	16.3	0.21	9.5	10.4				100	16.3	0.21	9.52	10.4
Exp.	70.9	14.2	0.17	8.4	7.4	400	3.5	0.2	65.7	20.2	1.8	8.3	3.8
Equl.	100	23.1	0.62	10.5	7.42				100	23.1	0.62	10.5	7.41
Exp.	90.6	21.7	0.55	10	7.9	450	3.5	0.2	85.3	27.7	1.9	10	3.4
Equl.	100	9.77	0.25	10.5	6.44				100	9.77	0.25	10.5	6.44
Exp.	89.7	12.9	0.51	10.7	4.6	400	2	0.6	70	14.7	2.4	9.6	1.1
Equl.	100	14.5	0.69	10.9	4.69				100	14.5	0.69	10.9	4.69
Exp.	96.1	15.9	1.05	10.9	3.2	450	2	0.6	88.0	19.7	2.7	10.4	1.1
Equl.	100	16.1	0.25	14.5	7.56				100	16.1	0.25	14.5	7.56
Exp.	91.7	20.3	0.54	14.6	4.3	400	3.5	0.6	64.3	17.9	2.7	11.9	0.44
Equl.	100	22.8	0.68	15	4.87				100	22.8	0.67	15	4.86
Exp.	96.2	25.7	0.96	15.3	3.2	450	3.5	0.6	82.3	24.6	2.7	13.2	0.43

The H_2 production rate was affected by T and S as those two factors boost the endothermic steam reforming reaction. Although, unlike the 15Ni catalyst, the O factor had a minor negative effect on H_2 production, the SO interaction effect was significant. To better visualize the SO interaction effect on H_2 %, a contrast diagram was constructed in Figure 5.4. The diagram shows that S has a stronger effect on H_2 than O, as increasing S to higher levels increased H_2 % for both O levels. However, at high S levels increasing O had a negative effect on H_2 %, while the same change had a small positive effect in the case of the 15Ni catalyst. This can be illustrated by comparing the highest H_2 % in all runs for both catalysts; it was at high levels of T (450) and S (3.5) and the low level of O (0.2) for the 0.3Mo catalyst, while it was at high levels of all three factors for 15Ni.

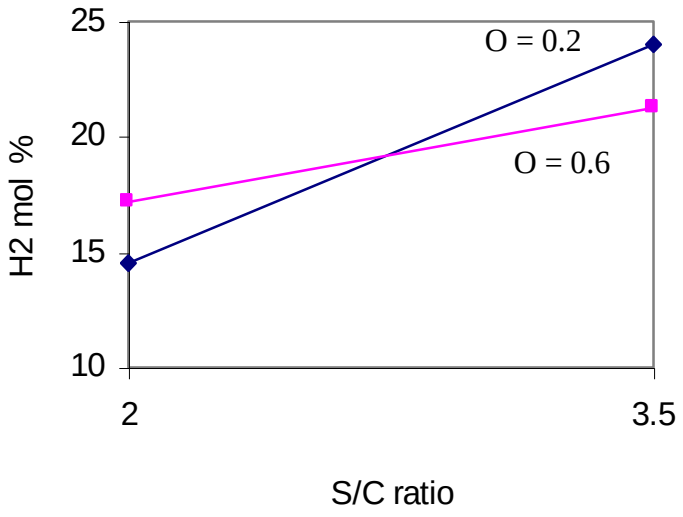

Figure 5.4: A contrast diagram of the SO interaction effect on H_2 mol % of the 0.3Mo catalyst

In fact, the H_2 % was higher for the Mo catalyst than the 15Ni except for the last two runs in Table 5.11. In these two runs the S and the O factors were at high levels for both temperatures. Another interesting observation for these last two runs in Table 5.11 is that like the H_2 %, the CO_2 % was lower for both runs compared to that of the 15Ni catalyst, while the CO_2 % in all other six runs was almost the same for both catalysts. This may indicate that under these conditions the catalyst does not favour the water gas shift

reaction as the CO % was not lower than other runs at high O levels. Both runs were repeated to ensure that these profiles were consistent. These observations do not only show that high O levels have a negative effect on H_2 production, but perhaps also on the stability of the 0.3Mo catalyst.

An important result from comparing the two catalysts is that for all runs in Table 5.11 the CO % from the 0.3Mo catalyst was higher than that of the 15Ni catalyst, while the CH_4 % was lower. This may indicate that the Mo catalyst does not favour the methanation reaction. and thus impedes further reaction of CO. In fact, further experiments (as described in Chapter 6) proved that methanation rate over Mo was very similar to that over the 15Ni catalyst. The explanation for the higher CO selectivity over the Mo catalyst will be given in Chapter 7.

Assuming that OSR for propane and butane over the 0.3Mo catalyst follows the reaction scheme given before, H_2 experimental, H_2 calculated and their error are given in Table 5.12 for each run. The results were in good agreement at higher S levels, while high O and low S resulted in more deviation from the scheme regardless of T, indicating the contribution of other reactions at these higher O levels, which are perhaps the total oxidation of the fuels to CO_2 and H_2O that was not included in the suggested scheme.

Table 5.12: Comparing H_2 production rates in mol/min for different runs of the factorial design for the 0.3Mo catalyst

Data	Conv.	H_2	CO	CO_2	CH_4	T	S	O	H_2 exp. mol/min	H_2calc mol/min	Error H_2 %
Equl. Mol%	100	9.79	0.22	6.73	9.01						
Exp. Mol%	61.8	12.1	1.7	5.5	3.6	400	2	0.2	79.25	84.18	6
Equl. Mol%	100	14.4	0.66	7.33	7.14						
Exp. Mol%	86.0	16.9	1.9	6.8	4.5	450	2	0.2	125.8	129.2	2.6
Equl. Mol%	100	16.3	0.21	9.52	10.4						
Exp. Mol%	65.7	20.2	1.8	8.3	3.8	400	3.5	0.2	111.3	112.1	0.7
Equl. Mol%	100	23.1	0.62	10.5	7.41						
Exp. Mol%	85.3	27.7	1.9	10	3.4	450	3.5	0.2	172.4	170.9	-0.8
Equl. Mol%	100	9.77	0.25	10.5	6.44						
Exp. Mol%	70	14.7	2.4	9.6	1.1	400	2	0.6	99.30	108.7	9
Equl. Mol%	100	14.5	0.69	10.9	4.69						
Exp. Mol%	88.0	19.7	2.7	10.4	1.1	450	2	0.6	142.6	151.5	6
Equl. Mol%	100	16.1	0.25	14.5	7.56						
Exp. Mol%	64.3	17.9	2.7	11.9	0.44	400	3.5	0.6	88.13	87.3	-0.9
Equl. Mol%	100	22.8	0.67	15	4.86						
Exp. Mol%	82.3	24.6	2.7	13.2	0.43	450	3.5	0.6	132.5	129	-2.7

5.4 Factorial Design Analysis of the Pt-15% Ni/Al_2O_3 Catalyst

A two level factorial design was also used to investigate and compare the activity of a Pt-containing catalyst to the 15Ni catalyst. In the preliminarily experiments for this catalyst different loadings of Pt were investigated, keeping these loadings as low as possible to account for the high cost of Pt. The loadings that were investigated were: 0.2, 0.5, 1 and 3% wt. The 3% loading showed a significant decrease in conversion and products compared to the three other loadings, and therefore was excluded. The other three loadings had comparable performance, with 0.5% showing intermediate results between the two other loadings. Therefore, the two Pt loadings that were chosen for the factorial design were; 0.2% as a low level (-) and 1% as a high level (+), while the other factors; T, S and O were the same as previously chosen for the other catalysts.

Catalysts at the two selected loadings were prepared following the co-impregnation method described earlier. The results of the 8 runs at each condition are compared to

those of the 15Ni catalyst are shown in Table 5.13. For each of the five considered responses different results were obtained for each loading under the conditions tested. This variation was also observed when comparing each loading to the 15Ni catalyst. In order to account for the variations related to Pt loadings and their interactions with the operational factors, a 2^4 factorial design was applied to include the loading factor (L) with a low level (-) at 0.2% Pt and a high level (+) at 1% Pt. The basis of the statistical analysis and calculations were the same as that illustrated earlier for the 2^3 factorial design. The center point runs were repeated three times at a Pt loading of 0.5% wt and are shown with the standard error for each response in Table 5.14. After constructing the contrast coefficient table and calculating the 95% confidence interval for each response, the main effects and their interactions for each response are summarized in Table 5.15.

Table 5.13: Comparing the results of factorial experiments of the 0.2Pt and 1Pt catalysts to the 15Ni catalyst

	0.2Pt								15Ni								1Pt				
	Conv.	H_2	CO	CO_2	CH_4	T	S	O	Conv.	H_2	CO	CO_2	CH_4	T	S	O	Conv.	H_2	CO	CO_2	CH_4
Equl. Mol%	100	9.79	0.22	6.73	9.01				100	9.8	0.22	6.73	9.01				100	9.79	0.22	6.73	9.01
Exp. Mol%	47.65	5.87	0.07	4.4	2.5	400	2	0.2	55.1	7.5	0.13	5.3	3.7	400	2	0.2	29.75	4.9	0.06	3.9	1.5
Equl. Mol%	100	14.4	0.66	7.33	7.14				100	14.4	0.66	7.3	7.14				100	14.4	0.66	7.33	7.14
Exp. Mol%	87.87	17.7	0.53	7.0	6.3	450	2	0.2	89.9	12.9	0.61	6.9	6.9	450	2	0.2	90.37	13.3	0.56	7.2	6.8
Equl. Mol%	100	16.3	0.21	9.52	10.4				100	16.3	0.21	9.5	10.4				100	16.3	0.21	9.52	10.4
Exp. Mol%	64.43	10.1	0.12	7.0	5.4	400	3.5	0.2	70.9	14.2	0.17	8.4	7.4	400	3.5	0.2	50.81	10	0.07	6.2	3.7
Equl. Mol%	100	23.1	0.62	10.5	7.42				100	23.1	0.62	10.5	7.42				100	23.1	0.62	10.5	7.42
Exp. Mol%	92.57	23.7	0.53	10.7	6.9	450	3.5	0.2	90.6	21.7	0.55	10	7.9	450	3.5	0.2	93.33	22.5	0.6	10.2	9.1
Equl. Mol%	100	9.77	0.25	10.5	6.44				100	9.77	0.25	10.5	6.44				100	9.77	0.25	10.5	6.44
Exp. Mol%	65.69	10.2	0.3	10.2	1.8	400	2	0.6	89.7	12.9	0.51	10.7	4.6	400	2	0.6	83.38	11	0.3	10.1	4.9
Equl. Mol%	100	14.5	0.69	10.9	4.69				100	14.5	0.69	10.9	4.69				100	14.5	0.69	10.9	4.69
Exp. Mol%	81.1	16.1	0.92	11.0	1.84\	450	2	0.6	96.1	15.9	1.05	10.9	3.2	450	2	0.6	92.46	19.3	1.07	11.2	4.3
Equl. Mol%	100	16.1	0.25	14.5	7.56				100	16.1	0.25	14.5	7.56				100	16.1	0.25	14.5	7.56
Exp. Mol%	89.21	19.4	0.4	14.6	4.0	400	3.5	0.6	91.7	20.3	0.54	14.6	4.3	400	3.5	0.6	89.82	18.8	0.41	14.4	5.0
Equl. Mol%	100	22.8	0.68	15	4.87				100	22.8	0.68	15	4.87				100	22.8	0.68	15	4.87
Exp. Mol%	95.74	25.6	0.97	15.1	3.7	450	3.5	0.6	96.2	25.7	0.96	15.3	3.2	450	3.5	0.6	94.99	23	0.89	14.8	4.2

Table 5.14: Replicates of center point runs and the standard error for each respond for a 0.5 % Pt-15 %Ni catalyst, at 425°C. S/C = 2.5 and O_2/C = 0.3

	Conv.	H_2	CO	CO_2	CH_4
Equilibrium	100	14.4	0.39	8.87	7.67
Run # 1	87.1	15	0.37	8.3	5.7
Run # 2	90.3	15.1	0.45	8.7	6.5
Run # 3	89.11	15.6	0.4	8.49	6.1
Standard Error (SD)	1.62	0.32	0.04	0.2	0.4

Under the examined conditions none of the five responses were affected by the Pt loading. The effect of loading appears mostly in the interaction term with O_2/C, which is not surprising since Pt is an oxidizing catalyst. Considering the cost factor this suggests that the optimized Pt loading may fall below 0.2 wt%. T, S and O had a major effect on conversion, H_2 % and CO_2 %. The effect of T and O was higher on conversion than S, and they should not be analyzed individually, since their interaction, TO, had a significant effect on conversion also. The contrast diagram for the TO interaction effect on conversion is shown in Figure 5.5. The diagram shows that when either factor is at low levels, increasing to high level will cause a dramatic increase in conversion. This is expected as Pt is a well known oxidation catalyst. However the effect of increasing temperature was not that significant at the high O level, as increasing O at high T did not have any effect on conversion. This TO interaction effect was the same for 15Ni as discussed in section 5.2. However, increasing both factors to high levels had a lower effect on conversion, while at high T increasing O still had a small positive effect, which means that at high T lower amounts of O_2 are needed for the Pt catalyst to achieve the same conversion of 15Ni. This is an indication of higher oxidation rates over the Pt catalyst at high T, as expected. The ability of Pt to oxidize propane and transfer that heat of oxidation to Ni sites for steam reforming was indeed suggested by Caglayan et al. (2005) in their study of propane reforming over a Ni-Pt/Al_2O_3 catalyst.

Table 5.15: The effect of each factor on conversion and mol % of different products over the Pt-Ni catalyst and their 95% confidence intervals

	Effect and deviation				
Response	Conv. %	H_2 mol%	CO mol %	CO_2 mol%	CH_4 mol%
Main Effects :					
Temperature, T	**25.96 ± 5.15**	**8.86 ± 1.02**	**0.54 ± 0.13**	**2.06 ± 0.64**	1.81 ± 1.27
Steam to carbon ratio, S	**11.58 ± 5.15**	**6.86 ± 1.02**	0.02 ± 0.13	**3.5 ± 0.64**	1.51 ± 1.27
Oxygen to carbon ratio, O	**16.95 ± 5.15**	**4.44 ± 1.02**	**0.34 ± 0.13**	**5.59 ± 0.64**	-1.56 ± 1.27
Loading, L (+)1Pt, (-)0.2Pt	0.08 ± 5.15	-0.74 ± 1.02	0.01 ± 0.13	-0.25 ± 0.64	0.88 ± 1.27
Two factor interaction:					
TS	-5.37 ± 5.15	0.26 ± 1.02	-0.04 ± 0.13	0.13 ± 0.64	-0.35 ± 1.27
TO	**-16.91 ± 5.15**	**-2.73 ± 1.02**	0.07 ± 0.13	**-1.34 ± 0.64**	-2.2 ± 1.27
TL	3.38 ± 5.15	-0.52 ± 1.02	0.02 ± 0.13	0.15 ± 0.64	0.55 ± 1.27
SO	0.2 ± 5.15	0.73 ± 1.02	0 ± 0.13	0.61 ± 0.64	-0.49 ± 1.27
SL	-3.33 ± 5.15	-0.38 ± 1.02	-0.03 ± 0.13	-0.21 ± 0.64	-0.38 ± 1.27
OL	7.15 ± 5.15	0.95 ± 1.02	0 ± 0.13	0.15 ± 0.64	0.88 ± 1.27
Three factor interaction:					
TSO	2.17 ± 5.15	-1.21 ± 1.02	-0.04 ± 0.13	-0.38 ± 0.64	0.21 ± 1.27
TSL	-0.13 ± 5.15	-0.27 ± 1.02	-0.02 ± 0.13	-0.12 ± 0.64	0.33 ± 1.27
TOL	-5.31 ± 5.15	0.65 ± 1.02	-0.01 ± 0.13	-0.1 ± 0.64	-0.81 ± 1.27
SOL	-3.97 ± 5.15	-1.41 ± 1.02	-0.03 ± 0.13	0.04 ± 0.64	-0.63 ± 1.27
Four factor interaction:					
TSOL	1.37 ± 5.15	-0.84 ± 1.02	-0.04 ± 0.13	-0.02 ± 0.64	-0.31 ± 1.27

Interestingly, promoting the Ni catalyst with Pt had no effect on fuel conversion. In fact, for almost all runs in Table 5.13 the conversion of the 15Ni catalyst was higher than that of 0.2Pt, while the conversion over the 1Pt catalyst was only higher than 15Ni at the fourth run, which was at higher levels of T and S, and low O.

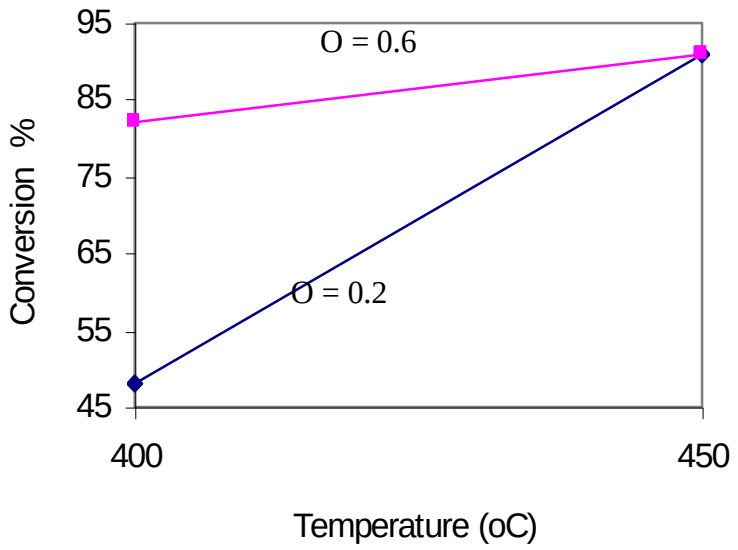

Figure 5.5: Contrast diagram of the TO interaction effect on the total conversion of the Pt-Ni catalyst

The three factors T, S and O also had a major effect on H_2 %. However, unlike the 15Ni catalyst where the S factor had the highest effect, in the case of the Pt promoted catalyst H_2 % was more affected by T. This observation also supports the suggestion that Pt particles work as micro heat exchangers, providing heat for the steam reforming reaction that is responsible for producing most of the H_2 during OSR (Caglayan et al, 2005). The effect of O and T are combined since their interaction was higher than the deviation. The contrast diagram for the TO interaction (Figure 5.6) shows a similar behaviour to that of TO effect on conversion. However, for H_2 %, increasing O at the high T level did have a slight positive effect. This is because at high O a higher amount of H_2 is produced from partial oxidation reactions.

Similar to the 15Ni catalyst, CO % was affected by T and O but not by their interaction, however, the effect of T was more significant than O. On the other hand, unlike all responses, CO_2 % was more affected by O than T. The effect of TO interaction was also significant on CO_2 % and is illustrated by the contrast diagram in Figure 5.7. The figure indeed shows a higher dependence of CO_2 % on O_2 % compared to T. In fact

at high O levels, CO_2 is almost independent of T. This is expected as Pt-based catalysts are known to be widely used as oxidation catalysts in automotive emission control at low T. CO_2 % was also positively affected by S as more steam shifts the water gas shift reaction towards producing more CO_2 and H_2.

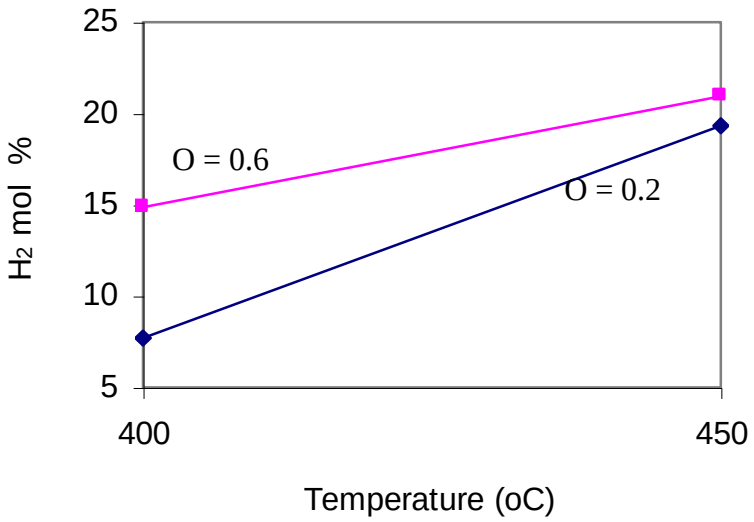

Figure 5.6: A contrast diagram of the TO interaction effect on H_2 mol % from the Pt-Ni catalyst

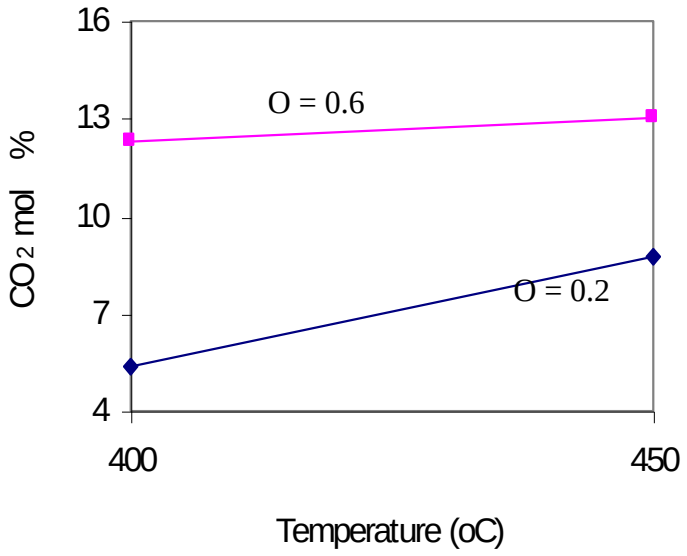

Figure 5.6: A contrast diagram of the TO interaction effect on H_2 mol % from the Pt-Ni catalyst

5.5 Stability Screening Experiments

In the previous sections of this chapter the comparison of the screened catalysts focused on the activity of the catalysts under different operating conditions, and the selectivity of each catalyst to different products under these conditions. In addition to a high activity and selectivity to desired products, the ability of an OSR catalyst to sustain stable activity is a key factor in promoting the catalyst for any application.

After long detailed studies on Ni-based steam reforming catalysts, Trimm (1999) stated that "Catalyst deactivation- either by coke formation or by thermal sintering- is a fact of life with steam reforming catalysts". In addition to coking and thermal sintering, Ni reforming catalysts can be deactivated by oxidation of the active metal phase to non-active phases [Tsipouriari et al. (1998); Bradford and Vannice (1999); Bengaard et al. (2002); Natesakhawat et al. (2005)]. However, coking is the main type of deactivation attacking reforming Ni based catalysts especially at higher hydrocarbon feeds (Bartholomew and Farrauto, 2006).

In this section the promoted screened catalysts were subjected to time-on-stream experiments. Time-on-stream experiments for the 1% Pt-15%Ni/Al_2O_3 (1Pt), 0.3% Mo-15% Ni/Al_2O_3 (0.3Mo) and 15%Ni/Al_2O_3 (15Ni) catalysts were run at 450°C, S/C = 3 and O_2/C = 0.3. These conditions are similar to the center point runs of the factorial analysis, except that the S/C ratio was increased from 2.5 to 3 since it is more commonly used in the literature. To ensure thermal stability of the catalysts, they were calcined in an external furnace at 700°C for 3 hr and left to cool down to room temperature before storage. Prior to each run the catalyst was reduced in-situ at 750°C for 30 min in a 10 % vol H_2/N_2 mixture, then cooled down to 450°C under a N_2 flow. Each experiment was run for 18 hours continuously, with product samples analyzed every 23 min by the GC.

Figure 5.8 shows the change in the total conversion of the three catalysts with time during the 18 hour runs, while Figures 5.9, 5.10, 5.11 and 5.12 represents production rates in mol/min × 10^{-5} of H_2, CO, CO_2 and CH_4, respectively. At the first 2 hours, the conversion and product flow rate trends were similar to those of the center points of the factorial experiments for each catalyst. The 1Pt and 15Ni conversions were almost the same, while the 0.3Mo conversion was 5-8% lower. H_2 and CO were higher for the 0.3Mo catalyst while CH_4 was lower. During the first two hours, product rates of the 15Ni and the 1Pt catalysts did not show any significant differences, a result which is in good agreement with the results of the factorial experiments of these two catalysts.

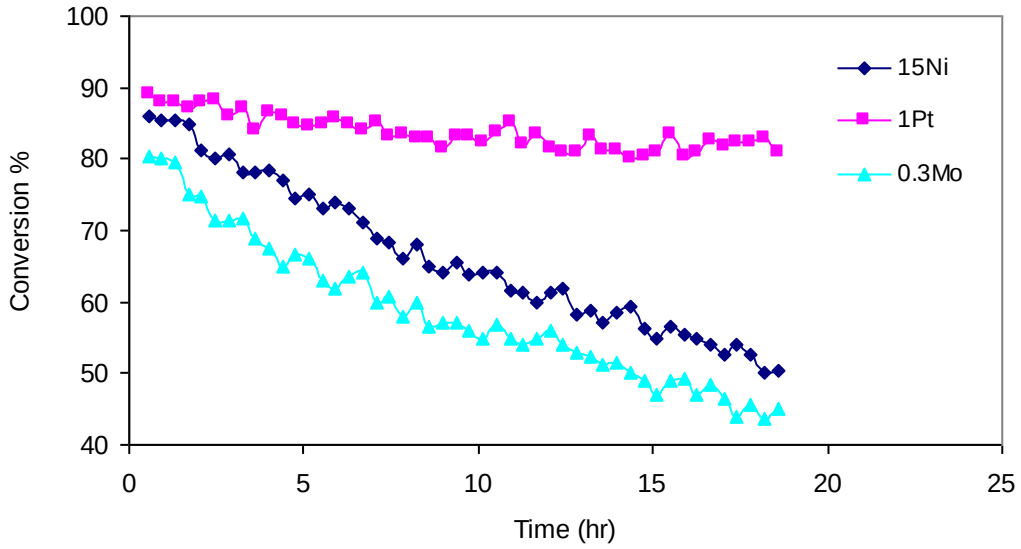

Figure 5.8: Total conversion as a function of time from 18 hours stability experiments of the three catalysts, at 450°C, S/C = 3 and O_2/C = 0.3

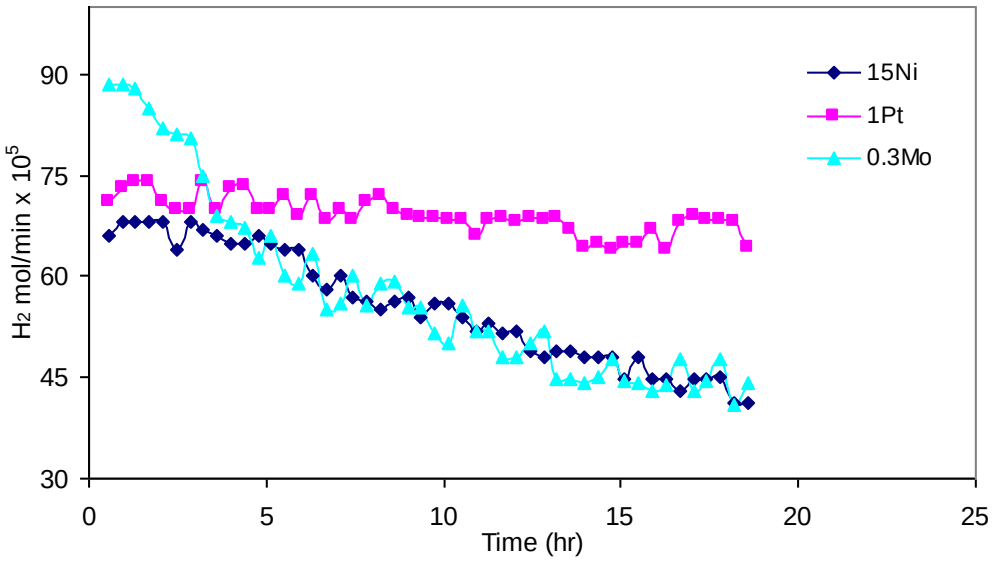

Figure 5.9: H_2 production rate as a function of time from 18 hours stability experiments of the three catalysts, at 450°C, S/C = 3 and O_2/C = 0.3

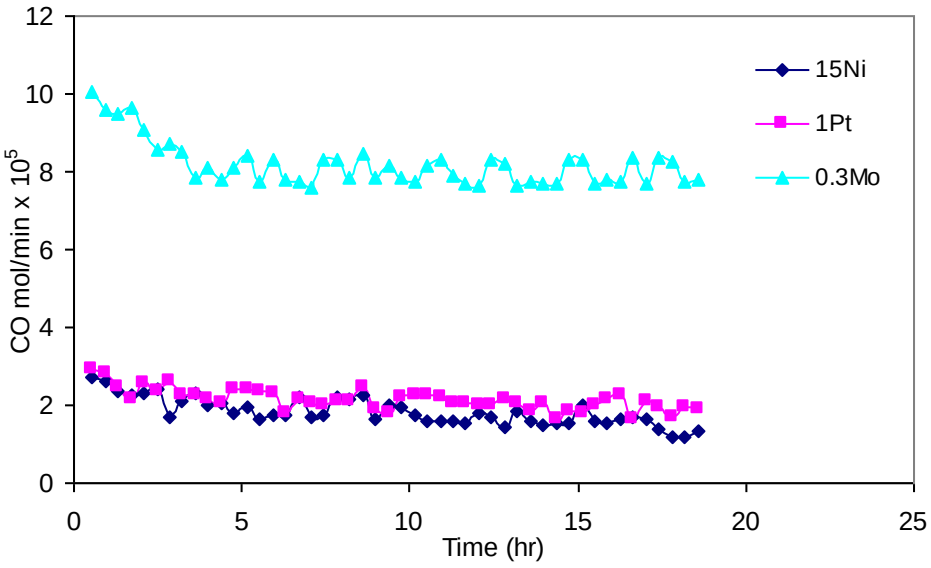

Figure 5.10: CO production rate as a function of time from 18 hours stability experiments of the three catalysts, at 450°C, S/C = 3 and O_2/C = 0.3

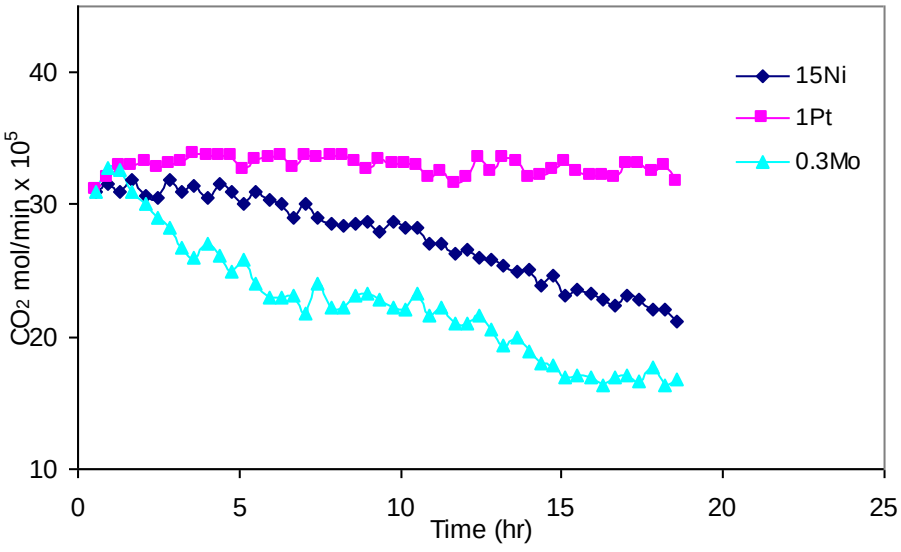

Figure 5.11 CO_2 production rate as a function of time from 18 hours stability experiments of the three catalysts, at 450°C, S/C = 3 and O_2/C = 0.3

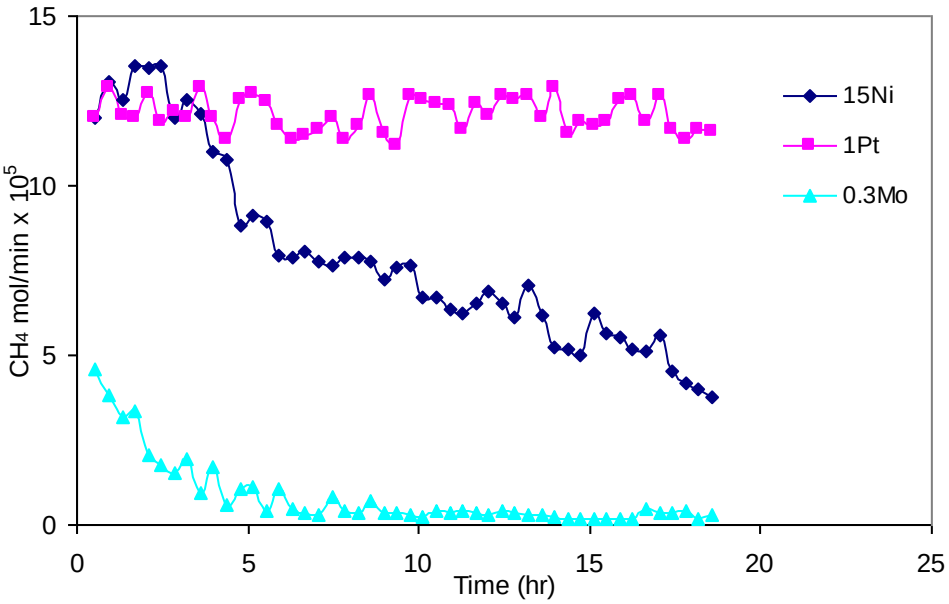

Figure 5.12 CH_4 production rate as a function of time from 18 hours stability experiments of the three catalysts, at 450°C, S/C = 3 and O_2/C = 0.3

After the 3rd hour, the conversion over the 15Ni sample began to decrease gradually, indicating loss of activity, and reached 50% by the 18th hour. This decrease in conversion was accompanied by a decrease in the production rate of the products. The decrease in the conversion of the 0.3Mo catalyst began even earlier, at the 2nd hour, to reach 45% by the end of the run. Product flow rates also decreased with time for the 0.3Mo catalyst, with CH_4 reaching a minimum value at the 9th hour. On the other hand, the Pt catalyst sustained a relatively constant conversion throughout the experiment period. All product rates were also stable for the 1Pt catalyst.

After each run the reactor was cooled down to room temperature under a N_2 flow and the catalyst bed was weighed. As expected carbon deposition could be visually detected over the 15Ni catalyst, with the bed weight increasing by 70%. Carbon formation on Ni catalysts during SR is a function of different factors. These factors include: catalyst structure, process feed, operating conditions and reactor design. Carbon formation can be

limited by designing a reactor with minimum void space to eliminate the occurrence of homogenous cracking of hydrocarbons. In our case, homogenous reactions for propane and butane were eliminated by lowering the reaction temperature to 450°C as shown in Chapter 4. In OSR processes, formation of carbon results from a balance between reactions that produce gaseous carbon precursors and the gasification of these precursors or carbon by H_2O, O_2 and H_2. Since thermal cracking of the fuels was not expected to occur, coking of the Ni catalyst under these experimental conditions were thought to be mainly caused by catalytic cracking of propane, butane and probably other smaller unsaturated hydrocarbons. Another reaction that may deposit carbon during OSR over Ni catalysts is the Boudouard reaction:

$$2CO \longleftrightarrow C + CO_2 \qquad (5.25)$$

However, the contribution of this reaction to carbon deposition is not expected to be significant, as the reaction is more active at lower temperatures and lower S/C ratios. Carbon deposition resulting from hydrocarbon cracking can have different forms, these include, gaseous carbon, carbon films, carbon fibres and whiskers and encapsulating carbon (Trimm, 1999). Each form of carbon has different reactivity towards gasifying agents. However, it should be noted that not all these types cause the deactivation of Ni catalysts. While encapsulating carbon are the hardest to gasify and cause direct deactivation of Ni sites, Ni particles continue to be active on tip of whiskers. However, higher whisker volumes will led to unacceptable pressure build ups in the reactor causing the process to be shut down.

As expected, no carbon deposition was detected on the 1Pt catalyst. Although the Pt catalyst did not show a significant effect on the activity and product distribution of the of the Ni catalyst, the promoting effect of Pt is obvious in sustaining the Ni catalyst activity. The role of Pt in resisting coking of Ni-Pt catalysts was discussed in the literature to some extent; however, different explanations were suggested for this role. In the early investigations on the resistance of a 15.7% wt Ni-0.5% wt Pt/Al_2O_3 catalyst to carbon deposition, Gardner and Bartholomew (1981) suggested that the addition of Pt reduces

the solubility of carbon in Ni particles. This leads to a lower rate of atomic carbon transformation to polymeric, hard to remove carbon. This suggestion was also confirmed later by other researchers; Bradford and Vannice (1996), Rostrup-Nielsen and Alstrup (1999) and Pompeo et al. (2007). In their earlier study, Gardner and Bartholomew (1981) also suggested that Pt may also act as a promoter for hydrogenation of atomic carbon at intermediate temperatures because of its well known ability to activate H_2. On the other hand, other studies on promoting Ni-based OSR catalysts with Pt suggested that Pt plays a textural role, in which it increases the degree of Ni dispersion providing smaller Ni ensembles not suitable for carbon formation [Dias and Assaf (2004); Lee et. al. (2009)].

Surprisingly, when examining the 0.3Mo catalyst after the 18 hour run, no carbon deposition was observed (through bed weight measurement and TPO) on the catalyst and there was no increase in the bed weight. A repeat of the 0.3Mo stability experiment was run, and the same trends were obtained again with no carbon deposition. It is clear that the 0.3Mo catalyst has the ability to resist carbon formation over the Ni catalysts even at this small loading; however, the catalyst activity was affected by a different type of deactivation. Perhaps the catalyst may have thermally degraded, or some non-active catalytic phase could have formed under the reaction conditions. The cause of deactivation of Ni- Mo catalysts at higher Mo loadings will be investigated in details in chapter 7 of this thesis.

Factorial experiments of Ni-Mo catalysts showed that for the higher Mo loading catalyst, 0.8% wt, Mo did not sustain activity under most of the examined conditions. However, under some conditions, even at low conversions, the catalyst had high H_2 production rates. When the loading of the catalyst was lowered to 0.3% wt Mo, the catalyst was more stable and sustained its higher H_2 rates. This led us to suggesting that lowering the loading of Mo under 0.3 % wt. may improve the catalyst stability while sustaining the Ni catalyst activity. Therefore, a 0.05 % wt Mo-15 % wt Ni/Al_2O_3 (0.05Mo) catalyst was prepared and pre-treated following exactly the same method of the 0.3Mo catalyst. 18 hour stability experiments were run for the 0.05Mo catalyst under the same conditions as for the other three catalysts; 15Ni, 1Pt and 0.3Mo. Conversion with

time results of the 0.05Mo catalyst are compared to the other three catalysts in Figure 5.13, while Figures 5.14, 5.15, 5.16 and 5.17 compares the molar flow rates of H_2, CO, CO_2 and CH_4 respectively.

The results were stunning: even a small loading of 0.05% Mo had a significant effect on conversion and products production. The most striking difference was the considerable increase in stability when adding just 0.05% Mo, as compared to 15Ni, and also as compared to 0.3Mo. The 0.05Mo sustained its performance throughout the experiment period maintaining stable conversions and product rates. The 18 hour stability experiment for the 0.05Mo catalyst was repeated and the same product trends and stable performance were obtained for the catalyst. After both runs, no carbon deposition was detected on the catalyst, as well as no increase in the bed weight. These results show that the 0.05Mo catalyst is not only capable of resisting coking, but it also prevented other types of degradation that caused the 0.3Mo catalyst to deactivate.

The conversion behaviour of 0.05Mo was comparable to that of the 1Pt over 18 hours time-on-stream. Benefits of the 0.05Mo compared to 1Pt are that the H_2 production rate was greater (80×10^{-5} mol/min vs. 70×10^{-5} mol/min) and the CH_4 production rate was lower (8×10^{-5} mol/min vs. 13×10^{-5} mol/min). On the other hand, the CO production rate was higher over 0.05Mo (4.5×10^{-5} mol/min) than over 1Pt (2×10^{-5} mol/min).

Over only the first two hours, where 15Ni and 0.3Mo did not experience much deactivation, conversion and products rate of 15Ni and 0.05Mo were similar. However, during this initial period 0.3Mo and 0.05Mo showed different conversion and products rates: conversion over 0.3Mo (80%) was lower than that over 0.05Mo (88%), H_2 and CO production rates were higher over 0.3Mo (89 and 10×10^{-5} mol/min, respectively) than over 0.05Mo (80 and 4.5×10^{-5} mol/min). Past 2 hours, the 0.05Mo maintained its performance, whereas 15Ni and 0.3Mo experience serious deactivation.

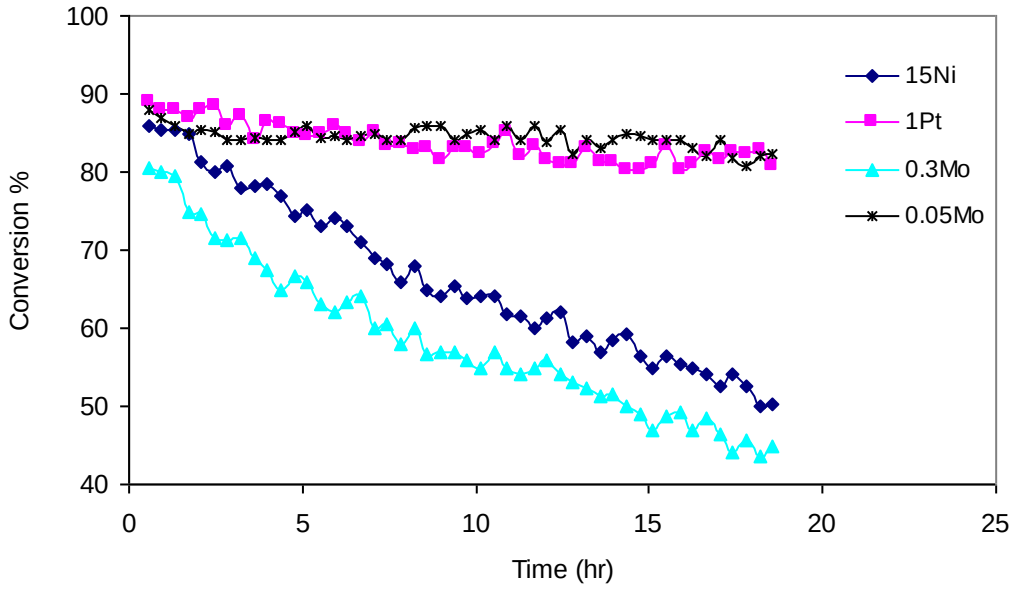

Figure 5.13: Total conversion as a function of time from 18 hours stability experiments of the 0.05Mo catalysts compared to the other three catalysts, at 450°C, S/C = 3 and O_2/C = 0.3

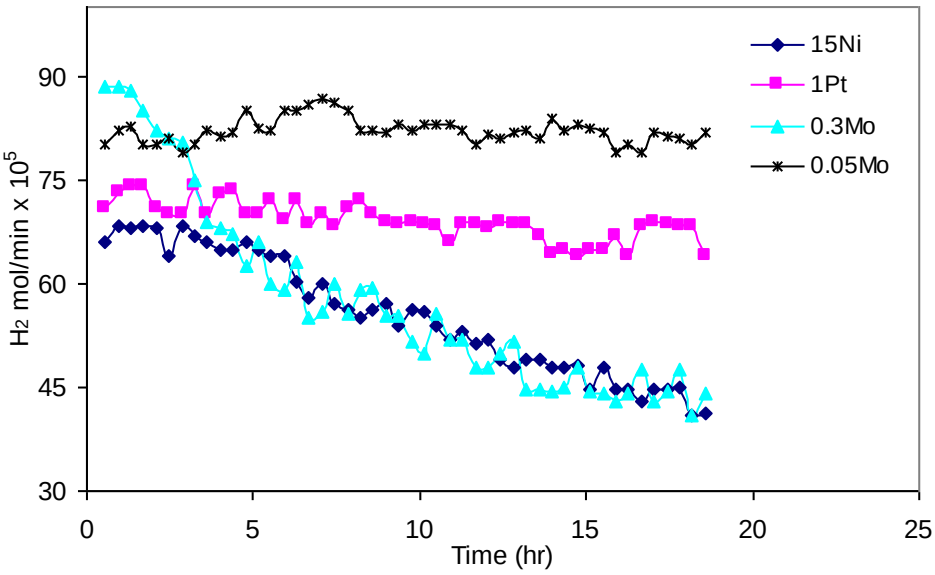

Figure 5.14: H_2 production rate as a function of time from 18 hours stability experiments of the 0.05Mo catalysts compared to the other three catalysts, at 450°C, S/C = 3 and O_2/C = 0.3

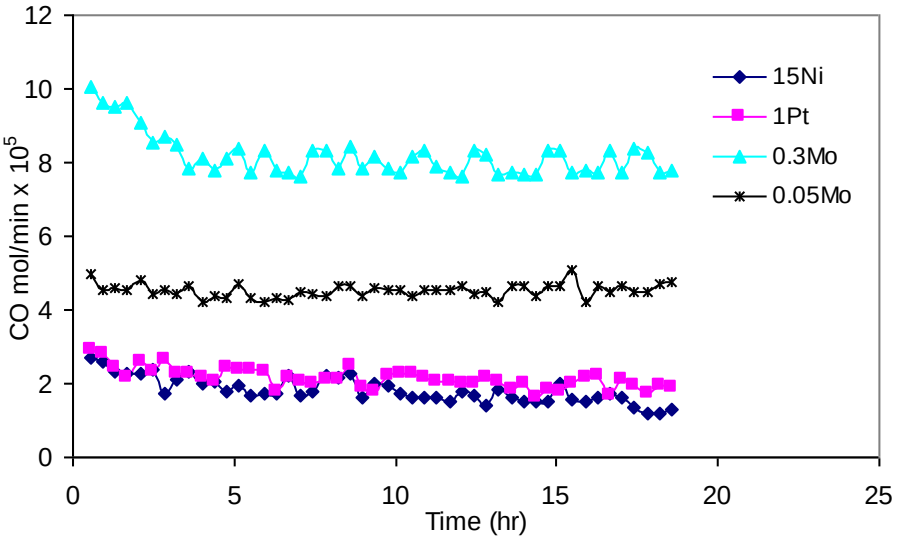

Figure 5.15: CO production rate as a function of time from 18 hours stability experiments of the 0.05Mo catalysts compared to the other three catalysts, at 450°C, S/C = 3 and O_2/C = 0.3

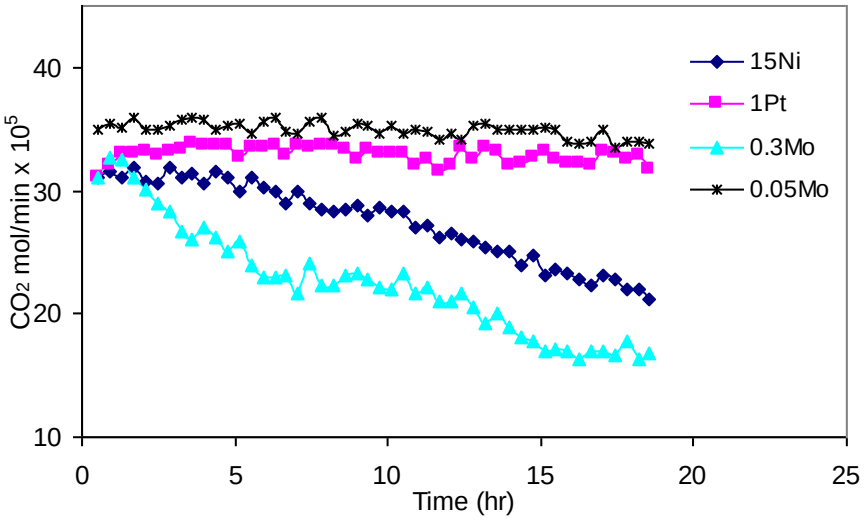

Figure 5.16: CO_2 production rate as a function of time from 18 hours stability experiments of the 0.05Mo catalysts compared to the other three catalysts, at 450°C, S/C = 3 and O_2/C = 0.3

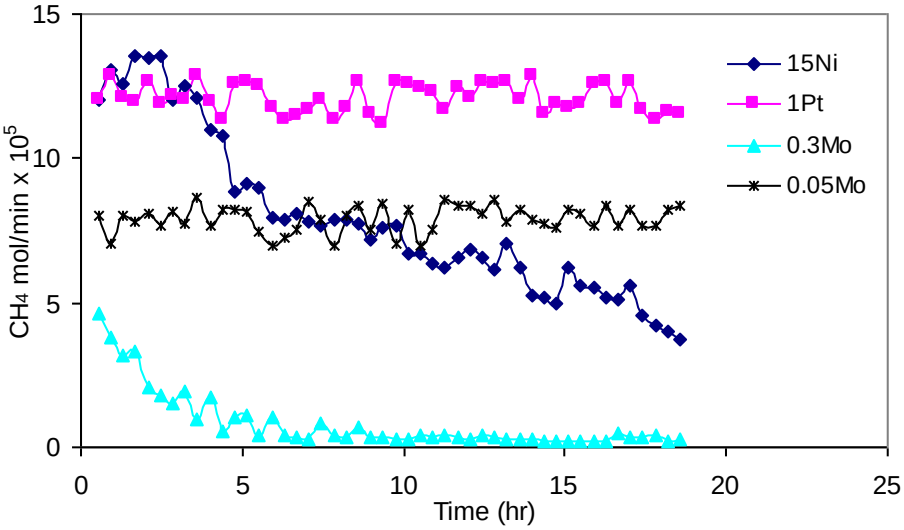

Figure 5.17: CH_4 production rate as a function of time from 18 hours stability experiments of the 0.05Mo catalysts compared to the other three catalysts, at 450°C, S/C = 3 and O_2/C = 0.3

5.6 Conclusions from the Catalysts Screening Study

A factorial experimental design illustrated the importance of screening the two chosen catalysts, Mo-Ni and Pt-Ni, under different operating conditions. Indeed it would have been misleading to compare activity or different product compositions of the catalysts under specified conditions, especially with the broad range of these conditions in the literature for both fuels. The importance of the factorial design was clearer when analyzing results for the Pt-Ni catalysts, as the catalyst showed different product compositions at the two selected loadings under different conditions compared to the unpromoted catalyst. The factorial design was also a useful tool to distinguish significant factors that affected the conversion and main product concentrations, and illustrated the importance of analyzing two factor interactions when they are significant. Although the factorial design was not conclusive about the effect of Pt loading on the performance of the Ni catalyst, it did show that increasing the amount of Pt above 0.2% did not have a major effect on the activity or selectivity of the catalyst, and hence lower loadings than

0.2% should be considered when optimizing the Pt loading under the specified conditions. This is an important direction when optimizing loadings for expensive noble metal catalysts.

Catalyst activity screening tests for all catalysts proved that increasing the reaction temperature to 450°C always had a positive effect on the total conversion of the fuel and on all products rates; however, the significance of this positive effect is more on the conversion of fuel for all catalysts. On the other hand, although increasing the other two operational conditions, S/C and O_2/C ratios, always improved the fuel conversion, their effects were not always positive for different products. This indicates that these ratios should be carefully optimized not only for cost considerations, but also to achieve the required product distributions. This conclusion was clearly illustrated when analyzing the H_2 % in the product for the 0.3Mo catalyst, as higher O_2 % in the feed resulted in lower H_2, which is the most highly desired product in the process.

Under all the conditions examined in the activity tests, none of the promoted catalysts showed a significant improvement in fuel conversion compared to the 15Ni catalyst. In fact, the 0.3Mo catalyst caused a decrease in conversion. However, the 0.3Mo catalyst showed higher syngas production rates under stable conditions for the first two hours, compared to the 15Ni catalyst. In addition, under all examined conditions the Mo catalyst always had a reformate lower in CH_4. To our knowledge these product composition variations were not reported before in the literature for hydrocarbon reforming reactions over Mo promoted catalysts. On the other hand, Pt promoted catalysts did not show a distinguishable trend for any of the products compared to the 15Ni catalyst, although it was expected to be more active in lowering the CO concentrations in the product stream.

Time-on-stream stability tests illustrated the high demand for sustaining conversion and product rates, when reforming LPG mixtures over monometallic Ni catalysts. Although the Ni catalyst showed distinguishable performance in the activity screening tests, it suffered from rapid deactivation by coking after only a couple of hours time-on-stream. This illustrates the high potential for solving the Ni stability problem associated

with reforming higher hydrocarbons, which was suggested in our case by promoting Ni catalysts with other transition metals. Indeed, promoting the Ni catalyst with Pt did stabilize the catalyst and improved its resistance to coking. On the other hand the 0.3Mo catalyst did not sustain a constant conversion or product composition showing a clear sign of deactivation with time. However, interestingly, deactivation of the 0.3Mo catalyst was not caused by coking, proving that the Mo catalyst did improve that ability of Ni to resist coking, but it accelerated its deactivation by another mode. This other deactivation type was prevented by reducing the amount of the Mo promoter to 0.05% wt, which resisted coking of Ni, while sustaining the same conversion of Ni and higher syngas production rates for the whole experiment time.

These distinguishable properties of the 0.05Mo catalyst led us to investigate it further as a promising active and stable catalyst for the oxidative steam reforming of LPG mixtures to produce H_2. Results of this investigation are presented in Chapters 6 and 7.

Chapter 6

LPG Reforming Over Ni-Mo/Al_2O_3 Catalysts: Analyzing Individual Reactions and Fuels

6.1 Introduction

In light of the conclusions from the catalyst screening and stability tests in Chapter 5, the addition of small amounts of Mo showed remarkable effects on the activity, selectivity and stability of Ni reforming catalysts. Although the addition of Pt also improved the stability of the Ni catalyst significantly by improving its resistance to coking, Pt did not have a significant effect on the activity and selectivity of the catalyst. Also, in addition to cost issue, promoting catalytic properties of Ni catalysts with different amounts of Pt in reforming reactions has already been covered extensively in the literature, as seen in Chapter 2. Therefore, in the remaining part of this study, the attention will focus on investigating the role of adding small amounts of Mo on the catalytic properties of Ni catalysts used in H_2 production reforming reactions. Specifically, the analysis will try to answer the following questions that arose from Chapter 5:

- How do small amounts of Mo (e.g. 0.05%) improve the stability of the Ni catalyst and its resistance to coking? And how do they affect the selectivity of the catalyst to different products?

- Why does the benefit of Mo addition vanish at higher (yet still small) Mo loading (e.g. 0.3%)?

- Although for the non-doped Ni catalyst, the main deactivation mechanism seems to be coking, such was not the case for the catalyst doped with 0.3% Mo. What is then the deactivation mechanism of the 0.3% Mo-Ni catalyst?

In this chapter we will investigate the effect of adding Mo to Ni catalysts on individual reactions that take place during oxidative steam reforming (OSR) of the two main components of LPG: propane and butane. This isolation will contribute to an understanding of the effect of each reaction on the four main products of OSR; H_2, CO, CO_2 and CH_4, and how the presence of Mo affects the selectivity of the catalyst to these products. The effect of Mo on carbon deposition reactions is presented in the last section of this chapter, in order to understand the role of Mo in preventing carbon formation from these reactions. On the other hand, structural effects of Mo on the Ni/Al_2O_3 catalyst that led to these activity, selectivity and stability changes will be discussed in detail in the next chapter (Chapter 7).

Classification of Individual Reactions

As illustrated earlier in Chapter 2, the oxidative steam reforming reaction (OSR) is actually a combination of two major reactions: an endothermic steam reforming reaction (SR) and exothermic partial oxidation reaction (PO). Also, from the background chapter we showed how LPG in most oil producing and/or refining countries is actually a mixture of two hydrocarbons: propane and butane. Therefore, OSR of LPG is a combination of saturated hydrocarbon reactions taking place at the same time and conditions. Other reactions that usually take place with these reactions under our conditions are the water gas shift reaction and the methanation reaction. In addition to these reactions, hydrocarbon SR over Ni-based catalysts is commonly associated with reactions that produce solid carbon such as hydrocarbon cracking and CO dissociation.

For investigation purposes, the reactions taking place during LPG OSR will be classified into three categories:

(1) Hydrogen producing reactions: include propane and butane partial oxidation (PO) and steam reforming (SR).

(2) CO consuming reactions: include the water gas shift reaction (WGS) and methanation reaction (ME).

(3) Carbon producing reactions: include coking of the Ni catalyst by propane and butane cracking and by the Boudouard reaction.

6.2 Literature Review on Ni-Mo Reforming Catalysts

Mo-Ni catalysts have been extensively studied in the literature as active and stable hydrodesulphurization catalysts. However, in these catalysts the Mo loading is higher than that of Ni, since Mo is the primary desulphurization metal, while Ni is added as a promoter. This is actually the opposite structure in our suggested Ni-Mo catalyst where Ni is the steam reforming metal and Mo a promoter. Moreover, our screening tests showed that the benefit of doping the Ni catalyst with Mo, occurs only within a very short window: obvious benefits with 0.05% Mo in term of stability, but Mo loadings as low as 0.8 %wt. resulted in an inactive catalyst, which suggests that Mo by itself will not activate reforming reactions. Therefore, it should be emphasized that the proposed Ni-Mo catalyst in this study is very different from Mo-Ni desulphurization catalysts in both catalytic and structural properties.

In the last decade, a number of studies in the literature did consider Ni-Mo catalysts for reactions other than desulphurization, especially those that consider Ni as the main activation metal. However, in these studies different Ni:Mo ratios were considered and the catalysts were prepared in different manners. Table 6.1 summarizes these studies highlighting the main findings. Although in most of these studies the resistance of Ni-Mo catalysts to coking was agreed upon, solid explanations for the role of Mo in this resistance were not conclusive, especially at very low Mo loadings. Moreover, in most of these studies the addition of Mo to Ni had a negative affect on the catalyst activity, while none of these studies discussed the effect of Ni-Mo catalysts on the selectivity to different steam reforming (SR) or oxidative steam reforming (OSR) reaction products. Although in a lot of industrial applications engineers will sacrifice activity and selectivity of catalysts to sustain their stability, high feed conversions and catalyst selectivities to desired products are important to reduce products separation costs and chemical waste treatment.

Table 6.1: A summary of studies that used Ni-Mo catalyst in reactions related to OSR

Author	Year	Fuels	Catalyst system	Reaction type & Temp. °C	Remarks
Gardner and Bartholomew	1981	CO	2.5%wt Ni-3%MoO_2/Al_2O_3	Methanation 300-475 °C	The promoted catalyst deactivated rapidly compared to the Ni catalyst. They suspected that Ni-MoO_2 is a poor hydrogenation catalyst.
Borowiecki et al.	1994-2002	CH_4 & Butane	A commertial Ni/α-Al_2O_3 catalyst promoted with (0.02-0.2) % wt Mo	SR 500-600 °C	Their extensive work was concentrated on understanding the role of Mo in preventing coking in hydrocarbons steam reforming. The work did not discuse product selectivity of the catalyst. Although their first publication (1994) did mention an improvement in CH_4 SR activity, lower activities of butane was reported over Ni-Mo catalysts (2002). This is thought to be due to their catalysts preparation method.
Silva et al.	1997	ground charcoal	2.5 % wt MoO_3, 2.5%wt NiO MoO_3-NiO	Oxidation and hydrogenation	Unsupported metal oxides were compared in the study for gasification of charcoal. NiO was more active than MoO_3 in both oxidation and hydrogenation of coal. When the oxides were combined only a slight effect was observer for the oxidation reaction.
Aksoylu et. al.	1998-1999	CO_2 & CO	Ni-Mo/Al_2O_3 Ni wt % (0, 5,10 and 15) Mo wt % (0, 5,10 and 15)	Methanation of CO_2 and CO 225-300 °C	Their studies tested the methanation of CO_2 and CO for a high range of Ni-Mo percentages. The lowest Mo % was 5. the activity of the catalyst for methanation decreased at high Mo % of 15. Mo was suggested to have a textural effect at low Mo concentrations, while electronic effects were suggested at higher concentrations.
Gonzalez et al.	2000	CH_4	3.3%wt Ni-(0.03, 0.3 and 3.3%wt) Mo/α-Al_2O_3	Dry reforming CO_2 650 °C	TEM results presented no change in the degree of Ni dispersion with Mo addition. Lower carbon deposition was accompanied with lower activity of Mo promoted catalysts. Kinetic measurements indicated that the addition of small amounts of Mo did not affect the mechanism of the CO_2 reforming reaction.
Quincoces et al.	2002	CH_4	2%wt Ni-0.12%wt Mo/α-Al_2O_3 0.12%wt Mo-2%wt Ni/α-Al_2O_3 2%wt Ni/α-Al_2O_3	Dry reforming CO_2 650 °C	Mo improved resistance to carbon but regardless of impregnation sequence, both Mo catalysts had lower activities than the Ni catalyst. They attributed this loss of activity to block of Ni active sites by Mo. Loss of stability of Mo catalyst was caused by catalyst sintering.
Xiao et al.	2003	CH_4	2% mol Ni-(0.67,2 and 6)% mol Mo/Al_2O_3	Dry reforming CO_2 700 °C	Mo lowered carbon deposition by improving the dispersion of Ni over Al_2O_3. However, all Mo catalysts had lower activity and CO selectivity than the Ni catalysts. XRD of reacted 2%Ni-6%Mo catalyst showed the formation of $NiMoO_4$.
Borowiecki et al.	2003	Butane	70%wt NiO-(1-10%wt) Mo/Al_2O_3	Hydrogenolosis 240-260 °C	XPS investigations showed that even after reduction at 800°C molybdenum exists on the surface at various oxidation states Mo^{+6}, Mo^{+x}, Mo^0

Table 6.1 cont.

Author	Year	Fuels	Catalyst system	Reaction type & Temp. °C	Main findings
Borowiecki et al.	2004	Butane	70%wt NiO-(1-10%wt) Mo/Al_2O_3	SR	Their attempts to investigate different states of Ni and Mo in a Ni-Mo catalyst with Mo loading < 1 %wt by XPS have failed, therefore, they used higher Mo loadings, maintaining the same Ni:Mo ratios. XPS, XRD, TPR and TGA results for these high Mo loading catalysts showed that the presence of Mo increased O_2 concentrations at the Ni-Mo catalysts surface as a result of different Mo oxidation states.
Wang et al.	2004	Methyl-cyclo-hexane	5%wt Ni- 2%wt Mo/Al_2O_3	SR 580 °C	The catalyst was compared to a $Ni-Re/Al_2O_3$ catalyst; the Mo catalyst had higher CO production and lower sulfur tolerance. No characterization of the catalyst was performed.
Youn et al.	2007	Ethanol	20%wt Ni-(3, 5, 7 and 9 % wt)Mo/ γ-Al_2O_3	ATR 550 °C	In contradiction to other reviewed studies, their TPR measurements showed that Mo increased the reducibility of Ni resulting in lower reduction temperatures. XRD results suggested a textural effect of Mo that reduced the interaction of Ni with the support. Low carbon deposition on Mo catalyst was attributed to high Mo dispersed species that served as barriers for preventing Ni partial growth.
Reqies et al.	2008	CH_4	5%wt Mo15%Ni/α-Al_2O_3 sequential impregnation with Mo first	PO and PO with small amounts of steam at 800 °C	The promoted catalyst improved the conversion from 88.9 to 90.6%. A slight improvement was also observed for the stability of the catalyst. These improvements were attributed to higher metal support interaction and to higher dispersion.
Wen et al.	2008	CO	Ni-MoO_2 produced from the reduction of ß-$NiMoO_4$	WGS 350-500 °C	Unsupported catalysts were tested for WGS reactions and found to be more active than Ni catalysts
Maluf and Assaf	2009	CH_4	Nominal Ni:Al molar ratio of 3:1 Mo loading: 0.05, 0.5, 1 and 2 (%w/w)	SR 700 °C	At S/C = 4 non-coking conditions, they suggested that the Mo promoter had a positive effect on the water gas shift reaction during SR since CO was lower with Mo and CO_2 was higher. The addition of Mo caused a significant decrease in metallic area of the catalyst.
Marin-Flores and Ha	2009	Iso-octane for gasoline	MoO_2	PO 700 °C	This is not a bimetallic catalyst. The catalysts is only MoO_2 so there are no metal-metal or metal-support interactions. The activity of the catalysts in PO was explained in terms of a Mars–van Krevelen-type mechanism, where the consumption of gas phase oxygen provided by the bulk structure to re-oxidize the active sites previously reduced during the interaction between the hydrocarbon molecules and the catalyst surface.
Marin-Flores et al.	2010	Dodecane for jet fuel	Nanoparticles MoO_2 from a reducing ethylene glycol/water solution	PO 850 °C	The catalyst was tested for internal reforming of jet fuel for SOFC. The catalyst had 90 %conversion and was more stable than Ni based catalysts and regular MoO_2.

6.3 Effect of Different Mo Loadings

In the screening stability test runs in Chapter 5 two loadings of Mo were tested. First, 0.3 wt% Mo, which was also used in the activity screening tests, was tested and lost its stability with time. When the Mo loading was decreased to 0.05% wt, the catalyst showed good stability for the whole period of the stability tests of 20 hr, maintaining a constant conversion and H_2 production rate. Therefore, the 0.05% Mo loading was chosen as a promising catalyst for further investigation. However, due to this significantly small loading of Mo it was hard to distinguish activity and product selectivity differences between the 15Ni catalyst and the promoted 0.05Mo-15Ni catalyst, in the first few hours prior to the deactivation of the Ni catalyst. This led to an attempt to vary the Mo loading between 0.3 and 0.05% in order to magnify the effect of Mo on conversion and product distribution during individual reforming reactions, while maintaining the catalyst's stability.

A Mo-Ni catalyst with a loading of 0.1Mo wt% was synthesized following the same preparation method as for the other Mo and Ni catalyst (previously discussed in detail in Chapter 3, Section 3.1). OSR for this catalyst was run under exactly the same feed and operating conditions as in the stability screening tests performed in Section 5.5. The 0.1Mo catalyst maintained its stability throughout the 6 hour reaction course. Compared to the 0.05Mo catalyst, 0.1Mo had a slightly, 2-3%, higher conversion. This percentage increase was also observed for the H_2 and CO production, while CO_2 and CH_4 did not show any significant differences between the two catalysts. Figures comparing conversions and product distributions (H_2, CO, CO_2 and CH_4) of the 0.3Mo, 0.1Mo and 0.05Mo catalysts can be found in Appendix C. Based on these tests, in the remaining part of this study, 0.1Mo will be evaluated and compared to 15Ni in the individual reactions and fuels tests.

6.4 H_2 Producing Reactions

In this section three reactions will be discussed for each fuel: partial oxidation (PO), steam reforming (SR) and oxidative steam reforming (OSR). The three reactions for each fuel will be compared over the 15Ni and the 0.1Mo catalysts. Prior to each run, catalysts were reduced in-situ under the same conditions used in the stability screening tests (section 5.5). OSR reactions were also run under the same stability test operating conditions. These conditions were selected because they resulted in reproducible data for both conversion and product distributions. Moreover, under these conditions the deactivation of the 15Ni catalyst was delayed for some time. These conditions are important in order to compare the activity and selectivity of the two catalysts in the absence of deactivation. However, we do need to look into the stability of each catalyst in each individual reaction. Therefore, in order to reduce the experiment run and see deactivation sooner, the amount of catalyst used in the bed was decreased from 50 to 30 mg, increasing the GHSV by 67%. Also, the amount of silicon carbide used as a heat sink was decreased from 2000 to 500 mg reducing the bed volume.

The feed fuel composition in the stability tests was 1mol% propane and 1mol% butane. Although this composition gave a 1:1 hydrocarbon ratio, the carbon:carbon and H_2:H_2 ratios were different, as butane has a higher carbon and hydrogen content. Since the major deactivation cause of Ni catalysts in reforming reactions was coking, a constant carbon feed composition was considered for each fuel in all individual reactions. Based on the stability test compositions, 1mol% propane + 1 mol% butane will result in a total of 7 mol% carbon. Considering a 7 mol% carbon basis for each fuel, the feed mol% will be 2.33 for propane (P) and 1.75 for butane (B). The S/C = 3 and O_2/C = 0.3, and were kept constant for all reactions so the GHSV was maintained at a constant value of 339,800 ml/hr.g_{cat} by adjusting the N_2 flow rate for each reaction.

***Bed Temperature Profile Experiments**:*

In order to investigate the effect of feed and operational condition changes on the bed temperature profile, bed temperature experiments were run for the 0.1Mo catalyst for all three H_2 production reactions; OSR, SR and PO. Bed temperature experiments were run in the main experimental setup described in section 3.2. The reactor was filled with a 30/500 mg of the catalyst/diluent mixture. The catalyst was reduced in a 30 mol% H_2/N_2 stream at 750°C for an hour. The reactor temperature was then cooled down to 450°C. the temperature inside the catalysts bed was measured using a K-type thermocouple positioned in the far end of the bed and touching the quartz frit (position Z= 0) as illustrated in Figure 6.1.

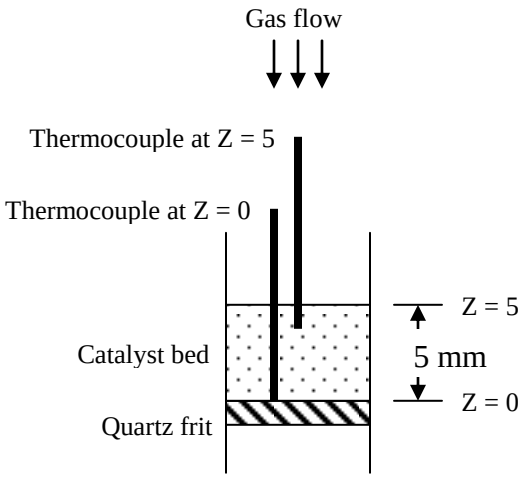

Figure 6.1: An illustrative diagram of measuring catalyst bed temperature at two positions during OSR, SR and PO of the 0.1Mo and 15Ni catalysts.

When the bed temperature was stabilized at 450°C, a feed of 1mol% prop 1 mol% butane, S/C= 3 and O_2/C= 0.3 was introduced to the reactor to run OSR. After 30 min the temperature inside the bed reached 456°C and was constant for an hour. After that the thermocouple was carefully pulled 4 mm to reach the top surface of the bed (position Z=5) as illustrated in Figure 6.1. The temperature was left to stabilize for 15 min and was

recorded to be 458°C. The O_2 flow to the reactor was then stopped and the N_2 flow was adjusted to keep a constant GHSV under steam reforming conditions. At position Z = 5 the temperature measured was 443°C, while it was 438°C at Z = 0. To measure the bed temperature during PO reactions O_2 was introduced again as OSR was regained and the temperature increased and was stable at 455°C at Z = 0. Then, the water pump was stopped and N_2 flow was adjusted to meantime a constant GHSV under PO conditions. Temperature increased to 466°C at Z = 0 and remained like that at Z = 5. Table 6.2 shows bed temperatures at the two positions illustrated in Figure 6.1 for 15Ni and 0.1Mo for the three reactions. From these measurements we conclude that running individual reactions under the selected operating conditions will not cause a significant offset from the reaction bed set-point temperature (450°C) for both catalysts.

Table 6.2: Bed temperatures measured at two thermocouple positions (Z = 0 and Z = 5) inside the catalyst bed for 0.1Mo and 15Ni catalysts during OSR, SR and PO reactions. The reaction set point temperature = 450°C

	0.1Mo		15Ni	
	Z = 0	Z = 5	Z = 0	Z = 5
OSR	456°C	458°C	460°C	463°C
SR	438°C	443°C	444°C	445°C
PO	466°C	466°C	470°C	465°C

6.4.1 Partial Oxidation Reactions (PO)

When running PO reactions at 450°C and O_2/C = 0.3 for both fuels, it is important to note that this ratio is lower than the PO stoichiometric ratio (O_2/C = 0.5) for both fuels to produce CO and H_2. In addition, the reaction temperature is lower than that reported in the literature for syngas production from propane or butane by PO. So, in reality only a portion of each fuel is partially oxidized while the rest catalytically cracked or did not react. Figure 6.2 shows the conversion of propane and butane over 15Ni and 0.1Mo with time. The two catalysts did not show significant differences for both fuels. The conversion decreased for both catalysts due to coking, with butane having a higher rate of

catalyst deactivation. In fact, for both catalysts the reaction with butane had to be stopped after 3 hr due to pressure build up in the reactor. On the other hand, for propane, the reactions with 15Ni and 0.1Mo were stopped after 4 and 5 hr, respectively. After each run the reactor was cooled under N_2 and the catalyst bed was weighed. The percentage increase in weight for each catalyst is presented in Table 6.3. Although all catalysts had a high amount of carbon deposition, for both fuels the 15Ni catalyst had a higher amount of carbon. It can also be seen that more carbon was deposited with butane PO than with propane PO.

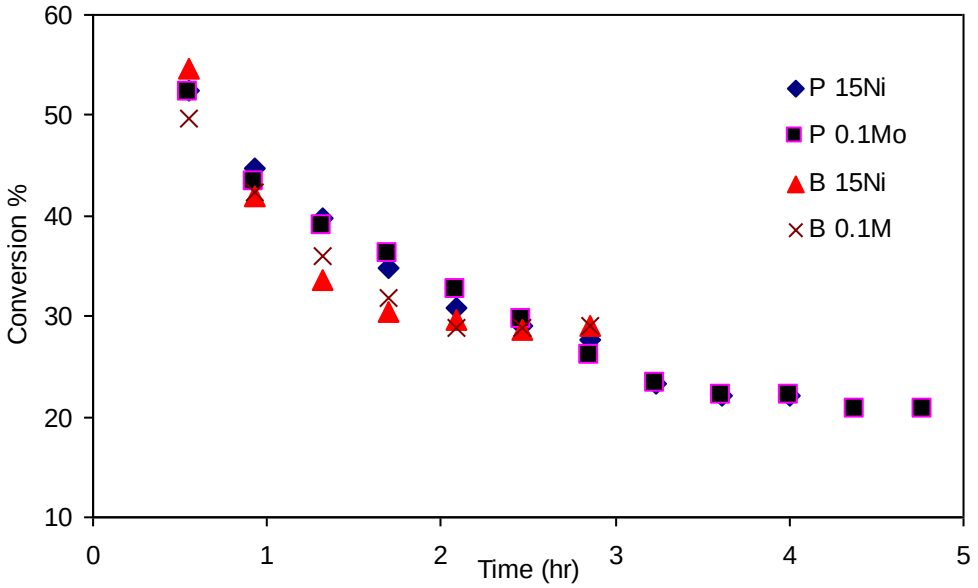

Figure 6.2: PO conversions for different catalysts and fuels at 450°C and O_2/C = 0.3. P is for propane and B is for butane

Although it is inappropriate to interpret selectivities of different catalysts under these unsteady state conditions, product compositions in the first hour could be assigned to PO as catalysts were not expected to be highly deactivated and conversions were above 50%, especially for propane. Table 6.3 presents the average values of the first two GC injections for each product taken within the first hour of the reaction.

Table 6.3: Average product flow rates and their standard deviation of the first two GC injections taken within the first hour of the reaction from PO (mol/min $\times 10^5$)

Catalyst & Fuel	H_2	CO	CO_2	CH_4	% Increase weight of catalyst after Reaction
P 15 Ni	21.6±2.5	3.2±0.5	7.1±0.8	0.6±0.1	302
P 0.1Mo	24.4±2.3	7.8±1.1	4.0±0.1	0.6±0.1	223
B 15Ni	21.8±3.2	2.0±0.9	6.1±0.2	0.4±0.1	480
B 0.1Mo	21.8±2.4	4.6±1.3	5.7±0.2	0.3±0.0	380

Not a lot can be concluded from these results regarding the two catalysts selectivities. However, for both fuels the 0.1Mo catalyst showed higher CO production rates than the unpromoted catalyst. This higher CO production for Mo was already seen in the OSR screening tests with both loadings of 0.3 % and 0.05 % Mo. Another observation is that more CH_4 is produced with propane as feed than with butane.

Although the present study focuses on propane and butane, it is worthwhile mentioning partial oxidation mechanisms for methane, because the later has been studied much more extensively. Two mechanism routes for CH_4 partial oxidation have been proposed [Dissanayake et.al. (1991); Hickman and Schmidt (1992); Goetsch and Schmidt (1996)]. In the first mechanism, part of CH_4 is first combusted to CO_2 and H_2O in the first section of the reactor, followed by reforming of the remaining CH_4 to CO and H_2. In the other suggested mechanism CO and H_2 are directly produced from recombination of CHx and O adsorbed on the surface of the catalyst as follows:

$$CH_4 + 5s \longrightarrow C\text{-}S + 4H\text{-}S \qquad (P1)$$

$$O_2 + 2s \longleftrightarrow 2O\text{-}S \qquad (P2)$$

$$C\text{-}S + O\text{-}S \longrightarrow CO\text{-}S \qquad (P3)$$

$$CO\text{-}S \longleftrightarrow CO \qquad (P4)$$

$2H\text{-}S \longleftrightarrow H_2$ (P5)

Where S is a catalytic surface site and X-S is an adsorbed specie.

For higher hydrocarbons, the mechanism of PO is not as fully developed as for CH_4. Subramanian et al. (2004) suggested a basic scheme beginning with dissociation of the hydrocarbon by stepwise dehydrogenation of the C bonds to produce H_2. This is followed by the reaction of C and H_2 with O_2 to produce CO, CO_2 and H_2O.

6.4.2 Steam Reforming (SR) and Oxidative Steam Reforming (OSR)

Steam reforming reactions for both propane and butane were run at 450°C and a S/C ratio of 3. The ratio is higher than stoichiometric, but the temperature is relatively low for complete conversion of the fuel during the highly endothermic SR reaction. Indeed, in all steam reforming reactions the temperature inside the bed decreased 7 to 13 degrees below the set point of 450°C. For both fuels the decrease in temperature was 3 to 5 degrees more for the 0.1Mo catalyst than for 15Ni, indicating a possibly higher SR rate in the presence of Mo. On the other hand, the addition of O_2 in the OSR reactions increased temperatures 7 to 11 °C above the set point. In order to have a better understanding of the effect of O_2 on SR for each fuel, OSR of either propane (P) or butane (B) was compared to SR with both catalysts. All reactions were run for six hours. Conversions of all eight runs are presented in Figure 6.3.

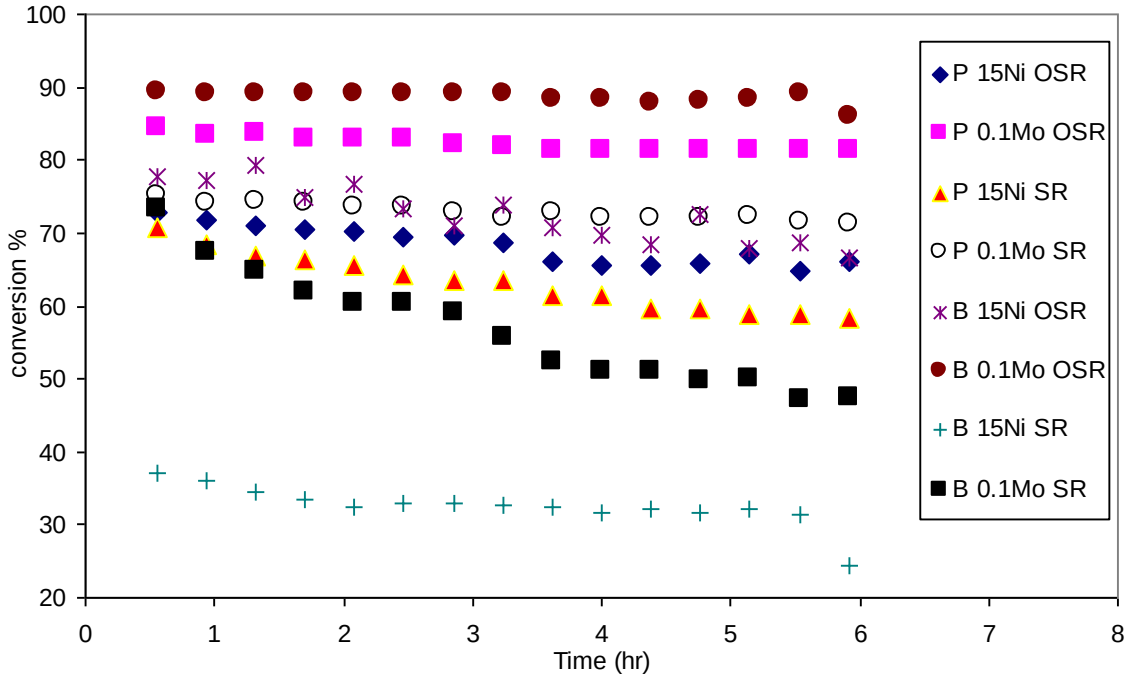

Figure 6.3: Conversions of SR and OSR reactions over 15Ni and 0.1Mo catalysts for propane and butane individual runs at 450°C, S/C = 3 and O_2/C = 0.3

A number of observations can be made from Figure 6.3. First considering SR, for a given catalyst, propane conversion is always higher than butane conversion. Also, comparison between 15Ni and 0.1Mo shows that the addition of 0.1% Mo increases the SR conversion and this is much more pronounced for butane where after one hour time-on-stream the conversion almost doubles from ~35% over 15Ni to ~68% over 0.1Mo. For propane the SR conversions at the beginning of the experiment are similar whether SR takes place over 15Ni or 0.1Mo catalyst. However, rapidly the propane SR conversion decreases over the 15Ni catalyst, whereas it is more stable over 0.1Mo. In the case of butane, the 0.1Mo conversion is not stable and the catalyst deactivates markedly over time.

The effect of the small amounts of O_2 added to SR reactions for both catalysts was more significant for butane. In fact, for the 15Ni catalysts, the addition of O_2 boosted the conversion of butane from 37 to 77% in the first two hours. This illustrates the

importance of OSR for LPG feeds with higher butane compositions. However, even with this improvement in activity for the 15Ni catalyst when adding O_2, the catalyst still shows deactivation (due to coking, as seen later) over only 6 hours for both fuels, proving the weakness of Ni catalysts in preventing coking even with the addition of O_2. The increase in the catalyst bed weight due to coking after the end of each run is shown in Table 6.4. The highest amount of carbon deposition, and by far, was for butane SR over 15Ni. Adding O_2 reduced considerably carbon deposition, but was still significant in the case of butane. For propane, the amount of carbon deposited was much lower than for butane and again addition of O_2 further reduced coking. Similar increases in bed weight were observed after SR reactions for both fuels over the 0.1Mo catalyst which kept deactivating over time, especially in the case of butane. However, the most notable result is that for the 0.1Mo catalyst, addition of O_2 resulted in no measurable increase in bed weight, at least during the first 6 hours, and this for both butane and propane. This can be related to the stable conversion in Figure 6.3 for both fuels for OSR over 0.1Mo. Finally, not only did butane and propane OSR over 0.1Mo showed good stability, they also yielded the highest conversions, as seen in Figure 6.3 (~90% for butane and ~82% for propane).

Table 6.4: Increase in the catalyst bed weight due to carbon depositions after 6 hours time-on-stream. For each run 30 mg of the catalyst was used in 500 mg SiC

Fuel, Catalyst and Reaction	Amount of Carbon Deposit = Final Bed Weight-Initial (mg)
Propane 15Ni SR	8.6
Propane 0.1Mo SR	1.7
Propane 15Ni OSR	3.1
Propane 0.1Mo OSR	0
Butane 15Ni SR	68.3
Butane 0.1Mo SR	2
Butane 15Ni OSR	14.1
Butane 0.1Mo OSR	0

Figures 6.4 and 6.5 show the H_2 and CO production rates, respectively. For both fuels, syngas (H_2+CO) production was higher over the 0.1Mo catalysts in OSR as well as SR. Butane OSR over 0.1Mo had the highest H_2 and CO productions among all runs. This indicates that LPG feeds with higher butane compositions will give higher activities and syngas production rates over Mo catalysts. This was also concluded by Gokaliler et al. (2008) when comparing the OSR of two mixtures of LPG over a Pt-Ni catalyst at an O_2/C = 0.5. However, in their experiments they had to use a higher S/C = 7, as at a lower S/C ratio of 5 the catalyst suffered from coking resulting in a rapid loss of activity for the enriched butane LPG mixture at a reaction temperature of 400°C.

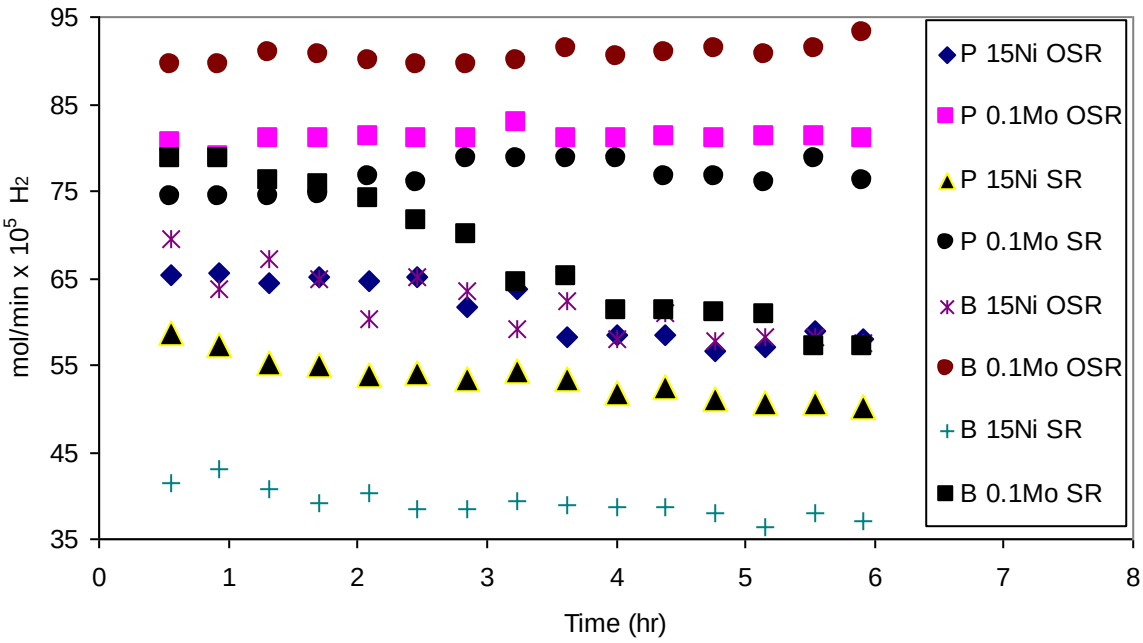

Figure 6.4: H_2 production from SR and OSR reactions over 15Ni and 0.1Mo catalysts for propane and butane individual runs at 450°C

The addition of O_2 to SR had a greater effect on H_2 production for butane, most likely by preventing fast catalyst coking as O_2 tends to play an important role in preventing the formation of unsaturated hydrocarbons like C_2H_4 and C_3H_6 which are known to be carbon precursors (Laosiripjana and Assabumrungrat, 2006). However, in the absence of SR

deactivation, it should be pointed out that at equilibrium, H_2 compositions in the product are higher in SR than OSR, as in OSR part of the fuel is oxidized. This cannot be concluded from these experiments, because due to the low reaction temperature, the conversions obtained in the experiments for SR were far from equilibrium conversions. However, H_2 produced from SR was significantly higher than that produced from PO (Table 6.3) over both catalysts. This low H_2 production rate from PO indicates that indeed the main role for introducing O_2 in OSR was to provide heat for the endothermic SR reaction. The O_2/C ratio in OSR reactions should be fixed at an optimum value as too much O_2 will result in oxidizing the H_2 and CO to H_2O and CO_2 as proven in the catalyst screening tests for both catalysts when using an O_2/C ratio of 0.6 (refer to Table 5.11 in Chapter 5).

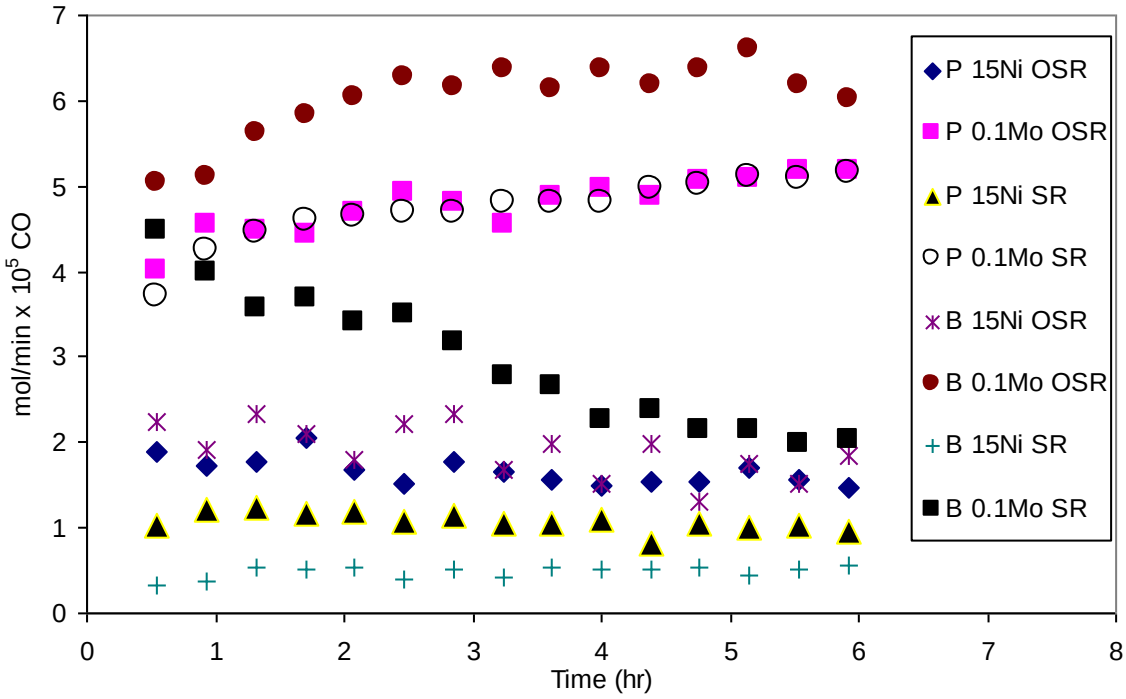

Figure 6.5: CO production from SR and OSR reactions over 15Ni and 0.1Mo catalysts for propane and butane individual runs at 450 °C

The CO_2 production rate is shown in Figure 6.6. As expected, OSR reactions for both fuels gave higher CO_2 production rates. Also CO_2 rates in Figure 6.6 indicate that for CO_2 produced over the 0.1Mo catalyst was slightly higher than over 15Ni.

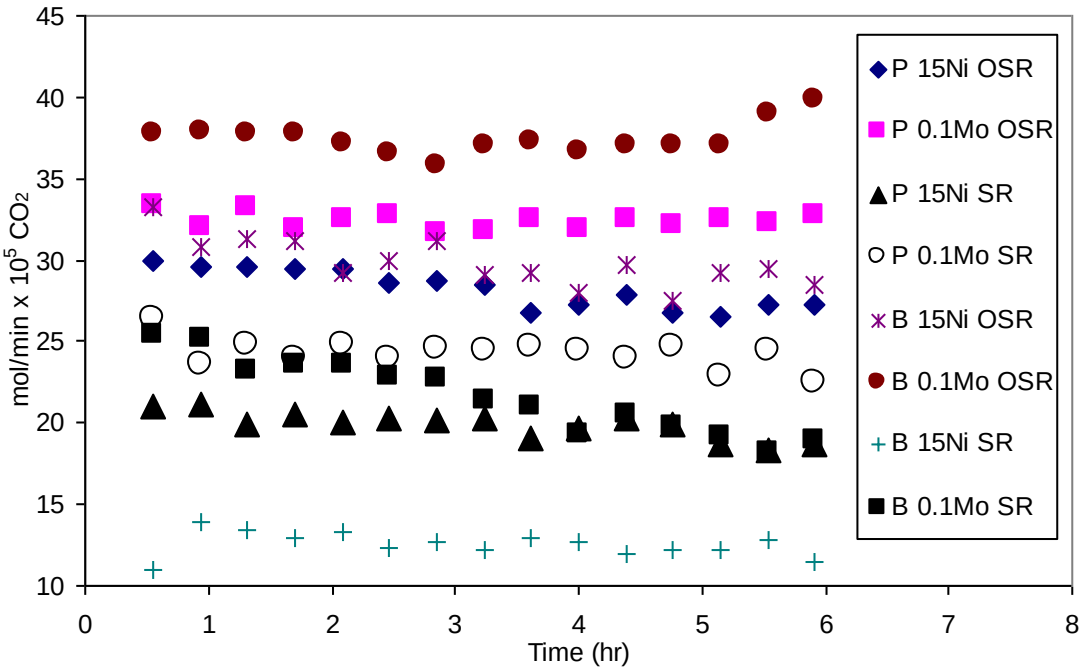

Figure 6.6: CO_2 production from SR and OSR reactions over 15Ni and 0.1Mo catalysts for propane and butane individual runs at 450 °C

One of the OSR mechanisms listed previously, and more commonly accepted, proposes that OSR reactors have two reaction zones; a combustion zone, where hydrocarbons are homogenously oxidized to CO_2 and H_2O followed by a catalytic zone where H_2 and CO are produced via SR. In chapter 4 we proved that under our OSR conditions, homogenous reactions including oxidation and thermal cracking are not favourable for propane and butane. Therefore, we speculate that both PO and SR are taking place heterogeneously in the catalytic zone. Moreover, due to the low O_2/C ratio it is expected that oxidation reactions are occurring in a relatively small section at the beginning of the catalyst bed with most of the bed utilized for SR. Lim and Bae (2010) proved this pathway for CH_4 OSR at 650°C by looking at the temperature profiles along

the catalyst bed for different O_2/C ratios. Using a 55 mm catalyst bed at a S/C ratio of 1.02 and an O_2/C ratio of 0.5, they found that within the first 4mm of the bed the temperature increased sharply to reach a maximum of 744°C, then it began decreasing broadly along the length of the bed to reach a minimum of 645°C 28 mm past the bed's entrance. This indicates that even at a stoichiometric value of O_2/C = 0.5, oxidation reactions only took place at the first 15-25% of the catalyst bed.

The fourth main detected product in SR and OSR reactions is CH_4, plotted for all reactions in Figure 6.7. Unlike the other three products (H_2, CO and CO_2), butane OSR over 0.1Mo did not give the highest CH_4 production. Thermodynamically, as previously proved in Chapter 4, CH_4 is favourable at low reaction temperatures. Once formed under these conditions it is very stable with a C-H bond energy of 439 kJ/mol, making it hard to dissociate. In agreement with the screening tests in Chapter 5 the 0.1Mo catalysts produced lower CH_4. This could be attributed to the Mo catalysts not favouring the methanation reaction which could be a source of CH_4 during SR reactions (this was proved not to be the case in the following section, section 6.5):

$$CO + 3H_2 \longleftrightarrow CH_4 + H_2O \qquad (6.1)$$

The possibility of CH_4 production through this reaction will be discussed in detail in the next section of this chapter. Other sources of CH_4 could be propane or butane hydrogenolysis (Rostrup-Nielsen and Alstrup, 1999):

$$C_3H_8 + H_2 \longrightarrow C_2H_6 + CH_4 \qquad (6.2)$$

$$C_4H_{10} + H_2 \longrightarrow C_3H_8 + CH_4 \qquad (6.3)$$

or carbon gasification by H_2:

$$C + 2H_2 \longleftrightarrow CH_4 \qquad (6.4)$$

The production of CH_4 by the gasification reaction (6.4) is not favoured under our conditions, because gasification of C by O_2 or H_2O has a higher rate than gasification by H_2 (Bartholomew and Farrauto, 2006).

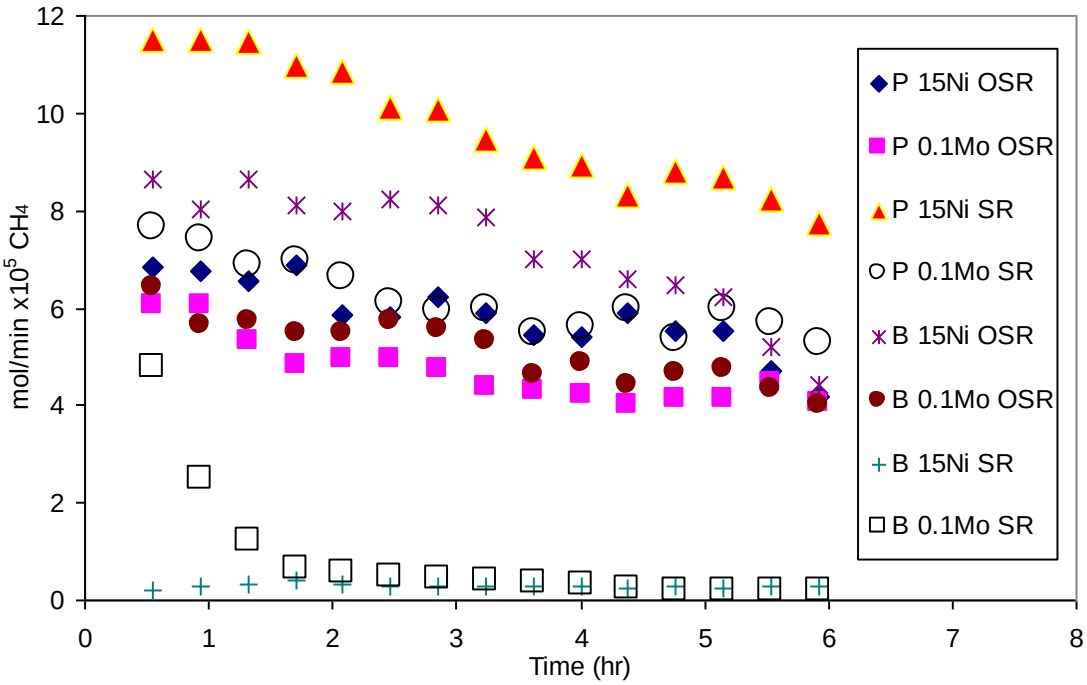

Figure 6.7: CH_4 production from SR and OSR reactions over 15Ni and 0.1Mo catalysts for propane and butane individual runs at 450 °C

In addition to CH_4, other small traces of hydrocarbons were detected by the FID detector. These hydrocarbons were identified for the propane tests, while not all of them were known for the butane tests because they covered a wider spectrum of unsaturated hydrocarbons with some small peaks overlapping, making them difficult to identify. Table 6.5 lists hydrocarbons associated with each experiment. Although it is difficult to quantify such small traces, peak areas could be compared to give an idea of their relative amounts in the product stream, especially in the case of propane where we were able to identify all the hydrocarbon by-products. These hydrocarbons can also promote different reaction routes. All propane reactions produced ethane rather than ethylene, the latter being a common by-product in propane SR at high temperatures. Because of the low

reaction temperature, hydrogenolysis of propane to ethane and CH_4 (reaction 6.2) is more favoured (Rostrup-Nielsen and Alstrup, 1999). Figure 6.8 shows ethane peak areas from the FID chromatograms for propane reactions. The other common hydrocarbon produced was acetylene, which is most likely produced from further dehydrogenation of adsorbed ethylene (Zaera and Hall, 1987). FID peak areas of acetylene may indicate a lower production over 0.1Mo catalysts as shown in Figure 6.9. An interesting observation when comparing Figures 6.8 and 6.9 is the mirror image of ethane and acetylene noticed for the 15Ni catalyst runs, demonstrating a change in reaction pathway as a function of time. Small traces of propylene were detected only over the 15Ni catalyst. Production routes for these hydrocarbons in propane OSR mechanism will be discussed in Chapter 7.

Table 6.5: Main hydrocarbon by-products from different reactions and fuels

Fuel, Catalyst and Reaction	Hydrocarbons By-products
Propane 15Ni SR	Acetylene, Ethane and Propylene
Propane 0.1Mo SR	Acetylene, Ethane
Propane 15Ni OSR	Acetylene, Ethane and Propylene
Propane 0.1Mo OSR	Acetylene, Ethane
Butane 15Ni SR	Acetylene, methylacetylene
Butane 0.1Mo SR	Acetylene, methylacetylene
Butane 15Ni OSR	Acetylene, methylacetylene
Butane 0.1Mo OSR	Acetylene, methylacetylene

The main by-products detected and identified in butane reactions were acetylene and methylacetylene (Propyne). Over both catalysts the addition of O_2 decreased the peak areas for both by-products, with OSR over the 0.1Mo catalysts having the lowest concentrations of all. It is hard to predict the exact production routes for these by-products since as mentioned earlier, other by-products from butane reactions could not be identified.

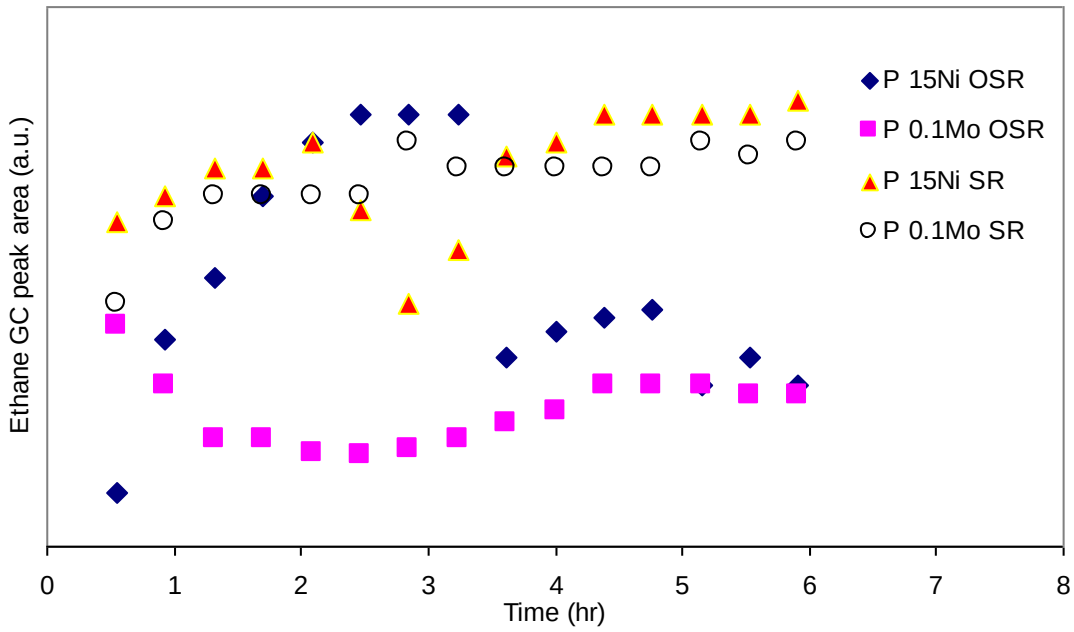

Figure 6.8: Ethane GC peak areas from propane SR and OSR reactions at 450 °C over 15Ni and 0.1Mo catalysts.

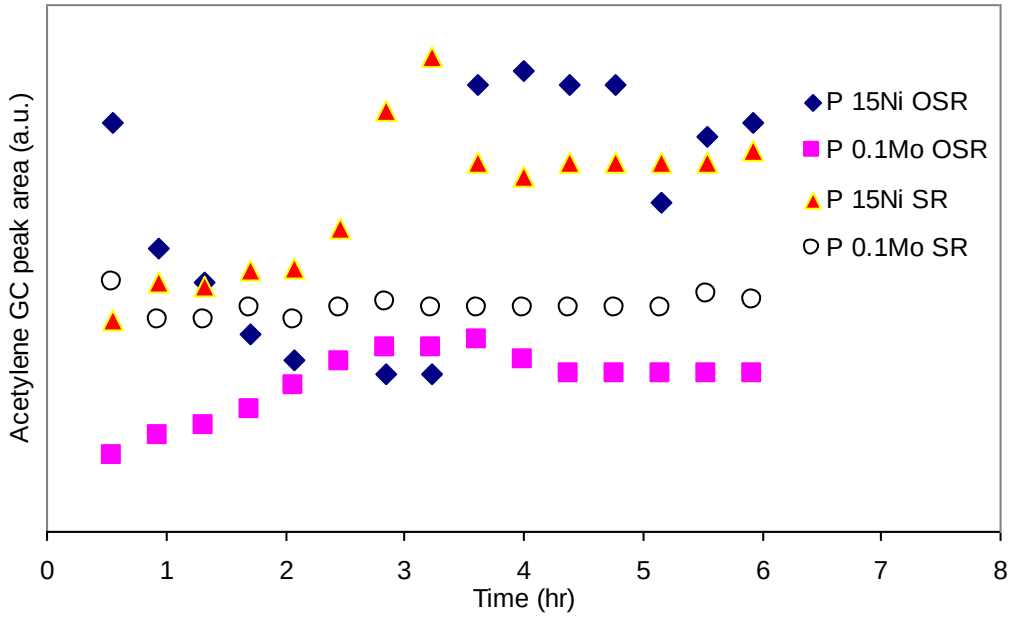

Figure 6.9: Acetylene GC peak areas from propane SR and OSR reactions at 450 °C over 15Ni and 0.1Mo catalysts.

CO_2 Dry Reforming

A reaction that is usually considered in the literature to produce syngas and takes place also during OSR or SR is CO_2 reforming:

$$C_3H_8 + 3CO_2 \longrightarrow 6CO + 4H_2 \quad (6.5)$$

$$C_4H_{10} + 4CO_2 \longrightarrow 8CO + 5H_2 \quad (6.6)$$

This highly endothermic reaction was assumed to be less probable to take place because of the low reaction temperature. However, this was also proven experimentally as the reaction was tested at a feed of 3 vol% propane and 12 vol% CO_2, with a CO_2 to carbon ratio of 1.33 at 450°C, with no significant results. This indicates that indeed CO and H_2 are mostly produced by the steam reforming reaction during OSR at these low temperatures and low O_2/C conditions. Excluding dry reforming in OSR of propane was also reported in the literature by Pino et al. (2006), as they assumed a low rate of dry reforming compared to steam reforming over a Pt/CeO_2 catalyst even at temperatures as high as 650°C.

6.5 CO Consuming Reactions

As concluded from the screening tests in chapter 5, and observed also from all individual reactions results in this chapter, the addition of even small amounts of Mo to the Ni catalysts resulted in a significant increase in the CO production. Therefore, in addition to investigating individual reactions that produced CO, it is necessary to look into reactions that consume CO which are known to take place as side reactions during OSR. One of these CO consuming reactions is the water gas shift (WGS) reaction:

$$CO + H_2O = H_2 + CO_2 \qquad (6.7)$$

A reaction that often accompanies the WGS reaction and is commonly considered in studies of the WGS reaction is the methanation reaction (reaction 6.1), which is also considered as a CH_4 production side-reaction during SR and OSR.

6.5.1 The Water Gas Shift Reaction (WGS)

In this section we investigate the effect of adding small amounts of Mo to the Ni catalyst on the product selectivities in the WGS reaction. The WGS reaction feed in this study consisted of only H_2O and CO in stoichiometric amount, 6 mol% each. N_2 was used to maintain the GHSV at a constant value (339,800 ml/hr.g_{cat}), similar to that of the individual reactions for both catalysts. The WGS reaction was run at 450°C.

No significant differences were observed in CO conversion for both catalysts (in the range of 62-67%) and the conversion remained constant during the 2 hours of the test. The production rates for CO, CO_2 and H_2 in the product stream for the first two hours are shown in Figure 6.10 for both 15Ni and 0.1Mo catalysts. All production rates remained constant, indicating steady-state conditions. It is seen that CO_2 and H_2 production were not affected by the addition of a small amount of Mo. It can be concluded that, compared to 15Ni, addition of 0.1% Mo does neither promote nor hinder the WGS reaction.

Stoichiometrically, according to equation 6.7, in the absence of any side-reactions, the amounts of CO_2 and H_2 produced should be equal, however, for both catalysts; CO_2

was higher than H_2. This is likely a result of the consumption of H_2 by the CO methanation reaction to produce CH_4. These amounts were detected for both catalysts and are shown in Table 6.6 for different time readings. The amounts of CH4 were higher over the 0.1Mo catalyst and were closer to the calculated value (~2 mol/min × 10^5) assuming that the methanation reaction is the only side reaction consuming H_2. However, in the case of the 15Ni catalyst the value was lower than the expected and hence other side-reactions were also taking place.

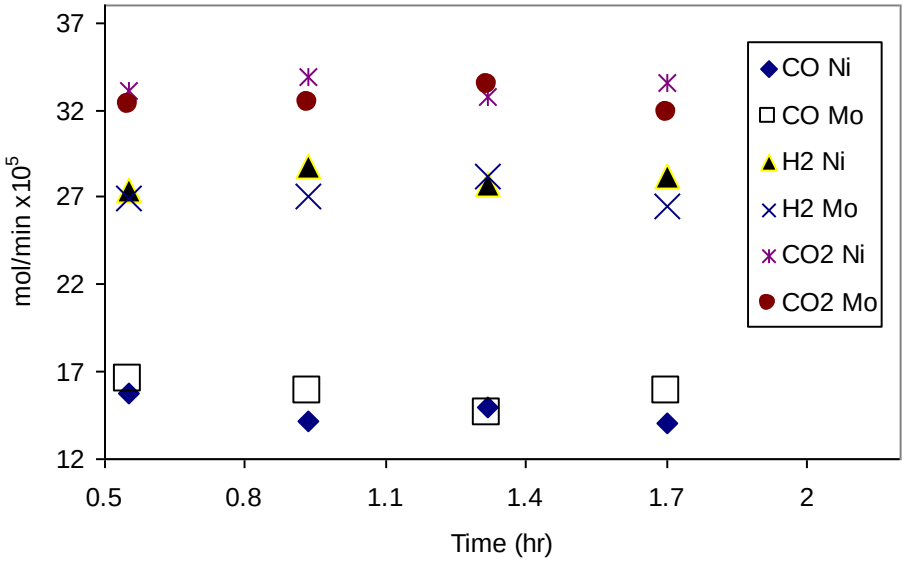

Figure 6.10: CO, CO_2 and H_2 produced from WGS reaction for 15Ni and 0.1Mo catalysts at 450°C, 6 mol % of H2O and CO and at GHSV = 339,800 ml/hr.g_{cat}

Table 6.6: CH_4 in mol/min×10^5 produced from WGS reactions at three GC readings

Reading Time (hr)	*0.93*	*1.5*	*1.7*
15Ni	0.7	0.6	0.6
0.1M-15Ni	1.8	2.3	1.8

6.5.2 The Methanation Reaction (ME)

Product distribution results from the screening tests of the 0.3Mo-15Ni catalyst in Chapter 5 and the individual reactions of the 0.1Mo-15Ni catalysts in this chapter showed that the addition of these small amounts of Mo resulted in higher CO and H_2 production and lower CH_4 production compared to the unpromoted catalyst. This led us to suggest that the addition of Mo to the Ni catalyst may cause a decrease in the catalyst's ability to consume CO and H_2 and produce CH_4 through the methanation reaction (reaction 6.1):

$$CO + 3H_2 = CH_4 + H_2O \qquad (6.1)$$

The ME reaction is a common side-reaction during hydrocarbon SR and OSR, especially at low H_2O/C ratios. Note that ME reaction is actually the reverse of the CH_4 SR.

In order to investigate the effect of Mo addition, ME reaction was run under the following conditions. All runs were carried out at 450°C. The GHVS was kept constant by maintaining the same amount of catalyst and total flow rate. The feed composition was 4 vol % CO and 8 vol % H_2, with a lower H_2/CO ratio than stoichiometric. This H_2/CO = 2 ratio was chosen based on preliminarily experiments for different H_2/CO ratios which showed that at stoichiometric H_2/CO = 3 ratio under the reaction conditions the CO conversion over the 15 Ni catalyst was 97-99 %. Therefore, in order to maintain similar reaction conditions with varying conversions of CO to compare the two catalysts, the H_2/CO ratio was lowered to 2 which also falls within the industrial application ratio range; 2-4 (Grander and Bartholomew, 1981).

The effluent molar flow rates with uncertainty error bars of CO, CO_2 and CH_4 for both catalysts 15Ni and 0.1Mo are shown in Figure 6.11, while H_2 rates in the product and are presented in Table 6.7. The activity and product selectivities of the two catalysts did not show any significant difference, although a slight increase in CH_4 was observed with 0.1Mo. This actually may contradict our suggestion that the addition of Mo to Ni decreased the activity of the ME reaction. In fact, the targeted ME experiments may suggest that increasing the amount of Mo may further increase the activity of the ME

reaction. This was investigated by Aksoylu and Onsan in 1998 as they studied the CO methanation reaction over a wide range of different Ni and Mo compositions in a Ni-Mo/Al_2O_3 bimetallic catalyst, where their lower Mo wt % was 5. They found that a 15%Ni-5%Mo catalyst had a higher methanation activity than the unpromoted 15% Ni catalyst at 250°C and at a H_2/CO ratio of 2. For low 5 wt % Ni loadings they related the promoter effect to increasing the total metal surface area by improving dispersion. However, at the 15% Ni composition they attributed the enhanced catalyst performance when adding 5 wt % Mo to electron transfer from MoOx species to active Ni sites, since they found that the monometallic Mo/Al_2O_3 catalyst gave no activity even at high Mo loadings, 15 wt %. Moreover, the addition of more than 10% wt Mo caused a decrease in the 15% Ni catalysts activity due to coverage of Ni sites by MoOx species at high Mo loadings. Although this study found a positive effect of Mo on the activity and product selectivity of the methanation reaction, the stability of the studied catalysts was not investigated.

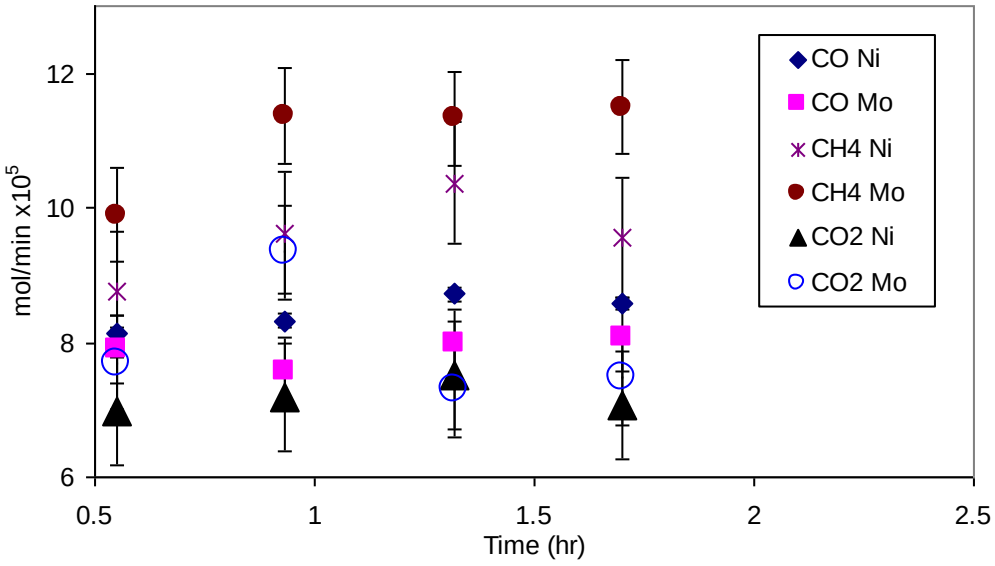

Figure 6.11: The effluent molar flow rates with uncertainty error bars of CO, CO_2 and CH_4 for both catalysts 15Ni and 0.1Mo from ME reaction at 450°C and H_2/CO = 2

Table 6.7: H_2 in mol/min×10^5 produced from ME reactions at four GC readings with uncertainty error

Reading Time (hr)	*0.55*	*0.93*	*1.5*	*1.7*
15Ni	22.2±1.1	22.1±1.1	22.3±1.1	22.2±1.1
0.1M-15Ni	21.1±2.3	21.1±2.3	20.9±2.3	21.1±2.3

The loss of catalyst stability during ME reactions is caused mainly by carbon deposition from the Boudouard reaction (Grander and Bartholomew 1981). In addition, exposure of the Ni based catalyst to temperatures higher than 600°C could lead to loss of active surface area via atom migration sintering (Rostrup-Nielsen et al, 2007). For both catalysts in our study no carbon deposited after the two hour run was observed. Although the lack of carbon deposition was expected due to the short run time, the presence of H_2 was thought to be the main reason. This was also concluded from the early work of Grander and Bartholomew (1981). As they studied carbon deposition from the Boudourad reaction under different methanation conditions over 15% Ni/Al_2O_3, they found that the presence of H_2 prevented carbon deposition during methanation reactions even at H_2/CO ratios as low as 0.5. They also studied carbon deposition rate in ME reactions over a 2.5% Ni-3% MoO_2/Al_2O_3 catalyst at $H_2/CO = 2$ and in the temperature range of 400-450°C. However, the promoted catalyst deactivated rapidly losing 90-95% of its activity compared to a loss of 40-60% for the unpromoted Ni catalyst under the same conditions. They attributed the low activity of the Ni-MoO_3 catalyst to its poor ability to hydrogenate atomic or polymeric carbon.

CO_2 was also produced over both catalysts as shown in Figure 6.11. This was expected as the relatively low H_2/CO ratio allows more CO to react with the produced H_2O through the WGS reaction to give CO_2 and H_2. Because of the low H_2/CO ratio we also expected to produce some C_2-C_4 hydrocarbons as they are known to be produced from ME reactions under our experimental conditions. However, no C_2-C_4 hydrocarbons were detected over both catalysts. This occurs mainly because of the high reaction temperature which accelerates methanation and prevents CHx species from polymerizing to higher hydrocarbons.

6.6 Considering Higher Mo Loadings (0.5 wt % Mo) in Further Investigations

An important observation from the screening experiments in Chapter 5 was that, although very low loading of Mo (e.g. 0.05 wt%) leads to stable catalysts, Mo loading of just above 0.3 wt% showed rapid loss of activity, but not due to coke formation. The activity investigation in Chapter 5 considered two Mo loadings; 0.3 and 0.8 % wt, while in the stability time-on-stream experiments only the 0.3 loading was examined since the 0.8 loading was not active. Therefore, in order to explain the effect of higher Mo loadings on the Ni catalyst and to help understanding the reasons for higher activity and stability at lower Mo loadings, a 15Ni-0.5Mo (0.5Mo) catalyst was considered.

Steam reforming experiments were run for the 0.5Mo catalyst and compared to the 0.1Mo and 15Ni catalysts. The purpose of these experiments was to see if the 0.5Mo is active under the analyzed conditions, unlike the 0.8Mo catalyst, and if so, to see if it follows the same product distribution patterns as the 0.3Mo and 0.1Mo catalysts. Experiments were repeated to ensure reproducibility of the data and error bars are reported. Figure 6.12 presents propane SR conversions for the 15Ni, 0.1M and 0.5Mo catalysts run at 450°C and S/C= 3. As expected, the 0.5Mo catalyst showed a lower conversion than the unpromoted Ni catalyst. This decrease in activity at higher Mo loadings is most likely caused by a structural effect of Mo on Ni active sites. Bengaard et al. (2002) found that during CH_4 SR over Ni catalysts, two active sites are involved with different reactivities; defect step sites which are more reactive, and less reactive close packed facets. They also suggested that carbon deposition is initiated on the same active step sites for SR. Therefore, when promoting Ni catalysts in SR reactions, the promoter prevents coking by binding to the step edges of Ni and hence blocking some of these active sites. A higher amount of the promoter will cause a total block of the step sites leaving only the less active close-packed facets which will lead to changes in activation energy barriers and reaction order. The change in activation energy of CH_4 formation during methanation reactions by the addition of 5% wt Mo to 15% wt Ni catalyst was also reported in the study of Aksoylu and Onsan (1998). Therefore, the addition of promoters to Ni catalysts should be optimized such that just enough promoter is present

to block carbon formation while allowing the SR reaction to take place. In this work (section 6.3), we found that, the optimized Mo amount added to 15% wt Ni catalysts for improving activity and cocking resistance during OSR and SR reactions is in the range 0.1-0.3 wt %.

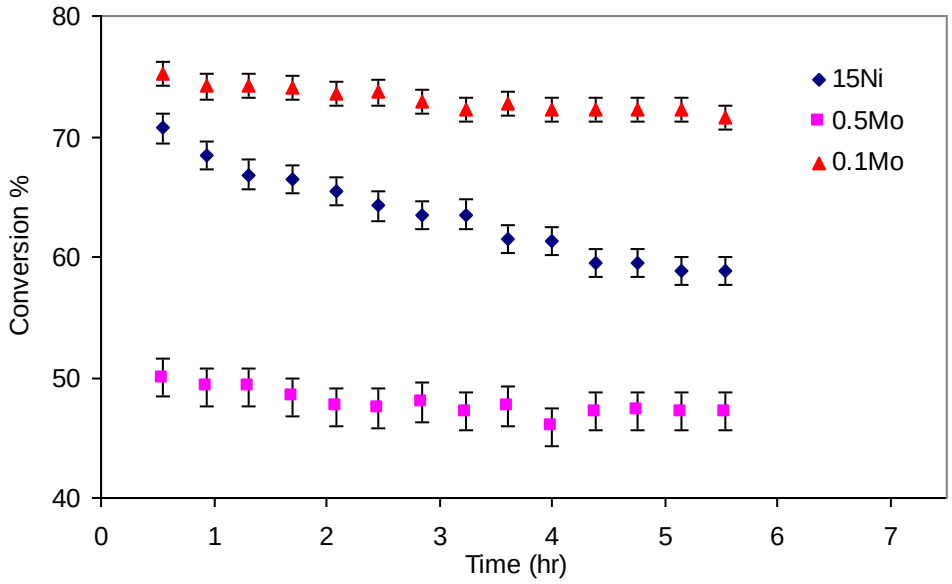

Figure 6.12: Propane SR conversions of 15Ni, 0.1Mo and 0.5Mo catalysts at 450 °C and S/C= 3

With the difference in conversion, product distributions for the three catalysts are normalized by presenting them as the yield of each product rather than the direct product mole flow rate as in the individual reactions results. The yield of a product Y_p was defined as:

$$Y_p = \frac{n_p}{n_{prop} \times X_{prop}} \qquad (6.10)$$

Where:
n_p: product molar flow rate mol/min×10^5
n_{prop}: propane feed molar flow rate mol/min×10^5
X_{prop}: propane conversion

Figures 6.13, 6.14, 6.15 and 6.16 present the yields of H_2, CO, CO_2 and CH_4, respectively for each catalyst. In agreement with our previous findings, Figures 6.13 and 6.14 show a higher syngas production when Mo is added, with the 0.5Mo catalyst having the highest yield for both H_2 and CO. On the other hand CH_4 yield was the highest for the unpromoted catalyst and the lowest for the 0.5Mo catalyst. CO_2 yields for the 15Ni and the 0.1Mo catalysts did not vary, while the 0.5Mo catalyst had the lowest CO_2 yield, which is a result of its high CO yield.

In light of the above results for the 0.5Mo catalyst, we speculate that the product selectivity mechanism for both 0.1Mo and 0.5Mo is somehow related since the same product patterns were observed. This also could be concluded for the role of the two catalysts in resisting carbon formation. Therefore, experiments will be run as well for the 0.5Mo catalyst to further investigate the effect of Mo on carbon deposition reactions, discussed in the next section. The 0.5Mo catalyst will also be considered when investigating the structural effect of Mo on the Ni catalyst in the next chapter (chapter 7).

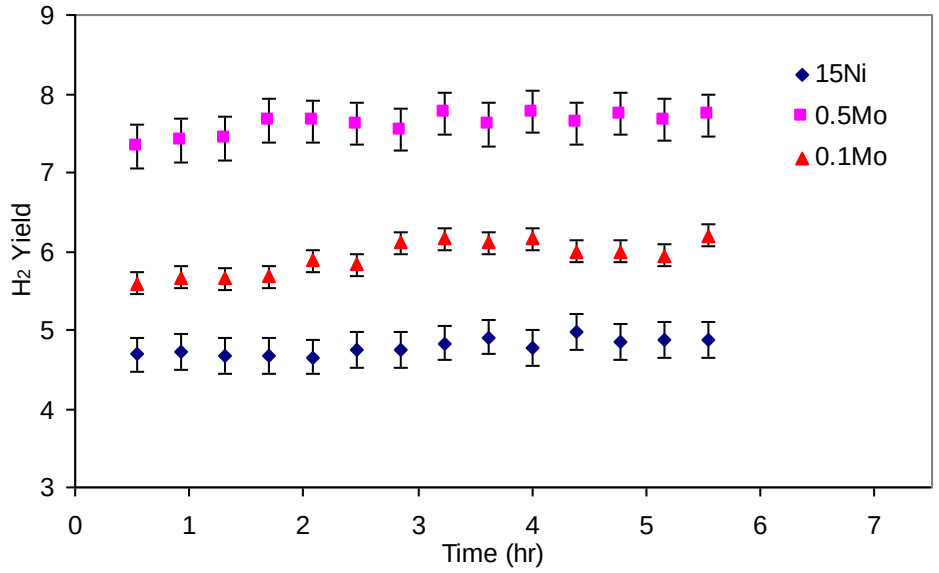

Figure 6.13: H_2 yield from propane SR of 15Ni, 0.1Mo and 0.5Mo catalysts at 450°C and S/C= 3

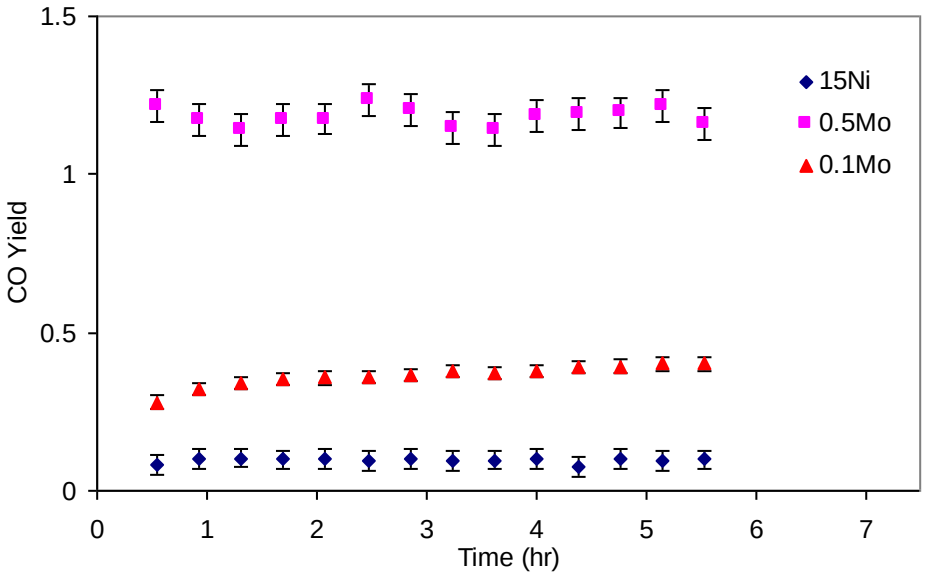

Figure 6.14: CO yield from propane SR of 15Ni, 0.1Mo and 0.5Mo catalysts at 450°C and S/C= 3

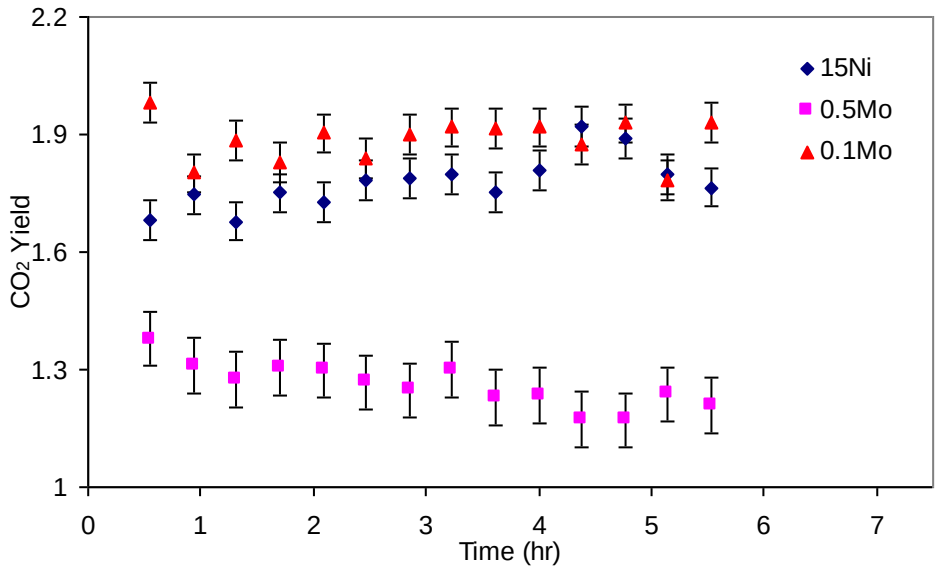

Figure 6.15: CO_2 yield from propane SR of 15Ni, 0.1Mo and 0.5Mo catalysts at 450 °C and S/C= 3

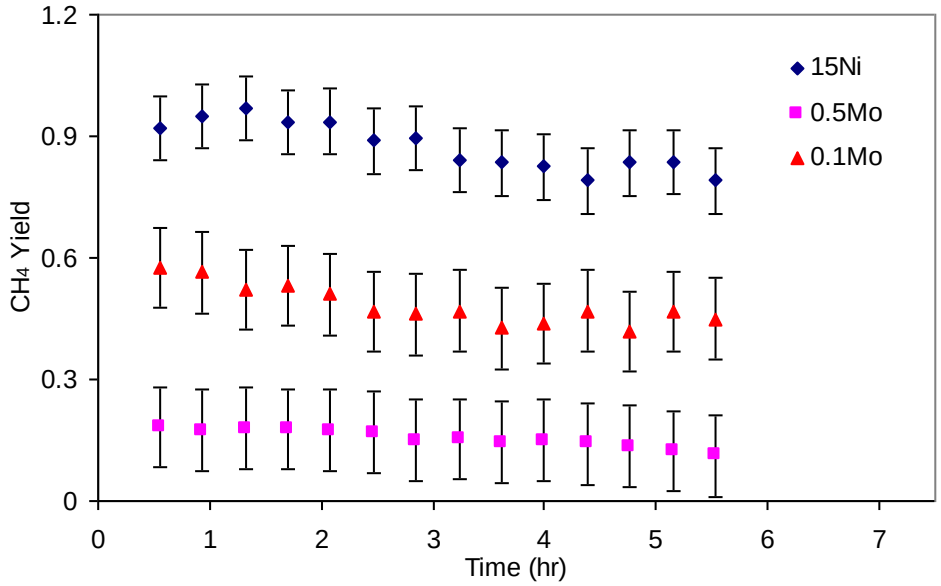

Figure 6.16: CH_4 yield from propane SR of 15Ni, 0.1Mo and 0.5Mo catalysts at 450 °C and S/C= 3

6.7 Effect of Mo on Carbon Deposition Reactions

As concluded from OSR stability experiments in Chapter 5, the addition of even small amounts of Mo (0.05 % wt) to the 15Ni catalyst had a significant effect in preventing the deactivation of catalyst by coking. The absence of carbon deposition was also observed in SR of propane over the 0.1Mo catalyst early in this chapter. Although Ni steam reforming catalysts can also be deactivated by sintering or oxidation of Ni to non-active phases, coking is the main type of deactivation affecting SR Ni-based catalysts especially at high hydrocarbons feeds. As a well-developed industrial process, deactivation of Ni catalysts in CH_4 SR was studied extensively in the literature. On the other hand, less attention was given to deactivation of LPG catalysts, as the feed was considered for H_2 production only in the last decade.

Carbon formation on Ni catalysts during SR is a function of different factors. These factors include the catalyst structure, the process feed and conditions and the reactor design. Carbon formation can be limited by designing a reactor with minimum void space to eliminate the occurrence of homogenous cracking of hydrocarbons. SR and OSR processes carbon formation results from a balance between reactions that produce gaseous carbon precursors and the gasification of these precursors or carbon by H_2O, O_2 and H_2. Therefore, an obvious way to reduce or prevent coking is choosing the right S/C and/or O_2/C ratios. Rostrup-Nielsen et al. (1993) have presented carbon limit diagrams which related carbon formation to the H:C and O:C ratios in the gas phase. However, for LPG hydrocarbons higher S/C and O_2/C ratios are needed to prevent coking, which means higher amounts of steam and O_2, thus increasing the cost of the process, and making it less economically feasible. Therefore, more attention is given to understanding the effect of the catalyst structure on carbon formation and how it can be modified or improved, to prevent carbon formation without losing catalyst activity.

In LPG, carbon formation during SR can be produced from a couple of reactions:
Decomposition of saturated hydrocarbons; butane, propane, ethane and methane:

$$C_nH_{2n+2} \longrightarrow nC + (n+1)H_2 \qquad \text{(B.1)}$$

Decomposition of unsaturated hydrocarbons; most likely ethylene and propylene:

$C_2H_4 \longrightarrow 2C + 2H_2$ (B.2)

$C_3H_6 \longrightarrow 3C + 3H_2$ (B.3)

Dissociation of CO (the Boudouard reaction):

$2CO = C + CO_2$ (B.4)

CO hydrogenation

$CO + H_2 = C + H_2O$ (B.5)

Reactions B.4 and B.5 are reversible and carbon formation from them can be avoided by optimizing S/C and O_2/C ratios. Thermodynamics dictates that they are also favoured at low temperatures while carbon from hydrocarbon decomposition is favoured at higher temperatures. Since in our OSR and SR reactions relatively high S/C ratios were used, reaction B.5 is expected to proceed in the steam carbon gasification direction. In addition, by-product analysis from SR and OSR in Section 6.4.2 showed that under our reaction conditions, it is not favourable to produce unsaturated hydrocarbons, as no ethylene or propylene were detected. However, both unsaturated carbons were detected when performing propane and butane cracking experiments. In addition these hydrocarbons were detected when PO reactions were run in section 6.4.1 where also propane and butane cracking were taking place because of the lower O_2/C = 0.3. Therefore, in order to investigate the effect of Mo on carbon formation under our reaction conditions, carbon deposition from reactions B.1 and B.4 were analyzed for the 15Ni, 0.1Mo and 0.5Mo catalysts.

6.7.1 Analysis of Carbon Deposition from Propane cracking

As mentioned earlier, since homogenous reactions were eliminated under our reaction conditions, the focus here will be on comparing propane catalytic cracking rather than thermal cracking for the three catalysts. In order to investigate the effect of Mo on coking rates, propane cracking over the three catalysts was first analyzed by TGA. Then, catalyst cracking was also run in the packed bed reactor setup to quantify H_2 production, and to identify different carbonaceous species via temperature program oxidation (TPO).

TGA Analysis

The description of the TGA apparatus was presented in Chapter 3. 20 mg of each catalyst was placed in the quartz holder. The catalyst was first reduced under a stream of 30 % vol H_2/N_2 at 750°C for 30 min, and then was cooled down under N_2 to the reaction temperature, i.e. 450°C. After stabilizing the weight, a stream of 1% vol propane was introduced and weight changes were recorded as the temperature was kept constant for an hour. Figure 6.17 presents the percentage increase in weight with time for the three catalysts. During the first 4 min a slight increase in carbon deposition was observed over the Mo catalysts. After the 5^{th} min coking rates were constant for the three catalysts. Coking rates of the three catalysts were calculated from the slope of the steady state coking period between 5 and 30 min as shown in Figure 6.18.The coking rate was exactly the same for the 15Ni and the 0.1Mo catalysts, while the 0.5Mo catalyst had a slightly lower rate.

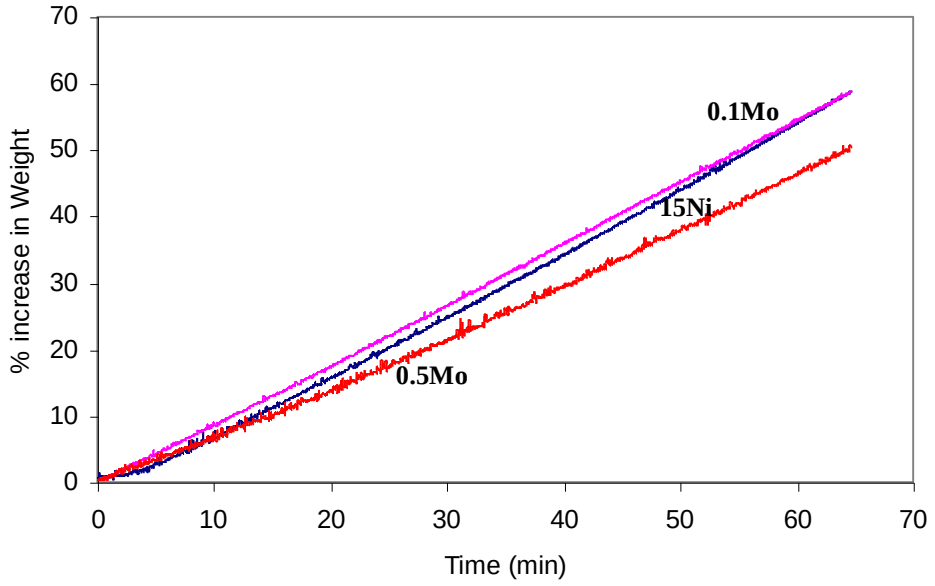

Figure 6.17: TGA of 1% vol propane cracking over the catalysts at 450°C

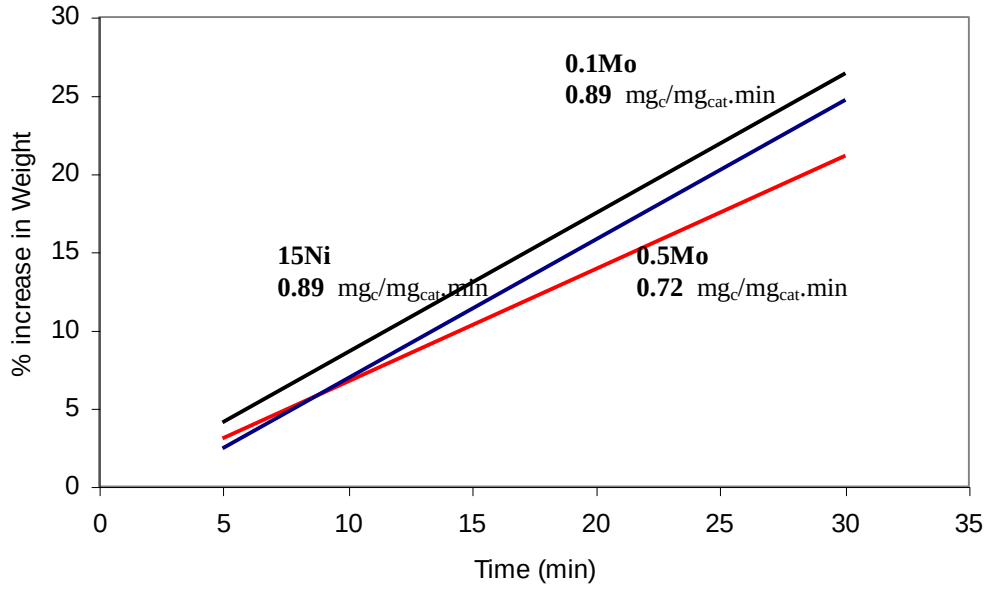

Figure 6.18: Coking rates calculated from slopes of TGA of 1% vol propane cracking over the catalysts at 450 °C

Propane Cracking in the Packed Bed Reactor

Propane catalytic cracking was also investigated in the packed bed reactor setup described in detail in Chapter 3. However, since the Varian 3800 GC used to analyze the products had a run time of 20 min, the effluent from the reactor was connected to an Agilent 3000 micro GC. The micro GC was fitted with a TCD which measured light gases concentrations throughout the course of the experiment. 30 mg of each catalyst was placed in the reactor and was pre-reduce with a 30 vol% H_2/N_2 stream at 750°C for 30 minutes before cooling down to 450°C. At 450°C a 3% vol propane stream was introduced and the micro GC started analyzing the product stream for an hour. After the reaction, propane was shut off and the reactor was cooled down under N_2 to 200°C. At 200°C TPO was begun by introducing a stream of 3% vol O_2 while ramping the temperature at 2°C/min up to 900°C. The micro GC was used to detect O_2, CO and CO_2 gases from the gasification of different types of carbon.

H_2 concentrations from propane cracking over the three catalysts are shown in Figure 6.19, while Figure 6.20 represents propane conversion. In agreement with TGA results, propane cracking rates were almost the same over the 15Ni and the 0.1Mo catalysts as propane conversions and H_2 production did not show significant differences between the two catalysts. The 0.5Mo catalyst had a lower propane conversion and H_2 production rate also indicating that less carbon would be deposited on the catalyst. H_2 production over all three catalysts reached a maximum before it decreased as the catalyst began deactivating. The period for H_2 to reach this maximum point was longer for the 0.5Mo catalyst indicating a slower coking rate than the other two catalysts. However, once all three catalysts began deactivating, deactivation rates were the same for the three catalysts, which may indicate same carbonaceous species on the catalysts.

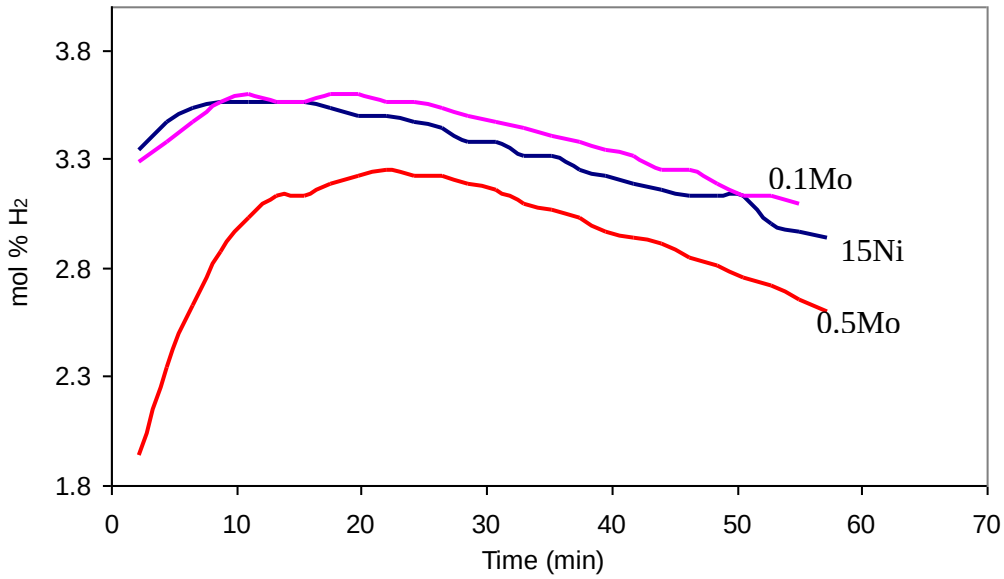

Figure 6.19: H_2 concentrations from 3 vol % propane cracking at 450°C in a packed bed reactor

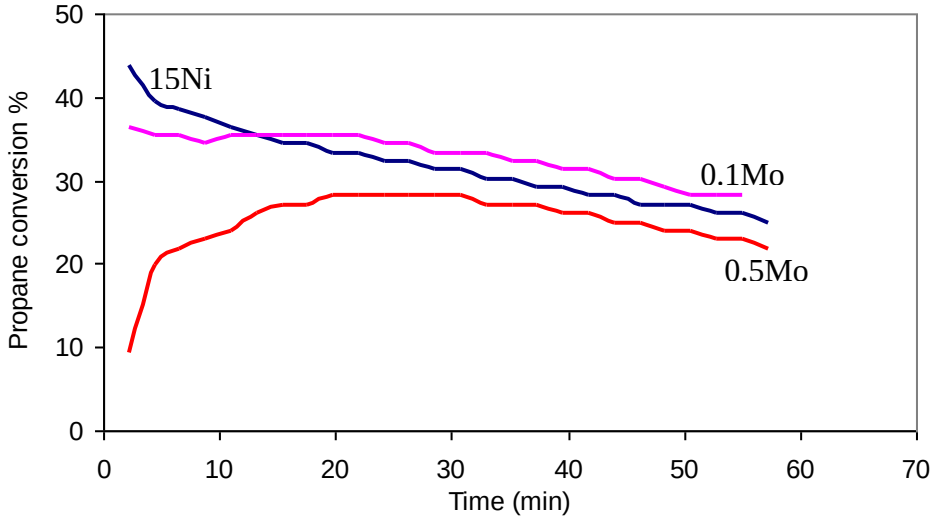

Figure 6.20: Propane conversion from 3 vol % propane cracking at 450°C in the packed bed reactor

Propane Cracking TPO Experiments

To identify and quantify carbonaceous species resulting form propane cracking over the three catalysts, TPO experiments were run in the packed bed reactor as described earlier. CO_2 and CO concentrations resulting from O_2 gasification of carbon at different temperatures are presented in Figure 6.21. CO_2 concentrations are represented by the solid lines, while the dotted lines are CO concentrations, which were only detected in a certain temperature range for all three catalysts. For all catalysts different CO_2 peaks were identified at certain temperature ranges. The dissociation of hydrocarbons over Ni is believed to begin with forming CHx fragments which will further dehydrogenate to monoatomic carbon (C_α). The first CO_2 peak in the 370 to 375°C range are assigned to these carbon species that can be easily gasified by O_2, H_2O or H_2 to form COx in SR reactions (Natesakhawat et al, 2005). However, in the absence of gasifying agents, or at slower gasification rates, these C_α carbons will polymerize to form layers of polymeric amorphous films of $C_ß$ carbons. $C_ß$ is less active than C_α and require higher temperatures to be gasified, and therefore it is believed to be responsible for the CO_2 peak in the 420 to 500°C range for all three catalysts in Figure 6.21. Since $C_ß$ is harder to gasify and is reported to begin forming at temperatures as low as 250°C (Bartholomew and Farrauto, 2006), it can further dissolve in Ni particles and form vermicular carbon (Cv) and further carbon fibres and whiskers.

The CO_2 peak in the 500 to 560°C range in Figure 6.21 is most likely attributed to carbon whiskers. This peak is accompanied by a CO peak in the same range for the three catalysts. Carbon whiskers are thought to be the most common type of carbon forming on Ni catalysts in hydrocarbon steam reforming and was detected by a number of authors under SR conditions using TPO and TEM techniques [Trimm (1997); Bengaard et. al. (2002); Laosiripojana and Assabumrungrat (2006); Bartholomew and Farrauto (2006); Zhang et al. (2009); Li et. al. (2009)]. Whiskers formation begins with the dissolution of carbon in Ni through the formation of nickel carbide (Ni_3C) which is thought to be unstable (Trimm, 1999). Once carbon has dissolved in Ni, it begins to diffuse through Ni particles that are suitable for filament growth. As carbon reaches the Ni/support interface it overcomes the interaction between them and begins lifting the Ni particle and

accumulating between the particle and the support surface. The steady state growth of carbon whiskers is sustained by continuous diffusion of carbon through the Ni particle driven by a carbon concentration gradient. The concentration gradient results from a carbon enriched front Ni surface, followed by atomic Ni layers with lower carbon concentrations to the bulk concentration of dissolved carbon (Bengaard et. al, 2002). Although, the concentration gradient is thought to be the driving force for the bulk diffusion of carbon through the Ni particles, a temperature gradient could play a role in the diffusion process also (Bartholomew, 1982). As whiskers continue growing, the Ni particles on the tip of them remain active; however, the accumulation of carbon whiskers blocks the catalyst bed and causes high pressure build-up across the reactor.

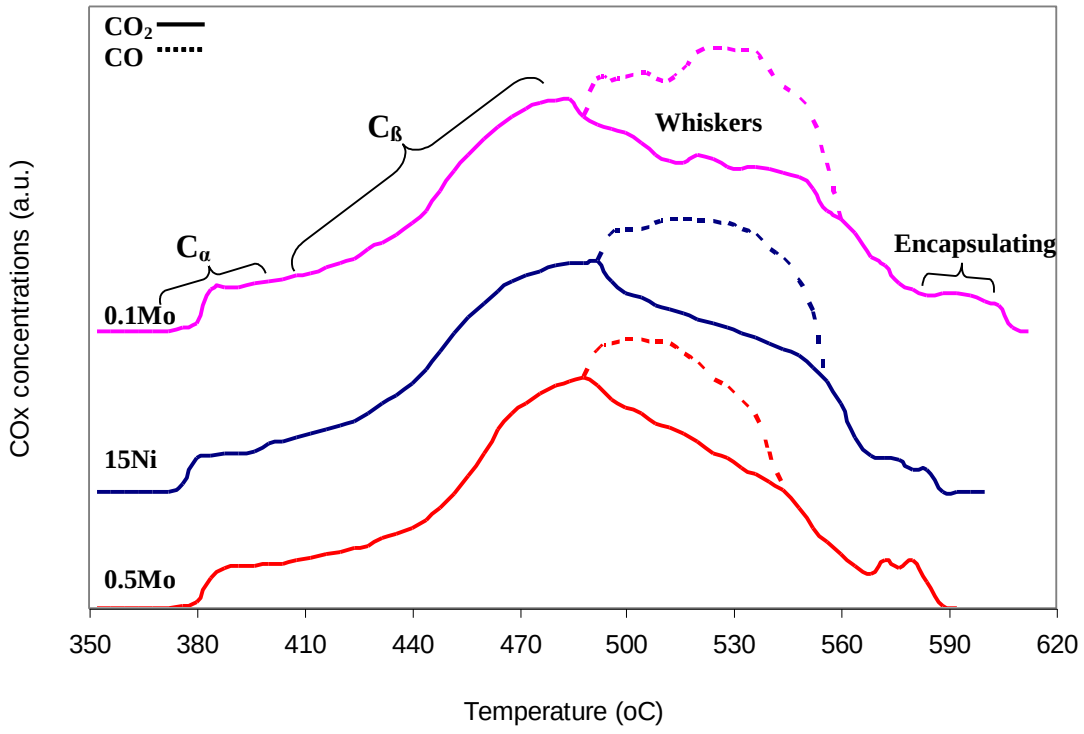

Figure 6.21: TPO after 3 vol. % propane cracking for 1 hour at 450°C

As gasification temperatures increased over 500°C, in the carbon whiskers region, CO was produced from carbon oxidation for all three catalysts. CO production is an indication of high oxidation rates, due to higher amounts of whiskers, and limited O_2 concentration. Whisker gasification is thought to occur in a reverse process to their growth, meaning that carbon should first diffuse back to the Ni surface in order to be gasified. This carbon back diffusion to the Ni surface was proposed to be the gasification rate determining step and the CO production is an indication of this step (Trimm, 1977). CO production was slightly higher from the 0.1Mo catalyst than from 15Ni, since CO production is related to back diffusion through Ni particles; this indicates that slightly more Ni sites were available for whisker formation over the 0.1Mo catalyst. More Ni sites for carbon formation indicates more active sites for steam reforming, as it was reported by Bengaard et al. (2002) that during CH_4 steam reforming over Ni catalysts both the reforming reaction and the formation of carbon are initiated at the same type of active site, which they refer to as defect step sites. Moreover, the steam reforming reaction requires a Ni ensemble of only 3 or 4 atoms while an ensemble of 6 or 7 Ni atoms is required to form a reactive surface carbon intermediate, which acts as a precursor for different carbon types [Edwards and Maitra (1995); Gonzalez et al. (2000)]. Therefore, higher SR conversions over the 0.1Mo catalyst could be a result of more Ni active sites.

Not all of the $C_ß$ carbon dissolves in Ni particles and forms carbon whiskers; some of theses carbon films will remain on the surface and encapsulate Ni particles. This encapsulation will lead to the formation of graphitic carbon, which will not only deactivate Ni, but also cause high pressure drops across the reactor (Bartholomew and Farrauto, 2006). The peaks in the 570-620°C range are attributed to these types of carbons. These peaks could also account for the gasification of graphite which is in direct contact with the alumina support and require high gasification temperatures (Natesakhawat et. al, 2005). Figure 6.22 is an illustrative scheme of different carbon forms resulting from hydrocarbon cracking over Ni SR catalysts and their possible transformation routes (adapted from Trimm, 1997).

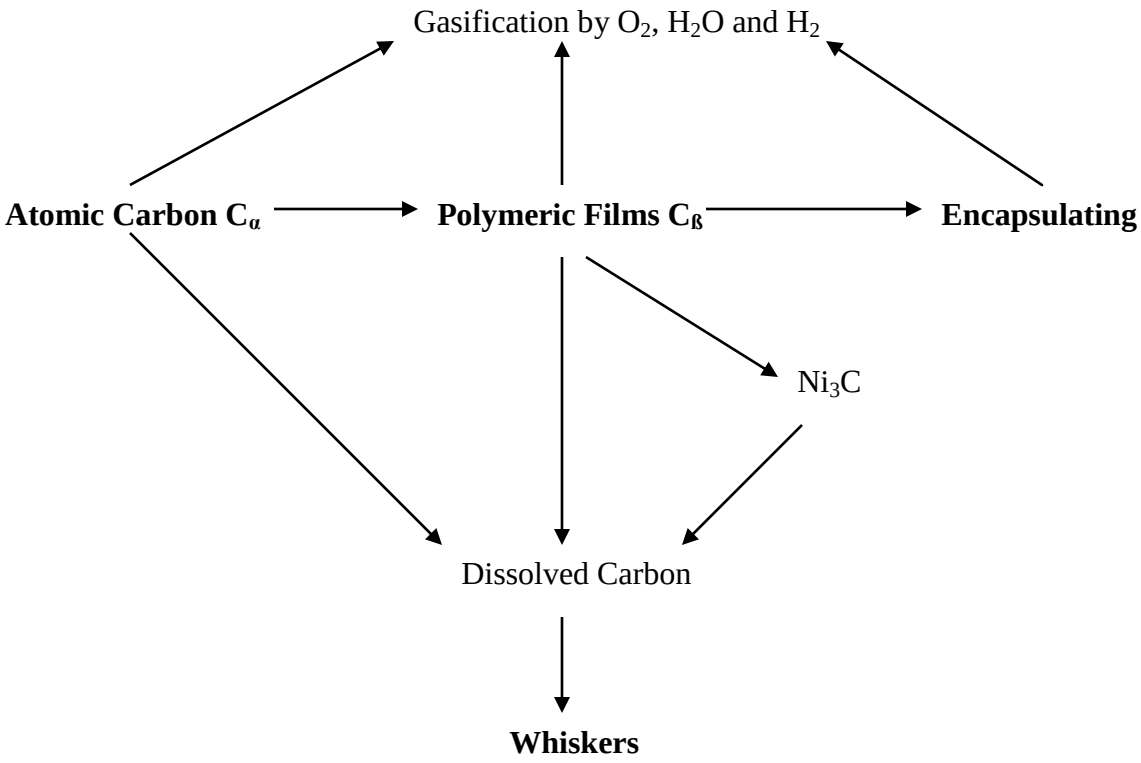

Figure 6.22: An illustrative scheme of different carbon forms resulting from hydrocarbon cracking over Ni steam reforming catalysts and their possible transformation routes (adapted from Trimm, 1997).

In general, propane cracking and TPO experiments did not show a significant difference between the catalysts that can explain the high resistance of 0.1Mo and 0.5Mo to catalyst coking during OSR reactions. These TPO results are in accord with the TGA results that showed similar carbon deposition rates for 0.1Mo and 15Ni. However, during SR experiments in section 6.4.2, much less carbon was deposited over the 0.1Mo catalyst than over the 15Ni catalyst. Furthermore, the types of carbon resulting from propane cracking were the same on the three catalysts, indicating that the Mo promoter does not affect the transformation mechanism of C_α to different carbon forms which are less reactive and more difficult to gasify. Therefore, propane cracking is not the reason for the difference in carbon deposition between 15Ni and 0.1Mo for SR and OSR.

Propane Catalytic Cracking in the Presence of O_2

Propane cracking with O_2 was run in the packed bed setup connected to a micro GC, to monitor different product concentrations from the reactor effluent every 90 seconds. Experiments were run for the three catalysts under exactly the same conditions as described earlier for the cracking experiments, but this time with the addition of 2.7 % vol. O_2 to obtain an O_2/C ratio of 0.3. The O_2/C ratio is similar to that of the propane partial oxidation (PO) individual reaction analyzed in Section 6.4.1 The feed propane mole fraction is 3 vol%. After running the experiment for one hour, TPO was run following the same procedure as described earlier.

Figures 6.23 shows propane conversion , while Figures 6.24, 6.25, 6.26 and 6.27 present concentrations recorded by the micro GC of H_2, CO, CO_2 and CH_4 respectively. It is important to note that the O_2/C ratio is lower than the stoichiometric ratio (O_2/C = 0.5) to produce CO and H_2. In addition, the reaction temperature is lower than that reported in the literature (Navarro et al, 2007). So, in reality only a portion of each fuel is partially oxidized while the rest is catalytically cracked or does not react. Although these experiments were run under more favourable coking conditions than in the PO experiments (because of higher propane concentration), the general trends of products were in good agreement with those of 0.1Mo and 15Ni PO presented in Section 6.4.1 earlier. Therefore, the trends of these two catalysts will not be discussed here as they were discussed earlier in detail. Similar to SR results in Section 6.6 the 0.5Mo catalyst had a lower propane conversion in the first 30 min, but it was more stable with time as the 15Ni catalyst began losing activity due to coking. Even at lower propane conversions, among all three catalysts, CO was the highest and CH_4 the lowest for the 0.5Mo catalyst. In terms of CO, these data indicate a higher capability of the 0.5Mo catalyst to oxidize C_α or CH_x fragments to CO and H_2. Higher CO concentrations and lower conversions resulted in lower CO_2 concentrations.

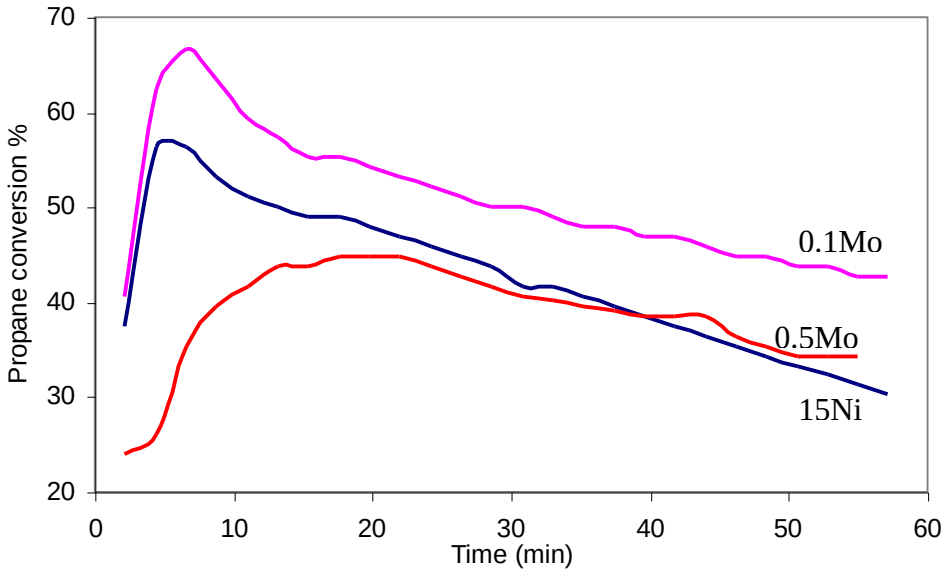

Figure 6.23: Propane conversion from 3 vol % propane cracking in the presence of O_2 at 450°C in the packed bed reactor

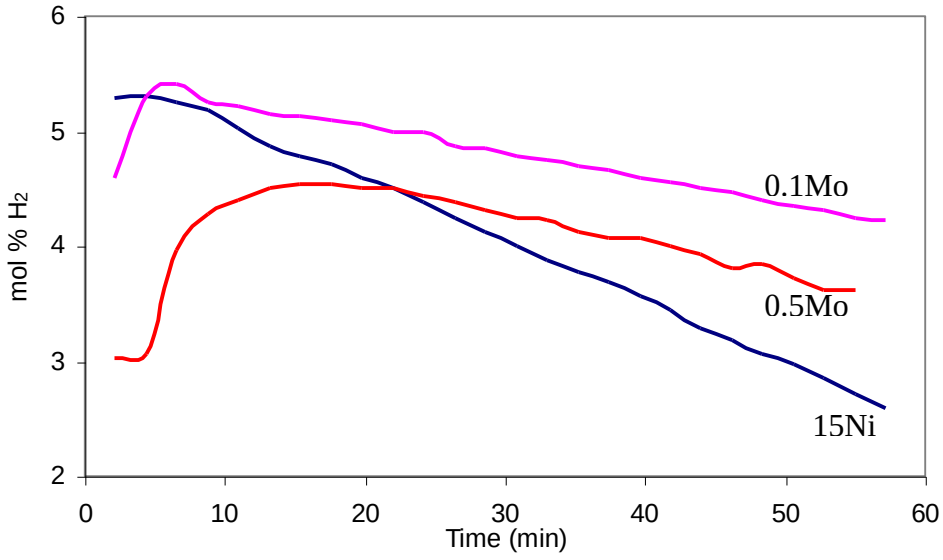

Figure 6.24: H_2 concentrations from 3 vol % propane cracking in the presence of O_2 at 450°C in the packed bed reactor

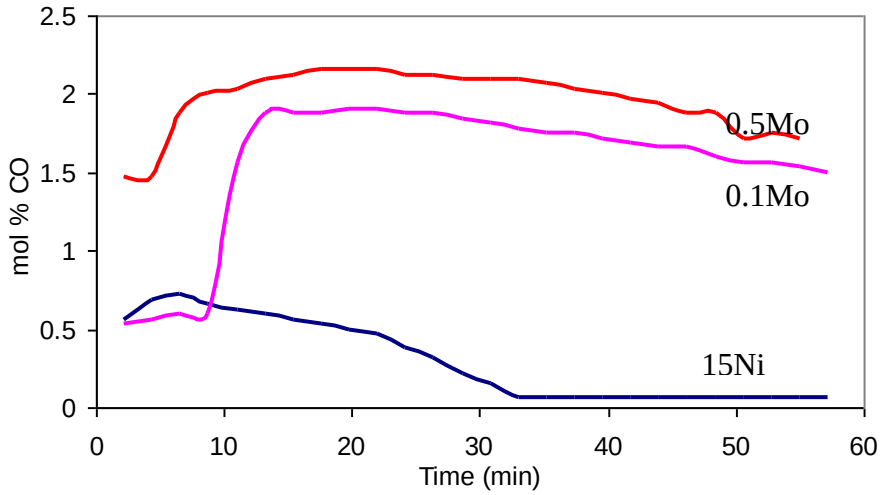

Figure 6.25: CO concentrations from 3 vol% propane cracking in the presence of O_2 at 450°C in the packed bed reactor

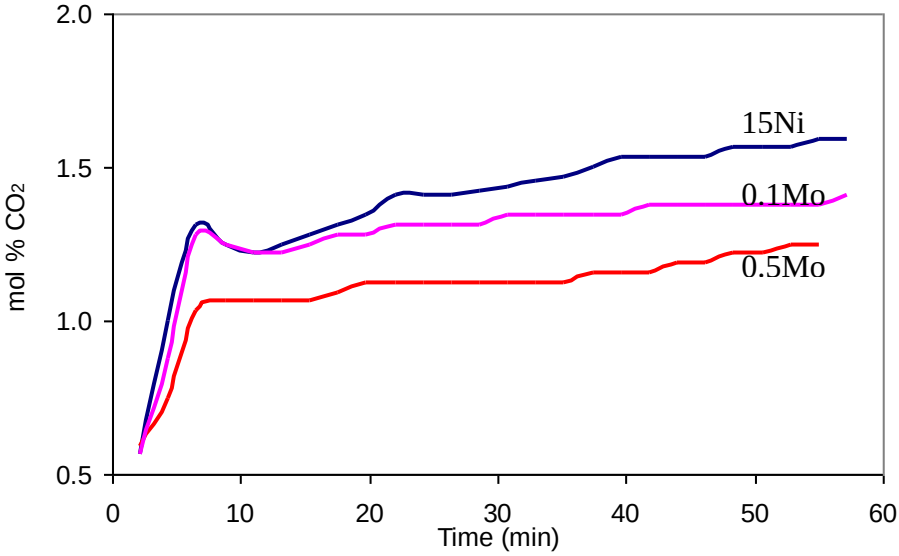

Figure 6.26: CO_2 concentrations from 3 vol% propane cracking in the presence of O_2 at 450°C in the packed bed reactor

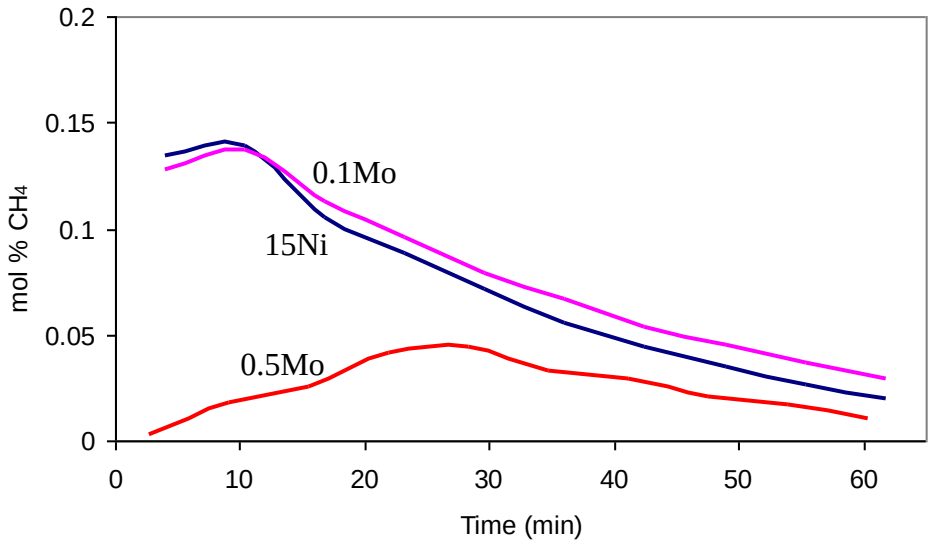

Figure 6.27: CH_4 concentrations from 3% vol propane cracking in the presence of O_2 at 450°C in the packed bed reactor

TPO Experiments of Propane cracking in the presence of O_2

Results of TPO runs for the three catalysts are shown in Figure 6.28, with the dotted lines representing CO concentrations. As expected the amount of carbon deposition was lower over the promoted catalysts than over the 15Ni catalyst. The lower amount of carbon on the 0.5Mo catalyst could be argued to be a result of lower conversions. However, the 0.1Mo catalyst had a higher conversion and yet a lower amount of carbon. In order to compare the amounts of carbon deposition of the three catalysts resulting from cracking with and without O_2, the area under each curve, including CO, in Figures 6.21 and 6.28 were integrated, and the results are presented in Table 6.8. The addition of O_2 decreased carbon deposition over 0.1M and 0.5Mo significantly, while no effect was observed on the 15Ni catalyst.

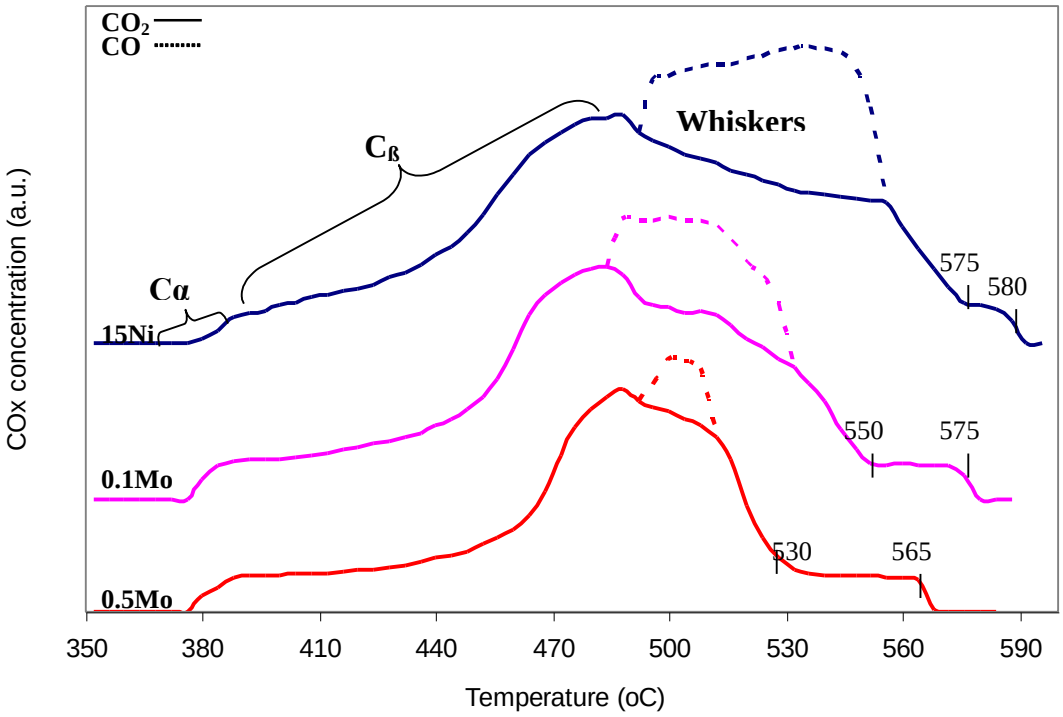

Figure 6.28: TPO after 1% vol. propane cracking in the presence of O_2 for 1 hour at 450°C

Table 6.8: Amounts of carbon from cracking with and without O_2 over the three catalysts

Catalyst	Carbon from Cracking (a.u.)	Carbon from Cracking with O_2 (a.u.)	% Decrease
15Ni	156	151	3.2
0.1Mo	158	130	17.7
0.5Mo	125	88	29.6

For all three catalysts, the four types of carbon previously identified in Figure 6.21 can also be identified when cracking in the presence of O_2 (Figure 6.28). However, small changes were observed for the gasifying temperature zones and the amount of each carbon type. The initial gasification temperature was the same for the three catalysts, which began at 377°C and was assigned to easy to gasify atomic carbon, Cα. A higher amount of this carbon was observed for the promoted catalysts compared to 15Ni. Higher CO concentrations in the carbon whiskers regions for 15Ni indicate higher amounts of fibrous carbon. The encapsulating carbon region was also different for the three catalysts. For 0.5Mo it was in the temperature range 530-565°C, it increased to a higher temperature range of 550-575°C for 0.1Mo, while higher temperatures were required to remove these types of carbon from the unpromoted catalyst; 575-580°C. In addition, the amount of carbon is higher in this encapsulating carbon region for the promoted catalysts. This could indicate that less carbon is dissolved in Ni particles to form whiskers for 0.1Mo and 0.5Mo. Instead, more filamentous encapsulating carbon is accumulating on the catalyst surface or support. Although we suggested earlier, based on the cracking TPO, that the presence of Mo did not have an effect on the dissolution of carbon into Ni particles to form whiskers, the presence of O_2 could have affected the dissolution process over the promoted catalysts. O_2 may have a structural effect on the Mo catalysts, oxidizing Mo to MoOx which can partially decorate Ni particles, and hence, prevent or limit carbon dissolution. On the other hand, if the dissolution is assumed to occur through the formation of a nickel carbide intermediate, then the high O_2 mobility over the Mo catalysts is expected to prevent dissolution by gasifying the unstable Ni_3C intermediate (Trimm, 1999).

Although the amounts of carbon were significantly lower over the promoted catalysts, the morphology of carbonaceous species was the same for the three catalysts, with no significant differences in gasification temperature ranges of the first three types. In other words, once $C_ß$, whiskers or encapsulating carbon are formed, the difficulty in gasifying them is the same on promoted and unprompted catalysts. In fact, Silva et al. (1997) studied air gasification of charcoal over Mo, Co and Ni oxides and found that Co and Ni had better gasification rates than Mo especially at the lower temperature ranges (300-

500°C). Even when mixing Mo with Ni, the improvement in gasification rates was not significant as they attributed this slight improvement to the role of Mo in preventing crystal growth or sintering. Therefore, in order for the Mo-promoted catalysts to have lower amounts of deposited carbon, the gasification process is most likely to occur before the complete dehydrogenation of CH_x fragments to C_α or $C_ß$ carbons. This led us to believe that Mo-promoted catalysts may play a role in preventing the complete dehydrogenation of CH_x fragments. This was also suggested by Wang et al. (1999) who studied the role of Mo in a Rh/Al_2O_3 catalyst in the process of CH_4 decomposition and hydrogenation to produce higher hydrocarbons at low temperatures (400°C). From different FTIR spectra studied, they found that the addition of Mo to the Rh catalyst increased the amount of CH_x species and decreased C_α.

6.7.2 Analysis of Carbon Depositions from CO Dissociation (the Boudouard Reaction)

Earlier studies on the Boudouard reaction over Ni-based catalysts were conducted in order to investigate the deactivation of methanation reaction catalysts (Gardner and Bartholomew, 1981). This occurred because methanation reactions were run at low temperatures (300-450°C) where the Boudouard reaction is more favourable than CH_4 decomposition. In high temperature steam reforming, CO dissociation is not a concern for carbon deposition; thermal and catalytic hydrocarbon cracking is usually the main problem. Furthermore, the presence of H_2 and H_2O proved to prevent CO dissociation even at small H_2/CO and H_2O/CO ratios. This was concluded from the early work of Grander and Bartholomew in 1981, as they studied carbon deposition from the Boudouard reaction under different methanation conditions over 14% Ni/Al_2O_3, and found that the presence of H_2 prevented carbon deposition during methanation reactions even at H_2/CO ratios as low as 0.5. Therefore, even at our relatively low reaction temperature of 450°C, the Boudouard reaction is not expected to be a major carbon contributor, because of high S/C ratios. However, the significantly high CO production over the Mo-promoted catalysts enhances the possibility of CO dissociation over the 0.1Mo and 0.5Mo catalysts. Moreover, CO dissociation is known to be a structure-sensitive reaction [Mavrikakis et al.(2002); Andersson et al. (2008)]; hence, it can be

utilized to probe structural differences between the catalysts, although explaining these differences may require further investigation.

In order to compare coking rates from CO to those previously obtained from propane cracking, CO dissociation over the three catalysts was first analyzed by TGA. Then the reaction was also run in the packed bed reactor setup to quantify and compare CO_2 production from the reaction over the three catalysts.

TGA Analysis

A description of the TGA apparatus was presented in Chapter 3. 20 mg of each catalyst was placed in the quartz holder. The catalyst was first reduced under a stream of 30% vol H_2 /N_2 at 750°C for 30 min, and then was cooled down under N_2 to the reaction temperature, i.e. 450°C. After stabilizing the weight, in order to maintain the same carbon content as in the propane cracking experiments, a stream of 3% vol CO was introduced and weight changes were recorded as the temperature was kept constant. Figure 6.29 presents the % increase in weight with time for the three catalysts. The carbon deposition rate for each catalyst was calculated at steady state coking from the 15^{th} min, and slopes representing these rates are also shown in Figure 6.29. As expected, coking rates from the Boudouard reaction were lower than propane cracking, however, unlike propane cracking these rates were significantly different between the catalysts. 0.1Mo had the highest coking rate while 0.5Mo had the lowest. The order followed that of the catalysts, activities for SR (section 6.6), where the 0.1Mo catalyst had the highest conversion while 0.5Mo had the lowest. Based on earlier studies a number of authors suggested the following sequence of elementary steps for the Boudouard reaction mechanism [Tørttrup (1976); McCarty and Wise (1979); Gardner and Bartholomew (1981)]:

$$CO = *CO \qquad (D.1)$$

$$*CO \longrightarrow *C\alpha + *O \qquad (D.2)$$

$$*C\alpha \longrightarrow C_\beta \qquad (D.3)$$

$$*CO + *O = CO_2 \qquad (D.4)$$

where * is a surface active site. The adsorption of CO was proved to be a relatively fast step (equation D.1). Based on his kinetic studies, Tørttrup (1976) suggested that the dissociation of CO (reaction D.2) is the rate determining step, while studies by McCarty and Wise (1979) and Gardner and Bartholomew (1981) concluded that the conversion of Cα atomic carbon to polymeric C is the rate determining step. If we assume reaction D.2 to be rate determining, then higher 0.1Mo carbon rates indicate higher rates of dissociation. This could result from a structural change effect by the small amount of Mo, or it could indicate more Ni available sites for the reaction. On the other hand, if reaction D.3 is assumed to be rate determining, higher 0.1Mo rates can be again related to more active Ni sites, but also it may indicate faster transformation of Cα to polymeric carbon. Since the most common type of carbon to form from the Boudouard reaction under our temperature conditions are filamentous Cß and whiskers, higher transformation rates to these types will lead eventually to faster deactivation of the 0.1Mo catalyst or higher pressure built-up. In order to further investigate these possibilities, deactivation of the three catalysts by the Boudouard reaction was accelerated and monitored by TGA.

Deactivation experiments were run in the TGA following exactly the same procedure described earlier, with the CO feed concentration raised to 70% vol. Figure 6.30 shows the increase in the weight of the three catalysts within the first 5 hours. Since the 0.5Mo catalyst had the lowest coking rate it was expected to deactivate slowly. However, with the 0.1Mo catalyst having the highest coking rate it was expected to deactivate faster than the 15Ni catalyst, which was not the case, as by the 5^{th} hour the increase in weight of the 15Ni catalyst began to plateau indicating no further carbon accumulation. Most carbon formed on the catalysts under these high CO concentrations were thought to be of whisker carbon type [Rostrup-Nielsen (1972); Tørttrup (1976); Gardner and Bartholomew (1981)]. As was discussed for Figure 6.29, more carbon was formed on the 0.1Mo catalyst and Ni particles on the tip of these whiskers are active.

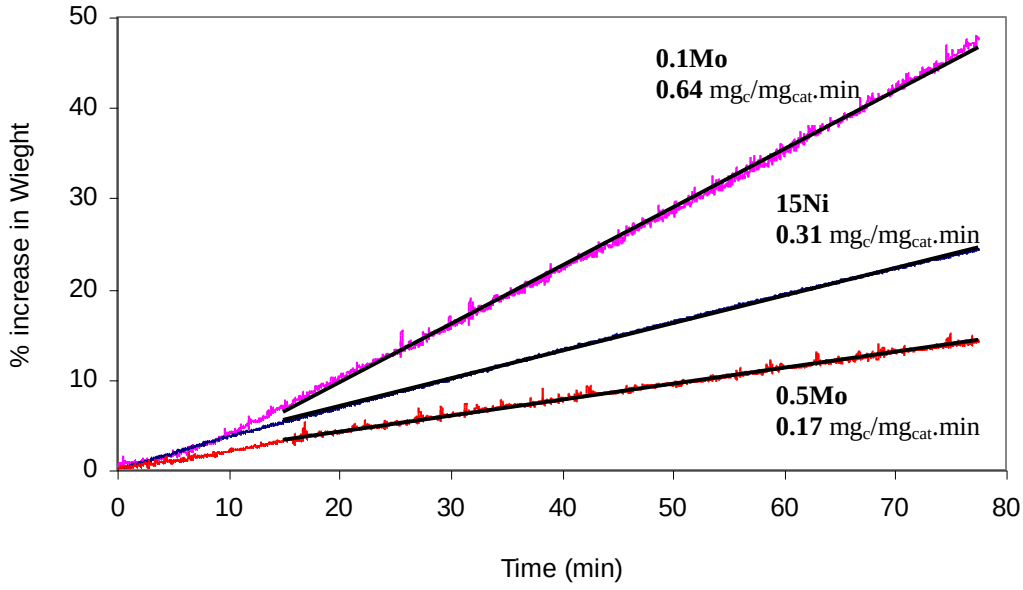

Figure 6.29: Coking rates calculated from slopes of TGA of 3% vol CO dissociation over the catalysts at 450°C

At these high CO feed concentrations, we speculate that the 15Ni catalyst deactivated as a result of losing active Ni sites due to the formation of inactive Ni carbonyls; $Ni(CO)_4$. Although this is not a common deactivation route for Ni catalysts, since it requires low temperatures and high CO pressures. A couple of authors did report the deactivation of Ni/Al_2O_3 methanation catalysts by the formation of inactive $Ni(CO)_4$ [Shen et al. (1981); Agnelli et. al. (1994)]. In fact, Bartholomew et al. (1982) suggested the loss of Ni phase even when performing CO chemisorption experiments. Since the formation of Ni $(CO)_4$ requires adsorption of CO on Ni sites, lower deactivation on the Mo-promoted catalysts may indicate weaker adsorption of CO on these catalysts. This weak adsorption of CO not only would explain the high CO and low CO_2 production over the promoted catalysts, but it would also be an indication of a catalyst surface structural change caused by the presence of these small amounts of Mo.

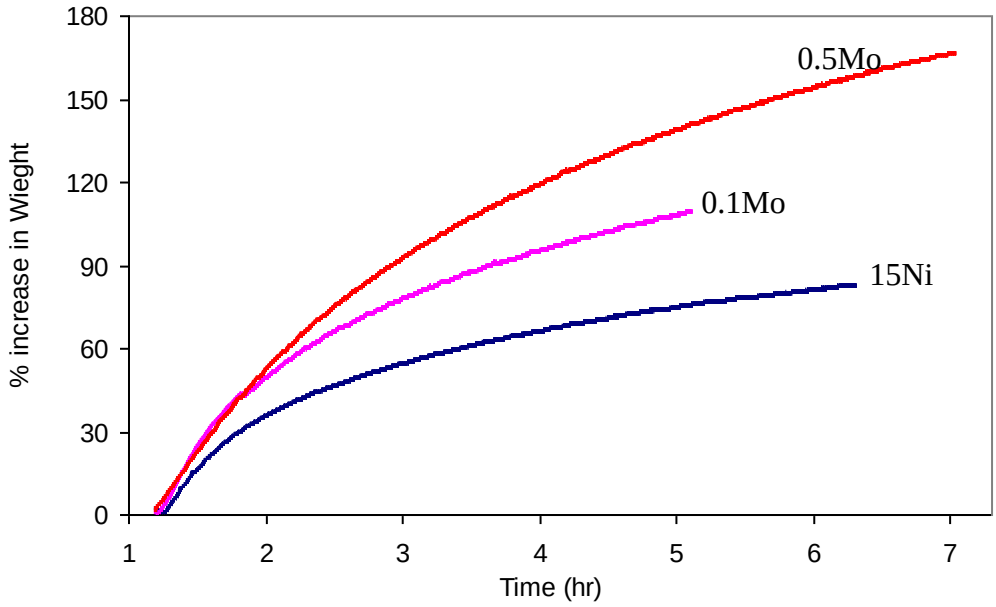

Figure 6.30: TGA of deactivation of the catalysts under 70 vol.% CO

CO Dissociation in the Packed Bed Reactor

The Boudouard reaction was also investigated in the packed bed reactor setup described in detail in Chapter 3. However, in order to continuously monitor CO_2 concentrations produced from the reaction, the Varian 3800 GC was substituted by the Agilent 3000 micro GC as described earlier in the propane cracking section. 30 mg of each catalyst was placed in the packed bed reactor, and was pre-reduced at 750°C for 30 min before cooling down to 450°C. At 450°C a 5% vol. CO stream was introduced and the micro GC started analyzing the product stream. Figure 6.31 presents CO_2 concentrations for the three catalysts. The trends are in good agreement with the TGA results as the 0.1Mo catalyst had the highest CO_2 concentrations while the 0.5Mo had the lowest. Moreover, the 0.1Mo run had to be shutdown after the first hour as the reactor was totally plugged, while it took 70 min to totally plug the 15Ni reactor. On the other hand the 0.5Mo catalyst did not plug the reactor even after 2 hours of reaction. This suggests that whisker

carbon was indeed formed during CO dissociation, and these whiskers were more over the 0.1Mo catalyst, probably indicating the availability of more active Ni sites.

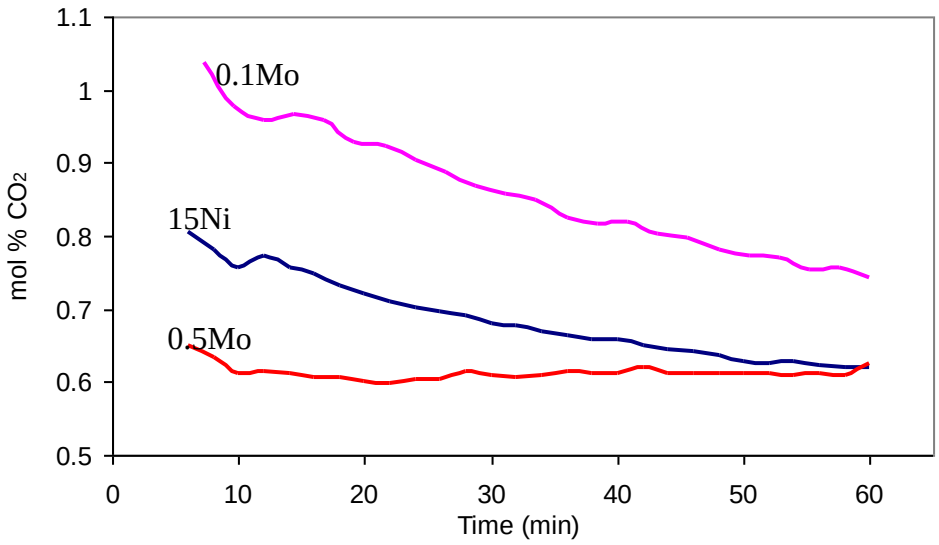

Figure 6.31: CO_2 concentrations from 5 vol.% CO dissociation at 450°C in the packed bed reactor

Chapter 7

Effect of Structural Interactions between Ni and Mo on Catalytic Properties of the Ni-Mo/Al_2O_3 Catalyst

The benefit of adding a metal to a monometallic catalyst is driven by the structural interaction between the two metals, or between the metals and the support within the new bimetallic catalyst. Generally, these structural interactions maybe of a textural nature affecting the physical properties of the catalyst such as the metal dispersion or metal crystal surface area, or they may be of an electronic nature changing electronic densities of different catalyst components, and hence affecting the adsorption and chemical interactions of these components with different reaction intermediates. Although the foundations of these interactions are set during the earlier catalyst synthesis and pre-treatment stages, the nature of these interactions may change during the course of the reaction and in many cases this interaction change will have a negative impact on catalytic properties, which will eventually lead to catalyst deactivation. Therefore, an understanding of the Mo–Ni and the Mo-Ni-Al_2O_3 interaction is essential to explain the effect of Mo on the activity, selectivity and stability of the promoted Ni catalyst.

Catalyst Characterization

The aim of the catalyst characterization was to investigate how does Mo affects the surface and bulk properties of the Ni/Al_2O_3 catalyst. Characterization studies of bimetallic catalysts containing Mo metal or MoOx showed that the interaction between the two metals could be of a physical nature or an electronic transfer interaction nature. In a Rh-Mo/Al_2O_3 catalyst, Lowenthal et al. (1995) found that Mo effectively prevents Rh agglomeration by isolating different sites. The same effect was observed in a Mo-Co catalyst, where MoOx species act as diluents in the catalyst matrix leading to a reduction in the size of Co sites (Chen et. al, 1994). Aksoylu and Onsan (1998) also found that the promotion of 5 wt %t Ni with Mo increased the metal surface area of Ni and hence, related the Mo promotion at the low Ni loading to a physical effect. However, for the same set of experiments, when they increased the Ni loading to 10 wt% they attributed the enhancement effect to electron transfer from MoOx to Ni sites. A negative effect of

Mo on the structure of bimetallic catalysts is coverage of the metal active sites at high Mo loadings leading to lost or lower catalyst activity (Youn et al., 2007).

All the characterization studies available in the literature were based on higher Mo to metal ratios than our Ni-Mo catalysts. Therefore, a big challenge in the characterization of our catalysts was the low loading of Mo, as most of traditional lab characterization methods were expected to fail in detecting theses small amounts or different phases related to them. However, any change in the Ni or Al_2O_3 structures due to the addition of Mo could be interpreted by comparing the unpromoted with promoted catalysts with different Mo loadings. Therefore, all characterization experiments were run for the three catalysts, 15Ni, 0.1Mo-15Ni and 0.5Mo-15Ni.

7.1 Temperature Programmed Reduction (TPR)

The main purpose of TPO and TPR in Chapter 4 was to determine calcination and reduction temperatures of the Ni/Al_2O_3 catalyst, which is an important property when using Ni catalysts in the SR reaction. This is because only metallic Ni is the active phase in SR reactions, while the other phases, like NiO, are not active. Therefore, a higher degree of reduced Ni will make more sites available for the reaction, leading to higher activities and turn over frequencies (TOF). An important factor that affects the reducibility of metal supported catalysts is the metal support interaction. This interaction between the Al_2O_3 support and different Ni phases is an important factor in controlling Ni reducibility. Although a strong metal support interaction will result in a lower degree of Ni reducibility, this strong interaction may affect the electronic properties of Ni or Al_2O_3 resulting in different product selectivities of the catalyst, or improving the catalyst resistance to different types of deactivation. Therefore, in this section, TPR experiments were run for promoted and unpromoted catalysts to investigate the effect of small amounts of Mo on these different interactions between Ni and Al_2O_3.

7.1.1 Experimental Methodology

TPR experiments were run in our regular reaction experimental setup described in detail in Chapter 3 based on a H_2 consumption measuring procedure. A smaller 0.3 mm ID quartz reactor was filled with 200 mg from the same catalyst batches used in the

individual reaction tests after calcination in the furnace with air circulation for 3 hr at 700°C. Temperature was ramped from room temperature to 950°C at a rate of 3°C/min. At 300°C a stream of 5% H_2 in N_2 was introduced. H_2O from reduction was removed through a silica gel trap before reaching the GC. H_2 concentrations were measured using an Agilent 3000 micro GC fitted with a TCD which measured H_2 concentrations throughout the course of the experiment every 90 seconds.

7.1.2 TPR Results and Discussion

In addition to running TPR for the three catalysts; 15Ni/Al_2O_3 (15Ni),0.1Mo-15Ni/Al_2O_3 (0.1Mo) and 0.5Mo-15Ni/Al_2O_3(0.5Mo), TPR was also run for a 1% wt Mo-15% wt Ni/Al_2O_3 (1Mo) catalyst prepared and pre-treated in the same way as the other three catalysts. Although we know that this is an inactive catalyst under our reaction conditions, TPR was run to magnify undetectable changes resulting from reduction of different MoOx species, especially for the 0.5Mo catalyst. Figure 7.1 presents the change in H_2 consumption with temperature recorded during TPR measurements for the four catalysts.

H_2 consumption for the unpromoted 15Ni catalyst began at 422°C, this first increase in H_2 consumption is attributed to the reduction of bulk NiO which is not or is weakly interacting with the alumina support. Unsupported bulk NiO is known to reduce to atomic Ni^0 in the 200-450°C range, however, the introduction of the support increases this temperature range to around 500°C [Richardson et al. (1994); Youn et al. (2007); Escritori et al. (2009)]. At 510°C another peak starts, maximizing at 620°C and ending at 665°C, this reduction stage covers a high range of NiO which are strongly interacting with the support NiO-Al_2O_3. Theses strong NiO-Al_2O_3 interactions are caused by the dissolution and incorporation of Al^{3+} ions in NiO crystallites which makes the disruption of the Ni-O bond difficult (Richardson et al, 1994). This process is more favourable at high calcination temperatures and lower Ni loadings. In addition, the high surface area γ-Al_2O_3 support increases the reduction temperature due to its interaction with H_2O vapor formed during NiO reduction (Borowiecki et al., 2004).

At 690°C a broad peak is observed for the 15Ni catalysts, reaching a maximum at 845°C, and then decreasing to the end of the run at 950°C. This broad high temperature reduction peak is associated with strongly dispersed spinel-like $NiAl_2O_4$ species which begin to form at calcination temperatures above 500°C (as proved from XRD analysis presented in the next section). As the calcination temperature is increased, more of these species are expected to form reaching a thickness of a few atomic layers. It is clear that the high 700°C calcination temperature of the 15Ni catalysts caused strong support/metal oxide interactions leading to higher reduction temperatures. However, it should be pointed out that the alumina/NiO strong interaction plays an important role in preventing the deactivation of the Ni catalyst by fouling and sintering. As stated before in chapter 6, it was reported by Bengaard et al. (2002) that during CH_4 steam reforming over Ni catalysts, both the reforming reaction and the formation of carbon are initiated at the same type of active site, which they refer to as defect step sites. However, the steam reforming reaction requires a Ni ensemble of only 3 or 4 atoms while an ensemble of 6 or 7 Ni atoms is required to form a reactive surface carbon intermediate which acts as a precursor for different carbon types [Edwards and Maitra (1995); Gonzalez et al. (2000)]. Strong interactions between alumina and NiO favour the formation of small NiO clusters, which enhances Ni dispersion and prevents the formation of large Ni ensembles during the course of the reaction (Zhang et al., 2009). Moreover, the formation of a solid solution between alumina and Ni at high calcination temperatures will suppress aggregation and sintering of the metal at high reaction temperatures, and hence, slows the catalyst aging rate, and improves its thermal stability [Wang and Ruckenstein (2001); Liu and Au (2003)].

The addition of 0.1Mo did not have a significant change on the TPR trend of the 15Ni catalyst. The 0.1Mo trend in Figure 7.1 has the same three reduction peaks described earlier. However, the first reduction peak of bulk NiO began at 416 to 488°C and the $NiO\text{-}Al_2O_3$ interaction peak was broader and covered a temperature range from 488 to 700°C. Overall, reduction temperatures are slightly shifted to lower temperatures indicating that Mo affected the strength of the $NiO\text{-}Al_2O_3$ interaction.

In the analysis of the TPR trends for the 0.5Mo catalyst, the three Ni reduction peaks can still be identified, in addition to smaller peaks related to the reduction of different phases of MoOx. These small peaks are clearer in the 1Mo TPR trend, and could be identified on a similarity basis between the two trends in Figure 7.1. The initial reduction temperature was lowered to 388°C for the 0.5Mo and was further lowed to 361°C for the 1Mo catalyst. Bulk NiO was reduced in a range from 388 to 432°C for the 0.5Mo catalyst while the range was 361 to 461°C for the 1Mo catalyst. For the Mo catalysts, it is hard to determine the exact range of the NiO-Al_2O_3 peak as some phases of MoOx began to reduce in the same range. However peak maxima for the NiO-Al_2O_3 phase can be identified for the 0.5Mo catalyst at 575°C, and for the 1Mo catalyst at 553°C, as these peaks were also shifted to lower temperatures with the addition of Mo.

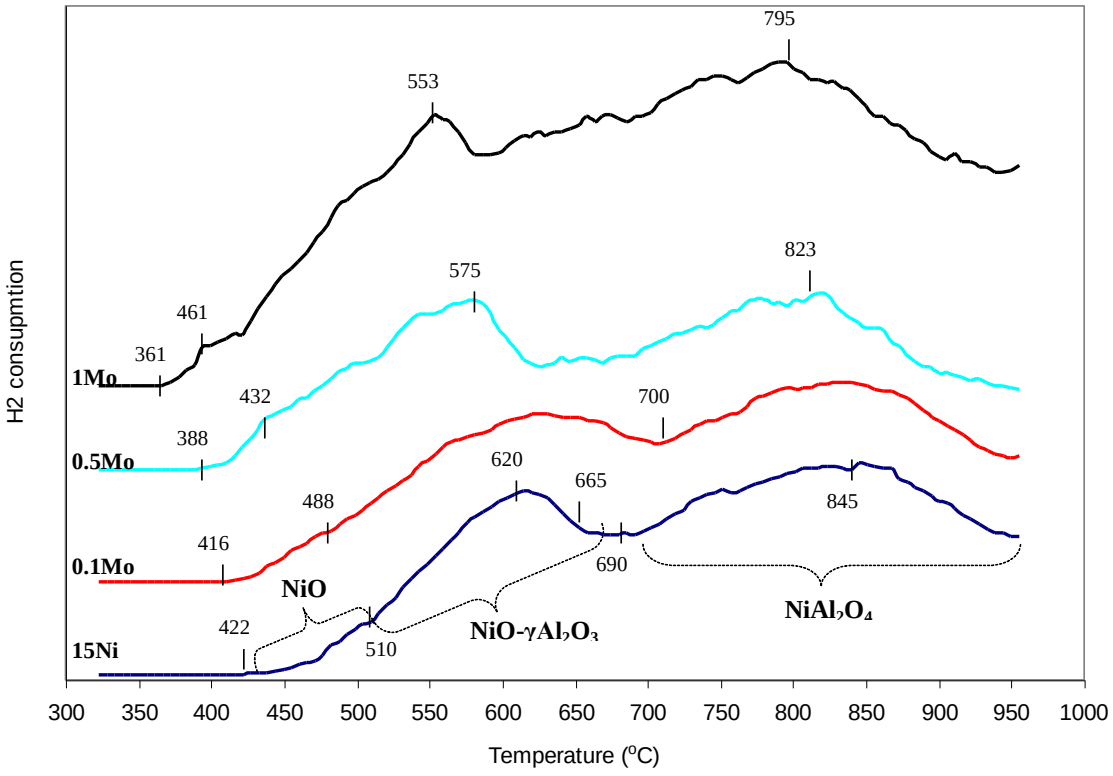

Figure 7.1: TPR profiles of unpromoted and promoted catalysts with different Mo loadings.

As the ramping temperature increases beyond the $NiO\text{-}Al_2O_3$ reduction range, for both catalysts (0.5Mo and 1Mo), H_2 consumption increases at different rates creating a series of small peaks and reaching maxima at 823 and 795°C for the 0.5Mo and the 1Mo catalysts, respectively. At these temperature ranges, $NiAl_2O_4$ is reduced together with different MoOx phases. Bulk MoO_3 is difficult to reduce and requires high temperatures to ensure a full reduction to metallic Mo^0. TPR profiles of bulk MoO_3 reveals two reduction peaks; the first in the 750-800°C range attributed to the reduction of MoO_3 to MoO_2, while a second occurring at 950-1000°C resulting from the reduction of MoO_2 to metallic Mo (Braithwaite, 1994). When MoO_3 is supported on Al_2O_3 in MoO_3/Al_2O_3 catalysts, two peaks are observed at lower temperatures. In the first peak, occurring at 400-450°C, polymeric structures of MoO_3 are reduced to MoO_2 while further reduction to Mo^0 is shifted to lower temperatures; 700-950°C, with bulk MoO_3 reducing between the two ranges [Borowiecki et al, (2004) ; Hercules et al. (1994); Yamada et al. (1991)].

Addition of Ni to Mo was found to lower MoOx reduction temperatures. In their TPR analysis of a Ni-Mo desulphurization catalyst, Brito and Laine (1993) found that NiO and MoOx reduced independently when calcined at low temperatures (400-600°C). However, they also found that each phase accelerates the reduction of the other. For NiO this is in agreement with our results as we illustrated earlier that the addition of Mo weakened the $NiO\text{-}Al_2O_3$ interactions causing its reduction to shift to lower temperatures. In the TPR profile of 1Mo in Figure 7.1, the series of small peaks in the $NiO\text{-}Al_2O_3$ peak occurring between 450 and 515°C could be attributed to the reduction of strongly dispersed polymeric structures of MoO_3 to MoO_2, while small peaks at higher temperatures, 600-800°C, are assigned to further reduction of these phases to Mo^0 (Maluf and Assaf, 2009).

A series of small peaks at relatively high temperatures in the range 830-950°C were observed for both 0.5Mo and 1Mo. Due to the small amounts of Mo it is hard to assign these small peaks to particular phases or compounds. However, some speculations can be made based on the literature. The small series of peaks at high temperatures could be attributed to the reduction of three phase component interactions $NiO\text{-}Al_2O_3\text{-}MoO_3$ which can be formed even in the presence of very small amounts of promoters (Mo:Ni ratios of

0.03-0.06) [Borowiecki et al, (2004); Siri et al (1991)]. In addition to these three phase components, direct interaction between NiO and MoOx resulting from high calcination temperatures when pre-treating our Ni-Mo catalysts could form a $NiMoO_4$ phase [Xiao et al. (2003); Youn et al. (2007)]. The reduction of $NiMoO_4$ takes place in stages and depending on the reduction temperature and environment could result in the formation of Ni_xMo compounds or Ni-Mo alloys and MoO_2 which are difficult to reduce. Therefore, in many cases formation of bulky $NiMoO_4$ will result in poor reducibility of the Ni catalyst and the loss of Ni active sites due to the decoration of these sites by different MoOx species (Youn et al, 2007).

Moreover, the formation of the difficult-to-reduce phases in Ni-Mo catalysts is highly affected by the impregnating sequence of the two metals at the catalyst preparation stage. It was reported in the literature that Ni-Mo catalysts prepared by co-impregnation or co-precipitation of the metals favours the formation of $NiMoO_4$ more than sequential impregnation with Mo first [Cordero and Agudo (2000); Brito et al. (1989)]. Therefore, in our case we expect the formation of $NiMoO_4$ even at small Mo ratios. However, it should be pointed out that contradictory to our lower reduction temperatures with the addition of Mo, TPR results in a few studies that sequentially impregnated Mo on Ni/Al_2O_3 catalysts showed that even small amounts of Mo shifted different NiO reduction peaks to higher temperatures [Quincoces et al. (2000); Borowiecki et al, (2004); Maluf and Assaf (2009)]. The increase in the reduction temperature of sequentially impregnated catalysts was attributed to stronger interactions between MoO_3 and NiO due to decoration of NiO with MoO_3, which led to the formation of a $NiO\text{-}MoO_3$ hard-to-reduce solid solution. On the other hand, when Ni was impregnated on a MoO_3/Al_2O_3 catalyst, TPR profiles were the same as the unpromoted Ni/Al_2O_3 catalyst (Quincoces et al., 2000) or slightly shifted to higher temperatures (Borowiecki et al, 2004). Therefore, since such low Mo loading (0.1-0.5wt%) on our co-impregnated $Ni\text{-}Mo/Al_2O_3$ catalyst shifted the reduction temperature of the Ni/Al_2O_3 catalysts to lower temperatures, we do not expect that changes of the catalyst properties are related to textural effects.

7.1.3 TPR Measurements Using TGA

Prior to conducting TPR analysis using the H_2 consumption technique in the earlier section, TPR was run in the TGA apparatus described in Chapter 3, following the same procedure for TPR-TGA preliminarily experiments in Chapter 4. 100 mg of pre-calcined catalyst was used in each run. Temperature was ramped at a rate of 5°C/min from room temperature to 900°C. The weight of the sample was measured every second, while a stream of 5% H_2 was introduced at 300°C. The percentage decrease in weight with change in temperature is plotted in Figure 7.2. As mentioned earlier, due to the high calcination temperatures it was hard to distinguish different reduction stages for both the 15Ni and the 0.1Mo catalyst, meanwhile, two distinct reduction stages were detected for the 0.5Mo catalyst.

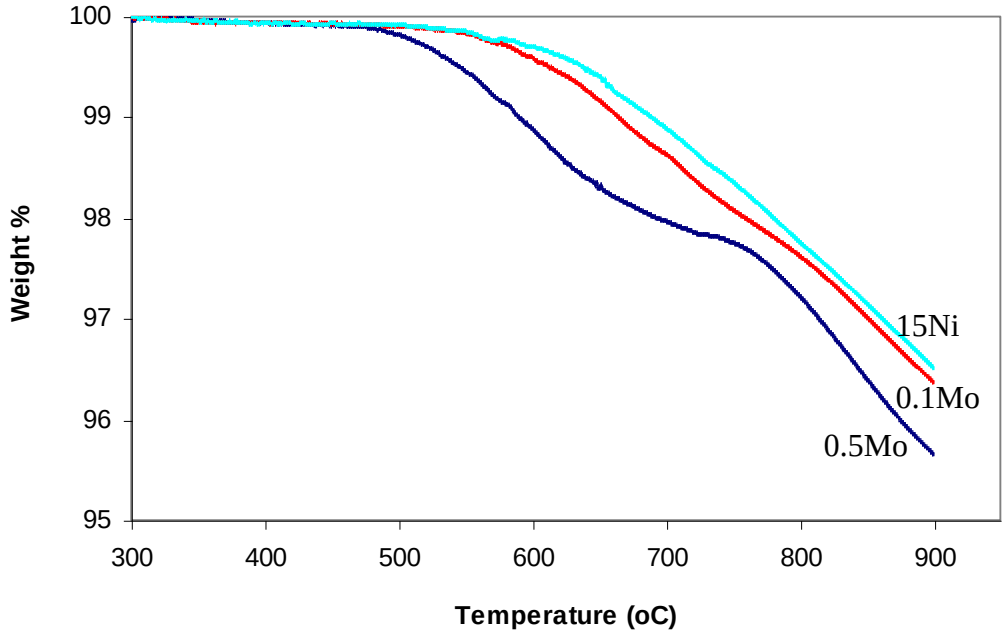

Figure 7.2: TPR-TGA profiles of unpromoted and promoted catalysts with different Mo loadings

Although these TGA results did not show a lot in terms of identifying different metal-support phases, they did agree with the TPR H_2 consumption results, showing that addition of small amounts of Mo caused a shift to lower reduction temperature for the

promoted catalyst, supporting the idea that the introduction of Mo weakened the NiO-Al_2O_3 interaction.

7.2 X-Ray Diffraction (XRD) Measurements

XRD is a commonly used technique to quantify and qualitatively characterize different chemical phases through the catalyst bulk. Another important piece of information that XRD can provide is the crystallization degree of different identified metals in the catalyst. This is important because catalyst active sites originate from the arrangement of atoms and molecules of the metal, and these arrangements are more likely to form from irregularities of amorphous structures or structures that have very small crystals. Therefore, if the catalyst structure is highly amorphous, this will limit the use of XRD since a certain degree of crystallinity is required to obtain diffraction patterns for each phase. Another XRD limitation is the amount of the chemical phase, as most XRD apparatuses are incapable of detecting amounts lower than 1% wt. The first limitation is not a concern for our catalysts, since the high calcination and reduction temperatures will crystallize the structure to a detectable degree. However, the second limitation was more of an issue in our study. In a couple of studies that used low Mo loadings, Borowiecki et al. (2004) could not identify any Mo related phases even at a loading of 3% wt MoO_3 in a 10%wt Ni/Al_2O_3 catalyst, while no Mo phases were identified in the XRD for a 5% wt Mo-20% Ni/Al_2O_3 catalyst examined by Youn et al. in 2007.

XRD patterns were measured on a Bruker AXS D8 Advance diffractometer using a Bragg-Brentano geometry with Ni-filtered Cu Kα radiation of λ= 1.5425 Å. Spectra were collected for a 2θ range of 15 to 80º using a step size of 0.02º and a count time of 1 second. XRD measurements were done with catalysts that were calcined in the furnace at 700°C for 3 hours, and for catalysts reduced under the same reaction pre-treatment condition; 750°C for 1 hour in 30% H_2 in the reactor. Reduced catalysts were cooled down to room temperature under a N_2 stream and stored in sealed sample bags. In addition to the three catalysts, XRD patterns were measured for pure γ-Al_2O_3 that was also calcined at the same catalyst conditions, in order to distinguish patterns related to the support.

XRD diffraction patterns for calcined and reduced 15Ni, 0.1Mo and 0.5Mo catalysts in addition to pure γ-Al_2O_3 are presented in Figure 7.3. The International Center of Diffraction Data (ICDD) was used to identify different phases for each chemical. The calcined support showed three diffraction patterns; Al_2O_3 (311), Al_2O_3 (400) and Al_2O_3 (440). These patterns were relatively broad indicating that heat treatment of the support at 700°C did not have a significant effect on its crystalinity which is expected, as changing the γ-Al_2O_3 to the next phase, δ-Al_2O_3, requires calcination temperatures higher than 850°C. The three alumina patterns appeared in the three calcined catalysts, with the Al_2O_3 (311) pattern having a higher intensity as it overlaps the NiO (111) pattern. Two other NiO patterns appear in the calcined catalysts profiles; NiO (200) at $2\theta = 43.8°$ and a much smaller one NiO (220) at $2\theta = 63.3°$.

Due to the small Mo loadings in the two Mo catalysts, no patterns were detected for any Mo-related phases. Moreover, some of the phases, such as MoO_2 and $NiMoO_4$ diffraction patterns overlap the higher intensity NiO and Al_2O_3 patterns making them harder to distinguish even at higher Mo loadings. For all three calcined catalysts, a slight shift in the Al_2O_3 (440) angle was observed from 67.2° to 66.8°. This slight decrease in the Al_2O_3 (440) angle with the addition of Ni indicates the formation of a $NiAl_2O_3$ spinel structure, as the incorporation of Ni in the Al_2O_3 structure causes an increase in the lattice parameters, due to the greater ionic radius of Ni^{2+} than Al^{3+} [Kim et al. (2004); Youn et al. (2007); Coleman (2008); Zhang et al. (2009)]. This Ni incorporation was also verified by the shift of the Al_2O_3 (440) peak back to its original angle after reducing the catalysts.

Reduced catalysts show three peaks attributed to Ni(111), Ni(200) and Ni(220). The peaks for all catalysts were broad and small as Ni was highly incorporated in Al_2O_3 due to the high Ni-Al_2O_3 interaction. Although NiO peaks disappeared in the reduced catalyst profiles, the intensity of the Al_2O_3(311)-NiO(111) peak was smaller for the 0.5Mo catalyst. This may indicate a lower amount of reducible NiO over the 0.5Mo catalyst. In general, Ni XRD patterns for the three catalysts were the same, therefore we do not

expect a significant effect of Mo on the average size of Ni crystallites and hence on Ni dispersion in the two promoted catalysts.

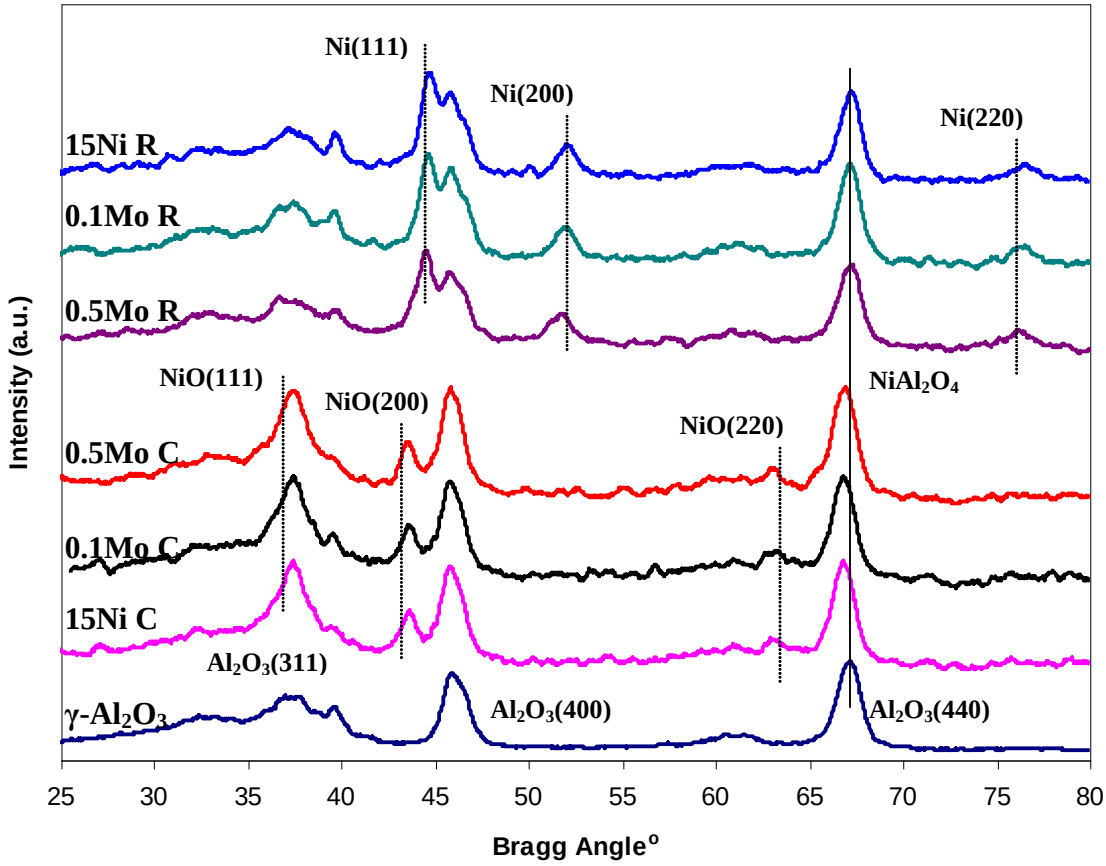

Figure 7.3: XRD patterns of γ-Al_2O_3, calcined (C) and reduced (R) catalysts

7.3 H_2 Chemisorption Measurements

Although XRD results indicate that the addition of Mo to the Ni catalyst did not affect the average Ni crystallite size, these results were not considered conclusive, as Ni XRD peaks could not be used to measure Ni crystallite size for the catalysts, because of the low intensities of the Ni(200) and Ni(220) peaks and the overlap of the high intensity Ni(111) peak with Al_2O_3 (311). An alternative, widely used characterization technique to measure average metal crystallite diameter and dispersion, is selective gas chemisorption. More specifically, the measurement of monolayer H_2 adsorption capacity is the most common

method used for supported noble and transition metal catalysts including Pt, Pd, Rh, Ru, Ni, Co and Fe. The purpose of H_2 chemisorptions in this study was to investigate the effect of Mo on the capacity and distribution of active Ni sites in freshly promoted reduced catalysts, which will in turn indicate if Mo has a textural effect on the Ni catalyst. It will also be used to determine the change in Ni dispersion as a result of aging the catalyst during time on stream experiments described in Chapter 5.

The fraction of total metal atoms or molecules of the active phase available at the surface for catalysis is known as the metal dispersion. Therefore, dispersion (D) is inversely proportional to the diameter (d) of a spherical metal crystallite hence:

$$d = k/D \qquad (7.1)$$

Where k is a constant for a given active metal phase and is 97 for Ni (Bartholomew and Farrauto, 2006). It is widely reported in the literature that for Ni-based catalysts each Ni surface atom chemisorbs one hydrogen atom, therefore, by measuring the H_2 chemisorption uptake, the dispersion can be calculated from the simple formula:

$$D = CX/fw \qquad (7.2)$$

Where: C: a constant related to the metal active phase = 1.17 for Ni
X: H_2 uptake in μmol/g
f: the fraction of Ni in zero valent state (not oxide)
w: Ni loading in wt % = 15

On the other hand, in addition to the small loadings of Mo in our catalysts; 0.1 and 0.5 % wt, it was reported in the literature that a 1% wt MoO_3/Al_2O_3 catalyst did not chemisorb any H_2 [Borowiecki et al, (1997); Maluf and Assaf (2009)]. Therefore, it is assumed in our measurements that Mo does not adsorb any H_2 even in the presence of Ni and all results are attributed to Ni dispersion over the support.

H_2 chemisorption measurements were performed in a Hiden CatLab reactor. 50 mg of fresh pre-calcined catalyst at 700°C for 3 hours was placed in a tube reactor of 4 mm ID. The catalyst was first reduced in a 5% vol H_2 stream at 750°C for 30 min then the temperature was cooled down to room temperature and the reactor was flushed with pure He. A dynamic flow technique was used to measure H_2 chemisorption uptake at room temperature. In this method, pulses of a 1% vol H_2/He stream were injected through the catalyst bed and H_2 uptakes were measured using a Hiden QIC mass spectrometer until no further H_2 uptake was detected. By calculating the amount of H_2 chemisorption uptake, a computer software fitted with parameters of equation 7.2 for different metal catalysts was used to calculate dispersion (D %) for each catalyst.

Dispersions for 15Ni, 0.1Mo and 0.5Mo catalysts in addition to the Ni crystallite diameter size calculated from equation 7.1, are shown in Table 7.1

Table 7.1: Ni dispersion (%) of fresh catalysts

Catalyst	Dispersion (%)	Ni crystallite diameter size (nm)
15Ni	9.8	9.9
0.1Mo	9.3	10.4
0.5Mo	9.4	10.3

Commercial Ni/Al_2O_3 catalysts with 10-30% loadings were reported to have dispersions in the 5-15% range (Bartholomew and Farrauto, 2006). Although it is inappropriate to compare the dispersion of the 15Ni catalysts with values reported in the literature, because of different preparation and pre-treatment conditions, the 15Ni catalyst had higher dispersion values than some Ni/Al_2O_3 catalysts prepared under similar conditions [Matsumura and Nakamori (2004); Borowiecki et al, (2004); Nagaoka et al. (2007); Zhang et al. (2009)], but close to that of an 18 % wt $Ni/MgAl_2O_4$ catalyst used in natural gas pre-reforming (Sperle et al, 2005). These data show that the Mo-promoted catalysts

did not have any significant effect on Ni dispersion and on Ni crystallite size, which is consistent with the XRD results.

7.4 Characterization of Aged Catalysts by H_2 Chemisorption and XRD

An interesting observation from the stability screening tests at the end of Chapter 5, was the loss of activity of the 0.3Mo-15Ni/Al_2O_3 (0.3Mo) catalyst after a period of time. The 0.3Mo catalyst had a lower initial conversion than the unpromoted catalyst, but the conversion loss rate was the same (refer to Figure 5.8). After the 18 hr run, no carbon was visually observed on the 0.3 Mo catalyst and no change in the catalyst weight was measured. Therefore, it was concluded that the 0.3Mo catalysts was not deactivated by fouling or carbon deposition, but by another type of deactivation.

It was frequently reported in the literature that deactivation of Ni-based steam reforming catalysts could be caused by coking, sintering or oxidation of the active metal phase [Tsipouriari et al. (1998); Bradford and Vannice (1999); Bengaard et al. (2002); Natesakhawat et al. (2005); Bartholomew and Farrauto (2006)]. Sintering and transformation of catalytic phases to non-active phases are sometimes discussed under the same deactivation category and referred to as thermal degradation. Sintering is typically the loss of catalytic surface area due to crystallite growth or support and pore collapse. The natural driving force for crystallite growth is the tendency of small metal particles to decrease their surface energy by agglomerating into larger crystallites, which results in the loss of metal surface area and hence, loss of metal active sites and/or their dispersion. Sintering implies the loss of metal surface area, metal dispersion decrease or metal crystal growth. H_2 chemisorption and XRD are among the most commonly used techniques to characterize sintering of supported metal catalysts. Therefore, in this section H_2 chemisorption and XRD results for aged catalysts are analyzed and compared to freshly reduced catalysts.

7.4.1 Aging Methodology

A simple and commonly used method to thermally age catalysts for sintering characterization is heating the catalyst in a ventilated furnace for a certain period of time.

Although this method is simple and fast, it does not consider the reaction atmosphere which is an important factor affecting supported metal catalyst sintering. Therefore, in order to account for this factor and to represent the actual deactivation environment, aging of the catalysts were run under regular oxidative steam reforming reaction conditions as those of the stability screening tests in Chapter 5 (Figure 5.8). However, the feed composition was slightly adjusted to avoid high accumulation of carbon deposition on the unpromoted catalysts; the concentrations of propane and butane were lowered from 1% to 0.8 vol. % for each, and the S/C and O_2/C ratios were increased from 3 and 0.3 to 4 and 0.4 respectively. The reaction temperature was kept constant at 450°C and experiments run for 10 hours for each of the three catalysts; 15Ni, 0.1Mo and 0.5Mo. For the sake of comparison, catalysts were pre-treated and analysed following exactly the same procedures for fresh catalyst H_2 chemisorption in Section 7.4 and XRD in Section 7.3.

7.4.2 Results and Discussion

Table 7.2 compares Ni dispersions, measured by H_2 chemisorption, of the three reduced catalysts before and after the aging process. While the 0.1Mo catalyst did not show any change in Ni dispersion, the two deactivated catalysts lost some exposed Ni sites, with the 0.5 Mo catalyst having a lower dispersion than 15Ni. When ageing experiments were repeated under the same conditions for a second time, and dispersion was measured by the same H_2 chemisorption method for both fresh and aged catalysts, the percentages decrease in dispersion followed the same order.

Table 7.2: Ni dispersions, measured by H_2 chemisorption, of the three reduced catalysts before and after the aging process

Catalyst	Dispersion of Fresh (%)	Dispersion of Aged (%)	Decrease in Dispersion (%)
15Ni	9.8	7.0	28
0.1Mo	9.3	9.2	1
0.5Mo	9.4	6.5	31

Although catalyst sintering rates increase exponentially with temperature, the reaction atmosphere has also a significant effect on sintering. Metal sintering is more rapid in the presence of O_2 and H_2O and slower in a H_2 atmosphere (Bartholomew and Sorensen, 1983). Moreover, in a reducing atmosphere, sintering increases with decreasing metal melting temperatures which is lower for Ni compared to common noble metal catalysts. Therefore, although 450°C is a low temperature for Ni/Al_2O_3 catalysts to be deactivated by Ni sintering, partial sintering of Ni could occur at this low temperature as a result of the oxidative reaction atmosphere caused by the presence of O_2 and H_2O. Ni sintering can occur through two proposed mechanisms; the first is called atomic migration and is more dominant at temperatures higher than 800°C for Ni-based catalysts (Wynblatt and Gjostein, 1976). It involves the emission of metal atoms from a metal particle to another one through diffusion of the atoms on the substrate or in the gas phase. The other mechanism, which is dominant at lower temperatures, involves the diffusion of metal particles on the substrate followed by collision and coalescence of the particles and is referred to as the metal particle coalescence mechanism. The work of Rasmussen et al. (2004) proved that the second mechanism was responsible for sintering of a Ni/Al_2O_3 catalyst in a H_2O/H_2 atmosphere in temperatures ranging from 500 to 750°C. Therefore, Ni sintering is expected to follow a metal partial coalescence mechanism under our low temperature reaction conditions. Moreover, the coalescence of metal particles in this mechanism results in larger particle sizes which are expect to give larger XRD Ni patterns.

XRD measurements were carried out for the three aged catalyst samples after reduction, and compared to the fresh reduced 15Ni catalyst in Figure 7.4. Diffraction patterns for Ni(111), Ni(200) and Ni(220) were identified for all three aged catalysts in addition to the three γ-Al_2O_3 patterns: Al_2O_3(311), Al_2O_3(400) and Al_2O_3(440). However, contrary to our expectations, all three Ni patterns for the aged catalysts were smaller than that of the fresh reduced catalysts. Moreover, for the 0.5Mo catalyst that had the highest decrease in Ni dispersion, these Ni patterns had the lowest intensity among all three aged catalysts. In addition, Ni peaks for the aged catalysts did not show any shift in position or a significant change in their broadness that can be attributed to an increase in crystallite

size. Therefore, the loss of Ni dispersion for the 15Ni and the 0.5Mo catalysts could not be attributed mostly to metal particle coalescence sintering, as suggested before.

The other thermal degradation type that can lead to losses of Ni active sites and result in smaller XRD Ni peaks is the transformation of active Ni to inactive, hard to reduce Ni phases. Metallic Ni is the active phase in steam reforming Ni/Al_2O_3 based catalyst, and therefore, fresh prepared catalysts are reduced at high temperatures to ensure full reduction of non-active NiO to Ni. During our ageing process, the reaction environment contains both oxidation agents such as O_2, H_2O and CO_2 as well as reduction agents, such as propane, butane, H_2, CO and CH_4. However, the presence of H_2O and O_2 favours a more oxidative atmosphere which not only results in the oxidation of Ni to NiO, but also in the formation of NiO surface layers that can block some active Ni sites (Rasmussen et al., 2004).

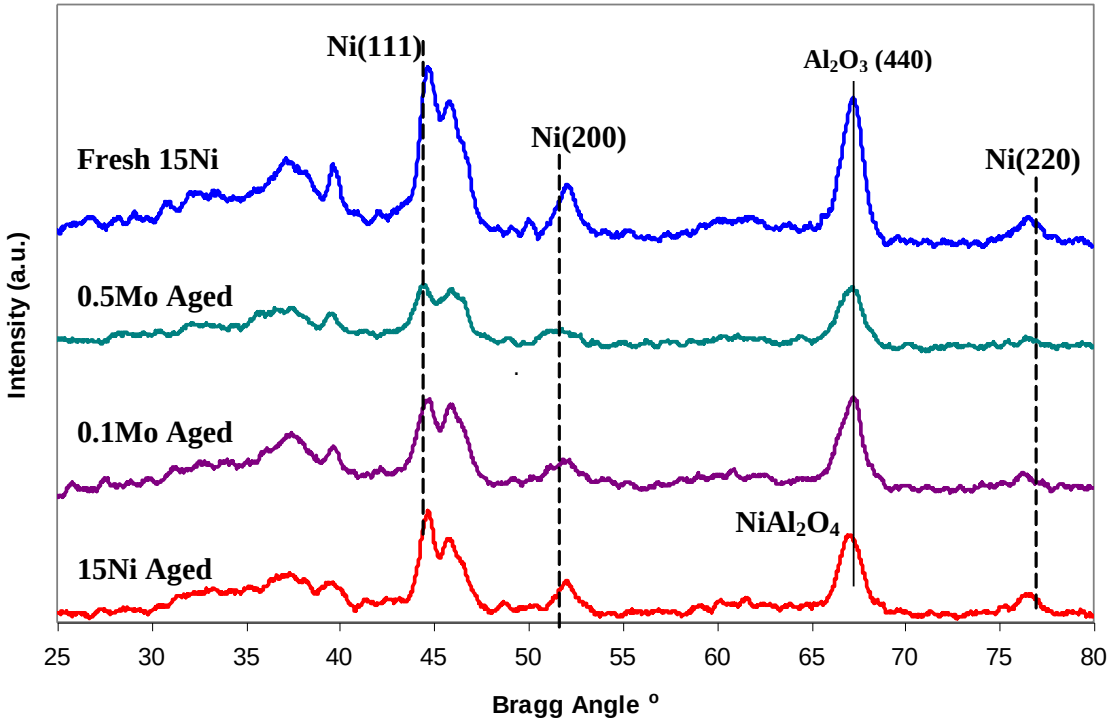

Figure 7.4: XRD patterns of 10 hr aged catalysts after reduction compared to fresh reduced 15Ni

As more Ni is lost by oxidation, lower conversions led to more unreacted H_2O and O_2 in the reaction atmosphere which is expected to accelerate metal oxidation. Although individual patterns could not be identified for $NiAl_2O_4$ in the aged catalysts, its presence can not be excluded. The peak of Al_2O_4(440) for the aged 15Ni catalyst was shifted to a slightly lower diffraction angle even after the reduction of the catalyst. As explained earlier in the fresh calcined catalyst XRD analysis, this shift indicates the presence of a $NiAl_2O_4$ spinel structure, as the incorporation of Ni in the Al_2O_3 structure causes an increase in the lattice parameters because of the greater ionic radius of Ni^{2+} than Al^{3+}.

For 0.1Mo and 0.5Mo catalysts shift of the Al_2O_4(440) peak was not observed. But, the presence of $NiAl_2O_4$ could not be excluded from the structure of aged 0.1Mo and 0.5Mo catalysts. However, it is not believed to be the only inactive phase that led to deactivation of the 0.5Mo catalyst, since obviously it did not cause the 0.1Mo catalyst to deactivate. Furthermore, the XRD patterns of the aged 0.5Mo showed a decrease in the Al_2O_3(440) lattice indicating a lower Ni incorporation degree in the support and hence lower $NiAl_2O_4$ formation. As the 0.5Mo catalyst is prepared by a co-pregnation, Mo and MoOx are in direct contact with the γ-Al_2O_3 support as well as Ni particles. In the oxidative reaction atmosphere, the formation of a three phase component interaction, NiO-Al_2O_3-MoO_3, which can be formed even in the presence of very small amounts of promoters is expected as reported in the literature [Borowiecki et al. (2004); Siri et al. (1991)].

Another inactive Ni phase that is initiated by the presence of Mo and the oxidative reaction atmosphere is $NiMoO_4$. Although XRD patterns for this phase were not identified for the 0.5Mo catalyst due to the small amount of Mo, its existence was reported in Ni-Mo catalysts at different Ni:Mo ratios [Xiao et al. (2003); Youn et al. (2007); Maluf and Assaf (2009)]. Further, reduction of $NiMoO_4$ takes place in a few stages and depending on the reduction temperature and environment could result in the formation of Ni_xMo compounds or Ni-Mo alloys and MoO_2, which are difficult to reduce. Therefore, formation of bulky $NiMoO_4$ will result in poor reducibility of the Ni catalyst and the loss of Ni active sites.

Since the 0.1Mo catalyst did not show any decrease in Ni dispersion compared to the two other catalysts, this indicates that promoting the Ni catalyst with such small Mo amounts not only improves the catalyst resistance to coking but also prevents the loss of Ni active sites to other inactive Ni phases. It should be pointed out that from an application point of view, a reforming catalyst used in domestic or automotive fuel cell compact reformers, should have a higher resistance to deactivation by oxidation than a large scale industrial application catalyst. Fuel cell reformers are subjected to repeated start-up and shutdown, and in between they should be purged by air or steam to enhance safety [Nagaoka et al. (2007); Li et al. (2009)]. Therefore, although the 0.5Mo catalyst was highly resistant to coking, it is not expected to be a suitable candidate for these reformers.

7.5 *In-Situ* DRIFTS Analysis of Propane Reactions

One of the most interesting results from the individual reaction experiments in Chapter 6 was the higher production rate and yield of CO in all reactions, SR, PO and OSR, when Ni catalysts were promoted with Mo. Even at lower conversions with the 0.5Mo catalyst the CO production rate was higher than the 0.1Mo catalyst. The higher CO production was first thought to be related to side reaction rates consuming or producing CO during the OSR process including the water gas shift and the methanation reactions. However, activity experiments for these reactions showed this to not be the case. Another speculation for the higher CO production was that the presence of Mo affects the surface chemistry of the Ni catalyst, and hence, affects the adsorption of CO on promoted catalysts. Therefore, in this section *in-situ* Diffusion Reflectance Infrared Fourier Transform Spectroscopy (DRIFTS) experiments were run to identify and quantify different adsorbed species on each of the three catalyst surfaces during propane reactions. This should give insight into CO adsorption, and will also point out to other intermediates on the catalysts surface that may assist in understanding the effect of Mo on the general reaction mechanism.

7.5.1 DRIFTS Apparatus Description

DRIFTS experiments were performed in a Nicolet Nexus spectrometer, equipped with a MCT detector and a KBr beam splitter. Around 100 mg of pre-reduced powder catalyst

was placed in a small cylindrical ceramic cell. The maximum cell temperature that could be reached was 400°C, controlled using a Thermo Scientific Cal 9500P temperature controller. Prior to each run, background normalization of the spectra was performed by subtracting the spectra recorded in a flow of He at the reaction temperature. In all experiments, spectra were averaged over 50 scans in the mid IR range (600-4000 cm^{-1}) to a nominal 4 cm^{-1} resolution. Scans were taken every minute until no change between spectra was observed, and then reaction gases were stopped and only He was flowed as desorption spectra were collected. Spectra were collected and analyzed using the OMNIC computer software.

7.5.2 CO and Propane Adsorption

CO adsorption experiments were run at room temperature (RT) for 15Ni and 0.1Mo catalysts. After flushing with He for 30 min, a 5 vol. % CO/He stream was introduced and spectra were collected every minute until equilibrium was reached after 12-14 min. The CO stream was then closed and only He was flowed while the desorption spectra was collected. CO adsorption was assumed to take place only on Ni particles, as it was reported in the literature that no CO adsorption was detected on a Mo/Al_2O_3 catalyst even at 15% wt Mo loadings [Scott et al. (1995); Aksoylua et al. (1998)]. Figure 7.5 presents the spectra of CO adsorption at the 15^{th} min for 15Ni and 0.1Mo in the range of CO adsorption wave numbers. Only two bands, at 2117 and 2175 cm^{-1}, were detected, and had the same absorbance for both catalysts. These bands are related to gaseous CO and disappeared after switching off the CO, indicating only physical adsorption of CO on both catalysts at room temperature.

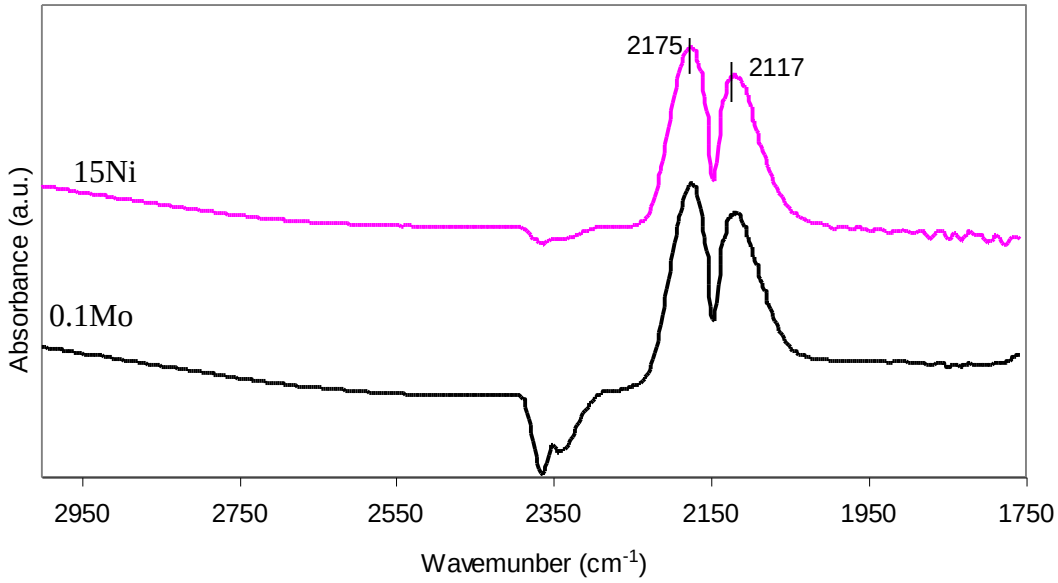

Figure 7.5: DRIFTS CO adsorption bands of fresh 15Ni and 0.1Mo at the 15th min, room temperature.

Propane adsorption experiments were run following the same procedure as in CO adsorption using a stream of 2 % vol propane/He. Figure 7.6 shows spectra of propane adsorption at the 15th min for the two catalysts. The high absorbance band at 2966 cm^{-1} is attributed to gaseous propane (Faria et al, 2009). This band overlaps bands 2940-2930 cm^{-1} which are assigned to asymmetric methyl ($\nu_{as}CH_3$) and methene ($\nu_{as}CH_2$) stretching, and bands around 2860 cm^{-1} assigned to symmetric methyl (ν_sCH_3) and methene (ν_sCH_2) stretching [Natesakhawat et al. (2005); He et al. (2009); Faria et al. (2009)]. Bands at lower wavenumbers; 1473 and 1388 cm^{-1} could be attributed to asymmetric methyl ($\delta_{as}CH_3$) and symmetric methyl (δ_sCH_3), respectively. All these bands were detected on both catalysts. However all the bands disappeared when switching to He for desorption, indication physical adsorption only.

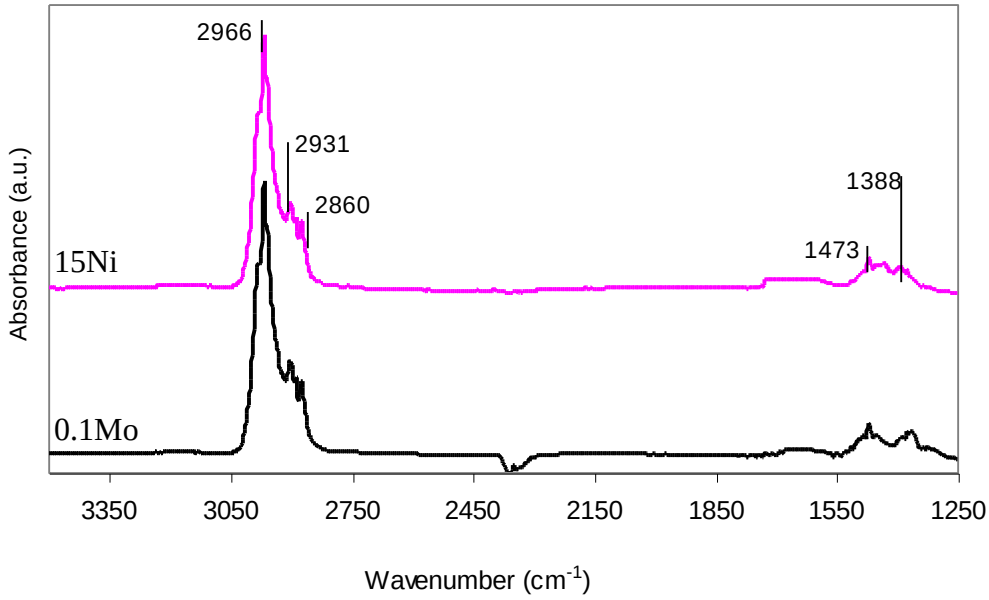

Figure 7.6: DRIFTS propane adsorption bands for fresh reduced 15Ni and 0.1Mo at the 15th min

7.5.3 *In-Situ* DRIFTS Analysis for Propane Partial Oxidation (PO)

Propane PO in-situ DRIFTS experiments were run for the three catalysts; 15Ni, 0.1Mo and 0.5Mo at 390°C. The cell temperature was raised to 390°C under a flow of He and was kept at these conditions for 30-45 min until a stable background signal was obtained. Then a stream of 1.2 vol. % propane, 1.62 vol. % O_2 and He was introduced, with an O_2/C of 4.5. Spectra were collected every minute until no change in the signal was observed after 12-14 min. The reaction mixture stream was then closed and only He was flowed while the desorption spectra were collected.

Figure 7.7 shows the adsorption spectra for the three catalysts at the 3rd and 5th minutes, while the adsorption at the 15th min, once steady-state was reached, is shown in Figure 7.8. At all three times a distinguishable difference between the three catalysts was observed for the bands ranging from 1760 – 2094 cm^{-1} which is attributed to CO

molecular adsorption. Bands from 2100-2000 cm^{-1} are assigned to linear CO adsorption which is favorable to form over isolated metal sites (corners and edges), while bands from 1900-1800 cm^{-1} are most likely a contribution of bridging CO, adsorbed on more flat and extensive metal sites [Xu et al. (2008); Faria et al. (2009); Eckle et al. (2010)]. For the 15Ni and the 0.1Mo catalysts, within the first 5 min of the reaction, CO is adsorbed more on the less reactive flat sites. As the conversion increases with time Ni surface ensembles change to smaller islands with more active edge sites, enhancing the linear adsorption of CO.

It was reported in the literature that CO adsorbs dissociatively on transition metals of the upper left corner of the periodic table and molecularly on transition metals on the lower right corner (Bengaard et al., 2002). Since Ni is located close to the border of the two groups, CO is expected to adsorb on Ni in both modes depending on the surface structure of the catalysts and its temperature. It was found that CO is adsorbed molecularly over Ni at RT and begins to desorb at 177°C (Bengaard et al, 2002). Therefore, we speculate that the high CO production over the 0.1Mo and 0.5Mo catalysts observed in the activity experiments is a result of weak adsorption or rapid desorption of CO in the presence of these small amounts of Mo. This is an indication that Mo caused a change in the surface structure of the Ni catalyst, which is thought to be more electronically driven due to the small amount of Mo compared to relatively large changes in CO adsorption bands. The differences in linear and bridged adsorbed CO bands between the three catalyst were sustained when stopping the reaction and when only He was flowing as the desorption spectra were collected (see Figure 7.9). CO bands for the 15Ni catalysts were detected even after 15 min desorption, while the 0.1Mo catalysts only showed the bridging CO band with a much smaller linear CO band at the 10^{th} min of desorption. On the other hand, the 0.5Mo catalyst lost both of its CO bands at the 3^{rd} min of desorption.

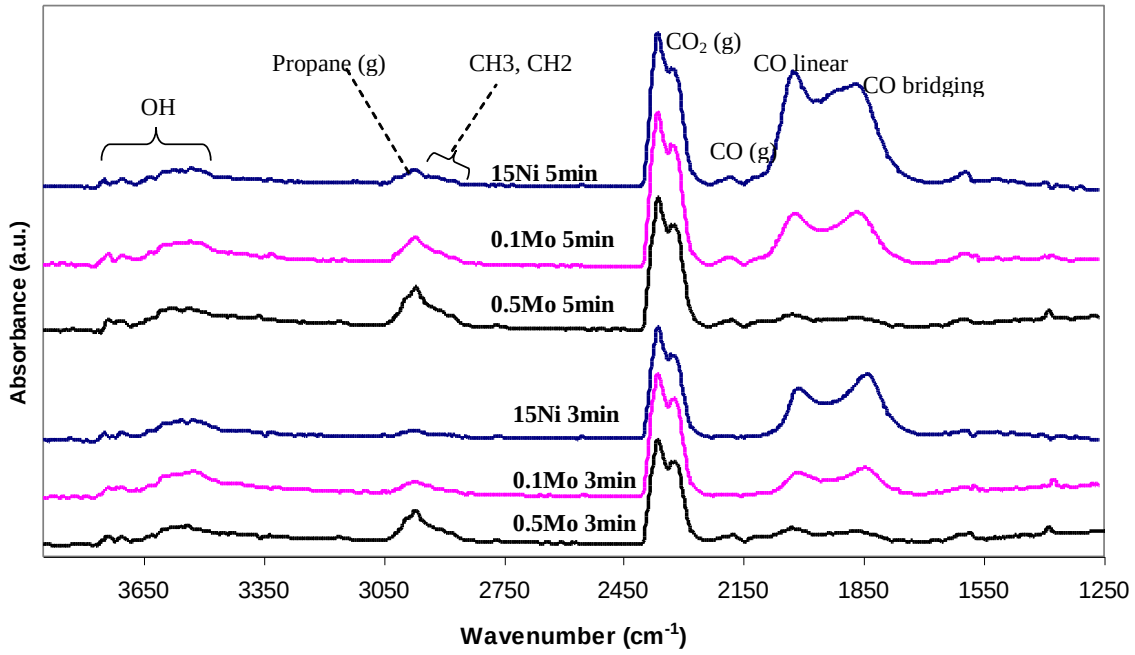

Figure 7.7: in-situ DRIFTS propane PO bands at the 3rd and 5th min, 390°C.

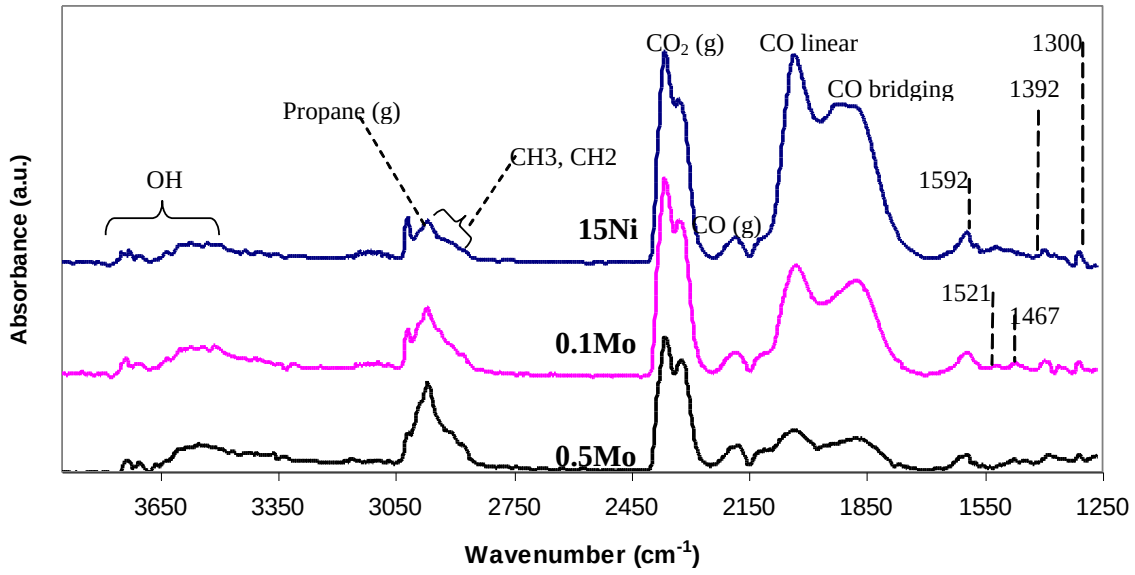

Figure 7.8: in-situ DRIFTS propane PO bands at the 15th min, 390°C.

Furthermore, the higher H_2 production over the 0.1Mo and 0.5Mo catalysts could contribute to the rapid CO desorption. CO adsorption and dissociation over Ni is not only structure sensitive, but also affected by the presence of H_2 in the reaction environment (Andersson et al, 2008). It was found that in the presence of H_2, chemisorbed CO can be rapidly displaced from the Ni surface by H_2 which will cause CO desorption at lower temperatures. Likewise, CO dissociation follows a different route when H_2 is present, as it dissociates through a CHO intermediate rather than a direct route in the absence of H_2 [Gland et al. (1988); Andersson et al. (2008)]. The formation of the CHO intermediates was not only reported for the CO dissociation reactions, but also it was suggested by a number of authors to be an intermediate in the formation of adsorbed CO during SR and PO reactions rather than the direct reaction between gaseous carbon and adsorbed oxygen to form CO [Rostrup-Neilsen and Hansen (1993); Bradford and Vannice (1999)].

High CO production over the Mo-promoted catalysts was not clearly distinguishable from the CO gaseous bands in the 2100 to 2250 cm^{-1} range, however, CO gaseous bands were detected early by the 3^{rd} min for the 0.5Mo catalyst while the spectra of the two other catalysts did not show any bands at that time (see Figure 7.7). Bands in the range 2200-2400 cm^{-1} are assigned to gaseous CO_2, with the 0.5Mo catalyst band having the lowest absorbance due to lower CO_2 production, which is in agreement with our catalyst activity experiments. These gaseous CO_2 bands disappeared rapidly after switching to the desorption mode.

As illustrated earlier in the propane DRIRTS experiments, the peak at 2966 cm^{-1} is attributed to gaseous propane and it overlaps bands in the range 2860-2940 cm^{-1} which are assigned to different symmetric and asymmetric CH_3 and CH_2 stretching. These bands had different absorbance for the three catalysts, as the intensities of the bands were higher for the 0.5Mo and 0.1Mo catalysts than the 15Ni. The higher intensity of the 0.5Mo band could be argued to be a result of more gaseous propane due to lower conversion. However, our PO individual reactions showed that the conversion of 0.1Mo and 15Ni are almost the same, yet there is a significant difference in the intensities of

these bands. Therefore we speculate that this difference is attributed to more CH_3 and CH_2 adsorbed on the surface of the Mo catalysts than Ni. For the unpromoted Ni catalyst CH_2 and CH_3 are unstable and tend to dehydrogenate rapidly to more stable carbon which can in turn change to more deactivating forms of carbon. Due to its instability, CH_3 can also react with adsorbed hydrogen to form CH_4, which was produced in smaller quantities over the Mo catalysts in the activity experiments discussed in Chapter 6. Therefore the role of Mo in preventing coking of the Ni catalyst could be attributed to preventing the dehydrogenation of CHx species to gaseous carbon.

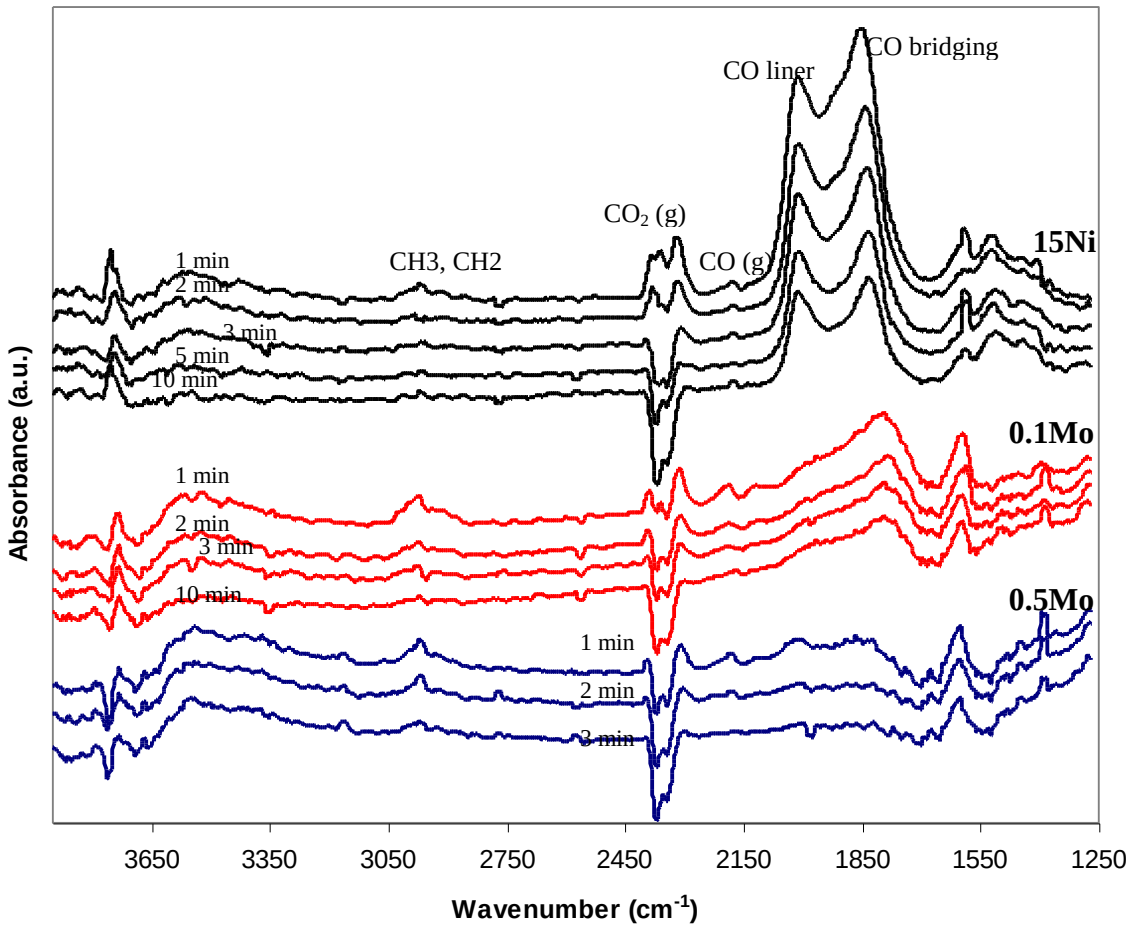

Figure 7.9: In-situ DRIFTS propane PO desorption bands at different times

From another perspective, as mentioned earlier, the formation of CO was argued by a number of authors to result through the reactions:

$*CHx + *OH = *CHxO + *H$

$*CHxO + *H = *CO + H_2$

where * is an absorbing site on the catalyst surface

rather than the direct reaction:

$*C\alpha + *O = **CO$

Therefore, higher CHx adsorbed species could result in higher CO production. Adsorbed OH bands appear in the spectral range 3500-3750 cm^{-1} for all three catalysts [Natesakhawat et al. (2005); Eckle et al. (2010)]. The intensities for the bands were higher for the Mo catalysts than Ni, indicating that more OH is available on the Mo catalyst for CHx gasification to CO, and promoting the OH gasification route rather than O only, even if gaseous carbon was formed on the Ni catalyst.

Smaller bands at 1300-1390 cm^{-1} are attributed to symmetric monodentate carbonates ($\nu_s COO^-$) while bands at 1470-1530 cm^{-1} are assigned to asymmetric monodentate carbonates ($\nu_{as} COO^-$) (Faria et al, 2009). Asymmetric ($\delta_{as} CH_3$) and symmetric ($\delta_s CH_3$) methyl can also co-exist in these two ranges with the formates. Bidentate carbonates are represented by bands in the range 1530-1620 cm^{-1}, however, these bands can also be attributed to olefinic C=C vibrations as they appear in the range 1580–1660 cm^{-1}[Watson and Ozkan (2003); Faria et al. (2009)]. The band at 3020 cm^{-1} is also assigned to olefinic sp2 C-H stretching and therefore bands at 1590 cm^{-1} are more likely to be attributed to olefinic C=C, initiating the formation of ethylene or propylene. All these bands were lower in intensity for the 0.5Mo catalyst due to its lower conversion.

7.5.4 In-Situ DRIFTS Analysis for Propane Steam Reforming (SR)

Propane SR in-situ DRIFTS experiments were run for the three catalysts; 15Ni, 0.1Mo and 0.5Mo at 390°C. The cell temperature was raised to 390°C under a flow of He that passed through water to saturate it. Due to irregularities on the catalyst surfaces caused by steam, the background signal had to be subtracted under the He and steam flow at 390°C. SR experiments were started by introducing a stream of 1.15 % vol propane with the He/steam stream. Assuming a maximum water vapor saturation of 2-3%, the S/C ratio was in the range 0.6-0.9. Spectra were collected every minute until no change in the signal was observed after 12-14 min.

The spectra at 5^{th} min and 15^{th} min are shown in Figures 7.10 and 7.11 respectively. Due to the presence of steam the spectra were higher in noise; however, the spectra for the three catalysts had the same features of the PO spectra. The linear and bridging CO were higher on the Ni catalyst and lower on 0.5Mo while CH_3 and CH_2 had an opposite trend. CO_2 gaseous bands were higher for 0.1Mo than the 15Ni due to higher conversions, which is in agreement with our SR activity experiments. Since the background signal was subtracted in the presence of steam, OH bands from H_2O dissociation were not detected: however, a negative OH band was clear on the 0.1Mo and 0.5Mo spectra at 3560 cm^{-1} which could be attributed to surface hydroxyl groups on the alumina support consumed upon the adsorption of propane (Natesakhawat et al, 2005). In general, conclusions from PO DRIFTS regarding CO and CHx species can also be made from the SR DRIFTS experiments.

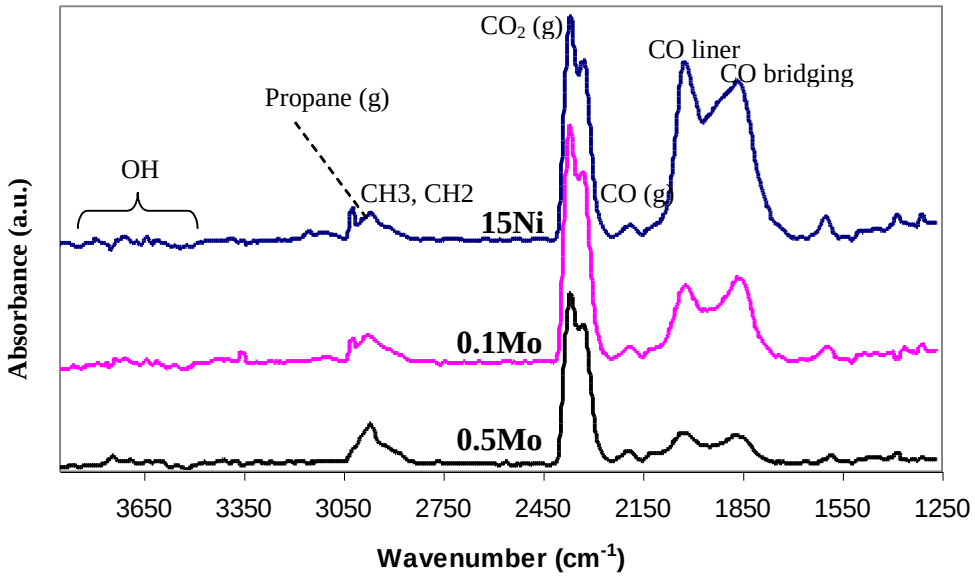

Figure 7.10: in-situ DRIFTS propane SR bands at the 5th min of adsorption

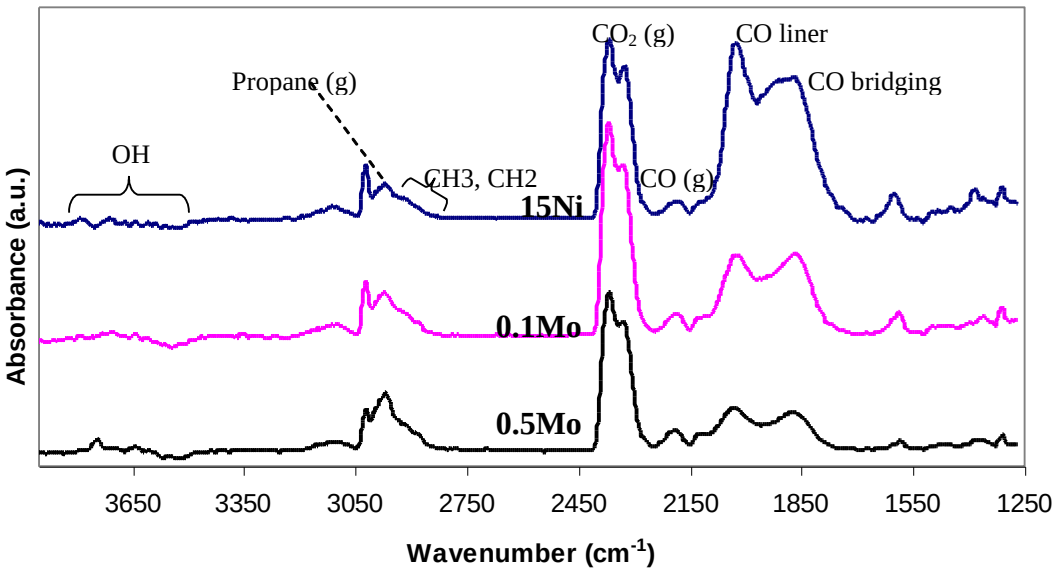

Figure 7.11: in-situ DRIFTS propane SR bands at the 15th min of adsorption

7.6 Oxygen Storage Capacity (OSC) Measurements

When propane cracking reactions were compared for 15Ni and 0.1Mo in Chapter 6, the rate of propane cracking was the same, as well as the amount of carbon deposition on both catalysts after a period of time. However, when small amounts of O_2 were introduced, TPO runs showed less carbon deposits and hence, lower deactivation rates over the 0.1Mo catalyst than over the 15Ni catalyst. Furthermore, DRIFTS spectra for the same reactions (PO of propane at 15 min) revealed the presence of higher amounts of adsorbed OH on the alumina surface for the Mo catalysts. These observations could indicate that the addition of Mo, even in these small quantities, improved the mobility of O_2 on the catalyst surface. To check this, oxygen storage capacity (OSC) was measured for the three catalyst; 15Ni, 0.1Mo and 0.5Mo at room temperature and at 400°C.

OSC is a measure of the ability of a metal or metal oxide to store and release oxygen through reduction-oxidation (redox) reactions.

OSC measurements were performed in a Hiden CatLab reactor. 50 mg of fresh pre-calcined catalyst at 700°C for 3 hours was placed in a tube reactor of 4 mm ID. The catalyst was first reduced in a 5% H_2 stream at 750°C for 30 min then the temperature was cooled down to room temperature and the reactor was flushed with pure He. A dynamic flow technique was used to measure O_2 uptake at room temperature. In this method, pulses of a 1% vol O_2/He stream were injected through the catalyst bed and O_2 uptakes were measured using a Hiden QIC mass spectrometer until no further O_2 uptake was detected. The same procedure was repeated to measure O_2 uptake at 400°C. O_2 uptakes at the two temperatures for the three catalysts are presented in Table 7.3.

Table 7.3: OSC measurements at RT and 400 °C

Catalyst	O_2 uptake at RT (ppm)	O_2 uptake at 400 °C (ppm)	% decrease at 400°C
15Ni	930	603	35
0.1Mo	2875	1800	37
0.5Mo	1613	1576	2

The addition of 0.1% wt Mo to the Ni catalysts increased its O_2 uptake by about 200% (3-fold increase) at both RT and 400°C, while increasing the Mo loading to 0.5% wt caused an increase of O_2 uptake by 73% at RT and by 160% at 400°C. As temperature was increased from RT to 400°C the O_2 uptake decreased for all catalysts due to lower O_2 chemisorption at the higher temperature. The % decrease in O_2 uptake between RT and 400°C was significantly higher for the 15Ni and 0.1Mo catalysts (32 and 37% decrease) compared to only 2% for the 0.5Mo catalyst. This is because the O_2 uptake for 0.5Mo at 400°C is not only a result of O_2 chemisorption, but also some O_2 is consumed in oxidizing Ni to NiO as our TPR measurements in section 7.1 showed that bulk NiO reduction over the 0.5Mo catalyst starts at 388°C while it is above 400°C for the other two catalysts.

TPR runs for the 0.5Mo and 1% Mo-15Ni catalysts revealed that Mo can exist in different oxidation states. This was also proven through XPS measurements of a reduced Mo-Ni catalyst by Borowiecki et al. (2003), as they indicated the presence of Mo in the forms: Mo^{+6}, Mo^{0} and Mo^{+n} ($4 < n < 5$). The existence of Mo in different oxidation states can facilitate redox properties of Mo-containing catalysts. Indeed, MoO_2 was found to be highly active in iso-octane partial oxidation (Marin-Flores et al, 2009). The high activity was attributed to the ability of MoO_2 to provide oxygen, sustaining a redox cycle on the catalyst surface. However, we do not believe that an increase of ca. 200 % in OSC for the 0.1Mo catalyst could be attributed to Mo oxidation state cycling alone. Furthermore, if that were the case, an increase in the Mo loading to 0.5 wt % should have further increased the OSC of the 0.5Mo catalyst, which was actually decreased to 73%. Therefore, the increase in OSC by the addition of small amounts of Mo could be attributed to an increase in oxygen ionic conductivity of Ni caused by an electronic interaction between Mo and Ni. This electronic effect allows cycling of Ni^{0} and Ni^{+2} depending on the reaction atmosphere, enhancing O_2 mobility on the catalyst surface and hence resulting in higher gasification rates of CHx species to CO and H_2. Lower OSC at higher 0.5% Mo indicates a decrease in the quantity of Ni particles available for the

cycling process although a high O_2 mobility is still sustain as high CO and H_2 levels were produced over the 0.5Mo catalyst in SR activity tests.

7.7 Combining Interpretations from Different Characterization Results

It was well said by Bartholomew and Farrauto (2006); "As in the parable of the 10 men and the elephant, each method or tool may feel a part of the elephant, but the combined use of several complementary tools may enable the entire elephant to be accurately described". Therefore, it is important to combine different interpretations from characterization techniques to better visualize the whole picture of the structural effect of Mo on activity, selectivity and stability of the Ni catalyst. The understanding of these combine interpretations is more demanding in our case, to overcome the lack of physical differences between the catalysts resulting from low Mo loadings.

The different characterization techniques point towards an electronic effect of these small amounts of Mo on the Ni catalyst structure and properties. In order to understand the nature of this effect, it is necessary to identify electronic properties of each phase existing on the catalyst during the course of the reaction, and how these phase properties affect each other, and affect reaction intermediates. TPR runs for the 15Ni catalysts showed that the high calcination temperature when pre-treating the catalyst caused relatively strong interactions between NiO and the alumina support. γ-Al_2O_3 has a structure of a defect hydrogen-aluminal spinel having a unit cell of $Al_{12}(Al_{12}H_4)O_{32}$ with 2 and 2/3 aluminum atoms missing (Bartholomew and Farrauto, 2006). This structure allows γ-Al_2O_3 to be a Brønsted proton donor acid due to surface hydroxyl groups and a Lewis acid electron acceptor at dehydrated aluminum sites. This moderate acidity has a crucial role in reactions involving acid sites; one of these reactions is hydrocarbon cracking which is also the major cause of Ni steam reforming catalyst deactivation as illustrated in Chapter 6. When γ-Al_2O_3 is impregnated with Ni, the bivalent metal cation occupies tetrahedral sites in the spinel structure (Coma et al, 1992), leading to a decrease in the cationic deficiency of γ-Al_2O_3 and hence, lowering its Lewis acidity and stabilizing the structure. The interaction between NiO and γ-Al_2O_3 plays also a physical role in reducing carbon formation, as it favours the formation of small NiO clusters, which

enhances Ni dispersion and prevents the formation of large Ni ensembles that are necessary to initiate carbon formation. Even with these Ni properties, coking of Ni/ γ-Al_2O_3 could not be avoided under industrial SR conditions, as was also the case in our stability tests in Chapters 5 and 6.

A negative effect of strong interactions between Ni and alumina is that in an oxidative environment, Ni can be oxidized form spinel $NiAl_2O_4$, which can begin to form at temperatures as low as 400°C. $NiAl_2O_4$ is inactive in SR, and TPR runs showed that it requires temperatures as high as 800°C to be reduced. Therefore, although O_2 facilitates the gasification of carbon, high ratios may cause the loss of Ni sites by oxidation to NiO or $NiAl_2O_4$ as proven by our aged 15Ni catalyst XRD runs. However, it should be noted that in the absence of O_2, studies proved that the oxidation of Ni to NiO is not observed in the presence of steam only, even at temperatures as high as 700°C (Borowiecki et al, 2004).

When 0.1 wt% Mo is co-impregnated with 15 wt% Ni over γ-Al_2O_3, reduction of NiO was shifted to lower temperatures and more Ni was present in the form of NiO rather than $NiAl_2O_4$, indicating that Mo weakened the NiO- γ-Al_2O_3 interactions. This led to a higher degree of Ni reduction as proven by the higher OSC of the 0.1Mo catalyst. We speculate that the effect of Mo on the metal support interaction strength is due to an electronegativity influence of Mo on Ni. Mo has an electronegativity of 2.16 on the Pauling scale while Ni electronegativity is 1.91, which makes Mo a higher electron acceptor. Moreover, MoOx is considered to be a strong Lewis acid while NiO is a mild base. TPR results of the higher Mo loadings showed that MoO_3 and MoO_2 are the two common oxides that exist on the promoted catalysts, and as the catalyst is further reduced, more MoO_2 is present. MoO_2 has higher electrical conductivity due to its higher density of state in the valence region and more free electrons, compared to MoO_3 where all neighbouring oxygen atoms form a covalent bond with Mo (Song et al, 2002). As Mo phases are imbedded in the Ni catalyst, these electronic properties affect the electronic state of Ni species, leading to a lower charge transfer between Ni and γ-Al_2O_3 acid sites, and hence, impeding the incorporation of the Ni species in the alumina lattice.

As Ni is less incorporated in γ-Al_2O_3, it will be easier to reduce and perhaps to oxidize at lower temperatures. Therefore, we expect Ni to be oxidized and reduced under our reaction conditions. This redox cycling will not only depend on the oxidative and reductive agents present in the reaction atmosphere, but also on different oxidation states of MoOx species. We speculate that the redox cycling of Ni species will improve their oxygen ion-conductivity, enhancing the mobility of O_2 on the catalyst surface and hence the gasification of CHx species.

The change in the electronic state of Ni species will also affect the stability of adsorbed reaction intermediates on the catalyst surfaces. Based on their DFT calculations, Bengaard et al. (2002) reported that during the dissociative chemisorption of CH_4 to different CHx species, adsorbed gaseous carbon (*C) is the most stable intermediate on step Ni(211) sites, compared to less stable CH_3 and CH_2 intermediates. Therefore, unpromoted Ni favours the complete dehydrogenation of CHx species to *C which is well adsorbed on Ni and can initiate the formation of more difficult to gasify forms of carbon, as illustrated in our cracking experiments in Chapter 6. On the other hand, in-situ DRIFTS experiments for propane PO and SR showed that there were more CH_3 and CH_2 adsorbed species over the 0.1Mo and 0.5Mo catalysts than 15Ni. We expect that the electronic change in Ni led to more stable adsorbed CHx species and prevented their further dehydration to carbon. CHx species are more active than gaseous carbon and can be highly gasified by the mobile O_2 available on the surface to CO and H_2. Moreover, TPO of carbon resulting from PO of propane in Chapter 6 showed that once nickel carbide is formed on the catalyst surface, the Mo catalyst did not have any effect on its gasification rate, as the carbon morphology was the same on promoted and unpromoted catalysts. This is another indication that inhibiting carbon formation on the Mo promoted catalysts was through the gasification of CHx rather than gaseous carbon. In addition, DRIFTS experiments for propane PO showed that there were more hydroxyl groups adsorbed on the surface of the Mo catalysts than unpromoted Ni, which led us to believe that when NiO is reduced during the redox cycle, Ni-OH is formed on the surface, which

is expected to be more reactive in the gasification of CHx species than the lattice Ni oxygen.

The dissociation of CO through the Boudoard reaction in Chapter 6 was affected by the change in the electronic structure of Ni in the two promoted catalysts. This was further justified by in-situ DRIFTS experiments of propane PO and SR which indicated lower adsorption of CO over the promoted catalysts. Therefore, although the O_2 mobility was improved over the catalyst surface, the oxidation of CO to CO_2 was lower due to the unstable adsorbed CO. Figure 7.12 is a schematic illustration of the effect of Mo on the Ni- γ-Al_2O_3 interaction and the stability of different reaction intermediates.

As Mo loadings are increased to 0.5Mo, Mo will have greater electronic effects on Ni species. These effects led to lower NiO reduction temperatures indicating weaker NiO-γ-Al_2O_3 interactions and hence, less Ni incorporated in the alumina lattice. As a result, Ni will be easier to undergo the redox cycle during the reaction and hence, we expect an increase in the O_2 ion conductivity. It is also expected that due to higher Mo loadings, MoOx will have a contribution to the O_2 ion conductivity. TPR experiments for 0.5Mo and 1Mo catalysts showed that MoOx exists in different oxidation states, and are reduced at lower temperatures in the presence of Ni. This was also proved when XPS measurements were performed for a reduced Mo-Ni catalyst by Borowiecki et al. (2003), as they indicated the presence of Mo in the forms: Mo^{+6}, Mo^{0} and Mo^{+n} ($4 < n < 5$). Therefore, MoOx species can also undergo redox cycling during the course of the reaction, contributing to the O_2 mobility on the catalyst surface and preventing coking of the catalyst. This higher O_2 ion conductivity indeed resulted in higher CO and H_2 yields than the 0.1Mo catalyst as proved by SR activity runs, and lower carbon deposition during TPO of propane PO. However, activity runs showed lower conversions for the 0.5Mo catalyst and loss of stability with time. In addition, H_2 chemisorption experiments indicated a 31 % loss in the Ni dispersion after ageing the catalyst. This was attributed to the loss of Ni sites due to the decoration of Ni or NiO by MoOx, or by the formation of difficult to reduce $NiMoO_4$, which can occur at the catalyst preparation stage as proved from TPR, or in highly oxidizing reaction atmospheres as concluded from aged catalyst XRD results. Indeed, the negative effect of the highly oxidizing atmosphere was also

observed in our first activity screening tests in Chapter 5 for the 0.3Mo catalyst (see Table 5.11). At both temperatures; 400 and 450°C, the conversion and the H_2 production was lowered when the O_2/C ratio was increased from 0.2 to 0.6 at a constant S/C ratio of 3.5. On the other hand, the unpromoted 15Ni catalyst had a reverse trend when the O_2/C ratio was increased. Therefore, although we expect that O_2 ion conductivity of 0.5Mo is higher than 0.1Mo, the density of the O_2 conductors are lower, which was also observed in OSC measurements. Consequently, optimizing the Mo loading in the Ni-Mo catalyst is a matter of finding the right ratio of the ion conductivity strength to the density of conductors.

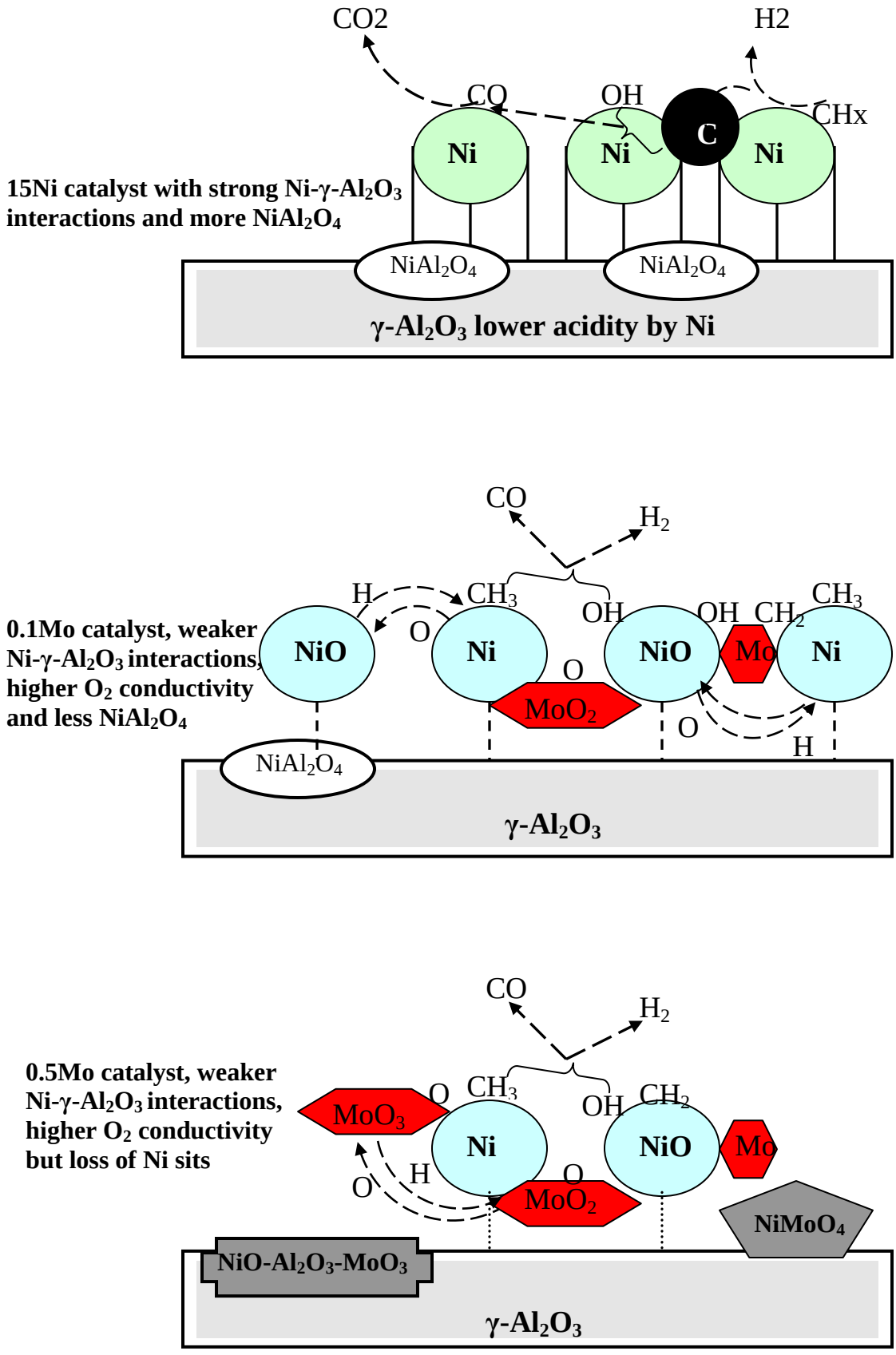

Figure 7.12: A schematic illustration of the effect of Mo on Ni- γ-Al_2O_3 interactions and the stability of different reaction intermediates.

7.8 Effects of Mo on the General Propane OSR Reaction Scheme

The mechanism of CH_4 steam reforming was studied extensively in the literature, however, less work has been proposed for propane and higher hydrocarbon steam reforming mechanisms. Some of the suggested pathways for propane SR by a couple of authors were discussed in Chapter 2. Although there were studies on the activity and stability of Ni-Mo catalysts in SR, to our knowledge no study has discussed the effect of the catalyst on propane OSR and its reaction scheme. In this section we investigate the effect of Mo in the Ni-Mo catalyst on different pathways of the propane OSR reactions, run under those conditions discussed in detail in Chapter 6. The selection of different pathways is also promoted by results of in-situ DRIFTS experiments for propane SR and PO discussed earlier in this chapter.

Generally, PO and SR reactions for higher hydrocarbons will precede through the dissociative adsorption of the hydrocarbon, in this case propane, which is thought to be an irreversible rate determining step under some reaction conditions. The adsorbed hydrocarbons undergo subsequent breakage to result in CHx species, which can dehydrate to produce H_2 and gaseous carbon Cα, that can be gasified by adsorbed oxygen to CO and CO_2. Adsorbed oxygen is produced from the dissociation of O_2 or H_2O:

$$O_2 + 2* \longleftrightarrow 2O* \quad \text{(R1)}$$

$$H_2O + * \longleftrightarrow O* + H_2 \quad \text{(R2)}$$

$$H_2 + 2* \longleftrightarrow 2H* \quad \text{(R3)}$$

$$O* + 2H* \longleftrightarrow OH* + H* \quad \text{(R4)}$$

Although this work does not present any evidence that Mo has an effect on H_2O dissociation, enhanced O_2 mobility on the catalyst can assist dissociation, as it was reported that adsorbed oxygen species auto-catalyze H_2O dissociation (Kasza et al.,

1996). However, higher levels of oxygen will slow the process due the occupation of Ni sites by oxygen.

In the presence of O or OH, propane is adsorbed on the catalyst to produce a propyl group. The propyl group may result from adsorption on a primary carbon 5
K'

$$CH_3CH_2CH_3 + 2* \longrightarrow CH_3CH_2{*}CH_2 + *H \qquad (R5)$$

or a secondary carbon:

$$CH_3CH_2CH_3 + 2* \longrightarrow CH_3{*}CHCH_3 + *H \qquad (R6)$$

If the propyl group was adsorbed on a secondary carbon it will result in the formation of propylene:

$$CH_3{*}CHCH_3 + *H \longrightarrow C_3H_6 + 2* + H_2 \qquad (R7)$$

Statistically, the propyl group is more likely to adsorb on a primary carbon (Huff et al., 1994). This agrees with our results, as propylene was detected only for the 15Ni catalyst in very small amounts compared to acetylene and ethane. Therefore, the propyl group is more likely to be adsorbed on a primary carbon. Adsorption of propyl on a primary carbon will result in an ethyl group and a methyl group:

$$CH_3CH_2{*}CH_2 + *H \longrightarrow CH_3{*}CH_2 + *CH_3 \qquad (R9)$$

Over some metal catalysts, such as Rh, propyl groups are more likely to undergo an α-hydrogen (the H atom on the same carbon metal bond) elimination (Huff et al., 1994). This leads to rapid dehydrogenation of propyl to produce more H_2 and *Cα with no or lower by-product hydrocarbons i.e. ethane, ethylene, methane, etc. This path was also suggested by Natesakhawat et. al. (2005) based on their DRIFTS experiments of propane

SR over a sol-gel Ni-Ce/Al_2O_3 catalyst. However, in our case, since on both types of catalyst, Ni and Mo-Ni, a significant amount of CH_4 together with traces of by-product hydrocarbons were detected especially during SR reactions, propyl is more likely to undergo a ß-elimination. Therefore, ethyl and methyl may further react with an adsorbed *H to produce ethane and methane respectively through hydrogenolysis:

$$CH_3{*}CH_2 + {*}H \longleftrightarrow CH_3CH_3 + 2{*} \quad \text{(R10)}$$

$$*CH_3 + {*}H \longleftrightarrow CH_4 + 2{*} \quad \text{(R11)}$$

However, steam reforming activity experiments showed lower CH_4 production over the Mo catalysts compared to Ni and in addition, in-situ propane SR DRIFTS experiments showed more adsorbed CHx species on the Mo catalyst surface. Therefore, we speculate that reaction (R11) is less favourable to occur in the presence of Mo. The lower CH_4 production in the presence of Mo is in agreement with results from the work of Boroweicki et al. (2003), as they studied butane hydrogenolysis over different loadings of Mo-Ni catalysts at low temperatures (240-260°C) and found that CH_4 selectivity was lower with the addition of Mo to the Ni catalysts. They also found that CH_4 selectivity decreased as they increased the Mo loading from 0.1 to 4% wt. They concluded from these results that the introduction of Mo caused a change in the properties of the active centers on the catalyst surface.

With methyl groups not converted to CH_4, they will further dehydrogenate to CHx, producing more H* and ultimately gaseous carbon *Cα:

$$*CH_3 + 6{*} \longleftrightarrow 3H{*} + *C\alpha \quad \text{(R12)}$$

Which can be gasified directly by *O to **CO:

$$*C\alpha + *O \longrightarrow **CO \quad \text{(R13)}$$

or by OH* first to **CHO then to CO** (Aparicio, 1997):

$$*C\alpha + *OH \longleftrightarrow **CHO \qquad (R14)$$

$$**CHO + 3* \longrightarrow **CO + *H + 2* \qquad (R15)$$

The complete dehydrogenation of CHx as it appears in equation (R12) and the gasification of *Cα to **CO was argued by a couple of authors in the literature. Bradford and Vannice (1999) argued that the reaction of *CHx with *OH to form a *CHxO intermediate is more likely to occur than the reaction of *OH with *Cα to form **CHO since *CHx species are more active than gaseous *Cα:

$$*CHx + *OH \longleftrightarrow *CHxO + *H \qquad (R16)$$

$$*CHxO + *H \longrightarrow *CO + H_2 \qquad (R17)$$

This was also suggested by Rostrup-Neilsen and Hansen (1993) as they postulated the reaction of *CHx with adsorbed *O rather than *OH to produce *CO and *H.

$$*CHx + *O \longrightarrow *CO + H_2 + 2* \qquad (R18)$$

When running TPO of carbon deposited from PO reactions of propane in Chapter 6, it was found that, although carbon deposition was low in quantity over the Mo catalysts, they were of the same carbon types as the unpromoted Ni catalyst. This was justified by the CO_2 and CO gasification peak shapes and temperatures, indicating similar carbon morphology (see Figure 6.28). This means that once carbon is formed, even on Mo-promoted catalysts, it is hard to gasify. In fact, Silva et. al. (1997) studied air gasification of charcoal over Mo, Co and Ni oxides and found that Co and Ni had better gasification rates than Mo especially at the lower temperature ranges (300-500°C). Even when mixing Mo with Ni, the improvement in gasification rate was not significant as

they attributed this slight improvement to the role of Mo in preventing crystal growth or sintering. Poor gasification of atomic and polymeric carbon over a Ni-MoO_2 catalyst was also reported by Gardner and Bartholomew (1981).

Therefore, in order to inhibit carbon formation on 0.1Mo and 0.5Mo catalysts, gasification during OSR should occur before the complete dehydrogenation of *CHx to *Cα; perhaps adsorbed *CHx is gasified rather than *Cα as we suggested earlier. This indicates the role of small amounts of Mo in decreasing the dehydrogenation degree of *CHx allowing them to be more easily gasified. Indeed, this was suggested by Wang et al. (1999) who studied the role of Mo in a Rh/Al_2O_3 catalyst in the process of CH_4 decomposition and hydrogenation to produce higher hydrocarbons at low temperatures (400°C). From different FTIR spectra studied, they found that the addition of Mo to the Rh catalyst increased the amount of *CHx species and decreased *Cα. Figure 7.13 is an illustrative diagram of the effect of Mo on the possible pathways of propane OSR over Ni catalysts.

On the left side of the scheme in Figure 7.13, the ethyl groups not converted to ethane can further under go an α-elimination:

$$CH_3{*}CH_2 + 2{*} \longleftrightarrow CH_3{**}CH + {*}H \qquad \text{(R19)}$$

This can result in rapid dehydrogenation of the intermediates to produce ultimately H_2 and adsorbed gaseous carbon *Cα. Or a ß-elimination can occur:

$$CH_3{*}CH_2 + 2{*} \longleftrightarrow {*}CH_2{*}CH_2 + {*}H \qquad \text{(R20)}$$

then further desorb to produce ethylene (Huff et al., 1994):

$$*CH_2*CH_2 \longleftrightarrow CH_2CH_2 + 2* \qquad \text{(R21)}$$

However, when studying chemisorption and decomposition of ethylene over Ni catalysts, Zaera and Hall (1987) found that unlike Pt and Pd, once dehydrogenated intermediates are formed on Ni they are difficult to desorb resulting in further dehydrogenation of these intermediates. They also found that the further decomposition of chemisorbed vinyl over Ni can result in the formation of acetylene. Since no ethylene was detected in our OSR and SR, the $*CH_2*CH_2$ intermediate can further dehydrogenate to produce an adsorbed vinyl group and further a desorbed acetylene as traces of acetylene were detected for both Ni and Ni-Mo catalysts:

$$*CH_2*CH_2 \longleftrightarrow CHCH + 4* + 2H_2 \qquad \text{(R22)}$$

The acetylene formation path can also be justified by analyzing by-product distributions from propane PO reactions on both catalysts in Chapter 6. PO reactions were run at low O_2/C ratio, allowing catalytic propane cracking to occur and deactivation of the catalysts by coking with time. For 15Ni and 0.1Mo, no ethylene was detected during the first three hours, only traces of acetylene were present. However, with time, acetylene peaks began to decrease and ethylene peaks began to appear, increasing in intensity with time. This is because, as more catalysts sites are blocked by carbon, no sites are available for further dehydrogenation, resulting in the desorption of ethylene rather that acetylene.

However, since very small traces of acetylene and ethane were detected over the 0.1Mo catalyst during OSR, compared to the other four main products; H_2, CO, CO_2 and CH_4, we expect that only a very small portion of ethyl in equation (R20) will follow the path suggested to produce acetylene or ethane. Most of the ethyl in equation (R20) will further undergo dissociative adsorption to fragments of methyl CH_3 and methylene CH_2 which will follow different routes suggested earlier to produce H* and *CO:

$$CH_3*CH_2 + 2* \longrightarrow **CH_2 + *CH_3 \qquad \text{(R23)}$$

Adsorbed **CO can further react with adsorbed oxygen *O to produce CO_2:

$$**CO + *O \longleftrightarrow CO_2 + 3* \quad \text{(R24)}$$

Propane PO reactions of 0.1Mo showed lower CO_2 production compared to the 15Ni catalysts, while CO_2 SR yields were the same for the two catalysts. Over the 0.5Mo catalyst, CO yields during SR were significantly higher than 15Ni and 0.1Mo, with the lowest CO_2 yield among the three catalysts. Considering the high CO production over the 0.5Mo catalyst, in-situ DRIFTS experiments for propane SR and PO indicated lower CO absorbance on 0.5Mo. Therefore, we speculate that in the presence of Mo, CO desorbed quickly lowering the production of CO_2:

$$**CO \longleftrightarrow CO + 2* \quad \text{(R25)}$$

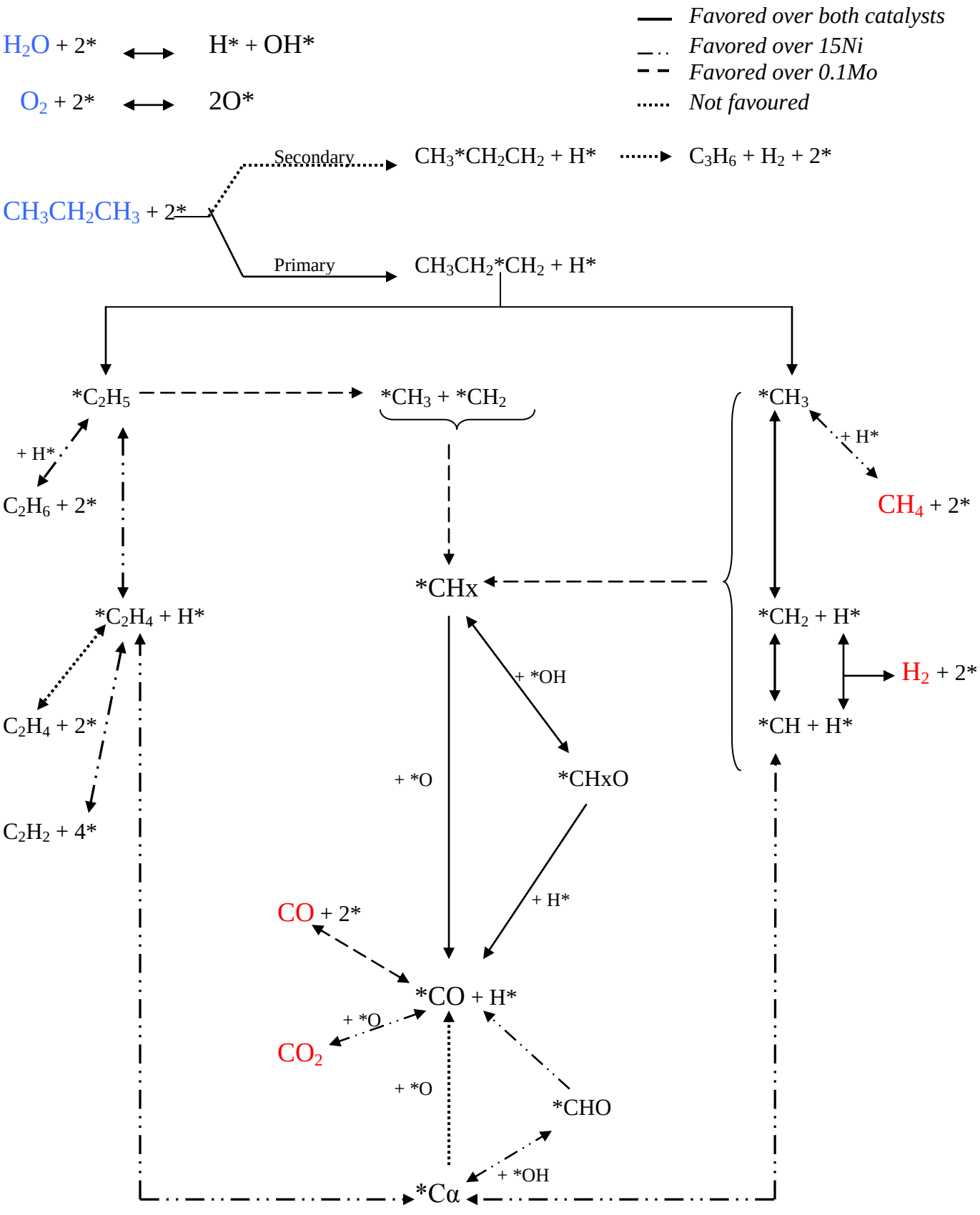

Figure 7.14: Possible pathways in reaction scheme of Propane OSR

Chapter 8

Conclusions and Recommendations

8.1 Conclusions

This study found that promoting a 15 wt% Ni/Al_2O_3 (15Ni) catalyst with 0.1 wt% Mo resulted in a 15Ni-0.1Mo/Al_2O_3 (0.1Mo) bimetallic catalyst which was active and stable under moderate operational conditions for H_2 production from LPG (propane butane mixture) oxidative steam reforming. Compared to the monometallic 15Ni catalyst under the same feed and operating conditions, the 0.1Mo catalyst had higher fuel conversion, higher H_2 yields and showed superior performance in resisting catalyst coking as well as Ni sintering and Ni oxidation to inactive phases.

In addition to its effect on catalyst's activity and stability, Mo addition affected the selectivity of the catalyst to different products. The 0.1Mo catalyst increased the catalyst selectivity to CO significantly under all examined conditions. On the other hand, the production of CH_4 was lower over the 0.1Mo catalyst compared to the unpromoted catalyst.

When propane and butane were tested individually for different reactions over the 0.1Mo catalyst, it was found that butane enriched LPG gave the highest fuel conversions and H_2 production rates, even though experiments for both fuels were run at the same carbon basis. Individual reactions runs also showed the benefit of oxidative steam reforming (OSR) compared to steam reforming (SR) as for both fuels higher conversions and H_2 production rates were achieved when small amounts of O_2 were introduced to SR reactions. However, due to relatively low reaction temperatures it was shown that the contribution of partial oxidation reactions in H_2 production is low and the main role of O_2 was to provide heat to the endothermic SR reaction. In addition, these small amounts of O_2 played an important role in preventing coking of the catalysts as for both fuels SR reactions resulted in carbon depositions over the catalyst.

The importance of O_2 in carbon gasification, especially in the presence of Mo, was also revealed. Comparison between propane catalytic cracking over the 15Ni and the 0.1Mo catalysts showed no difference in the amounts and morphology of deposited carbon. However, the introduction of small amounts of O_2 during the cracking process decreased the amount of carbon over the 0.1Mo catalysts while no effect on the amount of carbon deposited was detected over the unpromoted catalyst.

Characterization techniques were applied to understand the structural effect of small amounts of Mo on the Ni catalysts and revealed that the improvements in the catalytic properties of the catalyst and the change in its selectivity to different products were caused by an electronic effect of Mo and its different oxide phases on Ni species. The changes in the electronic state of different Ni species affected the catalyst properties in two ways:

1) It weakened the Ni-Al_2O_3 interactions leading to more reducible Ni and easier to reduce and oxidize (redox) Ni species under the reaction conditions. This redox cycling of Ni species improved their oxygen ion-conductivity, enhancing the mobility of O_2 on the catalyst surface and hence the gasification of CHx species. Higher CHx gasification rates prevented coking of the catalyst and increased H_2 and CO production rates.

2) It affected the stability of adsorbed reaction intermediates on the catalysts surface. It led to more stable adsorbed CHx species and prevented their further dehydrogenation to carbon. CHx species are more active than gaseous carbon and can be gasified to CO and H_2 by the mobile O_2 available on the surface. On the other hand, Ni electronic changes led to unstable adsorbed CO. These changes in intermediate species stabilities affected some pathways in the general propane OSR scheme. Weak adsorption of CO lowered their further oxidation to CO_2 while higher oxidation of CHx species lowered their hydrogenation to CH_4.

The present study also revealed that the amount of Mo used to promote the Ni catalysts should be carefully optimized. It was found that promoting the studied Ni catalyst with Mo loadings higher than 1 wt% led to inactive catalysts, while loadings higher than 0.3 wt% decreased fuel conversion and production rates. Moreover, when examining a 0.5 wt% Mo-15 wt% Ni /Al_2O_3 (0.5Mo) catalyst under LPG oxidative steam reforming conditions it was found that the catalyst did not only lower its activity but also lost its stability over time. However the deactivation of the catalyst was not due to coking.

Characterization of fresh and aged samples of the 0.5Mo catalyst showed that the lower catalyst activity and deactivation was caused by the oxidation of active Ni species to inactive Ni and Ni-Mo phases which resulted from the oxidative environment of the reaction. Although the 0.1Mo catalyst was not deactivated by the oxidation under the same 0.5Mo catalysts ageing conditions, activity tests at relatively high O_2/C ratios for a 0.3 wt% Mo-15 wt%/Al_2O_3 (0.3Mo) catalyst showed negative affects on H_2 production rates. Therefore, although steam reforming experiments with only butane showed high necessity of O_2 to maintain a stable catalyst, the reaction environment should be carefully controlled by optimizing the S/C and O_2/C ratios, such that a continuous redox cycle for the 0.1Mo catalysts is maintained.

8.2 Recommendations

The promising performance of the Mo-Ni/Al_2O_3 catalyst opens the potential for a couple of aspects to be investigated for further application of the catalyst in hydrocarbons reforming and scale-up of the process for large industrial applications. The following are recommended for further investigation:

- As the study illustrated the effect of small amounts of Mo on metal support interactions, it is recommended to investigate the effect of other supports on the bimetallic Ni-Mo combination. Other supports such as CeO_2 may reduce the CO production, typically for applications where CO poisoning is a concern. Also as the metal support interaction is highly affected by the catalyst synthesis

procedure, improving the consistency of the sequential impregnation method should be considered.

- The high catalyst resistance to coking suggests investigating the application of these catalysts in reforming for higher hydrocarbons such as gasoline and diesel. The application of the catalyst to these higher hydrocarbon contents may require increasing the amount of Mo in the catalyst and higher O_2/C and/or S/C ratios. Under these conditions the catalyst will be more exposed to deactivation by oxidation. Therefore, it is recommended to investigate recycling some H_2 with the feed to maintain a redox environment or regeneration of the catalyst.

- Another aspect related to applying the catalyst for high hydrocarbons is testing the catalyst tolerance to sulphur species.

- If the catalyst to be used in a compact reformers for domestic fuel cells, it is recommended to test the catalyst activity after air treatment. This is due to the fact that in domestic fuel cell applications between frequent start-up and shutdown the catalyst bed has to be purged by air.

- Conducting a kinetic study will be necessary to assist the scale-up of the process for industrial applications. The study will require well controlled reaction conditions including: ideal plug flow and isothermal conditions.

References

Aartun, Ingrid, Torbjrn Gjervan, Hilde Venvik, Oliver Gorke, Peter Pfeifer, Marcus Fathi, Anders Holmen, and Klaus Schubert. 2004. Catalytic conversion of propane to hydrogen in microstructured reactors. *Chemical Engineering Journal* 101 (1-3): 93-9.

Adesina, A. A., K. M. Hardiman, C. G. Cooper, and R. Lange. 2006. Post-mortem characterization of coke-induced deactivated alumina-supported co-ni catalysts. *Chemical Engineering Science* 61 (8) (04): 2565-73.

Agnelli, M., M. Kolb, and C. Mirodatos. 1994. Co hydrogenation on a nickel catalyst .: 1. kinetics and modeling of a low-temperature sintering process. *Journal of Catalysis* 148 (1) (7): 9-21.

Ahmed, S., and M. Krumpelt. 2001. Hydrogen from hydrocarbon fuels for fuel cells. *International Journal of Hydrogen Energy* 26 (4) (04): 291-301.

Aksoylu, A. Erhan, Zülal Mısırlı, and Z. lsen Önsan. 1998. Interaction between nickel and molybdenum in Ni–Mo/Al2O3 catalysts: I: CO2 methanation and SEM-TEM studies. *Applied Catalysis A: General* 168 (2) (3/27): 385-97.

Alvarez-Galvan, M., Domna A. Constantinou, Rufino M. Navarro, Jose A. Villoria, Jose Luis G. Fierro, and Angelos M. Efstathiou. 2011. Surface reactivity of LaCoO3 and Ru/LaCoO3 towards CO, CO2 and C3H8: Effect of H2 and O2 pretreatments. *Applied Catalysis B: Environmental* 102 (1-2): 291-301.

Andersson, M. P., F. Abild-Pedersen, I. N. Remediakis, T. Bligaard, G. Jones, J. Engbæk, O. Lytken, et al. 2008. Structure sensitivity of the methanation reaction: H2-induced CO dissociation on nickel surfaces. *Journal of Catalysis* 255 (1) (4/1): 6-19.

Aparicio, L. M. 1997. Transient isotopic studies and microkinetic modeling of methane reforming over nickel catalysts. *Journal of Catalysis* 165 (2) (1/15): 262-74.

Appleby, A. J. 1995. Electrochemical energy-progress towards a cleaner future: Lead/acid batteries and the competition. Paper presented at Fourth European Lead Battery Conference, .

Avcı, Ahmet K., Z. Ilsen Önsan, and David L. Trimm. 2001. On-board fuel conversion for hydrogen fuel cells: Comparison of different fuels by computer simulations. *Applied Catalysis A: General* 216 (1-2) (8/1): 243-56.

Avci, Ahmet K., David L. Trimm, A. E. Aksoylu, and Z. I. Onsan. 2004. Hydrogen production by steam reforming of n-butane over supported ni and pt-ni catalysts. *Applied Catalysis A: General* 258 (2): 235-40.

Avcı, Ahmet K., David L. Trimm, A. Erhan Aksoylu, and Z. Ilsen Önsan. 2004. Hydrogen production by steam reforming of n-butane over supported ni and pt-ni catalysts. *Applied Catalysis A: General* 258 (2) (2/20): 235-40.

Ayabe, S., H. Omoto, T. Utaka, R. Kikuchi, K. Sasaki, Y. Teraoka, and K. Eguchi. 2003. Catalytic autothermal reforming of methane and propane over supported metal catalysts. *Applied Catalysis A: General* 241 (1-2): 261-9.

Barbier Jr., J., and D. Duprez. 1993. Reactivity of steam in exhaust gas catalysis I. steam and oxygen/steam conversions of carbon monoxide and of propane over PtRh catalysts. *Applied Catalysis B: Environmental* 3 (1): 61-83.

Bartholomew and Farrauto. 2006. *Fundamentals of industrial catalytic processes*. second ed. New Jersey, USA: John Wiley & Sons INC.

Bartholomew, Calvin H. 1982. CARBON DEPOSITION IN STEAM REFORMING AND METHANATION. *Catalysis Reviews* 24 (1): 67-112.

Bartholomew, Calvin H., and Wayne L. Sorensen. 1983. Sintering kinetics of silica- and alumina-supported nickel in hydrogen atmosphere. *Journal of Catalysis* 81 (1) (5): 131-41.

Bengaard, H. S., J. K. Nørskov, J. Sehested, B. S. Clausen, L. P. Nielsen, A. M. Molenbroek, and J. R. Rostrup-Nielsen. 2002. Steam reforming and graphite formation on ni catalysts. *Journal of Catalysis* 209 (2) (7/25): 365-84.

Beretta, Alessandra, and Pio Forzatti. 2004. Partial oxidation of light paraffins to synthesis gas in short contact-time reactors. *Chemical Engineering Journal* 99 (3): 219-26.

Bharadwaj, S. S., and L. D. Schmidt. 1994. Synthesis gas formation by catalytic oxidation of methane in fluidized bed reactors. *Journal of Catalysis* 146 (1) (3): 11-21.

Borowiecki and Gotbiowski. 1994. Influence of molybdenum and tungsten additives on the properties of nickel steam reforming catalysts. *Catalysis Letters* 25 : 309-313.

Borowiecki, T., A. Gotebiowski, and B. Stasinska. 1997. Effects of small MoO3 additions on the properties of nickel catalysts for the steam reforming of hydrocarbons. *Applied Catalysis A:General* 153 (1-2): 141-.

Borowiecki, Tadeusz, Andrzej Denis, Wojciech Gac, Roman Dziembaj, Zofia Piwowarska, and Marek Drozdek. 2004. Oxidation-reduction of Ni/Al2O3 steam reforming catalysts promoted with mo. *Applied Catalysis A: General* 274 (1-2): 259-67.

Borowiecki, Tadeusz, Roman Dziembaj, Marek Drozdek, Grzegorz Giecko, Monika Panczyk, and Zofia Piwowarska. 2003. Studies of the model ni-Mo/alumina catalysts in the n-butane hydrogenolysis reaction. *Applied Catalysis A: General* 247 (1): 17-25.

Borowiecki, Tadeusz, Wojciech Gac, and Andrzej Denis. 2004. Effects of small MoO3 additions on the properties of nickel catalysts for the steam reforming of hydrocarbons: III. reduction of ni-Mo/Al2O3 catalysts. *Applied Catalysis A: General* 270 (1-2): 27-36.

Borowiecki, Tadeusz, Grzegorz Giecko, and Monika Panczyk. 2002. Effects of small MoO3 additions on the properties of nickel catalysts for the steam reforming of hydrocarbons: II. ni-Mo/Al2O3 catalysts in reforming, hydrogenolysis and cracking of n-butane. *Applied Catalysis A: General* 230 (1-2): 85-97.

Box, Hunter and Hunter. 2005. *Statistics for experimenters*. second ed. New Jersey. USA: John Wiley and Sons INC.

Bradford, Michael C. J., and M. Albert Vannice. 1996. Catalytic reforming of methane with carbon dioxide over nickel catalysts I. catalyst characterization and activity. *Applied Catalysis A: General* 142 (1) (8/1): 73-96.

Bradforda and Vannice. 1999. CO2 reforming of CH4. *Catalysis Reviews: Science and Engineering* 41 (1): 1-42.

Brito, J. L., and J. Laine. 1993. Reducibility of ni-Mo/Al2O3 catalysts: A TPR study. *Journal of Catalysis* 139 (2) (2): 540-50.

Brito, Joaquin L., Jorge Laine, and Kerry C. Pratt. 1989. Temperature-programmed reduction of ni-mo oxides. *Journal of Materials Science* 24 (2): 425-31.

Caglayan, Burcu Selen, Ahmet K. Avci, Z. Ilsen Onsan, and A. E. Aksoylu. 2005. Production of hydrogen over bimetallic pt-ni/-Al2 O3 I. indirect partial oxidation of propane. *Applied Catalysis A: General* 280 (2): 181-8.

Caglayan, Burcu Selen, Z. I. Onsan, and A. E. Aksoylu. 2005. Production of hydrogen over bimetallic pt-ni/-Al2O 3: II. indirect partial oxidation of LPG. *Catalysis Letters* 102 (1-2): 63-7.

Chan, S. H., and H. M. Wang. 2000. Effect of natural gas composition on autothermal fuel reforming products. *Fuel Processing Technology* 64 (1): 221-39.

Chen, H., and A. A. Adesina. 1994. Kinetic modelling of methanation reaction over a co-Mo/SiO2 catalyst. *Journal of Chemical Technology and Biotechnology* 60 (1): 103-13.

Cheng, Zhenxing, Qingle Wu, Jinlu Li, and Qiming Zhu. 1996. Effects of promoters and preparation procedures on reforming of methane with carbon dioxide over Ni/Al2O3 catalyst. *Catalysis Today* 30 (1-3) (6/17): 147-55.

Coleman, L. J. 2008. Preparation, characterization and evaluation of mg-al mixed oxide supported ni catalysts for the steam reforming of ethanol. A PhD thesis presented to the University of Waterloo., University of Waterloo.

Corbo, P., and F. Migliardini. 2007. Hydrogen production by catalytic partial oxidation of methane and propane on ni and pt catalysts. *International Journal of Hydrogen Energy* 32 (1) (01): 55-66.

Corma, A., V. Fornés, R. M. Martín-Aranda, and F. Rey. 1992. Determination of base properties of hydrotalcites: Condensation of benzaldehyde with ethyl acetoacetate. *Journal of Catalysis* 134 (1) (3): 58-65.

Costa-Nunes, O., J. M. Vohs, and R. J. Gorte. 2003. A study of direct-conversion SOFC with n-butane at higher fuel utilization. *Journal of the Electrochemical Society* 150 (7): A858-63.

Dadyburjor, Dady B., Tapan K. Das, and Edwin L. Kugler. 2011. Reactions for the partial oxidation of propane over pt-on-ceria. *Applied Catalysis A: General* 392 (1-2): 127-35.

Demirbas, A. 2002. Fuel properties of hydrogen, liquefied petroleum gas (LPG), and compressed natural gas (CNG) for transportation. *Energy Sources* 24 (7) (07): 601-10.

Dias, Joelmir A. C., and Jose M. Assaf. 2004. Autothermal reforming of methane over ni/-Al2O 3 catalysts: The enhancement effect of small quantities of noble metals. *Journal of Power Sources* 130 (1-2): 106-10.

Dimotakis and Pinnavaia. 1990. New route to layered double hydroxides intercalated by organic anions: Precursors to polyoxometalate-pillared derivatives. *Inorganic Chemistry* 29 (13).

Dinka, Peter, and Alexander S. Mukasyan. 2007. Perovskite catalysts for the auto-reforming of sulfur containing fuels. *Journal of Power Sources* 167 (2): 472-81.

Dissanayake, Dhammike, Michael P. Rosynek, Karl C. C. Kharas, and Jack H. Lunsford. 1991. Partial oxidation of methane to carbon monoxide and hydrogen over a Ni/Al2O3 catalyst. *Journal of Catalysis* 132 (1) (11): 117-27.

Eckle, S., Y. Denkwitz, and R. J. Behm. 2010. Activity, selectivity, and adsorbed reaction intermediates/reaction side products in the selective methanation of CO in reformate gases on supported ru catalysts. *Journal of Catalysis* 269 (2) (2/5): 255-68.

Edwards, J. H., and A. M. Maitra. 1995. Chemistry of methane reforming with carbon dioxide and its current and potential applications. *Fuel Processing Technology* 42 (2-3): 269-89.

Engler, B., Koberstein, E., Lindner, D. and Lox, E in: A. Crocq (Ed.). 1990. Catalysis and automotive pollution control II. Paper presented at Proceedings of the Second International Symposium on CAPOC 2, Brussels, September 10–13, 1990, Elsevier, Amsterdam, Stud. Surf. Sci. Catal. 71 (1991) 641. .

Erhan, Aksoylu, A., and Z. I. Onsan. 1998. Interaction between nickel and molybdenum in ni-Mo/Al2O3 catalysts: II CO hydrogenation. *Applied Catalysis A: General* 168 (2): 399-407.

Escritori, Janaina C., Sandra C. Dantas, Ricardo R. Soares, and Carla E. Hori. 2009. Methane autothermal reforming on nickel-ceria-zirconia based catalysts. *Catalysis Communications* 10 (7): 1090-4.

Faria, Wagner L. S., Lidia C. Dieguez, and Martin Schmal. 2008. Autothermal reforming of propane for hydrogen production over Pd/CeO2/Al2O3 catalysts. *Applied Catalysis B: Environmental* 85 (1-2): 77-85.

Faria, Wagner L. S., Carlos A. C. Perez, Deborah V. César, Lídia C. Dieguez, and Martin Schmal. 2009. In situ characterizations of Pd/Al2O3 and Pd/CeO2/Al2O3 catalysts for oxidative steam reforming of propane. *Applied Catalysis B: Environmental* 92 (1-2) (10/19): 217-24.

Fauteux-Lefebvre, C., N. Abatzoglou, J. Blanchard, and F. Gitzhofer. 2010. Steam reforming of liquid hydrocarbons over a nickel-alumina spinel catalyst. *Journal of Power Sources* 195 (10) (05/15): 3275-83.

Ferrandon, Magali, A. J. Kropf, and Theodore Krause. 2010. Bimetallic ni-rh catalysts with low amounts of rh for the steam and autothermal reforming of n-butane for fuel cell applications. *Applied Catalysis A: General* 379 (1-2): 121-8.

Finnerty, Caine, Geoff A. Tompsett, Kevin Kendall, and R. M. Ormerod. 2000. SOFC system with integrated catalytic fuel processing. *Journal of Power Sources* 86 (1): 459-63.

Gandhi, H., Piken, A., Stepien, H., Shelef, M., Delosh, R. and Heyde, M. 1977. SAE technical paper serial. no# 770166. Paper presented at Automotive Engineering Congress, Detroit.

Gardner, David C., and Calvin H. Bartholomew. 1981. KINETICS OF CARBON DEPOSITION DURING METHANATION OF CO. *Industrial & Engineering Chemistry, Product Research and Development* 20 (1): 80-7.

Ghenciu, A. F. 2002. Review of fuel processing catalysts for hydrogen production in PEM fuel cell systems. *Current Opinion in Solid State & Materials Science* 6 (5) (10): 389-99.

Goetsch, Duane A., and Lanny D. Schmidt. 1996. Microsecond catalytic partial oxidation of alkanes. *Science* 271 (5255): 1560-2.

Gokaliler, Feyza, Burcu Selen Caglayan, Z. Ilsen Onsan, and A. Erhan Aksoylu. 2008. Hydrogen production by autothermal reforming of LPG for PEM fuel cell applications. *International Journal of Hydrogen Energy* 33 (4): 1383-91.

Haber, J. 1994. *Molybdenum: An outline of its chemistry and use, studies in inorganic chemistry*. Vol. 19. Amsterdam: Elsevier.

Hardiman, Kelfin M., Cheng-Han Hsu, Tan T. Ying, and Adesoji A. Adesina. 2005. The influence of impregnating pH on the postnatal and steam reforming characteristics of a Co-Ni/Al2O3 catalyst. *Journal of Molecular Catalysis A: Chemical* 239 (1-2): 41-8.

Hardiman, Kelfin M., Tan T. Ying, Adesoji A. Adesina, Eric M. Kennedy, and Bogdan Z. Dlugogorski. 2004. Performance of a Co-Ni catalyst for propane reforming under low steam-to-carbon ratios. *Chemical Engineering Journal* 102 (2): 119-30.

He, Yunbing, Hongbing Ji, Jianhua Xu, and Lefu Wang. 2009. Deep oxidation in propane oxidative dehydrogenation to propene over V2O5/γ-Al2O3 studied by in-situ DRIFTS. *Journal of Natural Gas Chemistry* 18 (3) (9): 359-64.

HEARTH. *HEARTH gas appliance training manual, copyright 1997, HEARTH education foundation.*

Heitnes Hofstad, K., J. H. B. J. Hoebink, A. Holmen, and G. B. Marin. 1998. Partial oxidation of methane to synthesis gas over rhodium catalysts. *Catalysis Today* 40 (2-3) (4/17): 157-70.

Hercules, Proctor and Houalla. 1994. Quantitative analysis of mixed oxidation states in supported catalysts. *Acc. Chem. Res* 27 (12): 387-393.

Hickman, D. A., and L. D. Schmidt. 1992. The role of boundary layer mass transfer in partial oxidation selectivity. *Journal of Catalysis* 136 (2) (8): 300-8.

Hong-Joo Lee, Yoo-Soon Lim, Nam-Cook Park, and Young-Chul Kim. 2009. Catalytic autothermal reforming of propane over the noble metal-doped hydrotalcite-type catalysts. *Chemical Engineering Journal* 146 (2) (02/01): 295-301.

Huff, M., P. M. Torniainen, and L. D. Schmidt. 1994. Partial oxidation of alkanes over noble metal coated monoliths. *Catalysis Today* 21 (1): 113-28.

Jeong, Harim, and Misook Kang. 2010. Hydrogen production from butane steam reforming over Ni/Ag loaded MgAl2O4 catalyst. *Applied Catalysis B: Environmental* 95 (3-4): 446-55.

Kasza, R. V., K. Griffiths, J. G. Shapter, P. R. Norton, and D. A. Harrington. 1996. Interaction of water with stepped ni(760): Associative versus dissociative adsorption and autocatalytic decomposition. *Surface Science* 356 (1-3) (06/10): 195-208.

Kendall, K., and D. S. Williams. 1998. Catalysts for butane reforming in zirconia fuel cells. *Platinum Metals Review* 42 (4): 164-7.

Kepinski, L., B. Stasinska, and T. Borowiecki. 2000. Carbon deposition on Ni/Al2O3 catalysts doped with small amounts of molybdenum. *Carbon* 38 (13): 1845-56.

Kim, Pil, Younghun Kim, Heesoo Kim, In Kyu Song, and Jongheop Yi. 2004. Synthesis and characterization of mesoporous alumina with nickel incorporated for use in the partial oxidation of methane into synthesis gas. *Applied Catalysis A: General* 272 (1-2) (9/28): 157-66.

Kolb, Gunther, Ralf Zapf, Volker Hessel, and Holger Lowe. 2004. Propane steam reforming in micro-channels-results from catalyst screening and optimisation. *Applied Catalysis A: General* 277 (1-2): 155-66.

Laosiripojana, N., and S. Assabumrungrat. 2006. Hydrogen production from steam and autothermal reforming of LPG over high surface area ceria. *Journal of Power Sources* 158 (2) (08/25): 1348-57.

Laosiripojana, N., W. Sangtongkitcharoen, and S. Assabumrungrat. 2006. Catalytic steam reforming of ethane and propane over CeO2-doped Ni/Al2O3 at SOFC temperature: Improvement of resistance toward carbon formation by the redox property of doping CeO2. *Fuel* 85 (3): 323-32.

Laosiripojana, N., W. Sutthisripok, S. Charojrochkul, and S. Assabumrungrat. 2011. Steam reforming of LPG over ni and rh supported on gd-CeO2 and Al2O3: Effect of support and feed composition. *Fuel* 90 (1): 136-41.

Laosiripojana, N., W. Sutthisripok, P. Kim-Lohsoontorn, and S. Assabumrungrat. 2010. Reactivity of ce-ZrO2 (doped with La-, Gd-, Nb-, and Sm-) toward partial oxidation of liquefied petroleum gas: Its application for sequential partial oxidation/steam reforming. *International Journal of Hydrogen Energy* 35 (13) (07): 6747-56.

Lee, Hae Ri, Yeon Lee Kwi, Cook Park Nam, Soon Shin Jae, Dong Ju Moon, Gwon Lee Byung, and Chul Kim Young. 2006. Production of hydrogen by autothermal reforming of propane over ni/-Al2O3. *Journal of Nanoscience and Nanotechnology* 6 (11) (11): 3396-8.

Lee, Hong-Joo, Yoo-Soon Lim, Nam-Cook Park, and Young-Chul Kim. 2009. Catalytic autothermal reforming of propane over the noble metal-doped hydrotalcite-type catalysts. *Chemical Engineering Journal* 146 (2): 295-301.

Li, Dalin, Kazufumi Nishida, Yingying Zhan, Tetsuya Shishido, Yasunori Oumi, Tsuneji Sano, and Katsuomi Takehira. 2009. Sustainable Ru-doped Ni catalyst derived from hydrotalcite in propane reforming. *Applied Clay Science* 43 (1) (1): 49-56.

Lim, Seung-Soo, Hong-Joo Lee, Dong-Ju Moon, Jong-Ho Kim, Nam-Cook Park, Jae-Soon Shin, and Young-Chul Kim. 2009. Autothermal reforming of propane over ce modified Ni/LaAlO3 perovskite-type catalysts. *Chemical Engineering Journal* 152 (1): 220-6.

Lim, SeungSoo, DongJu Moon, JongHo Kim, YoungChul Kim, NamCook Park, and JaeSoon Shin. 2007. Autothermal reforming of propane over ni catalysts supported on a variety of perovskites.

Lim, Sungkwang, and Joongmyeon Bae. 2010. Autothermal reforming over a Pt/Gd-doped ceria catalyst: Heat and mass transport limitations in the steam reforming section. *International Journal of Hydrogen Energy* 35 (13) (07): 6717-25.

Liu, B. S., and C. T. Au. 2003. Carbon deposition and catalyst stability over La2NiO4/-Al2O3 during CO2 reforming of methane to syngas. *Applied Catalysis A: General* 244 (1): 181-95.

Lo Faro, Massimiliano, Daniela La Rosa, Patrizia Frontera, Pierluigi Antonucci, Vincenzo Antonucci, and Antonino Salvatore Arico. 2010. Propane-fed solid oxide fuel cell based on a composite Ni-La-CGO anode catalyst. *Catalysis Letters* 136 (1-2): 57-64.

López Cordero, R., and A. López Agudo. 2000. Effect of water extraction on the surface properties of Mo/Al2O3 and NiMo/Al2O3 hydrotreating catalysts. *Applied Catalysis A: General* 202 (1) (7/31): 23-35.

Lowenthal, E. E., S. Schwarz, and H. C. Foley. 1995. Surface chemistry of rh-mo/γ-Al2O3: An analysis of surface acidity. *Journal of Catalysis* 156 (1) (9): 96-105.

Ma, L., D. L. Trimm, and C. Jiang. 1996. The design and testing of an autothermal reactor for the conversion of light hydrocarbons to hydrogen I. the kinetics of the catalytic oxidation of light hydrocarbons. *Applied Catalysis A: General* 138 (2): 275-83.

Maluf, S. S., and E. M. Assaf. 2009. Ni catalysts with mo promoter for methane steam reforming. *Fuel* 88 (9): 1547-53.

Maria G. González1, Esther N. Ponzi1, Osmar A. Ferretti, Claudia E. Quincoces, P. Marecot and J. Barbier Studies on H2S Adsorption and Carbon Deposition Over Mo–Ni/Al2O3 Catalysts. 2000. Studies on H2S adsorption and carbon deposition over Mo–Ni/Al2O3 catalysts. *Adsorption Science & Technology* 18 (6): 541.

Marin-Flores, O., L. Scudiero, and Su Ha. 2009. X-ray diffraction and photoelectron spectroscopy studies of MoO2 as catalyst for the partial oxidation of isooctane. *Surface Science* 603 (15) (08/01): 2327-32.

Marin-Flores, Oscar, Timothy Turba, Caleb Ellefson, Kang Wang, Joe Breit, Jeongmin Ahn, M. G. Norton, and Su Ha. 2010. Nanoparticle molybdenum dioxide: A highly active catalyst for partial oxidation of aviation fuels. *Applied Catalysis B: Environmental* 98 (3-4): 186-92.

Matsumura, Yasuyuki, and Toshie Nakamori. 2004. Steam reforming of methane over nickel catalysts at low reaction temperature. *Applied Catalysis A: General* 258 (1) (2/10): 107-14.

Mavrikakis, M., M. Baumer, H. -J Freund, and J. K. Nrskov. 2002. Structure sensitivity of CO dissociation on rh surfaces. *Catalysis Letters* 81 (3-4): 153-6.

McCarty, J. G., and H. Wise. 1979. Hydrogenation of surface carbon on alumina-supported nickel. *Journal of Catalysis* 57 (3) (5): 406-16.

Minutillo, Mariagiovanna. 2005. On-board fuel processor modelling for hydrogen-enriched gasoline fuelled engine. *International Journal of Hydrogen Energy* 30 (13-14): 1483-90.

Moe, J. M. 1962. Design of water-gas shift reactors. *Chemical Engineering Progress* 58 (3): 33-6.

Nagaoka, Katsutoshi, Katsutoshi Sato, Hiroyasu Nishiguchi, and Yusaku Takita. 2007. Influence of support on catalytic behavior of nickel catalysts in oxidative steam prereforming of n-butane for fuel cell applications. *Applied Catalysis A: General* 327 (2) (8/15): 139-46.

Natesakhawat, Sittichai, Okan Oktar, and Umit S. Ozkan. 2005. Effect of lanthanide promotion on catalytic performance of sol-gel Ni/Al2O3 catalysts in steam reforming of propane. *Journal of Molecular Catalysis A: Chemical* 241 (1-2): 133-46.

Natesakhawat, Sittichai, Rick B. Watson, Xueqin Wang, and Umit S. Ozkan. 2005. Deactivation characteristics of lanthanide-promoted sol–gel Ni/Al2O3 catalysts in propane steam reforming. *Journal of Catalysis* 234 (2) (9/10): 496-508.

Navarro, R. M., M. A. Pena, and J. L. G. Fierro. 2007. Hydrogen production reactions from carbon feedstocks: Fossil fuels and biomass. *Chemical Reviews* 107 (10): 3952-91.

Nett. Nett technologies inc. website (2005). .

Park, Sun-Young, Jong-Ho Kim, Dong-Ju Moon, Nam-Cook Park, and Young-Chul Kim. 2010. Autothermal reforming of propane over ni-based hydrotalcite catalysts.

Pesce, L. and Jenks, W. 1992. *Handbook of industrial chemistry*. 9th ed. New York: Van Nostrand Reinhold.

Pino, Lidia, Antonio Vita, Francesco Cipiti, Massimo Lagana, and Vincenzo Recupero. 2008. Catalytic performance of Ce1-x nix O2 catalysts for propane oxidative steam reforming. *Catalysis Letters* 122 (1-2): 121-30.

Pino, Lidia, Antonio Vita, Francesco Cipiti, Massimo Lagana, and Vincenzo Recupero. 2006. Performance of Pt/CeO2 catalyst for propane oxidative steam reforming. *Applied Catalysis A: General* 306 : 68-77.

Pompeo, Francisco, Nora N. Nichio, Mariana M. V. M. Souza, Deborah V. Cesar, Osmar A. Ferretti, and Martin Schmal. 2007. Study of ni and pt catalysts supported on -Al2O3 and ZrO2 applied in methane reforming with CO2. *Applied Catalysis A: General* 316 (2): 175-83.

Quincoces, C. E., S. P. de Vargas, P. Grange, and M. G. Gonzalez. 2002. Role of mo in CO2 reforming of CH4 over mo promoted Ni/Al2O3 catalysts. *Materials Letters* 56 (5) (11): 698-704.

Race, H. 2000. *Handbook of commercial catalysts*. Vol. Heterogeneous CatalystsNew York.

Rakib, M. A., J. R. Grace, C. J. Lim, S. S. E. H. Elnashaie, and B. Ghiasi. 2010. Steam reforming of propane in a fluidized bed membrane reactor for hydrogen production. *International Journal of Hydrogen Energy* 35 (12) (06): 6276-90.

Rampe, T., A. Heinzel, and B. Vogel. 2000. Hydrogen generation from biogenic and fossil fuels by autothermal reforming. Paper presented at Sixth Grove Fuel Cell Symposium Fuel Cells - The Competitive Option for Sustainable Energy Supply, .

Rasmussen, Frank B., Jens Sehested, Herman T. Teunissen, Alfons M. Molenbroek, and Bjerne S. Clausen. 2004. Sintering of Ni/Al2O3 catalysts studied by anomalous small angle X-ray scattering. *Applied Catalysis A: General* 267 (1-2) (7/30): 165-73.

Recupero, V., L. Pino, A. Vita, F. Cipiti, M. Cordaro, and M. Lagana. 2005. Development of a LPG fuel processor for PEFC systems: Laboratory scale

evaluation of autothermal reforming and preferential oxidation subunits. *International Journal of Hydrogen Energy* 30 (9) (08): 963-71.

Resini, Carlo, Laura Arrighi, Maria Concepcion Herrera Delgado, Maria Angeles Larrubia Vargas, Luis J. Alemany, Paola Riani, Silvia Berardinelli, Rinaldo Marazza, and Guido Busca. 2006. Production of hydrogen by steam reforming of C3 organics over Pd-Cu/-Al2O3 catalyst. *International Journal of Hydrogen Energy* 31 (1): 13-9.

Resini, Carlo, Maria Concepcion Herrera Delgado, Laura Arrighi, Luis J. Alemany, Rinaldo Marazza, and Guido Busca. 2005. Propene versus propane steam reforming for hydrogen production over Pd-based and Ni-based catalysts. *Catalysis Communications* 6 (7): 441-5.

Richardson, J. T., M. Lei, B. Turk, K. Forster, and Twigg W. Martyn. 1994. Reduction of model steam reforming catalysts: NiO/-Al2 O3. *Applied Catalysis A: General* 110 (2): 217-37.

Rostrup-Nielsen, Dybkjaer, Christiansen. 1993. *Chemical reactor technology for environmentally safe reactors and products*. Dordrecht: Kluwer Academic Publishers.

Rostrup-Nielsen, J., K. Pedersen, and J. Sehested. 2007. High temperature methanation. sintering and structure sensitivity. *Applied Catalysis A: General* 330 (1-2): 134-8.

Rostrup-Nielsen, Jens, and Ib Alstrup. 1999. Innovation and science in the process industry steam reforming and hydrogenolysis. *Catalysis Today* 53 (3): 311-6.

Rostrupnielsen, J. R., and J. H. B. Hansen. 1993. CO2-reforming of methane over transition metals. *Journal of Catalysis* 144 (1) (11): 38-49.

Rostrup-Nielsen, Jens R. 1973. Activity of nickel catalysts for steam reforming of hydrocarbons. *Journal of Catalysis* 31 (2) (11): 173-99.

Rostrup-Nielsen, Jens R. 1972. Equilibria of decomposition reactions of carbon monoxide and methane over nickel catalysts. *Journal of Catalysis* 27 (3) (12): 343-56.

Sago, F., S. Fukuda, K. Sato, K. Nagaoka, H. Nishiguchi, and Y. Takita. 2009. Catalytic behavior of Ni/ZrxTi1-xO2 and the effect of SiO2 doping in oxidative steam reforming of n-butane. *International Journal of Hydrogen Energy* 34 (19) (10): 8046-52.

Sato, Katsutoshi, Fumiaki Sago, Katsutoshi Nagaoka, and Yusaku Takita. 2010. Preparation and characterization of active Ni/MgO in oxidative steam reforming of n-C4H10. *International Journal of Hydrogen Energy* 35 (11): 5393-9.

Schädel, Benjamin T., Matthias Duisberg, and Olaf Deutschmann. 2009. Steam reforming of methane, ethane, propane, butane, and natural gas over a rhodium-based catalyst. *Catalysis Today* 142 (1-2) (4/15): 42-51.

Schmidt, Lanny D., and Marylin Huff. 1994. Partial oxidation of CH4 and C2H6 over noble metal-coated monoliths. *Catalysis Today* 21 (2-3): 443-54.

Scott, Carlos E., Trino Romero, Estherina Lepore, Morela Arruebarrena, Paulino Betancourt, Carmelo Bolívar, M. Josefina Pérez-Zurita, Pedro Marcano, and José Goldwasser. 1995. Interaction between ruthenium and molybdenum in RuMo/Al2O3 catalysts. *Applied Catalysis A: General* 125 (1) (4/27): 71-9.

Seyed-Reihani, Seyed, and Gregory S. Jackson. 2010. Catalytic partial oxidation of n-butane over rh catalysts for solid oxide fuel cell applications.

Shen, W. M., J. A. Dumesic, and C. G. Hill. 1981. Criteria for stable ni particle size under methanation reaction conditions: Nickel transport and particle size growth via nickel carbonyl. *Journal of Catalysis* 68 (1) (3): 152-65.

Silberova, Bozena, Hilde J. Venvik, John C. Walmsley, and Anders Holmen. 2005. Small-scale hydrogen production from propane. Paper presented at Catalysis for a Sustaiable Future, .

Silva, I. F., D. W. McKee, and L. S. Lobo. 1997. A kinetic and in Situ-XRD study of carbon reactions catalyzed by nickel, cobalt, molybdenum, and their mixtures. *Journal of Catalysis* 170 (1) (8): 54-61.

Siri, Marchetti, Ferretti and Gonzalez. 1991. *Catalyst deactivation*. Amsterdam: Elsevier.

Song, Jae Hee, Peilin Chen, Seong Han Kim, G. A. Somorjai, Robert J. Gartside, and Frits M. Dautzenberg. 2002. Catalytic cracking of n-hexane over MoO2. *Journal of Molecular Catalysis A: Chemical* 184 (1-2): 197-202.

Sperle, Thomas, De Chen, Rune Lødeng, and Anders Holmen. 2005. Pre-reforming of natural gas on a ni catalyst: Criteria for carbon free operation. *Applied Catalysis A: General* 282 (1-2) (3/30): 195-204.

Stasinska, Beata, Tadeusz Borowiecki, Andrzej Golebiowski, and Kazimierz Stolecki. 1998. Influence of hydrogen on the properties of nickel-molybdenum catalysts in the steam reforming of hydrocarbons. *Adsorption Science and Technology* 16 (9): 705-13.

Su, B. and Guo, S. 1999. *Catalyst deactivation*. Amsterdam: Elsevier.

Subramanian, R., G. J. Panuccio, J. J. Krummenacher, I. C. Lee, and L. D. Schmidt. 2004. Catalytic partial oxidation of higher hydrocarbons: Reactivities and selectivities of mixtures. *Chemical Engineering Science* 59 (22-23) (11): 5501-7.

Tøttrup, Peter B. 1976. Kinetics of decomposition of carbon monoxide on a supported nickel catalyst. *Journal of Catalysis* 42 (1) (4): 29-36.

Trimm, D. L. 1999. Catalysts for the control of coking during steam reforming. *Catalysis Today* 49 (1-3): 3-10.

Trimm, D. L. 1997. Coke formation and minimisation during steam reforming reactions. *Catalysis Today* 37 (3): 233-8.

Trimm, David L. 1977. FORMATION AND REMOVAL OF COKE FROM NICKEL CATALYST. *Catalysis Reviews* 16 (2): 155-89.

Tsipouriari, V. A., Z. Zhang, and X. E. Verykios. 1998. Catalytic partial oxidation of methane to synthesis gas over ni-based catalysts: I. catalyst performance characteristics. *Journal of Catalysis* 179 (1) (10/1): 283-91.

Twigg, M., Catalyst Handbook, 2nd ed., Wolfe Press, London, (1989), Chapter 6: 'Water-gas shift'. 1989. *Catalyst handbook*. second ed. Vol. chapter6, 'Waterr gas shift. London: Wolfe Press.

Twigg, Martyn V., and Michael S. Spencer. 2001. Deactivation of supported copper metal catalysts for hydrogenation reactions. *Applied Catalysis A: General* 212 (1-2): 161-74.

Wang, H. Y., and E. Ruckenstein. 2001. CO2 reforming of CH4 over Co/MgO solid solution catalysts - effect of calcination temperature and co loading. *Applied Catalysis A: General* 209 (1-2): 207-15.

Wang, Wuyin, S. Q. Turn, V. Keffer, and A. Douette. 2007. Study of process data in autothermal reforming of LPG using multivariate data analysis. *Chemical Engineering Journal* 129 (1-3) (05/01): 11-9.

Wang, X., and R. J. Gorte. 2002. A study of steam reforming of hydrocarbon fuels on Pd/ceria. *Applied Catalysis A: General* 224 (1-2): 209-18.

Wang, X., and R. J. Gorte. 2001. Steam reforming of n-butane on Pd/ceria. *Catalysis Letters* 73 (1): 15-9.

Wang, Zhuojian, Colin H. Rochester, and James A. Anderson. 1999. Decomposition of methane and subsequent reaction of carbonaceous residues over Rh/Mo/Al2O3Catalysts. *Journal of Catalysis* 184 (1) (5/15): 213-23.

Watson, Rick B., and Umit S. Ozkan. 2003. Propane and propylene adsorption effects over MoOx-based catalysts induced by low levels of alkali doping. *Journal of Molecular Catalysis A: Chemical* 194 (1-2): 115-35.

Wen, Wen, Jean E. Calderon, Joaquin L. Brito, Nebojsa Marinkovic, Jonathan C. Hanson, and Jose A. Rodriguez. 2008. In situ time-resolved characterization of ni-MoO2 catalysts for the water - gas shift reaction. *Journal of Physical Chemistry C* 112 (6): 2121-8.

Wynblatt, P., and N. A. Gjostein. 1976. PARTICLE GROWTH IN MODEL SUPPORTED METAL CATALYSTS - 1. THEORY. *Acta Metallurgica* 24 (12): 1165-74.

Xiao, Tiancun, Thomas Suhartanto, Andrew P. E. York, Jeremy Sloan, and Malcolm L. H. Green. 2003. Effect of molybdenum additives on the performance of supported nickel catalysts for methane dry reforming. *Applied Catalysis A: General* 253 (1): 225-35.

Xu, Jiahui, Connie M. Y. Yeung, Jun Ni, Frederic Meunier, Nadia Acerbi, Martin Fowles, and Shik Chi Tsang. 2008. Methane steam reforming for hydrogen production using low water-ratios without carbon formation over ceria coated Ni catalysts. *Applied Catalysis A: General* 345 (2) (8/1): 119-27.

Yamada, Yasumaru, Houalla and Hercules. 1991. Distribution of molybdenum oxidation states in reduced molybdenum/alumina catalysts: Correlation with benzene hydrogenation activity. *The Journal of Physical Chemistry* 95 (18): 7037-7042.

Youn, Min Hye, Jeong Gil Seo, Pil Kim, and In Kyu Song. 2007. Role and effect of molybdenum on the performance of Ni-Mo/-Al2O3 catalysts in the hydrogen production by auto-thermal reforming of ethanol. *Journal of Molecular Catalysis A: Chemical* 261 (2): 276-81.

Zaera, F., and R. B. Hall. 1987. High-resolution electron energy loss spectroscopy and thermal programmed desorption studies of the chemisorption and thermal decomposition of ethylene and acetylene on Ni(100) single-crystal surfaces. *Journal of Physical Chemistry* 91 (16) (07/30): 4318-23.

Zaera, F., and R. B. Hall. 1987. Low temperature decomposition of ethylene over ni(100): Evidence for vinyl formation. *Surface Science* 180 (1) (02): 1-18.

Zeng, Guangming, Ye Tian, and Yongdan Li. 2010. Thermodynamic analysis of hydrogen production for fuel cell via oxidative steam reforming of propane. *International Journal of Hydrogen Energy* 35 (13) (07): 6726-37.

Zhang, Lingzhi, Xueqin Wang, Bing Tan, and Umit S. Ozkan. 2009. Effect of preparation method on structural characteristics and propane steam reforming performance of ni-Al2O3 catalysts. *Journal of Molecular Catalysis A: Chemical* 297 (1-2): 26-34.

Zhou, Kebin, Hongde Chen, Qun Tian, Dixin Shen, and Xiaobai Xu. 2002. Propane oxidation over Pd/LaFe0.8Co0.2O3 catalyst. *Reaction Kinetics and Catalysis Letters* 77 (1): 65-72.

Zhuang, Quan, Yongning Qin*, and Liu Chang. 1991. Promoting effect of cerium oxide in supported nickel catalyst for hydrocarbon steam-reforming. *Applied Catalysis* 70 (1): 1-8.

Appendix A

Sample Calculations for Fuel Conversion and Products molar Flow Rates

Sample calculations are provided for oxidative steam reforming of a 1: 1 propane to butane mixture over a 0.1% wt Mo-15 % wt Ni /Al_2O_3 catalyst. This experiment was part of the Mo loading optimization experiments discussed in section 6.1 and the results of these experiments are presented in Appendix C. the experiment was run for six hours under the following conditions:

Propane mol % = 1

Butane mol % = 1

S/C = 3

O_2/C = 0.3

Reaction Temperature = 450°C = 723 K

Reaction Pressure = 1 atm

GHSV = 339800 ml/h . g_{cat}

As illustrated earlier in section 3.2, as the product stream exists the furnace, it enters a condenser where H_2O is condensed and only gaseous products continue to the GC. Peak areas of different gases obtained from chromatograms of the TCD and FID at the 7^{th} GC injection (at steady state after 2.85 hr from the beginning of the reaction) are shown in Tables A.1 and A.2 respectively. The composition of the product gas exiting the reactor was determined by applying the calibration curves relating peak area of each gas to a volume % and is also shown in Tables A.1 and A.2.

Table A.1: Peak areas from a TCD chromatogram and vol % of each gas calculated from calibration curves.

Gas	Peak Area	vol % from calibration
H_2	2.4	11.76
O_2	2.4	0.04
N_2	921	81.32
CO	9.9	0.77
CH_4	11.5	0.83
CO_2	128	4.71

Table A.2: Peak areas from an FID chromatogram and vol % of each gas calculated from calibration curves.

Gas	Peak Area	vol % from calibration
Methane	681	0.89
Ethane	traces	out of calibration range
Ethylene	-	-
Propane	0.61	0.25
Propylene	-	-
Acetylene	traces	out of calibration range
n-Butane	0.69	0.08
Methyl Acetylene	traces	out of calibration range

Since N_2 was used to control the flow rate and dilute the fuel mixture, the total volumetric flow rate of the product gas stream was calculated from knowing the vol % of N_2 in the product gas and the volumetric flow rate of N_2 fed to the reactor:

$$F_T = \frac{F_{N_2}^{in}}{y_{N_2}^{out}} = \frac{138.89 ml/\min}{0.8132} = 170.79 ml/\min$$

By knowing the total product flow rate, the volumetric flow rate for each product can be calculated by multiplying the vol % of each product by the total flow rate for example:

$$F_{H_2} = F_T \times y_{H_2} = 170.79 ml/\min \times 0.118 = 20.08 ml/\min$$

The molar flow rate of each gas is achieved from the ideal gas low:

$$n_{H_2} = \frac{PF_{H_2}}{RT} = \frac{1atm \times 0.028L / \min}{0.082 \frac{L.atm}{mol.K} \times (25 + 273.15)K} = 82.19 \times 10^{-5} mol / \min$$

The molar flow rate for each gas product is shown in Table A.3:

Table A.3: molar flow rate for each gas product

Gas	Molar flow rate mol / min × 10^5
H_2	82.19
O_2	0.300
N_2	698.9
CO	5.42
CH_4	5.79
CO_2	32.93
propane	1.78
Butane	0.565

The total fuel conversion was calculated as:

$$X_{total} = \frac{(n_{prop}^{in} + n_{but}^{in}) - (n_{prop}^{out} + n_{but}^{out})}{(n_{prop}^{in} + n_{but}^{in})} \times 100$$

$$X_{total} = \frac{(7.59 \times 10^{-5} + 7.59 \times 10^{-5}) - (1.78 \times 10^{-5} + 0.565 \times 10^{-5})}{(7.59 \times 10^{-5} + 7.59 \times 10^{-5})} \times 100 = 84.54\%$$

The carbon balance for the injection was calculated as:

$$C_{bal} = \frac{3 \times n_{prop}^{out} + 4 \times n_{but}^{out} + 1 \times n_{CO}^{out} + 1 \times n_{CO_2}^{out} + 1 \times n_{CH_4}^{out}}{3 \times n_{prop}^{in} + 4 \times n_{but}^{in}} \times 100$$

$$C_{bal} = \frac{3 \times 1.78 \times 10^{-5} + 4 \times 0.565 \times 10^{-5} + 1 \times 5.42 \times 10^{-5} + 1 \times 32.93 \times 10^{-5} + 1 \times 5.79 \times 10^{-5}}{3 \times 7.59 \times 10^{-5} + 4 \times 7.59 \times 10^{-5}}$$

$$C_{bal} = 97.4\%$$

Appendix B

Reducibility of Results Obtained from Different Catalyst Batches

To ensure that the data produced from any single run is truly representative of the mean result, reproducibility experiments were performed for two batches of the 0.1Mo-15Ni/Al_2O_3 (0.1Mo) catalyst following exactly the same preparation and pre-treatment procedure. The performance of the two batches, B1 and B2, were compared under the same LPG OSR experimental conditions given below:

Propane mol % = 1, Butane mol % = 1

S/C = 3, O_2/C = 0.3

Reaction Temperature = 450°C = 723 K , Reaction Pressure = 1 atm

GHSV = 339800 ml/h . g_{cata}

Results of the 6 hour run for each batch are compared in Figures B.1, B.2 and B.3

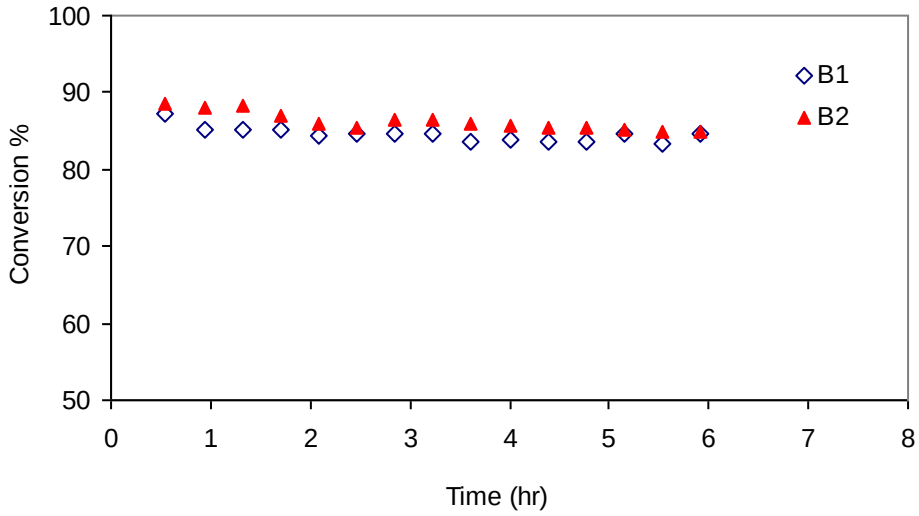

Figure B.1: Reducibility of fuel conversion of two 0.1Mo batches run under the same OSR conditions.

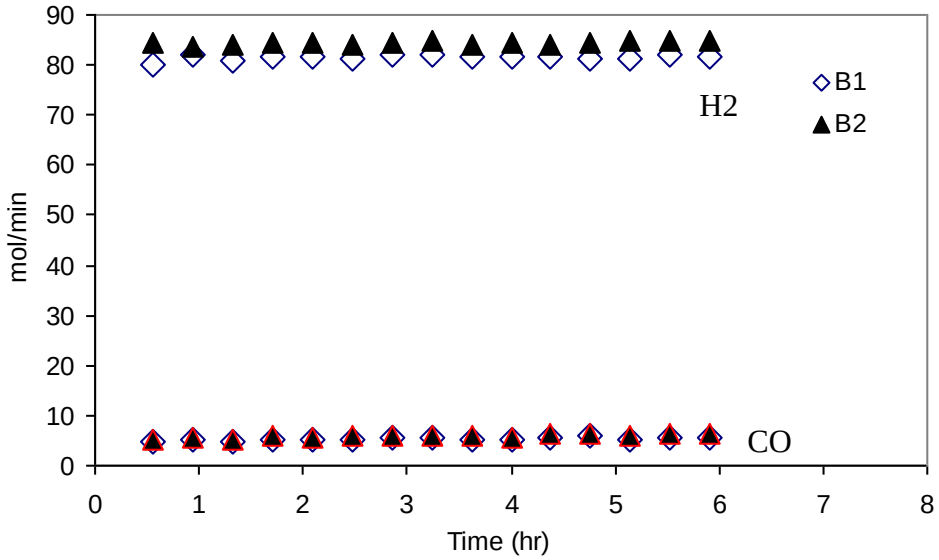

Figure B.2: Reducibility of H_2 and CO production rates of two 0.1Mo batches run under the same OSR conditions.

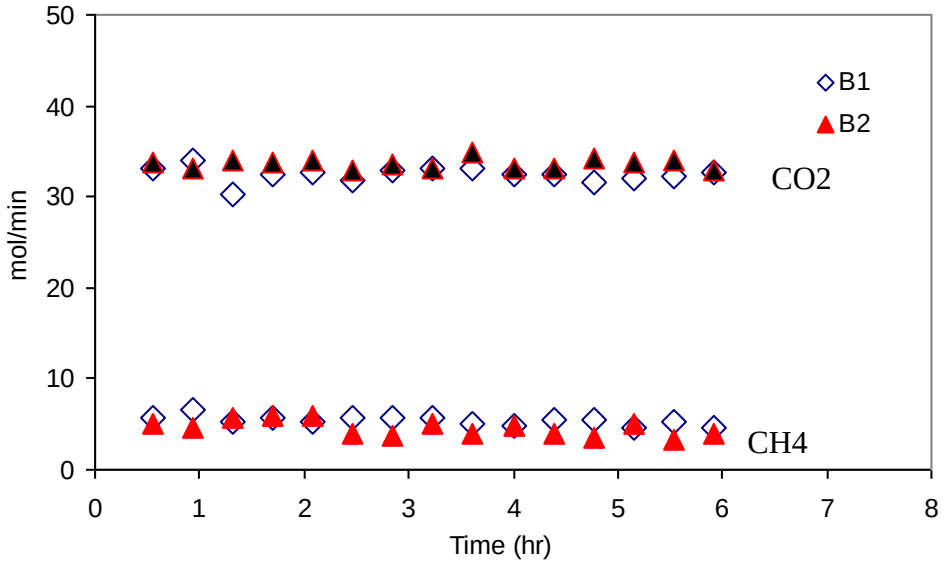

Figure B.3: Reducibility of CO_2 and CH_4 production rates of two 0.1Mo batches run under the same OSR conditions.

Appendix C

Results of Mo Loadings Optimization Experiments Discussed in Chapter 6, Section 6.3

In order to optimize Mo loading of the Mo-Ni /Al_2O_3 catalyst between 0.05 and 0.3 wt%, catalyst performance and stability of three Mo loadings; 0.05, 0.1 and 0.3 were compared under the same LPG OSR conditions given below:

Propane mol % = 1

Butane mol % = 1

S/C = 3

O_2/C = 0.3

Reaction Temperature = 450°C = 723 K

Reaction Pressure = 1 atm

GHSV = 339800 ml/h . g_{cata}

Results comparing the performance of the three loadings are shown in Figures C.1 to C.5

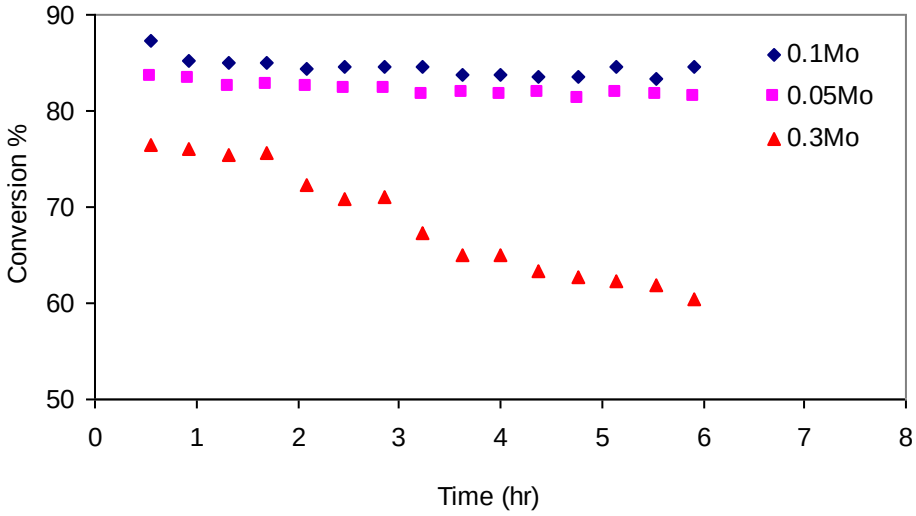

Figure C.1: Fuel conversion of three Mo catalyst loadings run under that same LPG OSR conditions.

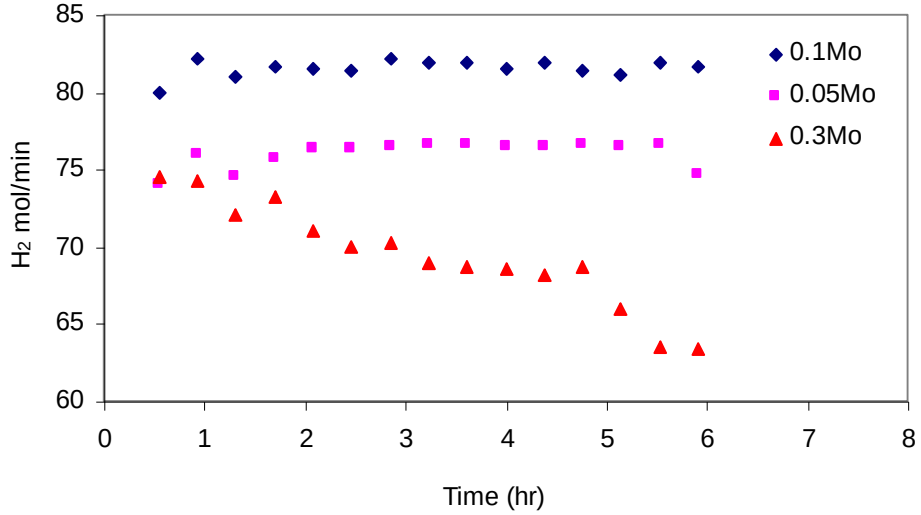

Figure C.2: H_2 production rate of three Mo catalyst loadings run under that same LPG OSR conditions.

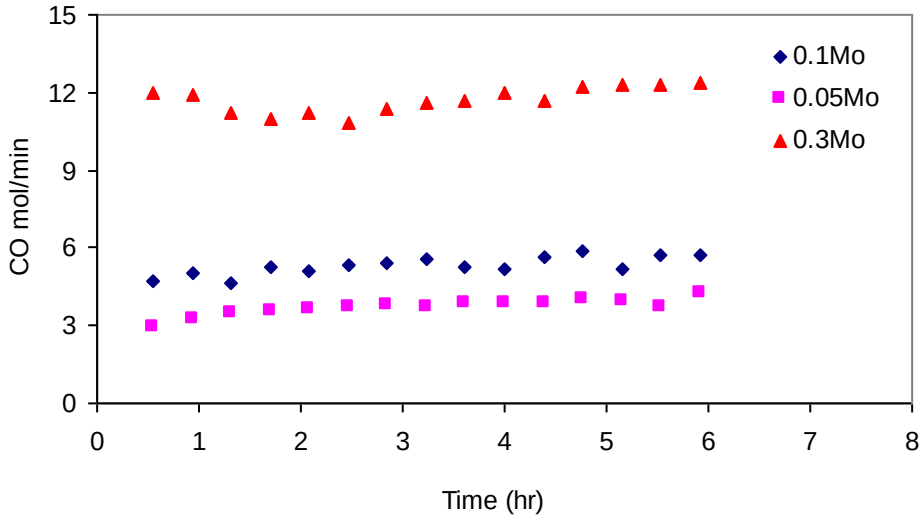

Figure C.3: CO production rate of three Mo catalyst loadings run under that same LPG OSR conditions.

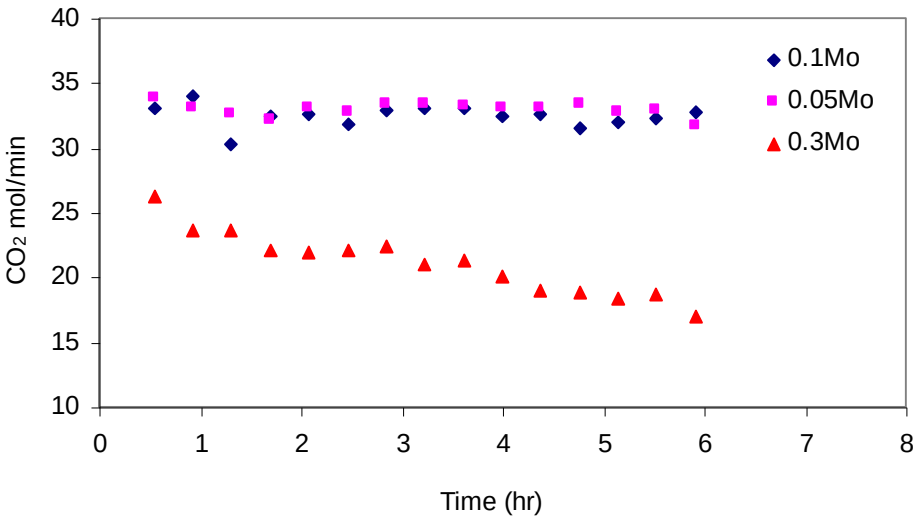

Figure C.4: CO_2 production rate of three Mo catalyst loadings run under that same LPG OSR conditions.

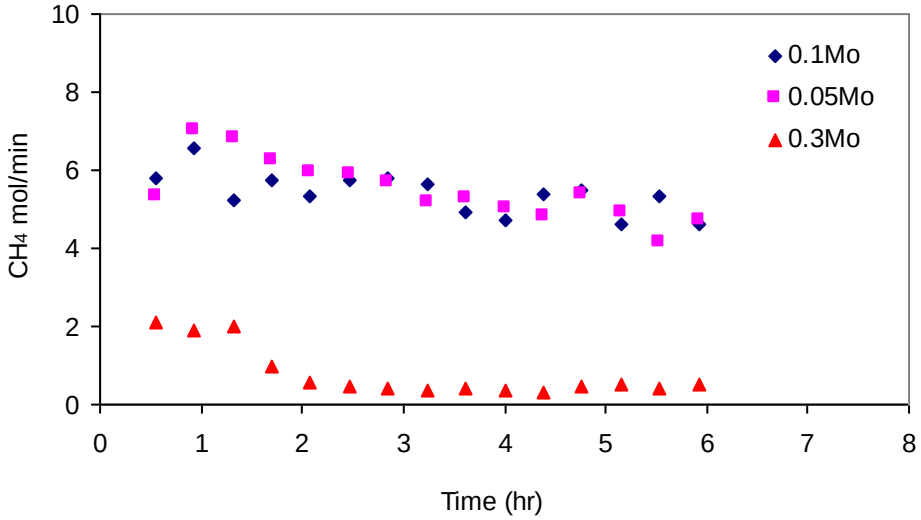

Figure C.5: CH_4 production rate of three Mo catalyst loadings run under that same LPG OSR conditions.